OFFICIAL JOURNAL OF THE SCIENTIFIC SOCIETY OF ANATOMISTS, HISTOLOGISTS, EMBRYOLOGISTS AND TOPOGRAPHIC ANATOMISTS OF UKRAINE

DOI: 10.31393
ISSN 1818-1295
eISSN 2616-6194

ВІСНИК МОРФОЛОГІЇ
REPORTS OF MORPHOLOGY

Vol. 30, №2, 2024

Scientific peer-reviewed journal in the fields of normal and pathological anatomy, histology, cytology and embryology, topographical anatomy and operative surgery, biomedical anthropology, ecology, molecular biology, biology of development

Published since 1993
Periodicity: 4 times a year

Vinnytsya · 2024

ВІСНИК МОРФОЛОГІЇ - REPORTS OF MORPHOLOGY

Founded by the "Scientific Society of Anatomists, Histologists, Embryologists, and Topographic Anatomists of Ukraine" and National Pyrogov Memorial Medical University, Vinnytsya in 1993

Certificate of state registration КВ №9310 from 02.11.2004

Professional scientific publication of Ukraine in the field of medical sciences in specialties 221, 222, 228, 229
According to the list of professional scientific publications of Ukraine, approved by the order of the Ministry of Education and Science of Ukraine No. 1188 of 24.09.2020
Professional scientific publication of Ukraine in the field of biological sciences in specialty 091
According to the list of professional scientific publications of Ukraine, approved by the order of the Ministry of Education and Science of Ukraine No. 1471 of 26.11.2020

Approved by the Academic Council of National Pyrogov Memorial Medical University, Vinnytsya, protocol №10 from 31.05.2024.

Indexation: Scopus, CrossRef, Index Copernicus, Google Schoolar Metrics, National Library of Ukraine Vernadsky

Address editors and publisher:
Pyrogov Str. 56,
Vinnytsya, Ukraine - 21018
Tel.: +38 (0432) 553959
E-mail: nila@vnmu.edu.ua

Computer page-proofs - Klopotovska L.O.
Translator - Gunas V.I.
Technical support - Levenchuk S.S.
Scientific editing - editorship

The site of the magazine - https://morphology-journal.com

CONTENT

DOI: 10.31393/morphology-journal-2024-30(2)-01 Reports of Morphology, Vol. 30, №2, Pages 5-12

ISSN 1818-1295 eISSN 2616-6194

REPORTS OF MORPHOLOGY

Official Journal of the Scientific Society of Anatomists, Histologists, Embryologists and Topographic Anatomists of Ukraine

journal homepage: https://morphology-journal.com

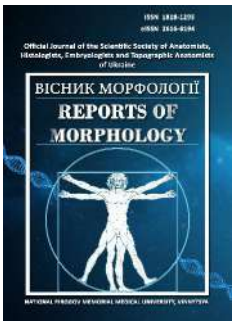

Density of lymphocytes in cortex and medulla substance of thymus particles of white rats in normal conditions and under influence of heavy metal salts during three months

Dobryanska E. S., Vatsyk N. S., Litvak V. V.
Uzhgorod National University, Uzhgorod, Ukraine

ARTICLE INFO
Received: 27 December 2023
Accepted: 15 February 2024

UDC: 591.443 612.438

CORRESPONDING AUTHOR
e-mail: erika.dobrianska@uzhnu.edu.ua
Dobryanska E. S.

CONFLICT OF INTEREST
The authors have no conflicts of interest to declare.

FUNDING
Not applicable.

DATA SHARING
Data are available upon reasonable request to corresponding author.

The consumption of clean water is the most relevant today, but natural water is delivered to our homes through plastic, iron and galvanized pipes. Metal ions, which are part of the pipe material, can get into drinking water and affect the human body, in particular the thymus. That is why the aim of the work was to determine the density of large, medium and small lymphocytes in the cortex and medulla of the thymus lobules of outbred white male rats of reproductive age when consuming small doses of heavy metal salts with water for three months. The study was conducted on 40 outbred white male rats of reproductive age, which were divided into 4 groups: 1 group - control animals that consumed distilled water; 2 group of animals that consumed aqueous solutions - $CuSO_4 \cdot 5H_2O$ at a dose of 0.247 mg/dm^3; 3 group - aqueous solution of $ZnSO_4 \cdot 7H_2O$ at a dose of 1.505 mg/dm^3; group 4 - aqueous solution of $FeSO_4 \cdot 7H_2O$ at a dose of 0.5 mg/dm^3. Histological, electron microscopic and morphometric research methods were used to study the density of large, medium and small lymphocytes in different zones of the thymus lobules. It was found that in the control group of rats, the density of large lymphocytes is the highest in the subcapsular zone, and the lowest in the medulla. The density of medium lymphocytes is the lowest in the subcapsular zone. The density of small lymphocytes is the lowest in the medulla, and the highest in the cortico-medullary zone. When using $CuSO_4 \cdot 5H_2O$ salts with drinking water for three months, there were no significant changes in the density of lymphocytes compared to the control group, except for a slight decrease in the density of large lymphocytes in the cortex of the thymus lobules. The density of lymphocytes in the third group of animals that consumed zinc salts ($ZnSO_4 \cdot 7H_2O$) with drinking water changes significantly: the density of large lymphocytes in the subcapsular zone decreases by 2.3 times, in the cortico-medullary zone it increases by 4.7 times, and in the medulla it increases by 2.7 times; the density of medium lymphocytes decreases in the subcapsular zone by 2 times; the density of small lymphocytes decreases by 1.5 times in the subcapsular zone, in the cortex and cortico-medullary zone - decreases by 1.2 times, and in the medulla by 1.1 times. When using $FeSO_4 \cdot 7H_2O$ salts with drinking water for three months, no special changes in the density of lymphocytes were noted: a decrease in the density of large lymphocytes in the subcapsular zone by 1.5 times and by 1.3 times in the cortex was observed; the density of medium lymphocytes decreases by 1.2 times in the cortex, and the density of small lymphocytes decreases by 1.2 times in the subcapsular zone and cortex, and increases by 1.2 times in the medulla, compared to the control group of animals. Ultrastructural changes in the structure of lymphocytes and reticuloepithelial cells were not detected when heavy metal salts were consumed with water. Thus, the study showed that the most toxic for the body are zinc salts ($ZnSO_4 \cdot 7H_2O$), the consumption of which with drinking water in small doses for three months led to significant changes in the density of lymphocytes, compared to the control group experimental animals.
Keywords: *thymus, lymphocytes, heavy metals, density.*

Introduction

The problem of clean drinking water is an urgent problem of many countries of the world. Currently, one of the reasons for the unsatisfactory quality of drinking water is mass pollution of surface water bodies, rivers, reservoirs,

and this can lead to a slowdown in the growth of molluscs [24] and other microorganisms that clean water bodies. Salts of heavy metals accumulate in plants [2, 3, 29], which we consume in food, add as spices or brew teas. Environmental exposure to many metals and metalloids is widespread, raising global concerns about the adverse health effects of mixed metal exposures, especially for young children living around industrial areas [19]. Salts of heavy metals play the role of trace elements [4]. These elements, like vitamins, are needed by the human body for its normal functioning. Lack of trace elements in the body or their excess causes various diseases. In connection with the ever-increasing pollution of the environment, salts of heavy metals constantly accumulate in living organisms, in particular, in the human body [19], in excess quantities, which leads to the development of various diseases [15, 22, 34, 35]. The problem of monitoring heavy metal ions is one of the main ones. Sensitive and reliable methods for the detection of heavy metal ions in various aptamer-based systems using nanoparticles have been developed [31]. Many scientists are working on the development of substances that could absorb excess salts of heavy metals [36]. It is about the development of inexpensive adsorbents for reducing the content of heavy metals in aqueous solutions [1, 17, 18, 31], as well as the generation of strains of Fe/Mn-oxidizing bacteria resistant to high concentrations of several heavy metals (loids) and their effective deactivation [14]. The thymus is the primary organ of hematopoiesis and immune protection, in which, under the influence of the microenvironment [13, 22, 23, 33], antigen-independent proliferation and differentiation of T-lymphocytes occurs, which provides cellular immunity [11, 13] and prevention of the development of autoimmune processes in organism [12, 20]. In addition, the cells of the cortico-medullary zone of the thymus produce a number of hormones that regulate many functions in the body, under their influence various tumors can develop, including thymomas [34, 35]. The thymus plays a central role in the production of lymphocytes and in ensuring the normal development of immunological ability [21], therefore the density of lymphocytes is one of the indicators of the functional state of the thymus. To this day, the influence of low concentrations of heavy metal salts on the thymus remains unexplored.

Research has paid little attention to morphological changes in the thymus under the influence of heavy metal salts. This is what determined *the purpose of our study* - to determine the density of large, medium and small lymphocytes in the cortex and medulla of the thymus lobes of outbred white male rats of reproductive age when consuming small doses of heavy metal salts with water for three months.

Materials and methods

The study was conducted on 40 outbred white male rats of reproductive age, which were divided into 4 groups of 10 individuals each: 1 group - control animals that consumed distilled water; 2 group of animals that consumed aqueous solutions - $CuSO_4 \cdot 5H_2O$ in a dose of 0.247 mg/dm^3, which corresponds to the content of the mineral chalcanthite in the floodplains of the Tysa River; group 3 - aqueous solution of $ZnSO_4 \cdot 7H_2O$ (zinc salt of sulfuric acid) in a dose of 1.505 mg/dm^3; group 4 - aqueous solution of $FeSO_4 \cdot 7H_2O$ (iron sulfate) in a dose of 0.5 mg/dm^3.

Animal care and all manipulations were carried out in accordance with the provisions of the "European Convention for the Protection of Vertebrate Animals Used for Experimental and Other Scientific Purposes" (Strasbourg, 1986), as well as the "General Ethical Principles of Animal Experimentation", adopted by the First National Congress on of bioethics (Kyiv, 2001) and the requirements of the Addendum to the "Rules for conducting work using experimental animals", approved by the order of the Ministry of Health No. 755 of August 12, 1977 "On measures to further improve organizational forms of work using experimental animals". The work was approved at the meeting of the Bioethics Commission of the Uzhhorod National University (Protocol No. 12/8 dated September 22, 2023).

The thymus was taken from the animals under anesthesia. The material for histological studies was fixed in AFA solution (formaldehyde - 100 ml, ethyl alcohol 96° - 60 ml, glacial acetic acid - 30 ml) and poured into paraffin blocks. Histological sections with a thickness of 5-7 μm were stained with hematoxylin and eosin.

Morphometric studies were carried out using Test-5, Stepanizer, KAAPA Image, Base, Microsoft Excel programs on a personal computer using a visual analysis system. Images of histological preparations were displayed on a computer monitor using an SEO SCAN microscope and a Vision CCD camera [26].

Statistical analysis was performed using the Jamovi 2.2.5 program (freely available under the AGPL3 license). The normality of the distribution was assessed by the Shapiro-Wilk test. Mean values were plotted as M±σ. The non-parametric Mann-Whitney test was used to assess the reliability of the difference between the experimental groups and the control. The significance of the difference was considered at $p<0.05$.

For electron microscopic examination, the material was fixed in a 2.5 % solution of glutaraldehyde in a 0.1 M phosphate buffer with a pH of 7.2-7.4 with additional fixation in a 2 % solution of osmium tetroxide. After dehydration in alcohols and acetone, the material was poured into araldite. Sections were made on an LKV 8800WI ultramicrotome and studied on an EOM-100AK microscope with an accelerating voltage of 75 kV.

Results

We found that the density of lymphocytes in the control group of animals decreases in the direction from the cortex to the medulla (Table 1). The number of large lymphocytes decreases by 4.5 times from the subcapsular zone of the

Table 1. Comparative characteristics of the density indicators of large, medium and small lymphocytes in the zones of the thymus lobe of white male rats of reproductive age on an area of 625.0 μm^2 of the control group and under the condition of exposure to heavy metal salts (M±y, n=40).

Zones of the thymus lobules	Density of lymphocytes on the area			
	Type of lymphocytes			
	groups	large lymphocytes	medium lymphocytes	small lymphocytes
Subcapsular zone of the cortex	1 gr.	3.881±0.410	2.634±0.321	6.158±0.421
	2 gr.	2.981±0.321	2.855±0.422	6.953±0.221
	3 gr.	1.183±0.641*	1.254±0.222*	4.151±0.621
	4 gr.	2.480±0.542	2.250±0.321	4.950±0.121
Cortex	1 gr.	2.743±0.291	3.481±0.520	6.212±0.461
	2 gr.	2.111±0.120	3.182±0.322	5.855±0.161
	3 gr.	2.293±0.290	3.486±0.253	5.251±0.360
	4 gr.	1.980±0.621	3.180±0.422	5.250±0.321
Cortico-medullary zone	1 gr.	0.613±0.330	3.331±0.461	6.511±0.522
	2 gr.	0.912±0.440	3.684±0.261	6.913±0.120
	3 gr.	2.834±0.641*	3.322±0.461	5.622±0.430
	4 gr.	0.900±0.241	2.850±0.662	6.210±0.141
Medulla	1 gr.	0.451±0.122	3.383±0.520	5.322±0.451
	2 gr.	0.454±0.361	3.243±0.420	5.851±0.251
	3 gr.	1.251±0.551*	3.183±0.521	4.844±0.652
	4 gr.	0.500±0.461	3.110±0.221	6.220±0.232

Notes: * - the reliability of the difference in the density of lymphocytes between the experimental groups and the control group at $p<0.05$.

cortex to the cortico-medullary zone, and in the medulla their density decreases by as much as 6 times (see Table 1). The density of average lymphocytes (see Table 1) is the lowest in the subcapsular zone, in other zones, that is, in the cortex itself, the corticomedullary zone, and the medulla, the density of lymphocytes increases. The density of small lymphocytes (see Table 1) is the highest in the cortex (subcapsular zone, cortex and cortico-medullary zone), the lowest density of small lymphocytes is in the medulla. In the cortex, there is a decrease in large lymphocytes and an increase in medium and small lymphocytes, compared to other areas of the thymus lobe. Therefore, in the control group of rats, the density of large lymphocytes (Fig. 1) is the highest in the subcapsular zone, and the lowest in the medulla, medium lymphocytes (see Fig. 1) is the lowest in the subcapsular zone, and in other zones (cortex, cortico-medullary zone, medulla) is almost the same. The density of small lymphocytes (see Fig. 1) is the lowest in the medulla, and the highest in the cortico-medullary zone. It should be noted that the density of small lymphocytes in the subcapsular zone and the cortex itself does not differ significantly.

When animals consume $CuSO_4 \cdot 5H_2O$ in water, the density of lymphocytes in the lobes of the thymus, compared to the control group of animals, does not change significantly (see Table 1): in the subcapsular zone, the density of large lymphocytes (Fig. 2) is the highest, but less than in the control group, their density decreases in the cortex (it is also somewhat less compared to the control group), in the cortico-medullary zone it decreases (it is slightly more than in the control group), and in the medulla it is the smallest, but similar in size to the control group. The density of average lymphocytes (see Table 1) is almost unchanged compared to the control group of animals. The highest density of medium lymphocytes (see Fig. 2) is determined in the cortico-medullary zone, and the lowest in the subcapsular zone (see Table 1). The density of small lymphocytes (see Table 1) increases unreliably, the highest is in the corticomedullary zone, and the lowest in the cortex and medulla. Therefore, when used for three months with drinking water $CuSO_4 \cdot 5H_2O$ at a dose of 0.247 mg/dm^3, no significant changes in the density of lymphocytes, compared to the control group, were detected, with the exception of a

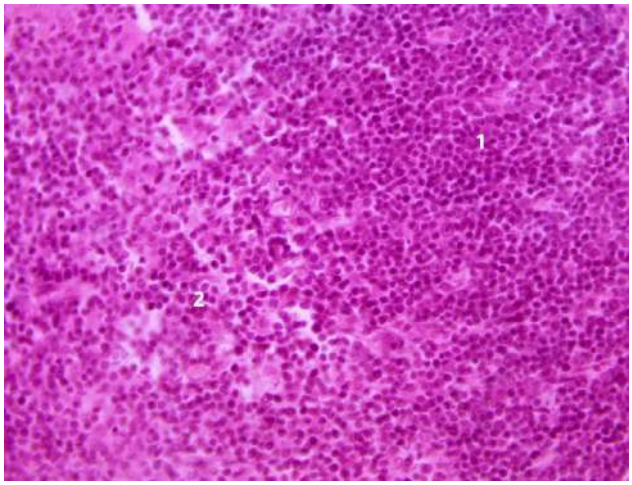

Fig. 1. Thymus of white male rats of reproductive age of the control group. Fragment of cortex (1) and medulla (2). Hematoxylin-eosin. x400.

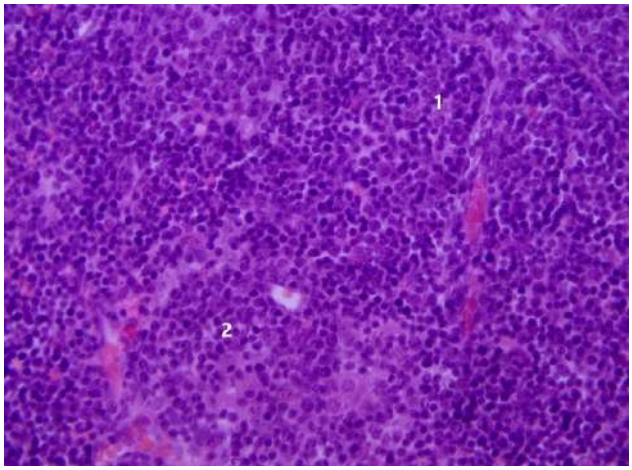

Fig. 2. Thymus of white male rats of reproductive age under the influence of $CuSO_4 \cdot 5H_2O$ for three months. Fragment of cortex (1) and medulla (2). Hematoxylin-eosin. x400.

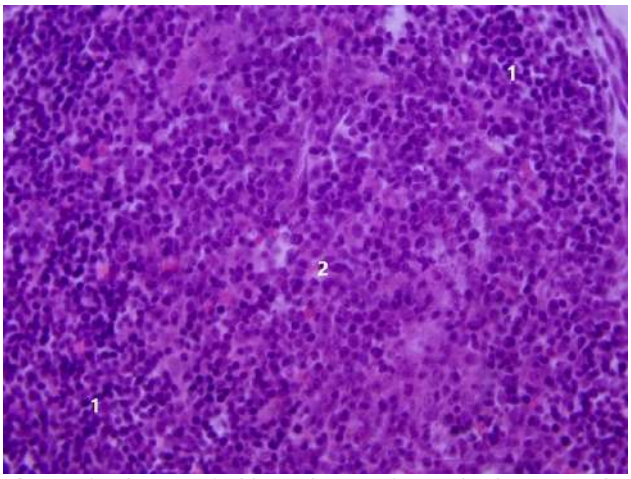

Fig. 3. The thymus of white male rats of reproductive age under the influence of $ZnSO_4 \cdot 7H_2O$ for three months. Fragment of cortex (1) and medulla (2). Hematoxylin-eosin. x400.

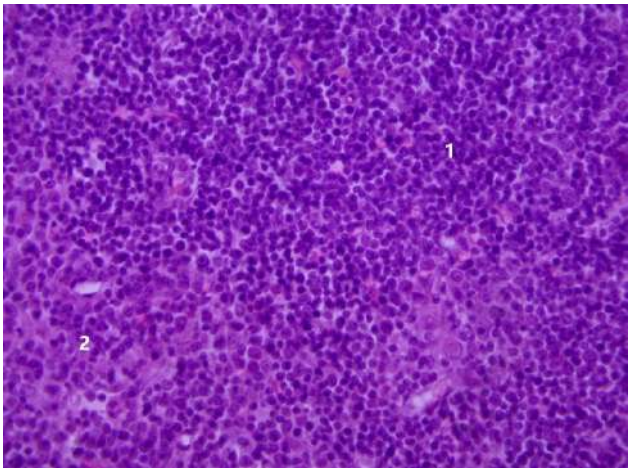

Fig. 4. Thymus of white male rats of reproductive age. Fragment of cortex (1) and medulla (2) under the influence of $FeSO_4 \cdot 7H_2O$ for three months. Hematoxylin-eosin. x400.

slight decrease in the density of large lymphocytes in the cortex of the thymus lobe.

The density of lymphocytes in the lobes of the thymus of animals of the third group, to which zinc salts ($ZnSO_4 \cdot 7H_2O$) were added to drinking water, changes significantly. Compared to the control group, the density of large lymphocytes (Fig. 3) in the subcapsular zone decreases by 2.3 times, in the cortex it decreases slightly (see Table 1), almost similar to the control group. In the corticomedullary zone - it increases by 4.7 times (see Table 1), in the medulla there is also an increase in the density of large lymphocytes by 2.7 times. The density of average lymphocytes (see Fig. 3) decreases in the subcapsular zone by 2 times (see Table 1) compared to the control group. In the cortex, corticomedullary zone, and medulla, the density of average lymphocytes (see Table 1) practically does not differ from the control group of animals. The density of small lymphocytes (see Fig. 3), compared to the control group (see Table 1), decreases in the subcapsular zone by 1.5 times, in the cortex, corticomedullary zone by 1.2 times, and in the medulla by 1.1 times. Therefore, when white rats consume an aqueous solution of $ZnSO_4 \cdot 7H_2O$ at a dose of 1.505 mg/dm^3 for three months, the density of large, medium, and small lymphocytes in all zones of the thymus lobe decreases, compared to the control group of animals.

In the fourth group, experimental rats consumed iron salts ($FeSO_4 \cdot 7H_2O$) with water, as in the second group, no particular changes in density were observed. A decrease in the density of large lymphocytes (Fig. 4) in the subcapsular zone by 1.5 times (see Table 1) and by 1.3 times in the cortex was noted, compared to the control group of animals. In the cortico-medullary zone and in the medulla, the density indicators were similar to those of the control group. The density of average lymphocytes (see Fig. 4) in the cortex decreased by 1.2 times, and in other areas of the lobes of the mammary gland it did not differ significantly from the similar indicators of the control group (see Table 1). The density of small lymphocytes (see Table 1) in the subcapsular zone and cortex decreases by 1.2 times, and in the medulla increases by 1.2 times compared to the control group of animals. In the cortico-medullary zone, the density of small lymphocytes is almost the same as in the control group.

At the submicroscopic level, no changes in the structure of large, medium and small lymphocytes (Figs. 5, 6, 7), reticuloepitheliocytes of the stroma (see Fig. 6) were detected.

Reticuloepitheliocytes form a stroma for lymphocytes, in which antigen-independent proliferation and differentiation of T-lymphocyte subpopulations occurs.

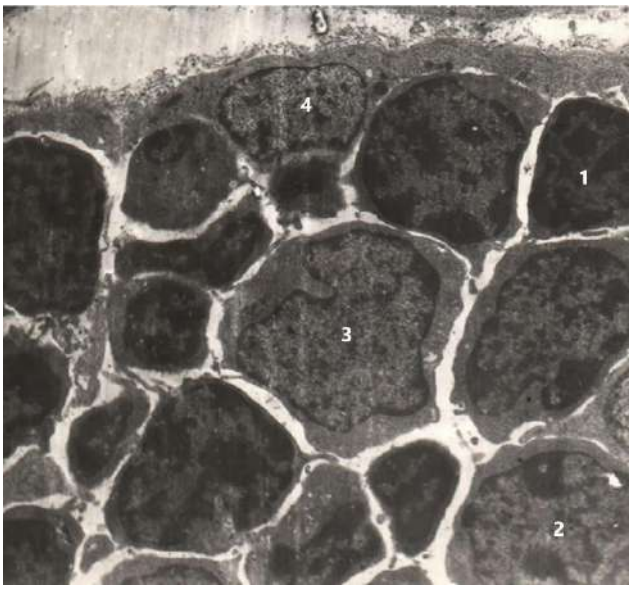

Fig. 5. Lymphocytes of the subcapsular zone of the cortex of the thymus lobules of white male rats of reproductive age: 1 - small lymphocyte, 2 - medium lymphocyte, 3 - large lymphocyte, 4 - nucleus of reticuloepitheliocyte. Electronic photography. x7000.

Fig. 6. Lymphocytes (1) in the cortex lobules of the thymus of white male rats of reproductive age. In the center is a reticuloepitheliocyte (2), the processes (3) of which branch out and surround lymphocytes. Electronic photography. x7000.

Reticuloepitheliocytes are extremely important because, together with macrophages, neutrophils, eosinophils and tissue basophils, they create a microenvironment for "maturing" T-lymphocytes. Reticuloepitheliocytes form numerous branched processes. The core in them is located in the center, mostly oval in shape. It has one nucleolus and a small amount of heterochromatin (see Fig. 6).

Lymphocytes are mainly small and medium. They have a rounded shape and a large nucleus that occupies the entire volume of the cytoplasm (see Fig. 6).

In the nuclei of different forms of lymphocytes, the amount of heterochromatin is not the same - it is more in the small ones, and less in the medium ones. Heterochromatin is mainly concentrated near the inner membrane of the nuclear envelope and, more rarely, freely in the nucleoplasm in the form of lumps of various shapes and sizes (see Fig. 6). At the submicroscopic level, no changes in the structure of large, medium, and small

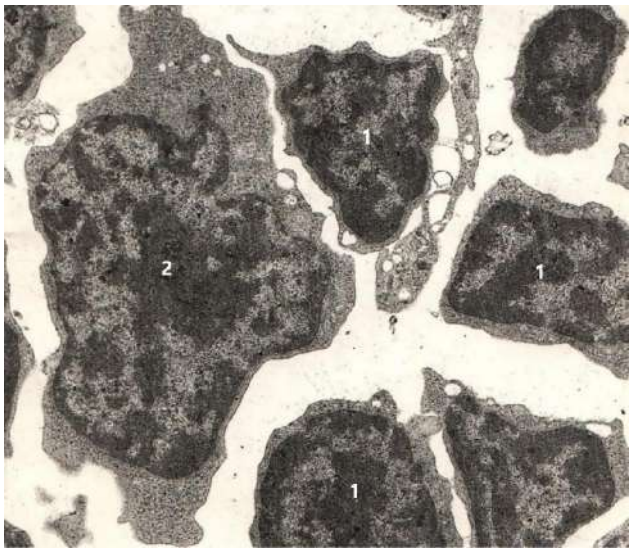

Fig. 7. Lymphocytes in the medulla lobules of the thymus of white male rats of reproductive age: 1 - small lymphocyte, 2 - medium lymphocyte. Electronic photography. x7000.

lymphocytes, reticuloepitheliocytes of the stroma of the cortex, medulla, and corticomedullary zone were detected (see Figs. 5, 6, 7).

Discussion

The study showed that the greatest influence on the change in the density of large, medium and small lymphocytes in different zones of the thymus lobe has an aqueous solution of $ZnSO_4 \cdot 7H_2O$ (zinc salt of sulfuric acid) at a dose of 1.505 mg/dm3 and an aqueous solution of $FeSO_4 \cdot 7H_2O$ at a dose of 0.5 mg/dm^3. It is in this concentration that all these heavy metals are found in nature, that is, in Ukraine, in the floodplains of the Tysa River. We did not take for research solutions of previously known toxic substances, such as cadmium, which penetrates the placental barrier and has a teratogenic effect [19]. An interesting fact was that in the blood of children living in industrial areas, the influence of As, Pb, Br, Cu and Se was increased, and the increased concentration of Tl was associated with obesity, and As, on the contrary, with underweight [19]. Such metals as Cu, Se and Br in high concentrations had a pronounced hepato- and nephrotoxic effect. Thus, salts of heavy metals, even in small concentrations, which we consume daily with water, food and breathe with air, are able to be deposited in the blood and other tissues of the body, thereby changing, for example, the density of lymphocytes in the thymus. According to Prykhodko O. O. [27], the thymus is involved in maintaining homeostasis and protecting the body from foreign antigens. With age, thymus tissue undergoes involutional changes, as a result of which the general condition of the human body worsens and the course of chronic diseases becomes more complicated. Age-related involution leads to a progressive decrease in the formation of new T-cells, that is, the density of lymphocytes in the thymus decreases.

This reduced output is compensated by the duplication of existing T cells, leading to a gradual dominance of memory T cells and a reduced ability to respond to new pathogens or vaccines [27]. That is, a decrease in the density of lymphocytes leads to a decrease in cellular immunity. In our study, it was established that under the conditions of exposure to zinc salts, the density of large and medium lymphocytes decreases by 2 times in the subcapsular zone - this is precisely the part of the thymus where T-lymphocytes migrate from the red bone marrow for "maturation". Thymic function is critical for reducing morbidity [15] and mortality associated with various clinical conditions, including infections, transplantation, and autoimmune diseases [20, 21]. Therefore, the study of changes in its structural components and vascular bed under the influence of various pathological factors, in particular heavy metal salts, is an important task of morphologists and clinicians.

Cellular immunity is not isolated from humoral immunity, so disturbances in the structure and function of the thymus and thymus-dependent antigens, which are themselves immunogenic, can induce the response of B cells that can neutralize, for example, viruses [11]. Under the conditions of short-term influence of any factor on the body of experimental animals, all changes in the thymus are a manifestation of a compensatory-adaptive reaction and are not specific. Obviously, such compensatory reactions of the body are an increase in the density of small lymphocytes in all zones of the thymus lobe and large lymphocytes in the cortico-medullary zone and medulla under the influence of zinc salts. Under the conditions of long-term exposure, a decrease in cell density, apoptosis of lymphocytes, loss of functional capabilities of the organ is observed [27].

Studies have shown that the thymus is involved in the development of hypertension. One interesting study aimed to evaluate the effect of thymus transplantation on blood pressure and target organ changes in hypertensive mice. The thymus of newborn mice was transplanted into the kidney capsule of the transplant group. The results of this study showed that thymus transplantation could improve the thymus function of hypertensive mice, which increased the expression of the thymic transcription factor FoxN1, affected the proportion of T cell subsets, and increased thymosin β4, thereby reducing blood pressure and halting the progression of target organ damage [8]. Many researchers study the influence of the reticuloepithelial stroma of the thymus [6, 13, 32] and the microcirculatory channel of the lobules in the norm and under the conditions of action of various antigens. Obviously, the age-related involution of the thymus, as a result of which the size of the cortex decreases, and, accordingly, the density of lymphocytes, is one of the mechanisms of aging, and that is why various viruses, such as COVID-19, often affect the elderly [25]. Immunocompromised patients living with HIV are at increased risk of co-infection and multiple tumors [30], as there is currently no effective strategy to restore their T-cell immune response [28, 35]. In patients with a positive result for the human immunodeficiency virus 1 (HIV-1), depletion of T-cells is observed [28] when receiving combined antiretroviral therapy. The study of Carvalho Silva W. H. V. et al. [5] demonstrate that reduced thymic function and death of CD4+ RTE T-cells by pyroptosis are the main mechanisms of immunological recovery failure in HIV-infected patients receiving combination antiretroviral therapy. An interesting fact is that thymus hormones (thymosin), which are produced by the cortico-medullary zone, play a significant role in promoting hair regeneration [7]. Thymosin, produced by the thymus, is a multifunctional peptide ubiquitously expressed in vertebrates and invertebrates. Many studies have found that β-thymosin is critical for wound healing, angiogenesis, cardiac repair, hair growth, and anti-fibrosis in vertebrates, and plays an important role in antimicrobial immunity in invertebrates [16]. It is an important regulator of stem cell proliferation and neuron regeneration. Epithelial cells of the thymus control the development of T-cells, imposing positive and negative selection on thymocytes [10, 13, 23, 33], so their study is necessary to assess the normal structure and function of the thymus.

The thymus is sensitive to damage caused by various endogenous and exogenous factors, and its capacity for self-repair decreases with age. Secondary and age-related forms of thymus dysfunction can lead to an increased risk of malignant neoplasms, the development of infectious and autoimmune diseases [12, 20, 22, 34]. That is why some researchers are considering the possibility of introducing soluble factors that promote thymus regeneration [6], but to date no therapy has been approved for clinical use.

Therefore, the density of lymphocytes in different zones of the thymus lobe should reflect a decrease or increase in the immune function of the thymus, but the morphologist cannot confirm this. In our opinion, it is necessary to conduct morphological studies simultaneously with physiological ones in order to simultaneously determine which morphological changes, for example, of the thymus increase or decrease cellular immunity.

Conclusions

1. Significant changes in the density of lymphocytes in the thymus are observed in the third group of animals that consumed zinc salts ($ZnSO_4 \cdot 7H_2O$) with drinking water, especially in the subcapsular zone and the cortico-medullary zone.

2. When using iron salts ($FeSO_4 \cdot 7H_2O$) and copper salts ($CuSO_4 \cdot 5H_2O$) with drinking water, changes in the density of lymphocytes are a manifestation of a compensatory and adaptive reaction.

3. No ultrastructural changes in the structure of lymphocytes and reticuloepithelial stroma cells were detected when heavy metal salts were consumed with water.

References

[1] AbdulKadir, W. A. F. W., Omar, R. C., Roslan, R., & Baharuddin, I. N. Z. (2023). Landfill leachate treatment in Malaysia: Continuous circulation motion using mixed agricultural wastes with an open grid-like Luffa's configuration. *Journal of Water Process Engineering,* 56(2023), 104532. doi: 10.1016/j.jwpe.2023.104532

[2] Adhikary, A., Kumar, R., Pandir, R., Bhardwaj, P., Ramakrishna, W., & Kumar, S. (2019). Pseudomonas citronellolis; a multi-metal resistant and potential plant growth promoter against arsenic (V) stress in chickpea. *Plant Physiology and Biochemistry,* 142, 179-192. doi: 10.1016/j.plaphy.2019.07.006

[3] Akhbarizadeh, R., Dobaradaran, S., Spitz, J., Mohammadi, A., Tekle-Röttering, A., De la Torre, G. E., & Keshtkar, M. (2023). Metal(loid)s in herbal medicines and their infusions: Levels, transfer rate, and potential risks to human health. *Hygiene and Environmental Health Advances,* 5, 100042. doi: 10.1016/j.heha.2022.100042

[4] Cao, K., Zhang, J., Wang, G., Lin, X., Zhan, F., Wu, K. …& Liu, C. (2022). Associations of trace element levels in paired serum, whole blood, and tissue: an example of esophageal squamous cell carcinoma. *Environmental Science and Pollution Research International*, 30(13), 38052-38062. doi: 10.1007/s11356-022-24960-z

[5] Carvalho Silva, W. H. V., Andrade Santos, J. L., Souto, F. O., Coelho, A. V. C., Crovella, S., & Guimarães, R. L. (2019). Immunological recovery failure in cART-treated HIV-positive patients is associated with reduced thymic output and RTE CD4+ T-cell death by pyroptosis. *Journal of Leukocyte Biology,* 107(1), 85-94. doi: 10.1002/jlb.4a0919-235r

[6] Cosway, E. J., White, A. J., Parnell, S. M., Schweighoffer, E., Jolin, H. E., Bacon, A., … & Anderson, G. (2022). Eosinophils are an essential element of a type 2 immune axis that controls thymus regeneration. *Science Immunology,* 7(69), eabn3286. doi: 10.1126/sciimmunol.abn3286

[7] Dai, B., Ri-Na, S., Yuan, J., & Liu, D. (2021). Multiple potential roles of thymosin β4 in the growth and development of hair follicles. *Journal of Cellular and Molecular Medicine*, 25(3), 1350-1358. doi: 10.1111/jcmm.16241

[8] Dai, X., Zhao, J., Li, H., Chen, H., & Liang, C. (2023). Thymus transplantation regulates blood pressure and alleviates hypertension-associated heart and kidney damage via transcription factors FoxN1 pathway. *International Immunopharmacology,* 116, 109798. doi: 10.1016/j.intimp.2023.109798

[9] Dong, X., Ding, A., Hu, H., Xu, F., Liu, L., & Wang, M. (2023). Placental Barrier on Cadmium Transfer from Mother to Fetus in Related to Pregnancy Complications. *International Journal of Women's Health,* 15, 179-190. doi: 10.2147/ijwh.s393067

[10] Dvorak, C. C., Haddad, É., Heimall, J., Dunn, E., Buckley, R. H., Kohn, D. B., … & Puck, J. M. (2023). The diagnosis of severe combined immunodeficiency (SCID): The Primary Immune Deficiency Treatment Consortium (PIDTC) 2022 Definitions. *The Journal of Allergy and Clinical Immunology,* 151(2), 539-546. doi: 10.1016/j.jaci.2022.10.022

[11] Feng, X., Zheng, Y., Zong, M. M., Hao, S. S., Guang, Z., Cao, R., … & Liu, T. Q. (2019). The immunomodulatory functions and molecular mechanism of a new bursal heptapeptide (BP7) in immune responses and immature B cells. *Veterinary Research,* 50(1), 1-12. doi: 10.1186/s13567-019-0682-7

[12] Fujimoto, S., Arinobu, Y., Miyawaki, K., Ayano, M., Mitoma, H., Kimoto, Y., … & Niiro, H. (2023). Anti-dsDNA IgE induces IL-4 production from basophils, potentially involved in B-cell differentiation in systemic lupus erythematosus. *Rheumatology,* 62(10), 3480-3489. doi: 10.1093/rheumatology/kead082

[13] Han, J., & Zúñiga Pflücker, J. C. (2021). A 2020 view of thymus stromal cells in T cell development. *The Journal of Immunology* (1950), 206(2), 249-256. doi: 10.4049/jimmunol.2000889

[14] Huang, C., Guo, Z., Peng, C., Anaman, R., & Zhang, P. (2023). Immobilization of Cd in the soil of mining areas by Fe Mn oxidizing bacteria. *Science of the Total Environment,* 873, 162306. doi: 10.1016/j.scitotenv.2023.162306

[15] Huang, K., Shojania, K., Chapman, K., Amiri, N., Dehghan, N., & Mezei, M. M. (2019). Concurrent inflammatory myopathy and myasthenia gravis with or without thymic pathology: A case series and literature review. *Seminars in Arthritis and Rheumatism,* 48(4), 745-751. doi: 10.1016/j.semarthrit.2018.05.004

[16] Huang, M., Gao, S., Gao, L., Liu, D., Liu, X., Sun, Z., … & Pang, Q. (2021). β-Thymosin is an essential regulator of stem cell proliferation and neuron regeneration in planarian (Dugesia japonica). *Developmental and Comparative Immunology/Developmental & Comparative Immunology,* 121, 104097. doi: 10.1016/j.dci.2021.104097

[17] Hussain, A. A., Kamran, K., Waseem, M., Umar, S., Hina, M., Altaf, M., … & Rafique, A. (2023). Effect of voltage gradient on energy consumption and chromium ions removal from salt-affected clayey soils. *Journal of Applied Electrochemistry,* 54(3), 635-646. doi: 10.1007/s10800-023-01987-9

[18] Lee, W. S., Aziz, H. A., & Tajarudin, H. A. (2023). Removal of Fe and Mn from the groundwater by using zeolite with Rossellomorea sp. *Water Environment Research,* 95(8), e10913. doi: 10.1002/wer.10913

[19] Mahmood, S., Tanvir, E. M., Komarova, T., Islam, M. N., Khatun, M., Hossain, M. F., … & Shaw, P. N. (2023). Relationships between growth indicators, liver and kidney function markers, and blood concentrations of essential and potentially toxic elements in environmentally exposed young children. *International Journal of Hygiene and Environmental Health,* 253, 114237. doi: 10.1016/j.ijheh.2023.114237

[20] Marković, I., & Savvides, S. N. (2020). Modulation of signaling mediated by TSLP and IL-7 in inflammation, autoimmune diseases, and cancer. *Frontiers in immunology,* 11, 541631. doi: 10.3389/fimmu.2020.01557

[21] Miller, J. F. (2020). The function of the thymus and its impact on modern medicine. *Science,* 369(6503), eaba2429. doi: 10.1126/science.aba2429

[22] Nishijima, H., Matsumoto, M., Morimoto, J., Hosomichi, K., Akiyama, N., Akiyama, T., … & Matsumoto, M. (2022). Aire controls heterogeneity of medullary thymic epithelial cells for the expression of Self-Antigens. *The Journal of Immunology,* 208(2), 303-320. doi: 10.4049/jimmunol.2100692

[23] Nitta, T., Ota, A., Iguchi, T., Muro, R., & Takayanagi, H. (2021). The fibroblast: An emerging key player in thymic T cell selection. *Immunological Reviews,* 302(1), 68-85. doi: 10.1111/imr.12985

[24] Park, K., & Kwak, I. (2023). Growth retardation and suppression of ubiquitin-dependent catabolic processes in the brackish water clam Corbicula japonica in response to salinity changes and bioaccumulation of toxic heavy metals. *Environmental Pollution,* 337, 122554. doi: 10.1016/j.envpol.2023.122554

[25] Pietrobon, A. J., Teixeira, F. M. E., & Sato, M. N. (2020). I mmunosenescence and Inflammaging: Risk Factors of Severe

COVID-19 in Older People. *Frontiers in Immunology, 1*1, 579220. doi: 10.3389/fimmu.2020.579220

[26] Poslavskaya, O. V. (2016). Determination of linear dimensions and square surfaces areas of morphological objects on micrographs using ImageJ software. Morfologiâ (Dnipropetrovsk), 10(3), 377-381. doi: 10.26641/1997-9665.2016.3.377-381

[27] Prykhodko, O. O. (2023). Structural changes in the thymus under the pathogenic factors action. *Вісник проблем біології та медицини=Herald of the Problems of Biology and Medicine*, 1(1), 62. doi: 10.29254/2077-4214-2023-1-168-62-72

[28] Qian, F., Hu, S., Zhu, Y., Wang, Y., Liu, J., Qiao, J., … & Zhu, C. (2022). CD56dim NK Cell is an Important Factor in T Cell Depletion of cART-Treated AIDS Patients. *International Journal of General Medicine,* 15, 4575-4583. doi: 10.2147/ijgm.s356771

[29] Rafya, M., Hafidi, A., Zehhar, N., & Benkhalti, F. (2023). Low-cost modified adsorbents derived from the solid residue of Rosmarinus officinalis L. for heavy metal uptake. *Industrial Crops and Products,* 195, 116317. doi: 10.1016/j.indcrop.2023.116317

[30] Savino, W., & Lepletier, A. (2023). Thymus-derived hormonal and cellular control of cancer. *Frontiers in Endocrinology,* 14, 1168186. doi: 10.3389/fendo.2023.1168186

[31] Sawan, S., Errachid, A., Maalouf, R., & Jaffrezic Renault, N. (2022). Aptamers functionalized metal and metal oxide nanoparticles: Recent advances in heavy metal monitoring. TrAC. *Trends in Analytical Chemistry* (Regular Ed.), 157, 116748. doi: 10.1016/j.trac.2022.116748

[32] Shichkin, V. P., & Antica, M. (2020). Thymus regeneration and future challenges. *Stem Cell Reviews and Reports* (Online), 16(2), 239-250. doi: 10.1007/s12015-020-09955-y

[33] Su, X., Li, X., Wang, S., Xue, X., Li, R., Bai, X., … & Shao, C. (2023). Nitric oxide-dependent immunosuppressive function of thymus-derived mesenchymal stromal/stem cells. *Biology Direct,* 18(1), 59. doi: 10.1186/s13062-023-00415-4

[34] Yang, Z., Luo, J., Zhang, M., Zhan, M., Bai, Y., Yang, Y., … & Lu, L. (2023). TMSB4X: A novel prognostic marker for non-small cell lung cancer. *Heliyon,* 9(11), e21505. doi: 10.1016/j.heliyon.2023.e21505

[35] Zhang, T., Zhao, Y., Li, L., Wang, H. Q., Song, J., Wu, Y., … & Fu, R. (2023). Clinical characteristics and prognosis of 21 patients with thymoma-associated pure red cell aplasia. *PubMed,* 44(12), 1031-1034. doi: 10.3760/cma.j.issn.0253-2727.2023.12.011

[36] Zheng, J., Li, D., Zeng, H., Yang, S., Zhang, Z., & Zhang, J. (2023). Effect of Fe(II) on manganese removal in biofilters: Microbial community, formation of manganese oxide and related mechanisms. *Journal of Water Process Engineering,* 56, 104519. doi: 10.1016/j.jwpe.2023.104519

ЩІЛЬНІСТЬ ЛІМФОЦИТІВ У КІРКОВІЙ ТА МОЗКОВІЙ РЕЧОВИНІ ЧАСТОЧОК ТИМУСА БІЛИХ ЩУРІВ В НОРМІ ТА ЗА УМОВ ВПЛИВУ СОЛЕЙ ВАЖКИХ МЕТАЛІВ ВПРОДОВЖ ТРЬОХ МІСЯЦІВ

Добрянська Е. С., Вацик Н. С., Литвак В. В.

Споживання чистої води є найактуальнішим сьогодні, але природна вода доставляється до наших домівок по пластиковим, залізним та оцинкованим трубам. Іони металів, котрі входять до складу матеріалу труб, здатні потрапляти до питної води і впливати на організм людини, зокрема на тимус. Саме тому метою роботи було визначити щільність великих, середніх та малих лімфоцитів у кірковій та мозковій речовині часточок тимуса безпородних білих щурів-самців репродуктивного віку при вживанні з водою незначних доз солей важких металів упродовж трьох місяців. Дослідження проведено на 40 безпородних білих щурах-самцях репродуктивного віку, яких розподілили на 4 групи: 1 група - контрольні тварини, які споживали дистильовану воду; 2 група тварин, які споживали водний розчин - $CuSO_4 \cdot 5H_2O$ в дозі 0,247 мг/дм^3; 3 група - водний розчин $ZnSO_4 \cdot 7H_2O$ в дозі 1,505 мг/дм^3; 4 група - водний розчин $FeSO_4 \cdot 7H_2O$ в дозі 0,5 мг/дм^3. Для дослідження щільності великих, середніх та малих лімфоцитів у різних зонах часточки тимусу використано гістологічні, електронно-мікроскопічні та морфометричні методи дослідження. Встановлено, що в контрольній групі щурів щільність великих лімфоцитів є найвищою у субкапсулярній зоні, а найнижчою у мозковій речовині. Щільність середніх лімфоцитів є найнижчою в субкапсулярній зоні. Щільність малих лімфоцитів найнижча у мозковій речовині, а найвища - у кортико-медулярній зоні. При вживанні упродовж трьох місяців з питною водою солей $CuSO_4 \cdot 5H_2O$ достовірних змін щільності лімфоцитів, порівняно з контрольною групою, не виявлено, окрім незначного зменшення щільності великих лімфоцитів у кірковій речовині часточки тимусу. Суттєво змінюється щільність лімфоцитів у третій групі тварин, які з питною водою споживали солі цинку ($ZnSO_4 \cdot 7H_2O$): щільність великих лімфоцитів у субкапсулярній зоні зменшується в 2,3 рази, у кортико-медулярній зоні збільшується в 4,7 разів, а у мозковій речовині збільшується у 2,7 рази; щільність середніх лімфоцитів зменшується в субкапсулярній зоні у 2 рази; щільність малих лімфоцитів зменшується в субкапсулярній зоні у 1,5 рази, у кірковій речовині та кортико-медулярній зоні - зменшується в 1,2 рази, а в мозковій речовині в 1,1 рази. При вживанні упродовж трьох місяців з питною водою солей $FeSO_4 \cdot 7H_2O$ особливих змін щільності лімфоцитів не відмічено: спостерігалось зменшення щільності великих лімфоцитів у субкапсулярній зоні у 1,5 рази та в 1,3 рази в кірковій речовині; щільність середніх лімфоцитів в 1,2 рази зменшувалась в кірковій речовині, а щільність малих лімфоцитів зменшувалась в 1,2 рази в субкапсулярній зоні та кірковій речовині, а у мозковій речовині в 1,2 рази збільшувалась, порівняно з контрольною групою тварин. Ультраструктурних змін у будові лімфоцитів та ретикулоепітеліальних клітин при вживанні з водою солей важких металів не виявлено. Таким чином, дослідження показало, що найбільш токсичними для організму є солі цинку ($ZnSO_4 \cdot 7H_2O$), споживання яких з питною водою у незначних дозах впродовж трьох місяців призвело до значних змін щільності лімфоцитів, порівняно з контрольною групою піддослідних тварин.

Ключові слова: *тимус, лімфоцити, важкі метали, щільність.*

Author's contribution

Dobryanska E. S. - conceptualization, research, project administration, methodology and original project writing, supervision, validation.
Vatsyk N. S. - review writing and editing, formal analysis.
Litvak V. V. - data visualization, software.

DOI: 10.31393/morphology-journal-2024-30(2)-02 Reports of Morphology, Vol. 30, №2, Pages 13-23

ISSN 1818-1295 eISSN 2616-6194

REPORTS OF MORPHOLOGY

Official Journal of the Scientific Society of Anatomists, Histologists, Embryologists and Topographic Anatomists of Ukraine

journal homepage: https://morphology-journal.com

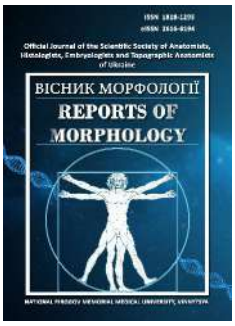

Correlations between amplitude rheovasographic indicators of the crus and anthropometric dimensions in volleyball players women of different somatotypes

Sarafyniuk L. A.[1], Stepanenko I. O.[1], Khapitska O. P.[1], Androshchuk O. V.[1], Borejko T. I.[1], Sarafyniuk P. V.[2], Nesterova S. Yu.[2]

[1]National Pirogov Memorial Medical University, Vinnytsya, Ukraine
[2]Vinnitsia State Mykhailo Kotsyubynskyi Pedagogical University, Vinnytsya, Ukraine

ARTICLE INFO
Received: 31 January 2024
Accepted: 04 March 2024

UDC: 572.087:612.13:796.071

CORRESPONDING AUTHOR
e-mail: Lsarafinyuk@gmail.com
Sarafyniuk L. A.

CONFLICT OF INTEREST
The authors have no conflicts of interest to declare.

FUNDING
Not applicable.

DATA SHARING
Data are available upon reasonable request to corresponding author.

Somatotypological features of the body can be considered as a lever of sports achievements, because they have an effect on the efficiency of the energy supply system, physical capacity, ability to adapt, and the state of the cardiovascular system. The purpose of our work is to reveal the correlations between the amplitude parameters of the crus rheovasogram and anthropometric indices in young volleyball players women of different somatotypes. A comprehensive clinical and laboratory study of the state of health and physical development of 108 volleyball players women aged 16-20 years (youth period of ontogenesis) of high sports ranks (from II adult to masters of sports) was conducted. Rheovasographic parameters of the crus in volleyball players women were determined by the method of tetrapolar rheocardiography on a certified computer diagnostic multifunctional complex. Anthropometric determination of the total dimensions of the body and chest, pelvis, limbs, and head was performed according to the recommendations of Shaparenko P. P. (2000), somatotypological - according to the Heath-Carter calculation method (1990). After somatotyping, it was established that 28 women volleyball players belonged to the mesomorphic type of constitution, 27 women athletes were assigned to the ectomorphic and ecto-mesomorphic somatotypes each, and 26 women volleyball players belonged to the medium intermediate type. The analysis of the obtained results was carried out in the license program "Statistica 5.5" using correlation analysis according to Spearman. We found that highly professional women volleyball players, who have different body types, differ in the strength and number of significant correlations between the amplitude rheovasographic parameters of the crus and anthropometric dimensions. The most numerous (18.64 % of the possible correlations, of which 6.82 % are reliable) and the strongest (3 strong with a correlation coefficient from -0.64 to -0.73) correlations between the amplitude indicators of the crus rheovasogram and parameters of the external body structure were recorded in volleyball players women of the middle intermediate somatotype. Ectomorphs had the lowest number and strength of relationships (3.18 % of possible correlations, only 1 reliable). Individual longitudinal dimensions of the body, chest girths and its diameters, transverse dimensions of the pelvis, and skinfold thickness were most often correlated with the amplitude indicators of the crus rheovasogram in women volleyball players of various constitutional types. Determining the features of the correlations is the basis for assessing the harmony of the physical development of women volleyball players and conducting further statistical modeling to determine their appropriate crus rheovasographic indicators.

Keywords: *correlations, peripheral hemodynamics, crus, anthropometry, somatotype, volleyball players women.*

Introduction

Features of the body structure, which are strongly influenced by genetic factors, are an important basis for sports results [11, 15]. Constitutional characteristics have an impact on the efficiency of the energy supply system, on

the manifestation and development of physical qualities, the maximum consumption of oxygen, and, therefore, on physical performance, the course of recovery processes, the ability to adapt to various exogenous factors. In particular, Summer L. C. and co-authors [25] note that the change in body weight composition during the competitive season in athletes is accompanied by a change in sports results. The constitutional approach makes it possible to study the organism at different levels, starting from the organ and ending with the system [8]. The most recent is the use of the factor of constitutional belonging as a basis for accentuating personality characteristics [3], in particular, the determination of such indicators in persons of different somatotypes as: the indicator according to the scale of insincerity according to Eysenck, extraversion-introversion according to Eysenck, personal anxiety according to Spielberger, character accentuation of different types, etc. [1, 2].

D. Berhtraum with co-authors [4] proved the importance of the state of the cardiovascular system for diagnosing the adaptation capabilities of the body, this hypothesis is also confirmed by other scientists [17, 18], this question acquires special importance in youth, because at this time it increases the importance of the respiratory and cardiovascular systems for the proper physical development of a young organism against the background of significant changes in living conditions [27]. The functional state of an athlete's cardiovascular system is an undeniable factor in sports performance [5, 12, 19, 22]. Many scientific studies have proven the importance of indicators of central [13, 18, 23, 30] and peripheral hemodynamics [26] in increasing the level of fitness of athletes and forming their high potential for adaptation to intensive physical exertion of various directions. In particular, Usova O. V. with co-authors [26] notes that as a result of a decrease in the functional capabilities of the body, a decrease in the speed of blood vessel filling will be observed. According to many scientists, the parameters of regional blood circulation are significantly influenced by the features of the external structure of the body [20, 28]. In particular, a change in the dynamics of venous blood flow in the elderly was established in the context of the peculiarities of the composition of the tissues of the lower extremities [24]. Significant differences were found in the value of regional blood circulation indicators, in particular on the crus, in representatives of different constitutional types of adolescence, the most pronounced differences were between girls of ectomorphic and mesomorphic somatotypes [7, 9]. A correlational analysis was conducted between body composition components and indicators of the cardiovascular system in young women [16]. But, unfortunately, there is a lack of works that would relate to the relationships between indicators of the external structure of the body and regional features of blood circulation in athletes.

The purpose of our work is to reveal the correlations between the amplitude parameters of the crus rheovasogram and anthropometric indices in young volleyball players women of different somatotypes.

Materials and methods

During 2017-2023, in the research center of National Pirogov Memorial Medical University, Vinnytsya, a comprehensive clinical and laboratory study of the state of health and physical development of 108 volleyball players women aged 16-20 years (youth period of ontogenesis) of high sports ranks (from II adult to masters of sports) was held. The average sports experience of volleyball players women was 6.361±2.865 years. Volleyball players women played as part of the teams: "Bilozgar - Medical University", "Dobrodiy - Medical University - ShVSM", student volleyball teams of Vinnytsia institutions of higher education, children's and youth sports schools of Vinnytsia and Kalynyvka. Each female athlete who had a sports experience of at least 3 years and the appropriate rank and age (inclusion criteria) gave informed consent to participate in such a study. All examinations were carried out at least 12 hours after training. Examination of volleyball players women was carried out in the period from day 5 to day 12 of their ovulatory-menstrual cycle. Eligibility for participation in further studies was a preliminary electrocardiographic and echocardiographic examination. Exclusion criteria were hypertension, pathological hypotension, arrhythmias, II-III degree mitral valve prolapse, pathological myocardial hypertrophy.

The research was carried out within the framework of the university-wide topic "Somato-viscerometric features of the human body in different periods of ontogenesis" (state registration number 0121U113772). The work was approved at the meeting of the Bioethics Committee of the National Pirogov Memorial Medical University, Vinnytsya (protocol No. 2) dated January 31, 2024.

The rheovasographic parameters of the crus in volleyball players women were determined by the method of tetrapolar rheocardiography on a certified computer diagnostic multifunctional complex (developers by scientists of National Pirogov Memorial Medical University, Vinnytsya and Vinnytsia National Technical University) and the amplitude, time and indicators of the ratio of amplitude and time rheovasographic parameters were evaluated (integral). An anthropometric study of the total dimensions of the body and chest, pelvis, limbs, and head was conducted according to the recommendations of Shaparenko P. P. [21]. All measurements were carried out with certified equipment with determination of the following dimensions: Martin's anthropometer was used to determine longitudinal dimensions, in particular body height and anthropometric points (cm); with a centimeter tape - girth measurements (cm), with a large thick compass - transverse and sagittal diameters of the body (cm), with a caliper - the width of the distal epiphyses of long tubular bones (cm), with a caliper - skinfold thickness (mm), on medical scales - body weight (kg). Body surface area (m^2)

was calculated using the Dubois formula [21]. The somatotypological study was carried out according to the Heath-Carter calculation method [6], which was based on anthropometric measurements, the value of the components of the somatotype (ectomorphic, mesomorphic, endomorphic) was determined in points (from 1 to 7). After somatotyping, it was established that 28 women volleyball players belonged to the mesomorphic type of constitution, 27 women athletes were assigned to the ectomorphic and ecto-mesomorphic somatotypes, and 26 women volleyball players belonged to the medium intermediate type.

The analysis of the obtained results was carried out in the licensed program "Statistica 5.5" using Spearman's non-parametric correlation analysis.

Results

After conducting a correlation analysis of the amplitude rheovasographic parameters of the crus with anthropometric dimensions in volleyball players women with a mesomorphic somatotype, we found few reliable correlations of average strength, therefore we also analyzed average connections that were unreliable (Table 1). In particular, *baseline impedance* had reliable direct correlations only with the height of the suprasternal point and the width of the distal femoral epiphysis. But unreliable straight correlations of the average strength were found between this indicator and body length, heights of 2 more anthropometric points (shoulder and finger), width of the distal epiphysis of the crus, transverse lower thoracic diameter, skinfold thickness on the side and thigh; and with skinfold thickness on the forearm, the correlation was inversely proportional. *The amplitude of the systolic* wave was reliably correlated in volleyball players women mesomorphs with 7 anthropometric dimensions: the width of the distal epiphyses of the thigh and crus, with the girth dimensions of the forearm in the upper part, the chest during inhalation, exhalation and at rest, skinfold thickness on the side. Unreliable average strength direct correlations were found between this indicator and the height of the suprasternal point, the circumference of the forearm in the lower part, intercristal distance and external conjugate. It should be noted that all connections were only direct. We determined that the *amplitude of the incisura* had only 1 reliable inverse relationship of average strength - with skinfold thickness on the chest; and with skinfold thickness on the front surface of the shoulder and forearm, the correlations were unreliable, medium, and inverse; with intercristal distance, the relationship was direct. *The amplitude of the diastolic* wave on the crus was statistically significantly correlated with the skinfold thickness on the side, still direct but unreliable connections were found with the width of the distal epiphysis of the crus, the circumference of the forearm in the upper part, the chest during inspiration and at rest, the size of the external conjugate. With crus circumference at the bottom, the

Table 1. Correlations of the amplitude indicators of the crus rheovasogram with anthropometric dimensions in mesomorph volleyball players women.

Anthropometric dimensions	Rheovasographic indicators				
	Z	h1	h2	h3	h4
body weight	0.15	0.17	-0.10	0.09	0.13
body length	**0.33**	0.23	-0.09	0.06	0.05
body surface area	0.20	0.18	-0.13	0.07	0.10
the height of the suprasternal point	**0.47**	**0.33**	0.05	0.20	0.21
the height of the pubic point	0.29	0.08	-0.11	-0.05	-0.06
the height of the shoulder point	**0.38**	0.25	0.01	0.10	0.17
fingertip height	**0.35**	0.20	-0.02	-0.03	0.12
the height of the trochanteric point	0.13	-0.01	-0.21	-0.09	-0.20
width of the distal epiphysis of the shoulder	0.07	0.26	-0.10	0.21	-0.10
width of the epiphysis of the distal forearm	0.11	0.18	-0.10	0.13	-0.09
width of the distal femoral epiphysis	**0.39**	**0.39**	0.16	0.29	0.27
width of the distal epiphysis of the crus	**0.35**	**0.46**	0.22	**0.36**	0.21
shoulder girth in a tense state	0.12	0.22	0.04	0.14	0.22
shoulder circumference in a relaxed state	0.26	0.29	0.13	0.22	**0.32**
forearm circumference at the top	0.25	**0.44**	0.15	**0.37**	0.22
the circumference of the forearm in the lower part	0.22	**0.37**	0.03	0.28	0.05
hip circumference	0.08	0.18	-0.02	0.13	0.15
the circumference of the crus at the top	-0.10	-0.08	-0.10	-0.09	-0.27
the circumference of the crus at the bottom	-0.20	-0.23	-0.10	**-0.31**	**-0.31**
neck circumference	0.05	0.28	-0.08	0.21	0.02
waist circumference	-0.01	-0.11	-0.28	-0.11	0.01
hips circumference	-0.05	-0.06	-0.16	-0.11	0.06
circumference of the hand	0.01	0.25	0.02	0.16	0.13
foot circumference	-0.10	-0.01	-0.19	-0.01	-0.20
chest circumference on inhalation	0.29	**0.47**	0.24	**0.36**	**0.41**
chest circumference on exhalation	0.17	**0.40**	0.21	0.29	**0.32**
chest circumference at rest	0.22	**0.44**	0.29	**0.33**	**0.38**
transverse mean thoracic diameter	-0.01	0.10	-0.13	-0.01	0.12
transverse lower thoracic diameter	**0.33**	0.25	0.04	0.18	0.23
sagittal mean thoracic diameter	0.03	0.12	0.20	0.08	0.26
acromial diameter	-0.24	-0.10	-0.26	-0.21	-0.27
interspinous distance	-0.01	0.07	0.12	0.05	-0.03
intercristal distance	0.27	**0.32**	**0.31**	0.20	0.22

Continuation of table 1.

Anthropometric dimensions	Rheovasographic indicators				
	Z	h1	h2	h3	h4
intertrochanteric distance	0.17	0.22	0.03	0.25	0.08
external conjugate	0.23	**0.32**	0.14	**0.33**	0.27
skinfold thickness on the back surface of the shoulder	-0.07	0.05	-0.02	-0.07	-0.06
skinfold thickness on the front surface of the shoulder	-0.22	-0.16	**-0.33**	-0.25	-0.19
skinfold thickness on the forearm	**-0.35**	-0.24	**-0.35**	-0.24	**-0.38**
skinfold thickness under the scapula	-0.10	0.10	-0.19	0.16	0.06
skinfold thickness on the chest	-0.25	-0.17	**-0.39**	-0.11	-0.27
skinfold thickness on the abdomen	0.28	0.25	-0.13	0.22	**0.34**
skinfold thickness on the side	**0.37**	**0.48**	0.19	**0.51**	0.20
skinfold thickness on the thigh	**0.31**	0.24	0.01	0.28	0.06
skinfold thickness on crus	0.22	0.16	-0.14	0.22	0.08

Notes: here and in the following, unreliable correlations of the average force are highlighted in red, reliable correlations of the average force are highlighted in blue, Z - basic impedance, h1 - amplitude of the systolic wave, h2 - amplitude of the notch; h3 - diastolic wave amplitude, h4 - rapid blood filling amplitude.

correlation was inverse. It was established that the *amplitude of rapid blood filling* had a reliable direct correlation only with the circumference of the chest during inspiration; with girth measurements of the shoulder in a relaxed state, chest on exhalation and at rest, skinfold thickness on the abdomen, the correlations were direct of medium strength, but unreliable; with skinfold thickness on the forearm and crus circumference in the lower part - reverse, average, unreliable (see Table 1).

In volleyball players women of ectomorphic somatotype, the amplitude parameters of the rheovasogram on the crus had only a few correlations of the average strength with indicators of the external structure of the body, so the *basic impedance* was correlated only with the girths of the crus in the lower part and the hand; these correlations were inverse, of medium strength, but unreliable (Table 2). *The amplitude of the systolic wave* did not correlate with any anthropometric measure. We determined that the *amplitude of the incisura* had only inverse relationships, reliable with skinfold thickness under the scapula, unreliable - with the width of the distal femoral epiphysis. *The amplitude of the diastolic wave* at the crus had no correlations with mean force. It was established that the *amplitude of rapid blood filling* had only 3 unreliable mean correlations, direct - with transverse lower thoracic diameter, inverse - with skinfold thickness on the chest and sagittal mid-thoracic diameter (see Table 2).

In the group of women volleyball players with an ecto-mesomorphic somatotype (Table 3), reliable direct correlations were found between the *basic impedance* on the crus and the heights of 3 anthropometric points

Table 2. Correlations of the amplitude indicators of the crus rheovasogram with anthropometric dimensions in volleyball players women ectomorphs.

Anthropometric dimensions	Rheovasographic indicators				
	Z	h1	h2	h3	h4
body weight	-0.03	0.02	-0.08	-0.06	-0.06
body length	0.01	-0.07	-0.18	-0.22	-0.19
body surface area	-0.01	-0.02	-0.09	-0.11	-0.13
the height of the suprasternal point	0.19	0.09	-0.07	-0.11	-0.04
the height of the pubic point	0.07	0.19	0.01	0.02	0.06
the height of the shoulder point	0.11	0.04	-0.13	-0.22	-0.12
fingertip height	0.28	0.11	-0.02	-0.09	-0.07
the height of the trochanteric point	-0.04	0.11	-0.14	-0.11	-0.07
width of the distal epiphysis of the shoulder	0.21	0.08	-0.05	-0.01	-0.04
width of the epiphysis of the distal forearm	0.15	0.04	-0.15	-0.12	-0.08
width of the distal femoral epiphysis	0.07	-0.09	**-0.33**	-0.30	-0.15
width of the distal epiphysis of the crus	0.11	-0.01	0.01	-0.05	0.08
shoulder girth in a tense state	0.04	0.15	0.10	0.09	0.14
shoulder circumference in a relaxed state	0.07	0.20	0.09	0.11	0.18
forearm circumference at the top	-0.09	0.19	-0.01	0.01	0.15
the circumference of the forearm in the lower part	-0.08	-0.07	-0.13	-0.14	-0.19
hip circumference	0.05	0.10	-0.13	-0.08	0.01
the circumference of the crus at the top	-0.26	-0.04	-0.05	0.01	-0.02
the circumference of the crus at the bottom	**-0.37**	-0.10	-0.09	-0.02	-0.15
neck circumference	-0.17	-0.02	-0.21	-0.19	-0.01
waist circumference	0.09	0.24	0.12	0.08	0.12
hips circumference	0.06	0.14	0.05	0.08	0.01
circumference of the hand	**-0.31**	-0.23	-0.10	-0.07	-0.22
foot circumference	-0.02	0.01	0.01	-0.05	-0.07
chest circumference on inhalation	-0.17	-0.01	0.01	-0.11	-0.03
chest circumference on exhalation	-0.15	-0.03	0.10	-0.02	-0.07
chest circumference at rest	-0.23	-0.03	0.05	-0.04	-0.03
transverse mean thoracic diameter	0.04	0.15	0.25	0.20	0.22
transverse lower thoracic diameter	0.23	0.25	0.18	0.22	**0.36**
sagittal mean thoracic diameter	-0.28	-0.29	-0.25	-0.29	**-0.33**
acromial diameter	-0.22	-0.08	0.11	0.04	-0.22
interspinous distance	-0.03	-0.07	-0.03	-0.11	-0.17
intercristal distance	-0.01	-0.01	-0.11	-0.14	-0.12

Continuation of table 2.

Anthropometric dimensions	Rheovasographic indicators				
	Z	h1	h2	h3	h4
intertrochanteric distance	-0.01	-0.04	0.02	-0.01	-0.14
external conjugate	0.21	0.27	-0.03	0.04	0.21
skinfold thickness on the back surface of the shoulder	0.10	-0.08	-0.01	-0.06	-0.21
skinfold thickness on the front surface of the shoulder	-0.01	-0.10	0.03	0.06	-0.15
skinfold thickness on the forearm	-0.11	-0.11	-0.21	-0.22	-0.23
skinfold thickness under the scapula	0.20	-0.02	**-0.41**	-0.28	-0.05
skinfold thickness on the chest	-0.30	-0.30	-0.10	-0.10	**-0.35**
skinfold thickness on the abdomen	-0.02	-0.17	-0.12	-0.12	-0.17
skinfold thickness on the side	0.05	-0.14	-0.14	-0.17	-0.12
skinfold thickness on the thigh	-0.13	-0.21	-0.23	-0.24	-0.11
skinfold thickness on crus	0.07	-0.03	-0.26	-0.20	-0.08

(suprasternal, brachial, digital), intercristal distance and intertrochanteric distance; direct, unreliable, medium-strength correlations - with the length and surface area of the body, the circumference of the shoulder in a relaxed state; reverse, unreliable, medium-strength correlations - with skinfold thickness on the forearm. *The amplitude of the systolic wave* does not have a reliable correlations with anthropometric dimensions, but unreliable average force direct correlations with the height of the suprasternal, brachial, and digital anthropometric points have been established. *Incisura amplitude* in volleyball players women ecto-mesomorphs had only one reliable feedback with skinfold thickness on the forearm. *The amplitude of the diastolic wave* on the crus had unreliable correlations of average strength: direct - with the circumference of the crus in the upper part and the sagittal mid-thoracic diameter, inverse - with the skinfold thickness on the forearm and abdomen. *Amplitude of rapid blood filling* had reliable small direct correlations with the length and surface area of the body, the height of the suprasternal, shoulder and digital anthropometric points, the circumference of the crus in the upper part, interspinous distance and intertrochanteric distance, inverse - skinfold thickness on the abdomen, unreliable direct correlations - with body weight and girth thighs, unreliable reverse - with the width of the distal epiphysis of the thigh and skinfold thickness on the side (see Table 3).

We established that in volleyball players women of the average intermediate somatotype, the *basic impedance* had a reliable direct correlation only with the transverse lower thoracic diameter, unreliable direct correlations of average strength - with the transverse average thoracic diameter and interspinous distance and intercristal distance, inversely reliable - with skinfold thickness on the front surface of the shoulder (r=-0.73), on the chest

Table 3. Correlations of the amplitude indicators of the crus rheovasogram with anthropometric dimensions in volleyball players women ecto-mesomorphs.

Anthropometric dimensions	Rheovasographic indicators				
	Z	h1	h2	h3	h4
body weight	0.27	0.23	0.05	0.14	**0.32**
body length	**0.36**	0.30	0.13	0.19	**0.36**
body surface area	**0.32**	0.28	0.11	0.17	**0.37**
the height of the suprasternal point	**0.37**	**0.32**	0.21	0.18	**0.37**
the height of the pubic point	0.11	0.26	-0.04	0.07	0.21
the height of the shoulder point	**0.39**	**0.34**	0.17	0.21	**0.39**
fingertip height	**0.48**	**0.35**	0.20	0.28	**0.44**
the height of the trochanteric point	0.15	0.28	0.02	0.16	0.25
width of the distal epiphysis of the shoulder	-0.17	-0.11	-0.03	0.05	-0.15
width of the epiphysis of the distal forearm	-0.14	0.03	-0.02	0.13	0.11
width of the distal femoral epiphysis	-0.16	-0.26	-0.09	-0.20	**-0.32**
width of the distal epiphysis of the crus	-0.11	-0.01	0.06	-0.04	0.09
shoulder girth in a tense state	0.28	0.18	0.07	0.10	0.21
shoulder circumference in a relaxed state	**0.34**	0.11	0.01	0.02	0.10
forearm circumference at the top	0.11	0.08	0.11	0.09	0.20
the circumference of the forearm in the lower part	-0.12	-0.24	-0.06	-0.11	-0.07
hip circumference	0.27	0.26	0.16	0.23	**0.31**
the circumference of the crus at the top	0.12	0.30	0.14	**0.32**	**0.37**
the circumference of the crus at the bottom	0.03	0.14	0.10	0.18	0.19
neck circumference	0.04	-0.14	-0.09	-0.05	-0.08
waist circumference	0.24	0.02	-0.11	-0.01	0.10
hips circumference	0.17	0.12	-0.04	0.08	0.26
circumference of the hand	0.05	0.04	0.01	0.08	0.11
foot circumference	-0.19	-0.03	-0.18	-0.06	0.03
chest circumference on inhalation	0.30	0.20	0.18	0.19	0.30
chest circumference on exhalation	0.21	0.09	-0.02	-0.01	0.19
chest circumference at rest	0.20	0.12	0.01	0.07	0.19
transverse mean thoracic diameter	0.07	-0.03	-0.12	0.01	0.05
transverse lower thoracic diameter	0.06	-0.11	0.06	0.10	-0.04
sagittal mean thoracic diameter	0.08	0.16	0.23	**0.36**	0.17
acromial diameter	-0.03	-0.04	-0.01	0.03	0.09
interspinous distance	0.30	0.22	0.20	0.20	**0.42**
intercristal distance	**0.38**	0.16	0.13	0.02	0.27

Continuation of table 3.

Anthropometric dimensions	Rheovasographic indicators				
	Z	h1	h2	h3	h4
intertrochanteric distance	**0.42**	0.30	0.11	0.18	**0.43**
external conjugate	0.08	-0.08	-0.05	0.10	0.03
skinfold thickness on the back surface of the shoulder	-0.24	-0.14	-0.02	-0.10	-0.23
skinfold thickness on the front surface of the shoulder	-0.17	-0.07	-0.13	-0.19	-0.19
skinfold thickness on the forearm	**-0.35**	-0.17	**-0.40**	**-0.32**	-0.26
skinfold thickness under the scapula	0.06	-0.20	0.30	-0.01	-0.04
skinfold thickness on the chest	-0.11	-0.07	-0.22	-0.24	-0.21
skinfold thickness on the abdomen	-0.23	-0.27	-0.25	**-0.35**	**-0.44**
skinfold thickness on the side	-0.16	-0.19	-0.21	-0.21	**-0.33**
skinfold thickness on the thigh	0.13	0.07	-0.07	-0.03	-0.09
skinfold thickness on crus	-0.13	-0.18	-0.10	-0.18	-0.26

(r=-0.49) and forearm (r=-0.41), unreliable inverse of medium strength - with acromial diameter (Table 4). *The amplitude of the systolic wave* had reliable direct correlations with the transverse lower thoracic diameter and intercristal distance, unreliable direct correlations of medium strength with interspinous distance and skinfold thickness on the side, reliable inverse correlations with skinfold thickness on the front surface of the shoulder, forearm, chest and crus. *The amplitude of the incisura* was reliably correlated only with the skinfold thickness on the front surface of the shoulder (r=-0.42), with the skinfold thickness on the forearm, a feedback of medium strength was also found, but it was unreliable; direct non-reliable mean correlations were with chest circumference on inhalation and at rest, sagittal mean thoracic diameter, skinfold thickness on the thigh. *The amplitude of the diastolic wave* on the crus in volleyball players women of the average intermediate somatotype had reliable correlations of the average force only inversely proportional: with skinfold thickness on the chest and front surface of the shoulder, with skinfold thickness on the crus (r=-0.40) and forearm (r=-0.41) and forearm circumference in the lower part (r=-0.31) revealed unreliable inverse correlations. Unreliable average strength direct correlations are established between this amplitude parameter of the rheovasogram and the circumference of the chest during inhalation and at rest, the width of the distal epiphysis of the shoulder, and the transverse lower thoracic diameter.

Amplitude of rapid blood filling had inverse reliable correlations with skinfold thickness on the front surface of the shoulder and forearm; reverse unreliable of medium strength - with forearm circumference in the upper part, acromial diameter and skinfold thickness on the chest and crus; straight lines of medium strength - with transverse lower thoracic diameter, interspinous distance and intercristal distance (see Table 4).

Table 4. Correlations of the amplitude indicators of the crus rheovasogram with anthropometric dimensions in volleyball players women of the average intermediate somatotype.

Anthropometric dimensions	Rheovasographic indicators				
	Z	h1	h2	h3	h4
body weight	0.12	0.13	0.01	0.16	-0.01
body length	0.10	0.15	-0.03	0.10	0.04
body surface area	0.09	0.15	0.01	0.14	0.01
the height of the suprasternal point	0.22	0.26	0.09	0.21	0.13
the height of the pubic point	-0.04	-0.01	-0.08	0.02	-0.19
the height of the shoulder point	0.22	0.25	0.13	0.22	0.12
fingertip height	0.13	0.12	0.13	0.13	0.05
the height of the trochanteric point	0.24	0.22	0.21	0.23	0.10
width of the distal epiphysis of the shoulder	**0.32**	0.24	0.21	**0.36**	0.21
width of the epiphysis of the distal forearm	-0.07	-0.05	-0.20	-0.09	-0.09
width of the distal femoral epiphysis	0.18	0.11	0.04	0.16	0.03
width of the distal epiphysis of the crus	0.28	0.22	0.17	0.17	0.20
shoulder girth in a tense state	-0.07	-0.14	-0.15	-0.08	-0.20
shoulder circumference in a relaxed state	-0.03	-0.16	-0.17	-0.09	-0.25
forearm circumference at the top	-0.23	-0.23	-0.08	-0.09	**-0.32**
the circumference of the forearm in the lower part	-0.10	-0.13	-0.28	**-0.31**	-0.20
hip circumference	0.13	0.09	0.15	0.23	0.04
the circumference of the crus at the top	-0.14	-0.21	-0.30	-0.29	-0.26
the circumference of the crus at the bottom	-0.21	-0.06	-0.21	-0.17	-0.14
neck circumference	0.03	0.05	-0.07	0.02	-0.04
waist circumference	-0.01	0.17	0.06	0.16	0.02
hips circumference	-0.03	-0.08	0.04	0.06	-0.08
circumference of the hand	-0.16	-0.09	-0.28	-0.21	-0.18
foot circumference	-0.14	0.01	-0.14	-0.11	-0.18
chest circumference on inhalation	0.11	0.23	**0.33**	**0.40**	0.07
chest circumference on exhalation	0.01	0.08	0.29	0.30	-0.04
chest circumference at rest	0.09	0.15	**0.37**	**0.40**	0.02
transverse mean thoracic diameter	**0.38**	0.27	0.04	0.17	0.20
transverse lower thoracic diameter	**0.43**	**0.49**	0.11	**0.31**	**0.38**
sagittal mean thoracic diameter	-0.16	0.01	**0.33**	0.28	-0.10
acromial diameter	**-0.33**	-0.14	-0.12	-0.02	**-0.35**
interspinous distance	**0.38**	**0.40**	0.09	0.21	**0.37**
intercristal distance	**0.36**	**0.41**	0.08	0.20	**0.34**

Continuation of table 4.

Anthropometric dimensions	Rheovasographic indicators				
	Z	h1	h2	h3	h4
intertrochanteric distance	0.03	0.29	0.01	0.17	0.16
external conjugate	0.22	0.17	0.17	0.25	0.09
skinfold thickness on the back surface of the shoulder	0.14	-0.08	-0.01	0.01	0.01
skinfold thickness on the front surface of the shoulder	**-0.73**	**-0.71**	**-0.42**	**-0.57**	**-0.64**
skinfold thickness on the forearm	**-0.41**	**-0.54**	**-0.37**	**-0.41**	**-0.50**
skinfold thickness under the scapula	0.01	-0.13	-0.20	-0.09	-0.15
skinfold thickness on the chest	**-0.49**	**-0.44**	-0.29	**-0.43**	**-0.41**
skinfold thickness on the abdomen	0.05	0.13	0.10	0.10	0.09
skinfold thickness on the side	0.24	**0.33**	0.01	0.17	0.17
skinfold thickness on the thigh	0.11	0.01	**0.31**	0.15	0.02
skinfold thickness on crus	0.12	**-0.47**	-0.25	**-0.40**	**-0.40**

Notes: reliable strong correlations are highlighted in green.

Discussion

In the body of highly professional athletes, under the influence of systematic practice of volleyball, adaptive or maladaptive changes occur in various organs, in particular, in the organs of the cardiovascular system. Moreover, representatives of different somatotypes within the same sport (with typical training and competitive activity) have significant differences. In particular, it was proven that volleyball players of young age, representatives of certain constitutional types, differ not only in anthropometric parameters, in particular, girth, transverse and sagittal dimensions of the chest [19], but also in morphological and functional indicators of the cardiovascular system [10, 29]. Thus, the integrative-anthropological approach has a clear practical direction when establishing relationships between indicators of the external structure of the organism and parameters of regional hemodynamics [29, 28].

According to the results of our study, it can be concluded that highly professional women volleyball players, who have different body types, differ in the strength and number of significant relationships between the amplitude rheovasographic parameters of the crus and anthropometric dimensions. In particular, in volleyball players women of the mesomorphic somatotype, it was found that the amplitude indicators of the crus rheovasogram with constitutional parameters had not very numerically significant correlations of average strength (a total of 39 connections, which is 17.73 % of 220 possible correlations in this group), of which reliable was only 5.45 %. Representatives of the mesomorphic constitutional type are characterized by the predominant development of skeletal muscles against the background of massive bones, therefore, most often, of all the body sizes that we studied, the significant correlations with the amplitude parameters of the crus rheovasogram were precisely those that determine constitutional belonging to the mesomorphic type (Fig. 1). Basic impedance, the value of which is determined by the resistance of body tissues to alternating current, which arises as a result of tissue resistance to current and reactive capacitive resistance [15], in volleyball players women of the mesomorphic somatotype, was correlated with the longitudinal dimensions of the body, the width of the epiphyses of the lower limb, and the indicators of subcutaneous fat deposition, so as the connections were direct. With an increase in body elongation, massiveness of the crus and thigh bones, skinfold thickness on the side and thigh of volleyball players women mesomorphs, the value of the basic impedance will increase. The amplitude of the systolic wave, which reflects the relative value of pulse blood filling in the studied section of the vascular bed, had the largest number of correlations (10 of average strength, 7 of which were reliable) with anthropometric dimensions. The revealed relationships indicate that with an increase in the width of the distal epiphyses of the lower limb, the girth of the forearm and chest, the skinfold thickness on the side of the systolic wave amplitude will also increase, and, therefore, the volumetric blood flow in the crus will increase. Incisura amplitude, which reflects peripheral resistance in arteries and arterioles of the smallest diameter [28], in the group of mesomorph volleyball players women had the least number of significant relationships (4 average strength, 1 of them reliable) with indicators of external body structure. The amplitude of the diastolic wave on the crus, which reflects the ratio of arterial and venous components of blood flow [20], was correlated with 6 anthropometric measurements, of which only the skinfold thickness on the side was reliably correlated. Rapid blood filling amplitude had only 1 significant direct relationship with inspiratory chest circumference. It should be noted that in volleyball players women mesomorphs with amplitude rheovasographic parameters of crus, the most numerous connections were established with the width of the distal epiphyses of the thigh and crus, the circumference of the forearm and chest, skinfold

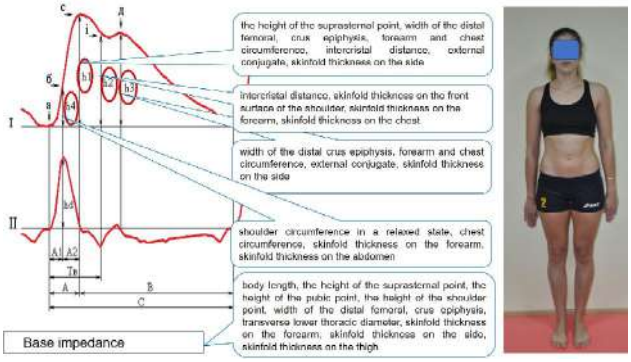

Fig. 1. Peculiarities of correlations of the amplitude indicators of the crus rheovasogram with parameters of the external body structure in volleyball players women of the mesomorphic somatotype.

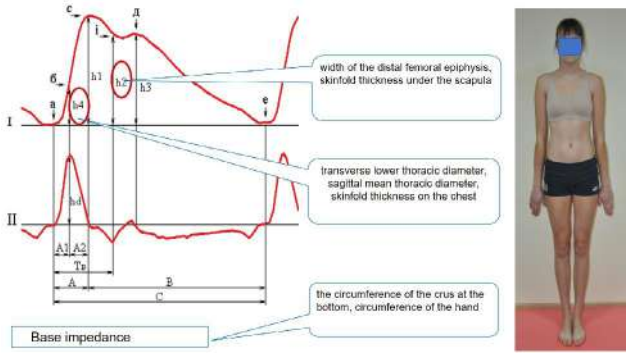

Fig. 2. Peculiarities of correlations of the amplitude indicators of the crus rheovasogram with the parameters of the external body structure in volleyball players women of the ectomorphic somatotype.

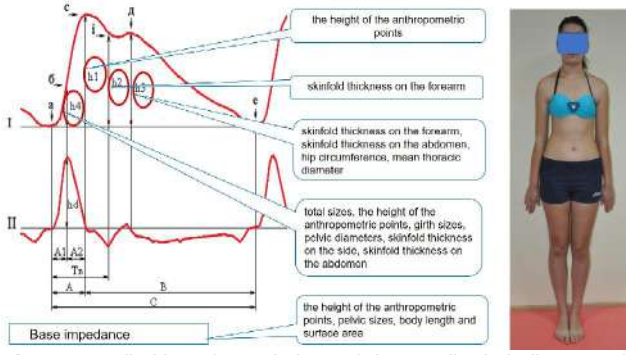

Fig. 3. Peculiarities of correlations of the amplitude indicators of the crus rheovasogram with the parameters of the external body structure in women volleyball players of the ecto-mesomorphic somatotype.

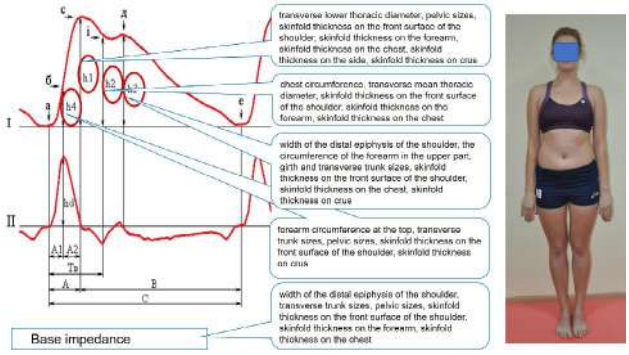

Fig. 4. Peculiarities of correlations of the amplitude indicators of the crus rheovasogram with parameters of the external body structure in volleyball players women of the average intermediate somatotype.

thickness on the side (see Fig. 1).

Only 7 (3.18 % of all possible correlations in this group) correlations of medium strength, of which only 1 is reliable, between amplitude indicators of regional blood circulation on the crus and constitutional characteristics were found in female volleyball players of ectomorphs (Fig. 2). Amplitudes of the incisura and diastolic wave had no significant correlations at all, only the amplitude of the systolic wave had the only inverse correlation with the skinfold thickness under the scapula. In volleyball players women ectomorphs, which are characterized by insignificant fat deposition, an increase in skinfolds under the scapula may indicate a decrease in pulse blood supply to the crus.

In volleyball players women of the ecto-mesomorphic somatotype, it was found that the amplitude indicators of the crus rheovasogram with constitutional parameters had 30 connections of medium strength (13.63 % of the possible correlations in this group), half of them were reliable (15 correlations - 6.82 %). In sportswomen of this somatotype, when the fold on the forearm is reduced and the longitudinal dimensions of the body, shoulder girth, and pelvis width are increased, the value of the basic impedance will increase. The amplitudes of the incisura and the diastolic wave did not have reliable correlations, but the detected unreliable average forces nevertheless indicate that the amplitude of the incisura will increase with the increase in the longitudinal body dimensions of women volleyball players of ecto-mesomorphs. And this may indicate an increase in peripheral resistance in small arteries and a decrease in their elasticity. In women volleyball players of the ecto-mesomorphic somatotype, the amplitude of the systolic wave had the only inverse reliable correlation with the skinfold thickness on the forearm. Amplitude of rapid blood filling had the most numerous relationships with indicators of the external structure of the body - 13 of medium strength, of which 9 were reliable. It should be noted that this rheovasographic indicator is determined by the tone and elasticity of the vascular wall [28]. In female ecto-mesomorph athletes, the amplitude of rapid blood filling will increase with an increase in all total body dimensions, most longitudinal dimensions, hip and crus girths, pelvic width and a simultaneous decrease in fat deposits on the abdomen and sides (Fig. 3).

The most numerous (18.64 % of the possible correlations, of which 6.82 % are reliable) and the strongest (3 strong with a correlation coefficient from -0.64 to -0.73) relationships between the amplitude indicators of the crus rheovasogram and parameters of the external body structure were recorded in volleyball players women of the middle intermediate somatotype Attention is drawn to the fact that in athletes of this somatotype, the amplitude indicators do not correlate with the total, longitudinal dimensions of the body, instead, skinfold thickness and the diameters of the pelvis and chest have multiple connections with the amplitude characteristics of the crus rheovasogram (Fig. 4).

It was established that with an increase in the width of the distal epiphysis of the shoulder and transverse diameters of the chest, and with a decrease in the width of the shoulders and indicators of subcutaneous fat deposition, the value of the basic impedance will increase, which was correlated with 20.45 % of all anthropometric measurements that we determined. The amplitude of the systolic wave was correlated with 18.18 % of the anthropometric parameters, while it was established that an increase in body size and a

decrease in skinfold thickness will be accompanied by a better functional state of the crus vessels [28], and, therefore, a greater pulse blood flow in female volleyball players with an average intermediate somatotype. The amplitude of the incisor correlated with 13.64 % of the anthropometric parameters. It should be noted that only with skinfold thickness on the front surface of the shoulder, the relationship was reliable, inverse. Each of the amplitudes of the diastolic wave and rapid blood filling was correlated with 20.45 % of anthropometric dimensions. The amplitude of the diastolic wave - a reflection of the arterial-venous ratio of blood flow [20] - increases with an increase in the width of the distal epiphysis of the shoulder, the size of the chest, and a decrease in the indicators of subcutaneous fat deposition. The amplitude of rapid blood filling in volleyball players women with an average intermediate somatotype will increase with larger values of transverse inferothoracic size, interspinous distance and intercristal distance, and, simultaneously, with smaller values of forearm girth, shoulder width and skinfold thickness. It is noteworthy that skinfold thickness on the front surface of the shoulder had inverse correlations with all amplitude parameters, and most of them were strong.

M. Mirramezani and co-authors [14] emphasize the need to find new methods for accurate assessment of peripheral hemodynamic indicators, in particular the possibility of accurate assessment of the functional significance of peripheral vascular damage, because there are no modern standardized methods or techniques for its assessment. Characterization of the relationship between the amplitude parameters of peripheral hemodynamics and the anthropometric body dimensions of volleyball players women of different body types will make it possible to predict the morphofunctional changes of the crus vessels based on changes in the body structure.

Conclusions

1. The most numerous and strongest correlations between the amplitude parameters of the regional blood circulation at the crus and indicators of the external structure of the body were established in women volleyball players of medium intermediate and mesomorphic somatotypes. Ectomorphs have the smallest number and strength of correlations.

2. In volleyball players women of the mesomorphic somatotype, the most numerous correlations with indicators of the external structure of the body were found for the amplitude of the systolic wave and the basic impedance; in ectomorphs - incisor amplitude; in ecto-mesomorphs - amplitudes of rapid blood filling and basic impedance; in sportswomen with an average intermediate somatotype - basic impedance, amplitude of rapid blood filling and diastolic wave.

3. In volleyball players women of the mesomorphic somatotype longitudinal dimensions, epiphyses of the thigh and crus, circumferences of the forearm and chest, diameters of the pelvis (only direct correlations), skinfolds (mostly direct); in ecto-mesomorphs - total and longitudinal dimensions of the body, circumferences of limb segments, dimensions of the pelvis (only direct correlations), skinfolds (only reverse); in the middle intermediate somatotype - the width of the distal epiphysis of the shoulder, the dimensions of the chest and pelvis (only direct correlations), skinfolds (mostly reverse) were most often correlated with rheovasographic indicators. Single correlations from different groups of anthropometric sizes were found in ectomorphs.

References

[1] Andriievskyi, I. I. (2021). Correlations of anthropo-somatotypological indicators with indicators of personality traits of practically healthy women with endo-mesomorphic somatotype. *Вісник Вінницького національного медичного університету=Reports of Vinnytsia National Medical University,* 25(2), 220-228. doi: 10.31393/reports-vnmedical-2021-25(2)-07

[2] Andriievskyi, I. I., Serebrennikova, O. A., Kyrychenko, I. M., Zhuchenko, I. I., & Gunas, V. I. (2020). Correlations of body structure and size indicators with personality indicators of practically healthy women with mesomorphic somatotype. *Biomedical and Biosocial Anthropology,* 39, 35-44. doi: 10.31393/bba39-2020-06

[3] Andriievskyi, I. I., Serebrennikova, O. A., Shayuk, A. V., Kovalchuk, V. V., & Likhitskyi, O. O. (2021). Correlations of body structure and size indicators with personality indicators of practically healthy women with ectomorphic somatotype. *World of Medicine and Biology,* 3(77), 16-21. doi: 10.26724/2079-8334-2021-3-77-16-21

[4] Berhtraum, D., Vovkanych, L., Strokun, M., & Kohut, Yu. (2023). Показники центральної гемодинаміки нетренованих студентів та студентів-бігунів на середні дистанції [Indices of central hemodynamics of the untrained students and students trained in middle-distance run]. *Науковий дискурс у фізичному вихованні і спорті=Scientific Discourse in Physical Education and Sport,* 2, 77-87.

[5] Braber, T. L., Mosterd, A., Prakken, N. H., Rienks, R., Nathoe, H. M., Mali, W. P., … & Velthuis, B. K. (2016). Occult coronary artery disease in middle-aged sportsmen with a low cardiovascular risk score: the measuring athlete's risk of cardiovascular events (MARC) study. *European Journal of Preventive Cardiology,* 23, 1677-1684. doi: 10.1177/2047487316651825

[6] Carter, J. L., & Heath, B. H. (1990). *Somatotyping - development and applications.* Cambridge University Press.

[7] Gunas, I. V., Serebrennikova, O. A., Hmel, L. L., Smolko, N. M., & Smolko, D. G. (2019). Indicators of thigh rheogram in practically healthy young men and young women of different somatotypes. *World of Medicine and Biology,* 3(69), 55-59. doi: 10.26724/2079-8334-2019-3-69-55-59

[8] Gunas, I., Prokopenko, S., & Melnik, M. (2016). Sonographic parameters of the pancreas and gall bladder in healthy men from Podillya region of Ukraine of different somatotypes. *Current Issues in Pharmacy and Medical Sciences*, 29(2), 94-96. doi: 10.1515/cipms-2016-0019

[9] Hmel, L. L., Gnenna, V. O., Serebrennikova, O. A., & Smolko, N. M. (2018). Features of indicators of crus rheogram in practically healthy teenagers of different somatotypes. *Biomedical and Biosocial Anthropology,* 33, 41-46. doi: 10.31393/bba33-2018-7

[10] Kyrychenko, Y. V. (2014). Показники електричної активності серця у юнаків і дівчат спортсменів і неспортсменів з різними типами будови тіла [Indicators of electrical activity of the heart in boys and girls athletes and non-athletes with different body types]. *Вісник Вінницького національного медичного університету=Reports of Vinnytsia National Medical University,* 18(1), 10-14.

[11] Liu, J., Lewis, G., & Evans, L. (2013). Understanding Aggressive Behavior Across the Life Span. *Journal of Psychiatric and Mental Health Nursing*, 20(2), 156-168. doi: 10.1111/j.1365-2850.2012.01902.x

[12] Liu, J., Sui, X., Lavie, C. J., Zhou, H., Park, Y. M., Cai, B., … & Blair, S. N. (2014). Effects of cardiorespiratory fitness on blood pressure trajectory with aging in a cohort of healthy men. *Journal of the American College of Cardiology,* 64, 1245-1253. doi: 10.1016/j.jacc.2014.06.1184

[13] McClean, G., Riding, N. R., Ardern, C. L., Farooq, A., Pieles, G. E., & Watt, V. (2017). Electrical and structural adaptations of the paediatric athlete's heart: a systematic review with meta-analysis. *British Journal of Sports Medicine,* 52, 230. doi: 10.1136/bjsports-2016-097052

[14] Mirramezani, M., Cimadomo, P., Ahsan, E., Shavelle, D., Clavijo, L. C., & Shadden, S. C. (2021). Mathematical modeling of blood flow to evaluate the hemodynamic significance of peripheral vascular lesions. *Journal of Angiology & Vascular Surgery,* 6, 076. doi: 10.24966/AVS-7397/100076

[15] Myer, G. D., Jayanthi, N., Difiori, J. P., Faigenbaum, A. D., Kiefer, A. W., Logerstedt, D., & Micheli, L. J. (2015). Does Early Sports Specialization Increase Negative Outcomes and Reduce the Opportunity for Success in Young Athletes? *Sports Health,* 7(5), 437-442. doi: 10.1177/1941738115598747

[16] Nalyvayko, N. V., Bardin, O. I., Pavlova, Iu. O., & Levkiv, L. V. (2020). Аналіз зв'язків між показниками компонентного складу тіла і серцево-судинної системи молодих жінок з різними типами гемодинаміки [Analysis of relationships between indicators of body component composition and cardiovascular system of young females with different types of hemodynamics]. *Український журнал медицини, біології та спорту=Ukrainian Journal of Medicine, Biology and Sport,* 5(5), 394-399. doi: 10.26693/jmbs05.05.394

[17] Pereira, L. A., Cal Abad, C. C., Leiva, D. F., & Oliveira G. (2019). Relationship Between Resting Heart Rate Variability and Intermittent Endurance Performance in Novice Soccer Players. *Research Quarterly for Exercise and Sport,* 90, 355-361. doi: 10.1080/02701367.2019.1601666

[18] Rave, G., Fortrat, J., Dawson, B., & Carre, F. (2018). Heart rate recovery and heart rate variability: use and relevance in European professional soccer. *International Journal of Performance Analysis in Sport,* 18, 168-183. doi: 10.1080/24748668.2018.1460053

[19] Sabato, T. M., Walch, T. J., & Caine, D. J. (2016). The elite young athlete: strategies to ensure physical and emotional health. *Open Access Journal of Sports Medicine,* 7, 99-113. doi: 10.2147/OAJSM.S96821

[20] Serheta, I. V., Vysochanskiy, O. V., & Cherepaha, O. L. (2015). Features of correlation indicators rheovasography of thigh and shin with anthropometric body parameters a in healthy girls with different somatotypes. *Світ медицини та біології=World of Medicine and Biology*, 3(51), 86-89.

[21] Shaparenko, P. P. (2000). *Антропометрія [Anthropometry].* Vinnytsya: Printing house of the Vinnytsia State Medical University named after M. I. Pirogov.

[22] Sharma, S., Merghani, A., & Mont, L. (2015). Exercise and the heart: the good, the bad, and the ugly. *European Heart Journal,* 36, 1445-1453. doi: 10.1093/eurheartj/ehv090

[23] Shevchuk, T., Romaniuk, A., Aponchuk, L., Usova, O., & Shevchuk, A. (2021). Стан центральної гемодинаміки підлітків залежно від спортивної спеціалізації [The state of the adolescents` central hemodynamics depending on sports specialization]. *Фізичне виховання, спорт і культура здоров'я у сучасному суспільстві=Physical Education, Sport and Health Culture in Modern Society,* 2(54), 126-132. doi: 10.29038/2220-7481-2021-02-126-132

[24] Skomudek, A., Gilowska, I., Jasiński, R., & Rożek-Piechura, K. (2017). Analysis of the dynamics of venous blood flow in the context of lower limb temperature distribution and tissue composition in the elderly. *Clinical interventions in aging,* 12, 1371-1378. doi: 10.2147/CIA.S137707

[25] Summer, L. C., Cheng, R., Moran, J. T., Lee, M., Belanger, A. J., Taylor, W. L., & Gardner, E. C. (2024). Changes in Body Composition and Athletic Performance in National Collegiate Athletic Association Division I Female Field Hockey Athletes Throughout a Competitive Season. *Journal of Strength and Conditioning Research,* 1, 38(1), 146-152. doi: 10.1519/JSC.0000000000004591

[26] Usova, O. V., Sologub, O. V., Ulianytska, N. Ya., Yakobson, O. O., Ushko, Ia. A., Sitovskyi, A. M. & Shevchuk, T. Ya. (2022). Біомеханіка кровообігу підлітків різних медичних груп фізичного виховання [Biomechanics of blood circulation of teenagers in different medical groups of physical education]. *Медична наука України=Medical Science of Ukraine,* 18(3), 73-82. doi: 10.32345/2664-4738.3.2022.11

[27] Voloshyn, O. S., Humeniuk, H. B., Voloshyn, V. D., & Smorshchok, Yu. S. (2023). Оцінка адаптаційних можливостей осіб юнацького віку з різним рівнем ефективності функціонування серця [Evaluation of adaptive capabilities of adolescents with different levels of efficiency of the heart functioning]. *Здобутки клінічної і експериментальної медицини=Achievements of Clinical and Experimental Medicine,* 4, 83-88. doi: 10.11603/1811-2471.2022.v.i4.13502

[28] Vysochanskiy, O. V. (2015). Відмінності кореляцій показників реовазограми стегна та гомілки з антропо-соматометричними параметрами у здорових хлопчиків Поділля різних соматотипів [Differences of correlation indices of rheovasography of hip and shin with anthropo-somatometric parameters in healthy podillya boys with different somatotypes]. *Світ медицини та біології=World of Medicine and Biology,* 3(51), 15-19.

[29] Yakusheva, Yu. I. (2015). Показники центральної гемодинаміки у волейболісток з різними типами статури тіла [Indicators of central hemodynamics in volleyball players with different body types]. *Вісник проблем біології і медицини=Bulletin of Problems Biology and Medicine,* 3, 2(123), 344-347.

[30] Zhang, Y., Qi, L., van de Vosse, F., Du, C., Yao, Y., Du, J., … & Xu, L. (2020). Recovery responses of central hemodynamics in basketball athletes and controls after the bruce test. *Frontiers in Physiology,* 11, 593277. doi: 10.3389/fphys.2020.593277

ОСОБЛИВОСТІ ВЗАЄМОЗВ'ЯЗКІВ АМПЛІТУДНИХ РЕОВАЗОГРАФІЧНИХ ПОКАЗНИКІВ ГОМІЛКИ З АНТРОПОМЕТРИЧНИМИ РОЗМІРАМИ У ВОЛЕЙБОЛІСТОК РІЗНИХ СОМАТОТИПІВ

Сарафинюк Л. А., Степаненко І. О., Хапіцька О. П., Андрощук О. В., Борейко Т. І., Сарафинюк П. В., Нестерова С. О.

Соматотипологічні особливості організму можна розглядати як важіль спортивних досягнень, тому що вони мають вплив

на ефективність системи енергозабезпечення, фізичну працездатність, здатність до адаптації, стан серцево-судинної системи. Мета нашої роботи - виявити взаємозв'язки між амплітудними параметрами реовазограми гомілки та антропометричними показниками у волейболісток юнацького віку різних соматотипів. Проведено комплексне клініко-лабораторне дослідження стану здоров'я та фізичного розвитку 108 волейболісток віком 16-20 років (юнацький період онтогенезу) високих спортивних розрядів (від II дорослого до майстрів спорту). Реовазографічні параметри гомілки у волейболісток визначали методом тетраполярної реокардіографії на сертифікованому комп'ютерному діагностичному багатофункціональному комплексі. Виконано антропометричне визначення тотальних розмірів тіла та грудної клітки, таза, кінцівок, голови за рекомендаціями Шапаренка П. П. (2000), соматотипологічне - за розрахунковим методом Heath-Carter (1990). Після соматотипування встановили, що до мезоморфного типу конституції належали 28 волейболісток, до ектоморфного та екто-мезоморфного соматотипів були віднесені по 27 спортсменок, до середнього проміжного типу - 26 волейболісток. Аналіз отриманих результатів проведений у ліцензійній програмі "Statistica 5.5" з використанням кореляційного аналізу за Спірменом. Нами встановлено, що високопрофесійні волейболістки, які мають різний тип статури тіла, різняться за силою та кількістю значущих зв'язків між амплітудними реовазографічними параметрами гомілки й антропометричними розмірами. Найчисельніші (18,64 % із можливих кореляцій, із них 6,82 % достовірних) і найбільшої сили (3 сильних з коефіцієнтом кореляції від -0,64 до -0,73) взаємозв'язки між амплітудними показниками реовазограми гомілки та параметрами зовнішньої будови тіла зафіксовані у волейболісток середнього проміжного соматотипу. У ектоморфів була найменша кількість та сила взаємозв'язків (3,18 % із можливих кореляцій, лише 1 достовірна). З амплітудними показниками реовазограми гомілки у волейболісток різних конституціональних типів найчастіше корелювали окремі поздовжні розміри тіла, обхвати грудної клітки та її діаметри, поперечні розміри таза, товщина шкірно-жирових складок. Визначення особливостей кореляцій є підґрунтям для оцінки гармонійності фізичного розвитку волейболісток та проведення у подальшому статистичного моделювання для визначення у них належних реовазографічних показників гомілки.

Ключові слова: *кореляції, периферична гемодинаміка, гомілка, антропометрія, соматотип, волейболістки.*

Author's contribution

Sarafyniuk L. A. - conceptualization, research, project administration.
Stepanenko I. O. - methodology and writing of the original draft, data visualization.
Khapitska O. P. - resources, methodology and writing of the original draft.
Androshchuk O. V. - review writing and editing, software.
Borejko T. I. - formal analysis and validation, supervision.
Sarafyniuk P. V. - research, data visualization.
Nesterova S. Yu. - review writing and editing.

DOI: 10.31393/morphology-journal-2024-30(2)-03 **Reports of Morphology, Vol. 30, №2, Pages 24-30**

ISSN 1818-1295 eISSN 2616-6194

REPORTS OF MORPHOLOGY

Official Journal of the Scientific Society of Anatomists, Histologists, Embryologists and Topographic Anatomists of Ukraine

journal homepage: https://morphology-journal.com

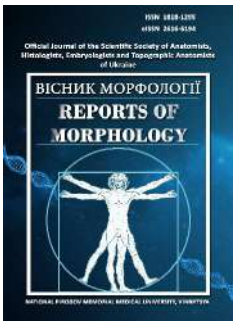

Forensic characteristics of injuries from thermo-baric explosive device

Mykhaylenko O. V.[1], Mishalov V. D.[2], Kozlov S. V.[3], Varfolomeiev Y. A.[4]

[1]Kyiv City Clinical Bureau of Forensic Medicine, Kyiv, Ukraine
[2]Shupyk National Healthcare University of Ukraine, Kyiv, Ukraine
[3]Dnipro State Medical University, Dnipro, Ukraine
[4]Bogomolets National Medical University, Kyiv, Ukraine

ARTICLE INFO
Received: 16 January 2024
Accepted: 12 March 2024

UDC: 614.83.001(048)

CORRESPONDING AUTHOR
e-mail: mihaylenko36@ukr.net
Mykhaylenko O. V.

CONFLICT OF INTEREST
The authors have no conflicts of interest to declare.

FUNDING
Not applicable.

DATA SHARING
Data are available upon reasonable request to corresponding author.

Since the beginning of the Russian Federation's invasion of Ukraine in 2022, explosive trauma has become an extremely urgent problem, as the main source of bodily injury among both the military in the combat zone and the civilian population in cities has been the impact of explosive devices. The aim of the study is the examination of the forensic characteristics of damage to biological objects that were formed from thermal exposure and shock wave as a result of the explosion of a cumulative munition and in the conditions of an experimental explosion model. The objects of the study were the materials of two examinations on the death of Ukrainian soldiers who died in the war zone (archival "Conclusions of the medical examination" of the Kyiv City Clinical Bureau of Forensic Medical Examination in 2023). Under the conditions of the experiment, studies of pathomorphological changes in the liver and small intestine of 30 white outbred rats from the action of an artificially created air shock wave with an overpressure of 31.62±4.84 kPa were carried out. The injuries were examined macroscopically and using standard laboratory histological techniques. Microscopy of histological sections was performed using an Axio Imager 2 microscope (Zeiss, Germany) at magnifications of x200 and x400. Statistical processing of the obtained quantitative results was carried out using the STATISTICA 6.1 software product. Under the condition of the explosion of the ammunition with the cumulative effect of the rocket-propelled infantry flamethrower "Bumblebee" on sectional incisions of the skin and muscles of the thigh in the projection of areas of redness, a picture of a gelatinous consistency of bright red color was macroscopically determined due to abundant blood impregnation of muscles and subcutaneous fat and partial loss of muscle structure with the release of myoglobin. The bright red color of the skin of the thigh and pelvis without burning the hair may indicate the superficial thermal effect of the explosive device and the protection of the skin by clothing. Diffusely located numerous both paired and single abrasions and shallow wounds, small rounded, oblong, circular in shape, which are the result of fragments of a rocket-propelled grenade equipped with a fire mixture, were also determined. The effect of an air shock wave with an overpressure of 31.62±4.84 kPa on the liver parenchyma of rats was determined by focal hemorrhages with rupture of the terminal central vein of the hepatic lobule, edema of the parasinusoidal spaces, and sludges in the sinusoids. In the wall of the small intestine, acute hemodynamic disorders occurred in the form of vasodilation of arterial vessels, venular and capillary stasis. There was layering and swelling of the small intestine wall, rupture of veins, focal hemorrhage. Thus, the revealed characteristic pathomorphological signs of the destructive effect of overpressure as a result of a blast wave (barotrauma) are typical and common both in the areas of the human thigh and pelvis, and in biological objects of experimental animals. The obtained results are consistent with the pathomorphological manifestations of barotrauma in areas of the human body as a result of the action of an explosive device with a cumulative effect.

Keywords: *forensic medical examination, biological objects, thermo-baric trauma.*

Introduction

Since the beginning of the large-scale invasion of the troops of the Russian federation on the territory of Ukraine in February 2022, the problem of blast-induced trauma has become extremely topical in connection with the use by the enemy of a significant arsenal of explosive devices such as grenades, artillery shells, aerial bombs, rockets, etc. According to the head of the Main Directorate of Mine Action, Civil Protection and Environmental Safety of the Ministry of Defense of Ukraine, since the beginning of the invasion of the russian federation in Ukraine, 950 people have been injured by explosive objects, of which 289 have been killed and 661 have been injured [2].

An explosion is a rapid release of energy due to the action of physical, chemical, nuclear processes with the expansion of the initial explosive substance or products and the formation of extremely high pressure [17]. The damaging and traumatic factors of an explosion are its products (a wave of explosive gases, particles of an explosive substance, soot from an explosion), a shock and sound wave, fragments and particles of explosives, special striking objects (mechanical, chemical, thermal), secondary projectiles [7]. In the literature, considerable attention is paid to morphological changes in biological objects under the influence of fragments and parts of explosive devices that have significant kinetic energy and penetrating ability [23, 24, 30]. It should be noted that the powerful damaging effect of explosive devices is also realized due to the thermo-baric effect, and the shock wave, which acts on the human body as a blunt solid object, accounts for 70 % of the energy of the explosion [25]. As a result, extensive damage to the outer coverings of the body and internal organs, detachment of limbs, parts of the body, and with lower power, barotrauma of the ear, contusion of the lungs, and other internal organs occurs [9, 27]. In a number of clinical and pathomorphological studies based on macro- and microscopic, immunohistochemical, morphometric and microelemental changes, it was found that the brain, lungs, intestines, bladder, and kidneys are the most sensitive to the action of the blast wave in the human body [14, 31].

The severity of damage to these organs is influenced by the distance from the epicenter of the explosion to the biological object, the power of the explosion, the presence of obstacles, the peculiarities of the body position, the presence of protective equipment [7, 11].

Thus, at the time of our research, a whole series of literature information is already known, in which the clinical, pathomorphological and pathogenetic traumatic and post-traumatic processes, as well as changes in internal organs after exposure to a shock wave, are sufficiently fully covered. However, some issues related to the morphological features and the mechanism of action of the blast wave on biological objects with thermo-baric effect remain insufficiently elucidated and require further research.

The aim of the study is the examination of the forensic characteristics of damage to biological objects that were formed from thermal exposure and shock wave because of the explosion of a cumulative munition and in the conditions of an experimental explosion model.

Materials and methods

The material of the study was "Conclusions of a medical expert examination" from the archive of the Kyiv City Clinical Bureau of Forensic Medical Examination, which related to 2 cases of death of servicemen in the combat zone from explosive devices, in particular, from the reactive infantry flamethrower "Bumblebee", which is a thermobaric reactive grenade. equipped with a fire mixture (Fig. 1). Studies in forensic medicine were performed in accordance with current Ukrainian legislation, in particular Order No. 6 of the Ministry of Health from 1995 [22].

In addition, in order to increase the objectivity of study, an experiment was conducted, namely, studies of pathomorphological changes in the liver and small intestine of purebred white rats weighing 177.5±15.8 g as a result of the action of an artificially created air shock wave with an excess pressure of 31.62±4.84 kPa. The generation of the shock wave was carried out on a self-made device. The animals were kept in the vivarium of the Dnipro State Medical University. During the study we followed the requirements of the "General Ethical Principles of Animal Experiments" adopted by the Fifth National Congress on Bioethics (Kyiv, 2013), the recommendations of the European Convention for the Protection of Vertebrate Animals (Strasbourg, 2005), and the Law of Ukraine "On the Protection of Animals from harsh treatment". The work was approved at a meeting of the Commission on Bioethics of Dnipro State Medical University (Protocol № 12 dated October 23, 2024). All animals (n=30) were randomly divided into three groups: 1 group consisted of intact rats (n=6), 2 - control (halothane anesthesia with fixation) (n=12), 3 (n=12) - experimental animals (halothane anesthesia with fixation, traumatic single action of an air shock wave with excess pressure 31.62±4.84 kPa). The objects for the study were fragments of the liver and intestine of 30 male rats, which were removed on the first day of the post-traumatic period after euthanasia of the animals (decapitation under halothane anesthesia). The pieces were fixed in a 10 % solution of neutral formalin (pH 7.4) with exposure for 24 hours. The samples were then dehydrated in increasing concentrations of ethanol, cleared

Fig. 1. Jet infantry flamethrower "Bumblebee" of Soviet production (Wikipedia).

Table 1. Point assessment of signs of traumatic injuries.

Morphological sign		Characteristics of the sign	Point assessment
1	Post-traumatic hemorrhages	absent in all fields of vision	0
		diapedesis hemorrhages	1
		small focal hemorrhages	2
		large focal hemorrhages	3
2	Intratissue traumatic ruptures of layers, membranes, vessels	absent in all fields of vision	0
		tears in the walls of capillaries, venules	1
		ruptures of arterioles, interstitial tears	2
		multiple tears of all tissue components	3
3	Expression of post-traumatic edema	absent in all fields of view	0
		moderate perivascular edema	1
		foci of perivascular and pericellular edema	2
		widespread perivascular and pericellular edema	3
4	Alterative post-traumatic cell changes	there are no signs of irreversible cell changes	0
		necrosis, apoptosis	2

in xylene, and embedded in paraffin. After that, the paraffin-soaked fragment of soft tissues was embedded in paraffin blocks, from which serial sections with a thickness of no more than 4 μm were obtained using a Thermo HM 355S microtome (Thermo Scientific, Germany). Sections of each tissue sample were used for general histological tissue staining with hematoxylin and eosin. Before staining, sections were deparaffinized in xylene, rehydrated in descending (100, 95, 70 %) concentrations of ethanol and placed in Bouin's fluid (10 % formalin in saturated picric acid solution) for additional fixation to enhance nuclear staining for 1 hour. Then samples were dehydrated in increasing concentrations of alcohol, clarified in xylene and placed in the final medium under coverslips glasses. Microscopy of histological sections was carried out using an Axio Imager 2 microscope (Zeiss, Germany) at magnifications of x100, x200 and x400. In each group, based on the results of histological examination of the liver and small intestine, the integral index of traumatic injury was calculated in accordance with Table 1.

Mathematical and statistical processing of the obtained quantitative results was carried out using the software product STATISTICA 6.1 (StatSoftInc., serial number AGAR909E415822FA), Excel program (Microsoft Office, USA). The significance of differences between groups was assessed using the Mann-Whitney U-test for a confidence level of at least 95 %, ($p<0.05$).

Results

Macroscopically, redness of the skin of a local nature was detected - areas of the outer and inner surfaces of the right and left thigh, as well as the pelvic area (Fig. 2). They were bright red in color with no hair burning, which may indicate superficial thermal effects and skin protection by clothing. In addition, diffusely located numerous both paired and single abrasions and shallow wounds, small in size of rounded, oblong, circular shape (see Fig. 2), which were the result of the action of fragments of a rocket-propelled grenade, were determined. On the sections of the skin and muscles of the thigh in the projection of areas of redness, macroscopically, there was blood impregnation of muscles and subcutaneous fat, as well as a partial loss of muscle structure, presumably with the release of myoglobin, which gave them a state of gelatinous consistency of bright red color (Fig. 3).

Microscopic qualitative analysis of histological sections of the liver and intestine of rats exposed to an air shock wave revealed a number of structural changes at both the cellular and tissue levels. In most of the studied objects of the liver, typical changes were damage of the vascular system. Thus, in the liver of experimental rats, at the border of media of different densities, small focal hemorrhages occurred as a result of rupture of microvessels, ruptures of the terminal central vein of the hepatic lobule. The endotheliocytes of the sinusoidal capillaries thinned and acquired a spindle-like shape, the parasinusoidal spaces expanded, the sinusoidal capillaries in this part of the liver

Fig. 2. Local redness of the skin of the outer and inner surfaces of thigh after the action of a thermobaric reactive grenade equipped with a fire mixture.

Fig. 3. Macropreparation. Blood seepage of the muscles and subcutaneous fatty tissue of the right and left thigh areas after the action of a thermobaric reactive grenade equipped with a fire mixture.

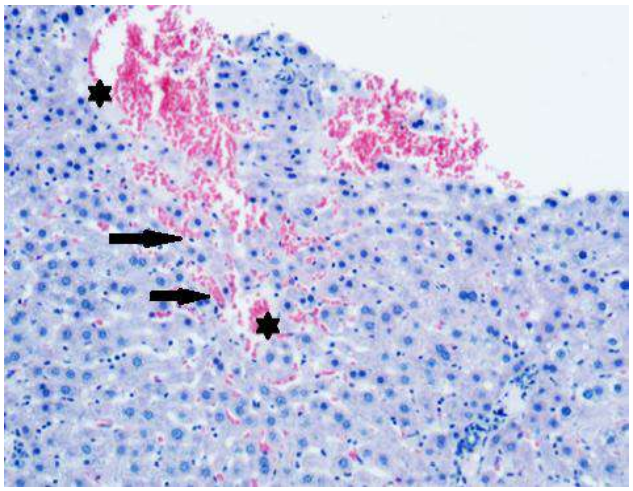

Fig. 4. Focal hemorrhages with rupture of the terminal central vein of the hepatic lobe (asterisks), swelling of the parasinusoidal spaces and sludge in the sinusoids (arrows) of the rat liver after exposure to an air shock wave. Hematoxylin and eosin staining. x100.

were empty (Fig. 4). The nuclei of the endothelial cells of the sinusoidal capillaries in some places protruded into the lumen of the sinusoids, which were full of blood with the phenomena of sludge syndrome. The lumen of the interlobular veins was increased compared to the control and intact groups. Inflammatory infiltrates with polymorphonuclear leukocytes formed around the interlobular vessels. Individual hepatocytes were destroyed, the swelling of stromal components grew rapidly, the sizes of parasinusoidal and periportal spaces increased.

The intercellular spaces increased not only in the area of the lateral but also the apical surfaces of hepatocytes. There were areas with a violation of the beam structure of the liver lobules with focal small foci of parenchymal destruction.

Acute hemodynamic disturbances in the form of vasodilatation of arterial vessels, venular and capillary

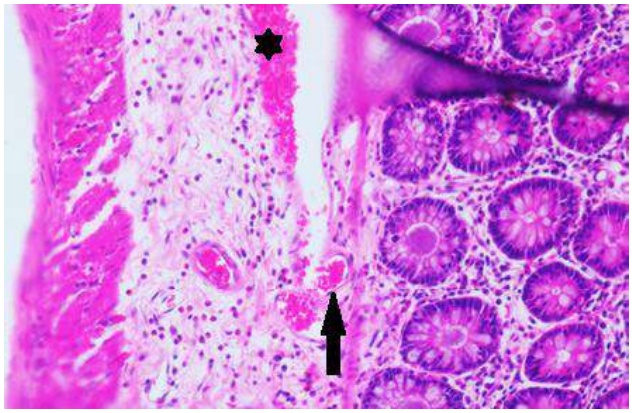

Fig. 5. Layering and swelling of the wall of the small intestine of a rat. Rupture of venules (asterisk). Focal hemorrhage (arrow). Hematoxylin and eosin staining. x100.

Table 2. The results of calculating the integral indicator of traumatic damage to the liver and small intestine (M±σ).

Characteristics of groups	Integral indicator of damage, conventional units
Control, liver	1.672±0.490
Experiment, liver	4.830±1.113*
Control, small intestine	1.834±0.391
Experiment, small intestine	5.421±1.440**

Notes: * - differences with the corresponding control group are statistically significant ($p<0.01$); ** - differences with the corresponding control group are statistically significant ($p<0.01$).

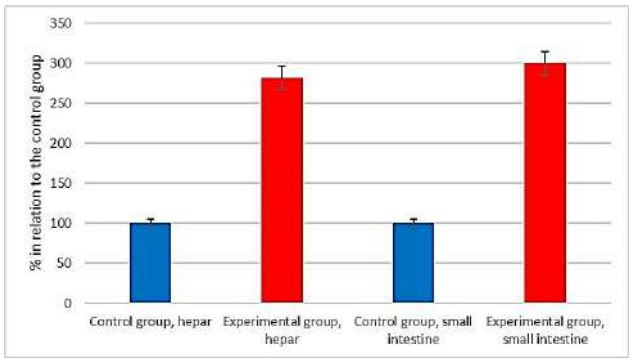

Fig. 6. The effect of shock airwave on changes in the integral index of damage to the liver and small intestine of rats in the experiment.

stasis also occurred in the wall of the small intestine on the background of alterative changes (Fig. 5). Hemodynamic disturbances were accompanied by an increase in the edematous component. There were delamination and swelling of the intestinal wall, rupture of a vein, focal hemorrhage.

The calculation of the integral indicator of traumatic damage to the liver and small intestine showed significant changes in comparison with the control group (Table 2, Fig. 6).

Discussion

Therefore, as a result of the conducted research, a pronounced destructive effect on the biological objects of the human body (regions of the thigh and pelvis) and experimental animals (liver and small intestine of rats) of the shock wave with excess pressure, which was formed as a result of the explosion of ammunition with a cumulative effect, was revealed as well, as after the action of the experimental model of the explosive device. The explosion of the rocket-propelled infantry flamethrower "Bumblebee" is accompanied by the formation of very compressed, high-temperature gas jets, which penetrate at high speed into a room, vehicle, or other space, forming overpressure and high temperature. Overpressure creates a shock wave that acts on biological objects like a blunt object. Its short-term pulsed, centripetal and unilateral action can last from 0.1 to 0.001 seconds, causing a variety of injuries: from abrasions and bruises to the separation of body parts, and the thermal effect is accompanied by the formation of skin burns of varying degrees. In both cases, the blast wave acted on biological objects as a blunt object, the main mechanism of which was the shock, which was accompanied by the destruction of the vascular bed, thigh muscles, liver parenchyma and small intestine. The thermal effect of the ammunition with a cumulative effect was accompanied by skin burns.

As it turns out from the literature, the use of explosive devices is a fairly common negative form of impact on the health and life of people, ranging from suicides [26, 29], to accidents [18, 20] and terrorist attacks [8, 12]. They are most common in military conflicts [1, 25]. It should be noted that since February 2022, over the past three years, in the context of the armed conflict on the territory of Ukraine, the hot phase of hostilities has been going on, the victims of which are both military personnel and civilians. At the same time, the number of victims is constantly increasing, and the dominant lesions are blast trauma, which is accompanied by bodily injuries of varying severity, high-risk somatic and mental illnesses [3, 28].

Practice has shown that explosive devices, such as grenades, mines and others, have both a blast wave and penetrating shrapnel wounds, and the severity of injuries in a mine-blast wound depends on the location of a person at the time of the explosion, which coincides with the opinion of Kalebi A. Y. and Olumbe A. K. [19], Chopna V. V. et al. [5], as well as the authors Christensen A. M. and Smith V. A. [6]. The obtained own data on numerous paired and single abrasions and wounds of the skin of small sizes of rounded, oblong, circular shape, as well as the bright red color of the skin of the thigh and pelvis, which were the result of the action of fragments of a rocket-propelled grenade equipped with a fire mixture, correspond to the features of injuries given in the literature [9, 13, 15].

During the explosion of the rocket-propelled infantry flamethrower "Bumblebee", a shock wave was formed, with a short-term pulse, centripetal and unilateral effect on the body or part of the human body as a blunt object. The consequences of such a destructive effect on the areas of the thigh and pelvis were the loss of the integrity of the vascular bed and the impregnation of muscles and subcutaneous fat with blood, as well as a partial loss of muscle structure, which generally gave them a gelatinous consistency of bright red color. Manifestations of the destructive effect of overpressure as a result of a blast wave (barotrauma) were also typical on biological objects of experimental animals.

In general, the results obtained by us regarding the destructive effect of a blast wave with a thermal effect on biological objects are original and consistent with the data of known literature sources [4, 10, 17, 25].

The microscopically changes in the liver and small intestine identified and evaluated by us after exposure to an airborne shock wave under experimental conditions are generally consistent with the experimental results of other researchers [16, 21], but there are still debates about the degree and duration of reactive changes in parenchymal-stromal and vascular elements, which may be of significant importance in determining the age of the damage.

Conclusions

1. The established pathomorphological signs of the destructive effect of overpressure as a result of a blast wave (barotrauma) were typical and common both in the areas of the human hip and pelvis, and in biological objects of experimental animals. In particular, during the explosion of ammunition with a cumulative effect of the rocket infantry flamethrower "Bumblebee" on sectional incisions of the skin and muscles of the thigh in the projection of areas of redness, a picture of a gelatinous consistency of bright red color was macroscopically determined due to abundant blood impregnation of muscles and subcutaneous fat and partial loss of muscle structure, with the release of myoglobin.

2. The bright red color of the skin of the thigh and pelvis without burning the hair may indicate the superficial thermal effect of the explosive device and the protection of the skin by clothing.

3. The effect of an air shock wave with an excess pressure of 31,62±4,84 kPa on the liver parenchyma of rats was primarily determined by destructive changes in its vascular system, namely, focal hemorrhages with

rupture of the terminal central vein of the hepatic lobe, swelling of the parasinusoidal spaces, sludge in the sinusoids. In the wall of the small intestine, there were acute hemodynamic disturbances in the form of vasodilatation of arterial vessels, venular and capillary stasis, delamination and swelling of the intestinal wall, rupture of veins, focal hemorrhage. And all this is consistent with the pathomorphological manifestations of barotrauma on parts of the human body as a result of the action of an explosive device with a cumulative effect.

References

[1] Babkina, O. P., Stogniev, Y. O., & Benaissa, M. V. (2016). Судово-медична експертиза летальної мінно-вибухової травми в умовах надзвичайної ситуації в Україні [Forensic medical examination of a fatal mine-explosive injury in the conditions of an emergency in Ukraine]. *Актуальні проблеми сучасної медицини=Actual Prob. Mod. Med.*, 16(3), 37-41.

[2] Beregulya, R. (2022). *Since February 2022, 950 civilians have been injured by explosive devices in Ukraine*. https://www.ukrinform.ua/rubric-ato/3841397-z-lutogo-2022-roku-v-ukraini-vid-vibuhonebezpecnih-predmetiv-postrazdali-950-civilnih-minoboroni.html

[3] Bukowski, J., Nowadly, C. D., Schauer, S. G., Koyfman, A., & Long, B. (2023). High risk and low prevalence diseases: Blast injuries. *The American Journal of Emergency Medicine*, 70, 46-56, doi: 10.1016/j.ajem.2023.05.003

[4] Champion, H. R., Holcomb, J. B., & Young, L. A. (2009). Injuries from explosions: physics, biophysics, pathology, and required research focus. *Journal of Trauma and Acute Care Surgery,* 66(5), 1468-1477. doi: 10.1097/TA.0b013e3181a27e7f

[5] Chopna, V. V., Zavodyak, A. Y., Matviychuk, M. V., Ivashkevich, E. M., Sivak, V. M., Slobodian, V. V., & Lunko, O. D. (2023). Тяжкість ушкоджень при мінно-вибуховій травмі залежно від місцязнаходження особи на момент вибуху [Severity of injuries in case of a mine-explosive trauma depending on the location of the person at the time of the explosion]. *Актуальні аспекти діагностики і лікування=Curr Asp Diag Treat,* 4(3), 70-77. doi: 10.46847/ujmm.2023.3(4)-070

[6] Christensen, A. M., & Smith, V. A. (2015). *Blast trauma. Skeletal trauma analysis: case studies in context.* John Wiley & Sons. doi: 10.1002/9781118384213.ch13

[7] Cullis, I. G. (2001). Blast waves and how they interact with structures. *BMJ Military Health,* 147(1), 16-26. doi: 10.1136/jramc-147-01-02

[8] Delannoy, Y., Plu, I., Sec, I., Delabarde, T., Taccoen, M., Tracqui, A., & Ludes, B. (2020). Terrorist attacks: cutaneous patterns of gunshot and secondary blast injuries. *Forensic sciences research,* 5(3), 208-213. doi: 10.1080/20961790.2020.1771859

[9] Demining, H. (2017). *Explosive weapon effects - final report.* GICHD, Geneva, February. ISBN: 978-2-940369-61-4

[10] Dettmeyer, R. B., Verhoff, M. A., Schütz, H. F., Dettmeyer, R. B., Verhoff, M. A., & Schütz, H. F. (2014). *Gunshot and blast wounds.* Forensic Medicine: Fundamentals and Perspectives, 155-170. doi: 10.1007/978-3-642-38818-7_10

[11] Duan, Z. X., Li, G. H., Zhang, J. Y., Deng, M. S., Chen, K. J., Zhang, L. C., ... & Wang, J. M. (2023). Effects of orientation and distance of goats on blast lung injury characteristics on a plateau above 4500-meter. *Chinese journal of traumatology,* 26(03), 139-146. doi: 10.1016/j.cjtee.2022.09.001

[12] Franceschetti, L., Galante, N., Del Sordo, S., Casali, M. B., & Genovese, U. (2021). Forensic considerations on the two major civilian terrorist events occurred in Milan: A retrospective autopsy-based study. *Forensic Science International,* 326, 110929. doi: 10.1016/j.forsciint.2021.110929

[13] Galante, N., Franceschetti, L., Del Sordo, S., Casali, M. B., & Genovese, U. (2021). Explosion-related deaths: An overview on forensic evaluation and implications. *Forensic Science, Medicine and Pathology,* 17(3), 437-448. doi: 10.1007/s12024-021- 00383-z

[14] Goeller, J., Wardlaw, A., Treichler, D., O'Bruba, J., & Weiss, G. (2012). Investigation of cavitation as a possible damage mechanism in blast-induced traumatic brain injury. *Journal of neurotrauma,* 29(10), 1970-1981. doi: 10.1089/neu.2011.2224

[15] Greer, N., Sayer, N., Kramer, M., Koeller, E., & Velasquez, T. (2017). *Prevalence and epidemiology of combat blast injuries from the military cohort 2001-2014.* VA ESP Project #09-009; 2016. PMID: 28813129

[16] Haussner, F., Maitz, A., Rasche, V., Hoffmann, A., Braumüller, S., Lupu, L., ... & Huber-Lang, M. (2022). Intestinal damage and immune response after experimental blunt abdominal trauma. *Shock,* 58(4), 332-340. doi: 10.1097/SHK.0000000000001986

[17] Horrocks, C. L. (2001). Blast injuries: biophysics, pathophysiology and management principles. *BMJ Military Health,* 147(1), 28-40. doi: 10.1136/jramc-147-01-03

[18] Hull, J. B. (1992). Traumatic amputation by explosive blast: pattern of injury in survivors. *Journal of British Surgery,* 79(12), 1303-1306. doi: 10.1002/bjs.1800791220

[19] Kalebi, A. Y., & Olumbe, A. K. O. (2006). Forensic findings from the Nairobi US Embassy terrorist bombing. *East Afr Med J,* 83(7), 380-388. doi: 10.4314/eamj.v83i7.9450

[20] Kunz, S. N., Zinka, B., Peschel, O., & Fieseler, S. (2011). Accidental head explosion: an unusual blast wave injury as a result of self-made fireworks. *Forensic science international,* 210(1-3), e4-e6. doi: 10.1016/j.forsciint.2011.04.013

[21] Maitz, A., Haussner, F., Braumüller, S., Hoffmann, A., Lupu, L., Wachter, U., ... & Palmer, A. (2021). Temporal-spatial organ response after blast-induced experimental blunt abdominal trauma. *FASEB J,* 35(12), e22038. doi: 10.1096/fj.202100995R

[22] Order of the Ministry of Health of Ukraine (1995). Про розвиток та вдосконалення судово-медичної служби України [On the development and improvement of the forensic medical service of Ukraine]. Наказ Міністерства охорони здоров'я України № 6 від 17.01.1995=Order of the Ministry of Health of Ukraine No. 6, dated January 17.1995. https://zakon.rada.gov.ua/laws/show/z0248-95#Tex

[23] Perebetiuk, A. M., Gunas, V. I., Terehovska, O. I., Prokopenko, S. V., & Sergeeva, Y. Y. (2023). Indicators of the temporary cavity during shots from non-lethal firearms: an experimental study using the "FORT 9R" and "FORT 17R" pistols. *Odesa Medical Journal,* 183(2), 21-25. doi: 10.32782/2226-2008-2023-2-3

[24] Pollak, S., & Saukko, P. J. (2009). Blunt force trauma. Wiley Ency. Forensic Sci. doi: 10.1002/9780470061589.fsa037

[25] Popivanov, G., Mutafchiyski, V. M., Belokonski, E. I., Parashkevov, A. B., & Koutin, G. L. (2014). A modern combat trauma. *BMJ Military Health,* 160(1), 52-55. doi: 10.1136/jramc-2013-000132

[26] Sacco, M. A., Ricci, P., Gratteri, S., Scalise, C., & Aquila, I. (2021). The forensic analysis of homemade explosive

suicides: Case report and systematic review of the literature. *Journal of Forensic Sciences*, 66(5), 2013-2019. doi: 10.1111/1556- 4029.14757

[27] Salzar, R. S., Treichler, D., Wardlaw, A., Weiss, G., & Goeller, J. (2017). Experimental investigation of cavitation as a possible damage mechanism in blast-induced traumatic brain injury in post-mortem human subject heads. *Journal of neurotrauma,* 34(8), 1589-1602. doi: 10.1089/neu.2016.4600

[28] Spiegel, P. B., Kovtoniuk, P., & Lewtak, K. (2023). The war in Ukraine 1 year on: the need to strategise for the long-term health of Ukrainians. *The Lancet,* 401(10377), 622-625. doi: 10.1016/S0140-6736(23)00383-5

[29] Tsokos, M., Türk, E. E., Madea, B., Koops, E., Longauer, F., Szabo, M., ... & Barz, J. (2003). Pathologic features of suicidal deaths caused by explosives. *The American Journal of forensic medicine and pathology,* 24(1), 55-63. doi: 10.1097/01.PAF.0000052752.18930.44

[30] Turillazzi, E., Monaci, F., Neri, M., Pomara, C., Riezzo, I., Baroni, D., & Fineschi, V. (2010). Collection of trace evidence of explosive residues from the skin in a death due to a disguised letter bomb. The synergy between confocal laser scanning microscope and inductively coupled plasma atomic emission spectrometer analyses. *Forensic Science International,* 197(1-3), e7-e12. doi: 10.1016/j.forsciint.2009.12.012

[31] Zhang, J. K., Botterbush, K. S., Bagdady, K., Lei, C. H., Mercier, P., & Mattei, T. A. (2022). Blast-related traumatic brain injuries secondary to thermobaric explosives: implications for the war in Ukraine. *World neurosurgery,* 167, 176-183. doi: 10.1016/j.wneu.2022.08.073

СУДОВО-МЕДИЧНА ХАРАКТЕРИСТИКА УШКОДЖЕНЬ ВІД ТЕРМОБАРИЧНОЇ ДІЇ ВИБУХОВОГО ПРИСТРОЮ

Михайленко О. В., Мішалов В. Д., Козлов С. В., Варфоломеєв Є. А.

З початку вторгнення російської федерації на територію України у 2022 р., вибухоіндукована травма стала надзвичайно актуальною проблемою, оскільки основним джерелом тілесних ушкоджень як серед військових в зоні бойового зіткнення, так і цивільного населення в містах, стала дія вибухових пристроїв. Мета роботи - вивчення судово-медичної характеристики ушкоджень біологічних об'єктів, які утворились від термічного впливу та ударної хвилі внаслідок вибуху боєприпасу з кумулятивною дією та в умовах експериментальної моделі вибуху. Об'єктами дослідження були матеріали двох експертиз з приводу смерті українських військових, які загинули в зоні бойових дій (архівні "Висновки експертного дослідження" Київського міського клінічного бюро судово-медичної експертизи за 2023 р.). В умовах експерименту були проведені дослідження патоморфологічних змін печінки та тонкої кишки 30 білих безпородних щурів від дії штучно створеної повітряної ударної хвилі з надлишковим тиском 31,62±4,84 кПа. Ушкодження досліджували макроскопічно та за допомогою стандартних лабораторних гістологічних методик. Мікроскопію гістологічних зрізів проводили за допомогою мікроскопу Axio Imager 2 (Zeiss, Німеччина) на збільшеннях х200 та х400. Статистичну обробку отриманих кількісних результатів проводили за допомогою програмного продукту STATISTICA 6.1. За умови вибуху боєприпасу з кумулятивною дією реактивного піхотного вогнемету "Джміль" на секційних розрізах шкіри і м'язів стегна в проекції ділянок почервоніння макроскопічно визначалась картина драглистої консистенції яскраво-червоного кольору за рахунок рясного просочування кров'ю м'язів і підшкірно жирової клітковини та часткової втрати структурованості м'язів із виходом міоглобіну. Яскраво-червоний колір шкіри стегна і таза без обгоряння волосся може свідчити про поверхневу термічну дію вибухового пристрою та захист шкіри одягом. Також визначались дифузно розташовані чисельні як парні, так і поодинокі садна та неглибокі рани, невеликих розмірів округлої, довгастої, циркулярної форми, які є наслідком дії уламків реактивної гранати, спорядженої вогневою сумішшю. Вплив повітряної ударної хвилі з надлишковим тиском 31,62±4,84 кПа на паренхіму печінки щурів визначався вогнищевими крововиливами з розривом кінцевої центральної вени печінкової часточки, набряком парасинусоїдальних просторів та сладжами в синусоїдах. У стінці тонкої кишки відбувалися гострі порушення гемодинаміки у вигляді вазодилятації артеріальних судин, венулярного та капілярного стаза. Мали місце розшарування та набряк стінки кишки, розрив вен, вогнищевий крововилив. Таким чином, виявлені характерні патоморфологічні ознаки руйнівної дії надлишкового тиску внаслідок вибухової хвилі (баротравми) є типовими і загальними як на ділянках стегна і таза людини, так і на біологічних об'єктах експериментальних тварин. Отримані результати узгоджуються з патоморфологічними проявами баротравми на ділянках тіла людини в результаті дії вибухового пристрою з кумулятивною дією.

Ключові слова: *судово-медична експертиза, біологічні об'єкти, термобарична травма.*

Author's contribution

Mykhaylenko O. V. - conceptualization, research, review writing and editing.
Mishalov V. D. - project administration, research, methodology and writing of the original draft, formal analysis and validation.
Kozlov S. V. - data visualization.
Varfolomeiev Y. A. - software, resources.

DOI: 10.31393/morphology-journal-2024-30(2)-04 Reports of Morphology, Vol. 30, №2, Pages 31-36

ISSN 1818-1295 eISSN 2616-6194

REPORTS OF MORPHOLOGY

Official Journal of the Scientific Society of Anatomists, Histologists, Embryologists and Topographic Anatomists of Ukraine

journal homepage: https://morphology-journal.com

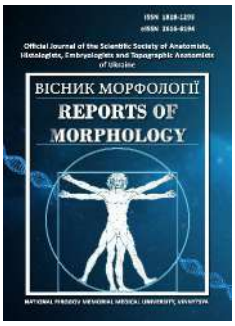

Morphological features of the pons in human fetuses 14-15 weeks of intrauterine development

Lopatkina O. P., Tykholaz V. O., Shkolnikov V. S., Zalevskyi L. L.
National Pirogov Memorial Medical University, Vinnytsya, Ukraine

ARTICLE INFO
Received: 30 November 2023
Accepted: 13 March 2024

UDC: 611.81+612.82]:57.017.642

CORRESPONDING AUTHOR
e-mail: lopatkinaksyusha@gmail.com
Lopatkina O. P.

CONFLICT OF INTEREST
The authors have no conflicts of interest to declare.

FUNDING
Not applicable.

DATA SHARING
Data are available upon reasonable request to corresponding author.

Knowledge of human embryonic development is essential to improve our understanding of human fetal anatomy and for better understanding the etiology of congenital malformations. Currently, the structures of the posterior cranial fossa and the brain stem are of great interest to researchers, because of a large number of nuclei are located in the pons area, which play an important role in ensuring vital functions. The aim of the scientific work is to establish the morphological features of the pons of human fetuses at 14-15 weeks of gestation, the size and area of the nuclei of cranial nerves and neurons which are located in the area of the pons. Anatomical and histological research was carried out on 6 human fetuses aged 14-15 weeks of gestation. The cadaver material for research was obtained as a result of late abortions which were conducted according to medical indications in Vinnytsia maternity hospitals. Preparations were fixed in a 10 % solution of neutral formalin, stained with hematoxylin-eosin, toluidine blue modified by Nissl. Computer histometry (Toup View) was used for morphometric research. Statistical digital data were processed on a personal computer using Microsoft Excel 2016 and "Statistica 6.1" software. We established that in human fetuses at 14-15 weeks of intrauterine development, the nuclei of the trigeminal, abductor and vestibulocochlear nerves were detected. The nucleus of the facial nerve on 14-15 weeks of gestation is represented by single polygonal nerve cells with eosinophilic cytoplasm. The nucleus of the abductor nerve had the largest area, the cochlear nucleus of the vestibulocochlear nerve had the smallest area. The largest area of neurons was in the nuclei of the VIII pair of cranial nerve, the smallest - in the nucleus of the abductor and facial nerves. At 14-15 weeks of intrauterine development of human fetuses, the area of the cell nucleus could be determined only in the nuclei of the vestibulocochlear nerve, while the cell nuclei of the trigeminal, facial, and abductor nerves were represented by nerve cells of a spherical shape with a nucleus in which a basophilic nucleolus and a homogeneous eosinophilic cytoplasm were noted. Thus, in human fetuses of 14-15 weeks of intrauterine development, differences in the sizes and areas of the nuclei of cranial nerves and neurons that form nuclei in the pons area were found.

Keywords: *human fetuses, gestational age, embryonic development, pons, pons nuclei, neurons of pons nuclei.*

Introduction

Knowledge of human embryonic development is essential to improve our understanding of human fetal anatomy and to help understand the etiology of congenital malformations [3, 13, 29].

In the conditions of a difficult demographic situation in Ukraine, the problem of saving newborns is becoming more and more urgent. Environmental pollution, non-observance of a healthy lifestyle, unbalanced nutrition leads to the development of birth defects, sometimes to disability and death of newborns [5, 17, 18, 23].

Timely detection of a birth defect allows you to make a decision to terminate a pregnancy or prepare for the birth of a sick child. Early prenatal diagnosis allows adequate monitoring of the course of pregnancy, childbirth and the neonatal period. Modern methods of analysis make it possible to investigate placental insufficiency - the cause of fetal development delay, intrauterine hypotrophy and hypoxia, and ultimately - the possibility of intrauterine death

of the fetus [22, 28].

Most often, congenital malformations of the brain were diagnosed before the 22nd week of intrauterine development, which were the result of a violation of the main processes of brain development - the formation of the neural tube, the division of its cranial division into paired formations, migration and differentiation of nerve cell elements [4, 11].

According to some studies [7, 21, 27], at the 7th week of pregnancy, the development of the pons as a derivative of the metencephalon is observed, at the 12th week of intrauterine development, the differentiation of the basilar and tegmental parts of the pons occurs, at the 14th week, migrating neurons are identified in the basilar part of the pons, which form pons nuclei among the white matter, at the 18th week of gestation in the pons cover, the nuclei of the abductor and facial nerves are identified, at 28 weeks, formed cells are observed in the nucleus of the abducens nerve, at 32 weeks of intrauterine development, multipolar cell complexes that form the nuclei of the abductor and facial nerves increase, at 36 weeks, the size of neurons increases, they have clearly defined nuclei and nucleoli.

In the 2nd trimester of pregnancy, the organ of hearing begins to develop in human fetuses. R. Lim and A. Brichta [15] described the development of the human hearing organ with intussusception of the ear sac at 4 weeks of gestation, the growth of the semicircular canals from 5 weeks and the formation of the auricle from 10 weeks of gestation. A number of authors proved that from the 12th week, the vestibular node of the vestibulocochlear nerve was gradually filled with glial cells, and in the cochlear nerve, at the 22nd week, the peripheral processes began to be myelinated, which suggests that the maturation of peripheral glial cells in the hearing organ of the human fetus begins its development from 9 to 22 weeks of gestation [10, 16, 19].

Embryonic development of the pons, according to literary sources of foreign and domestic scientists, was studied on animals, which could not always be extrapolated to humans [14]. Currently, the structures of the posterior cranial fossa and brain stem are of great interest to researchers, because a large number of nuclei are located in the pons area, which play an important role in ensuring vital functions [1].

The aim of the scientific work is to establish the morphological features of the pons of human fetuses at 14-15 weeks of gestation, the size and area of the nuclei of cranial nerves and neurons located in the pons area.

Materials and methods

The work was performed as part of the SRW of the Department of Human Anatomy, National Pirogov Memorial Medical University, Vinnytsya "Establishment of patterns of organ and histogenesis and topography of internal organs of the thoracic and abdominal cavities, as well as structures of the central nervous system of human fetuses (macroscopic, histological, immunohistochemical and ultrasound examination)".

The study was approved at the meeting of the Biomedical Ethics Committee of the National Pirogov Memorial Medical University, Vinnytsya (Excerpt from the minutes of the meeting of the Bioethics Committee of the National Pirogov Memorial Medical University, Vinnytsya No. 10 dated November 23, 2017), in compliance with the basic provisions of GCP (1996), Convention on the Protection of Human Rights and Dignity in Connection with the Application of Advances in Biology and Medicine (1996). The research materials do not contradict the basic bioethical norms of the Declaration of Helsinki on the ethical principles of conducting scientific and medical research involving human subjects, adopted by the 59th General Assembly of the World Medical Association in 2008.

Anatomical and histological research was performed on 6 human fetuses aged 14-15 weeks of gestation. The average fetuses weight was 93.30±4.66 g, parietal-coccygeal length - 118.9±5.9 mm.

The cadaver material for the study was obtained as a result of late abortions according to medical indicators from the maternity hospitals of the city of Vinnytsia, Ukraine.

The weight of the fetus and the weight of the pons were determined using electronic scales. According to the method of Avtandilov G. G. [2], with the help of a ShC-125 caliper, the dimensions of the head were determined, the height of the pons (sulcus bulbopontinus from below and the legs of the midbrain from above), the width of the pons (the most prominent point from one angulus pontocerebellaris to the other), the thickness of the pons (the most prominent point from the posterior surface to the anterior surface of the pons). The obtained pons preparations from human fetuses were fixed in a 10% solution of neutral formalin according to our own method. Subsequently, serial sections of the pons were made from paraffin and celloidin blocks with a thickness of 8-9 microns. Preparations were stained with hematoxylin-eosin, toluidine blue modified by Nissl. Microscopic research was carried out using the MBS-9 microscope and the Euromex iScope series and the Euromex Microscope camera B. V. DC. 1359 F100 using the following magnifications: x1, x4, x10, x40, x100, x400. Computer histometry (Toup View) was used for morphometric research.

Statistical digital data were processed on a personal computer using Microsoft Excel 2016 and "Statistica 6.1" software (license number BXXR901E246122FA).

Results

In human fetuses at 14-15 weeks of gestation, the following head sizes are established: circumference - 110.6±5.5 mm, height - 44.60±2.23 mm, transverse size - 30.91±1.54 mm, longitudinal size - 38.58±1.93 mm. The size of the front fontanelle: longitudinal - 22.00±1.10 mm, transverse - 19.17±0.96 mm. The size of the posterior fontanelle: longitudinal - 10.71±0.53 mm, transverse - 11.10±0.55 mm.

Macrometric dimensions of the pons: height - 6.751±0.337

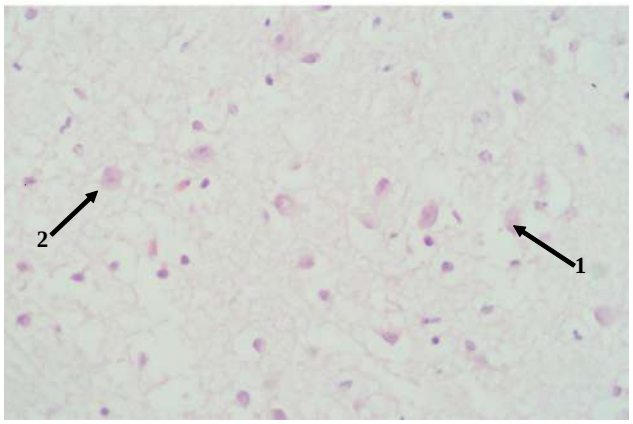

Fig. 1. Pons of a human fetus with a gestation period of 14-15 weeks. 1, 2 - neuroblasts of the nuclei of the trigeminal nerve. Hematoxylin-eosin, x400.

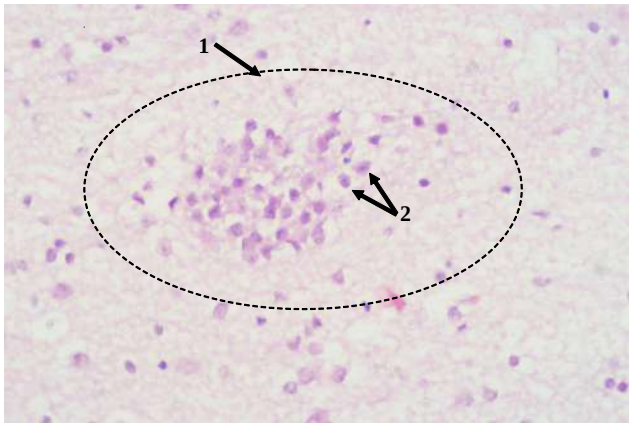

Fig. 2. Pons of a human fetus with a gestation period of 14-15 weeks. 1 - cochlear nuclei of vestibulocochlear nerve, 2 - neuronal cells of cochlear nuclei of vestibulocochlear nerve. Hematoxylin-eosin, x100.

mm, thickness - 6.354±0.318 mm, width - 9.152±0.458 mm. The weight of the pons was 4.757±0.238 g.

On the histological preparation of the pons, the roof, the base, and the nucleus of the trapezoidal body are clearly defined at the boundary between them by the gestation period of 14-15 weeks.

The boundaries of the nucleus of the trigeminal nerve in human fetuses at 14-15 weeks of fetal development are unclear. The nucleus has an oval, somewhat elongated shape, with an area of 0.024±0.002 mm^2. Neurons of the nucleus are single, most of them are represented by neuroblasts (Fig. 1).

The nucleus of the abducens nerve is located near the cavity of the fourth ventricle on the posterior surface of the pons. The boundaries of the nucleus are unclear, the nucleus is elongated and has a rounded shape. The core area is 0.183±0.009 mm^2. Neurons are unformed, almost identical, spherical or oval in shape. The area of neurons is 35.29±1.76 μm^2. Nerve cells with a large round nucleus, in which a dense basophilic nucleolus and a homogeneous eosinophilic cytoplasm are defined.

Between the nucleus of the trigeminal nerve and the abducens nerve, closer to the trapezoidal body, the nucleus of the facial nerve is located. The nucleus is represented by single polygonal nerve cells with eosinophilic cytoplasm, the boundaries of the nucleus are unclear. The core area is 0.031±0.001 mm^2. The area of neurons is 47.85±0.24 μm^2.

The vestibular nuclei of the vestibulocochlear nerve are located in the posterior-lateral area of the pons in human fetuses at 14-15 weeks of gestation. The nucleus has no clear boundary, it is just beginning to form, the area of the nucleus is 0.053±0.002 mm^2. Neurons are at the stage of differentiation, their number is small, but they already have processes. The average value of the neuron area is 140.1±7.0 μm^2. The area of the cell nucleus is on average 60.14±3.01 μm^2. The nucleolus and chromatin are clearly visualized in the nuclei.

The cochlear nuclei of the vestibulocochlear nerve are located above the vestibular nuclei in the lateral part of the pons preparation. The nucleus has an irregular oval shape, the boundaries of the nucleus are not clear. Its area is 0.014±0.001 mm2 (Fig. 2). Neurons are immature, rounded in shape, and do not have appendages. The sizes of the nuclear cells are almost the same, represented by poorly differentiated nerve cells of a spherical shape with a nucleus in which a dense basophilic nucleolus and a homogeneous eosinophilic cytoplasm are noted. The area of the neuron is 113.8±5.7 μm^2. The area of the cell nucleus is 36.01±1.80 μm^2 on average.

Discussion

According to Hamano S. I. at al. [6], as well as Hossain M. I. at al. [8], who studied the development of the nuclei of the trigeminal nerve, at the 12th week of gestation, the nuclei have not yet been determined. In our study of human fetuses of 14-15 weeks of gestation, vague, slightly elongated, oval-shaped borders of the trigeminal nerve nucleus with single neurons were found.

Neurons of the main nucleus of the trigeminal nerve in terms of cell location, number of Nissl bodies, and neuron morphology approached adult neurons at approximately 33 weeks of gestation [24]. In their work, Lavezzi A. M., Mehboob R. and Matturri L. [12] pointed out that the structures of the human trigeminal nucleus are still poorly studied. But the trigeminal nerve has a functional significance in the early phases of the development of the central nervous system and in the regulation of autonomic functions.

K. Yamaguchi and K. Honma [30] indicated that the nucleus of the abducens nerve was identified at 20 weeks. Core neurons were clearly distinguished from glial cells by their clear nuclei. The cells of the nuclei of neurons had different shapes and sizes, larger neurons were located in the center of the nucleus. At the same time, Padmini M. P. and Rao B. N. [21] proved that the nucleus of the abductor nerve was identified at the 18th week of gestation in the covering of the pons. According to our research, the

boundaries of the nucleus of the abducens nerve at 14-15 weeks of gestation are unclear, the neurons are not formed, and are almost the same in size.

A morphometric study by Rao B. N. and Padmini M. P. [25] showed that primitive migrating cells of the nucleus of the facial nerve settle down at 10 weeks of fetal development, and rounded neuroblasts form at 12-18 weeks. Our results confirm the results of this study that from 12 to 18 weeks of gestation, the nuclei of the facial nerve are formed by rounded neuroblasts.

S. Jang et al. [9] studied the development of the vestibular nuclei of the vestibulocochlear nerve in human fetuses of different gestational periods. Morphometric analysis of the study showed that vestibular nuclei neurons differed from glia only after 16 weeks of gestation, cytoarchitectonically divided into medial and lateral at 21 weeks. When examining human fetuses at the stage of 14-15 weeks, we established that the vestibular nuclei of the vestibulocochlear nerve are just beginning to form, the nucleus without a clear boundary, the nucleolus and chromatin are clearly visualized in the nuclei.

S. Saini et al. [26] in their study indicated that the cochlear nuclei can be identified at 10 weeks of fetal development, and dorsal and ventral cochlear nuclei can be identified at 16 weeks. A sudden jump in the growth of the total area of nuclei, the number of neurons and astrocytes occurs at week 18, and at week 22, an increase in proliferation and apoptosis is observed. In his scientific work, Mishra S. et al. [20] concluded that the morphological and functional maturation of the cochlear nuclei of the vestibulocochlear nerve in humans occurs simultaneously in the middle of pregnancy, which is a critical period of development, and lasts until the 37th week of gestation. Data from the scientific work of Saini S. et al. [26] also confirm the results of our study that at 14-15 weeks of intrauterine development in human fetuses, irregular oval-shaped cochlear nuclei of the vestibulocochlear nerve with immature neurons are determined.

Thus, in human fetuses of 14-15 weeks of intrauterine development, differences in the sizes and areas of cranial nerve nuclei and neurons that form nuclei in the pons area were found.

In the future, further studies plan to establish patterns of expression of immunohistochemical markers in the prenatal period of human ontogenesis.

Conclusions

1. In human fetuses at 14-15 weeks of intrauterine development, we found the nuclei of the trigeminal, abducens and vestibulocochlear nerves. The nucleus of the facial nerve at the stage of 14-15 weeks of gestation was represented by single polygonal nerve cells with eosinophilic cytoplasm.

2. The nucleus of the abductor nerve had the largest area, the cochlear nuclei of the vestibulocochlear nerve had the smallest area.

3. The largest area of neurons was in the vestibular and cochlear nuclei of the vestibulocochlear nerve, the smallest - in the nuclei of the abducens and facial nerves.

4. At 14-15 weeks of intrauterine development of human fetuses, the area of the cell nucleus could be determined only in the nuclei of the vestibulocochlear nerve, while the cell nuclei of the trigeminal, facial, and abducens nerves were represented by spherical nerve cells with a nucleus in which a basophilic nucleus and a homogeneous eosinophilic cytoplasm.

References

[1] Ajeigbe, S. O., Muazu, T. A., & Nzalak, J. O. (2021). Histomorphological Study of The Pons and Medulla Oblongata of African Striped Group Squirrel (Xerus erythropus). *Egyptian Journal of Veterinary Sciences,* 52(3), 361-372. doi: 10.21608/ejvs.2021.75614.1232

[2] Avtandilov, G. G. (2002). *Основы количественной патологической анатомии [Basics of Quantitative Pathological Anatomy].* M.: Медицина=M.: Medicine. ISBN 5225007538.

[3] De Bakker, B. S., de Jong, K. H., Hagoort, J., De Bree, K., Besselink, C. T., de Kanter, F. E. C., … & Moorman, A. F. (2016). An interactive threedimensional digital atlas and quantitative database of human development. *Science,* 354(6315). doi: 10.1126/science.aag0053

[4] Dovjak, G. O., Schmidbauer, V., Brugger, P. C., Gruber, G. M., Diogo, M., Glatter, S., ... & Kasprian, G. J. (2021). Normal human brainstem development in vivo: a quantitative fetal MRI study. *Ultrasound in Obstetrics & Gynecology*, 58(2), 254-263. doi: 10.1002/uog.22162

[5] Fitzgerald, E., Hor, K., & Drake, A. J. (2020). Maternal influences on fetal brain development: The role of nutrition, infection and stress, and the potential for intergenerational consequences. *Early Human Development,* 150, 105190. doi: 10.1016/j.earlhumdev.2020.105190

[6] Hamano, S. I., Goto, N., Nara, T., Okada, A., & Maekawa, K. (1997). Development of the human principal sensory trigeminal nucleus: a morphometric analysis. *Early Human Development,* 48(3), 225-235. doi: 10.1016/S0378-3782(96)01859-2

[7] Horn, A. K., Horng, A., Buresch, N., Messoudi, A., & Härtig, W. (2018). Identification of functional cell groups in the abducens nucleus of monkey and human by perineuronal nets and choline acetyltransferase immunolabeling. *Frontiers in Neuroanatomy,* 12, 45. doi: 10.3389/fnana.2018.00045

[8] Hossain, M. I., Horie, M., Yoshioka, N., Kurose, M., Yamamura, K., & Takebayashi, H. (2018). Motoneuron degeneration in the trigeminal motor nucleus innervating the masseter muscle in Dystonia musculorum mice. *Neurochemistry International*, 119, 159-170. doi: 10.1016/j.neuint.2017.10.009

[9] Jang, S. H., Lee, M. Y., Yeo, S. S., & Kwon, H. G. (2018). Structural neural connectivity of the vestibular nuclei in the human brain: a diffusion tensor imaging study. *Neural Regeneration Research,* 13(4), 727. doi: 10.4103/1673-5374.230304

[10] Kandathil, C. K., Stakhovskaya, O., & Leake, P. A. (2016). Effects of brain-derived neurotrophic factor (BDNF) on the cochlear nucleus in cats deafened as neonates. *Hearing Research,* 342, 134-143. doi: 10.1016/j.heares.2016.10.011

[11] Komshuk, T. S., & Pishak, V. P. (2013). Морфологія структур судинних сплетень шлуночків головного мозку в онтоге-

незі людини [Morphology of structures of vascular plexuses of cerebral ventricles in human ontogeny]. *Вісник проблем біології і медицини=Bulletin of Problems in Biology and Medicine,* 1(1), 191-195.

[12] Lavezzi, A. M., Mehboob, R., & Matturri, L. (2011). Developmental alterations of the spinal trigeminal nucleus disclosed by substance P immunohistochemistry in fetal and infant sudden unexplained deaths. *Neuropathology*, 31(4), 405-413. doi: 10.1111/j.1440-1789.2010.01190.x

[13] Lee, J. H., Shin, H., Shaker, M. R., Kim, H. J., Park, S. H., Kim, J. H., ... & Sun, W. (2022). Production of human spinal-cord organoids recapitulating neural-tube morphogenesis. *Nature Biomedical Engineering,* 6(4), 435-448. doi: 10.1038/s41551-022-00868-4

[14] Leibovitz, Z., Lerman-Sagie, T., & Haddad, L. (2022). Fetal brain development: regulating processes and related malformations. Life, 12(6), 809. doi: 10.3390/life12060809

[15] Lim, R., & Brichta, A. M. (2016). Anatomical and physiological development of the human inner ear. *Hearing Research*, 338, 9-21. doi: 10.1016/j.heares.2016.02.004

[16] Locher, H., de Groot, J. C., van Iperen, L., Huisman, M. A., Frijns, J. H., & Chuva de Sousa Lopes, S. M. (2014). Distribution and development of peripheral glial cells in the human fetal cochlea. *PLoS One*, 9(1), e88066. doi: 10.1371/journal.pone.0088066

[17] Lytvynenko, N. V., Purdenko, T. Y., Gladka, V. M., & Silenko, G. Ya. (2017). Морфофункціональні особливості розвитку нервової системи в онтогенезі [Morphofunctional features of the development of the nervous system in ontogenesis]. *Світ медицини та біології=The World of Medicine and Biology,* 13(1 (59)), 202-208.

[18] Mai, C. T., Isenburg, J. L., Canfield, M. A., Meyer, R. E., Correa, A., Alverson, C. J., ... & National Birth Defects Prevention Network. (2019). National population-based estimates for major birth defects, 2010-2014. *Birth Defects Research,* 111(18), 1420-1435. doi: 10.1002/bdr2.1589

[19] Manis, P. B., Kasten, M. R., & Xie, R. (2019). Classification of neurons in the adult mouse cochlear nucleus: Linear discriminant analysis. *PloS One*, 14(10), e0223137. doi: 10.1371/journal.pone.0223137

[20] Mishra, S., Roy, T. S., & Wadhwa, S. (2018). Morphological and morphometrical maturation of ventral cochlear nucleus in human foetus. *Journal of Chemical Neuroanatomy*, 93, 38-47. doi: 10.1016/j.jchemneu.2017.03.002

[21] Padmini, M. P., & Rao, B. N. (2019). A study on morpho-histogenesis of human foetal pons. *Indian Journal of Clinical Anatomy and Physiology,* 6(1), 41-44. doi: 10.18231/2394-2126.2019.0010

[22] Priymak, S. G., & Priymak, K. V. (2020). Пренатальна діагностика вроджених вад розвитку плода в I триместрі вагітності [Prenatal diagnosis of congenital malformations of the fetus in the first trimester of pregnancy]. *Південноукраїнський медичний науковий журнал=South Ukrainian Medical Scientific Journal,* 25(25), 54-56. doi: 10.36074/05.06.2020.v3.13

[23] Prokopchuk, N., Nikolenko, M., Korinets, Ya., & Ivaniv, Yu. (2023). Оцінка результатів пренатальної діагностики вроджених вад розвитку плоду у жінок в різні терміни гестації [Evaluation of the results of prenatal diagnosis of congenital malformations of the fetus in women at different periods of gestation]. *Перспективи та інновації науки=Perspectives and Innovations of Science*, 10(28), 796-808. doi: 10.52058/2786-4952-2023-10(28)-796-808

[24] Rahman, M., & Tadi, P. (2020). *Neuroanatomy, Pons.* StatPearls Publishing, Treasure Island (FL). PMID: 32809424

[25] Rao, B. N., & Padmini, M. P. (2009). Histogenesis of neurons in the nucleus of facial nerve-a study in. J. Anat. Soc. India, 58(2), 135-139.

[26] Saini, S., Kaur, C., Pal, I., Kumar, P., Jacob, T. G., Thakar, A., ... & Roy, T. S. (2019). Morphological development of the human cochlear nucleus. *Hearing Research,* 382, 107784. doi: 10.1016/j.heares.2019.107784

[27] Smit, J. A., Jacobs, K., Bais, B., Meijer, B., Seinen, M. N., de Bree, K., ... & de Bakker, B. S. (2022). A three-dimensional analysis of the development of cranial nerves in human embryos. *Clinical Anatomy,* 35(5), 666-672. doi: 10.1002/ca.23889

[28] Solovei, V. M. (2020). Діагностика плацентарної дисфункції та прогнозування перинатальних ускладнень у жінок із невиношуванням у ранні терміни гестації (огляд літератури) [Diagnostics of placental dysfunction and prognosis of perinatal complications in women with miscarriage at early gestation (literature review)]. *Клінічна та експериментальна патологія=Clinical and Experimental Pathology,* 19(2), 91-97. doi: 10.24061/1727-4338.XIX.2.72.2020.13

[29] Vlasenko, O. V., Gunas, I. V., Semenenko, A. I., Dovgan, A. V., & Bobruk, V. P. (2023). Morphogenesis of the human brain and cerebellum in the early prenatal period. *Вісник Вінницького національного медичного університету=Reports of Vinnytsia National Medical University,* 27(2), 204-208. doi: 10.31393/reports-vnmedical-2023-27(2)-04

[30] Yamaguchi, K., & Honma, K. (2012). Development of the human abducens nucleus: A morphometric study. *Brain and Development,* 34(9), 712-718. doi: 10.1016/j.braindev.2011.12.009

МОРФОЛОГІЧНІ ОСОБЛИВОСТІ МОСТА У ПЛОДІВ ЛЮДИНИ 14-15 ТИЖНІВ ВНУТРІШНЬОУТРОБНОГО РОЗВИТКУ

Лопаткіна О. П., Тихолаз В. О., Школьніков В. С., Залевський Л. Л.

Знання ембріонального розвитку людини необхідні для покращення нашого розуміння анатомії плода людини, а також для того, щоб допомогти зрозуміти етіологію вроджених вад розвитку. На даний час велику зацікавленість у дослідників викликають структури задньої черепної ямки і стовбура мозку, тому що в ділянці моста локалізується велика кількість ядер, які відіграють важливу роль у забезпеченні життєвих функцій. Метою роботи є встановлення морфологічних особливостей моста плодів людини 14-15 тижнів гестації, розмірів та площі ядер черепних нервів та нейронів, які розташовуються в ділянці моста. Анатомо-гістологічне дослідження проводили на 6 плодах людини віком 14-15 тижнів гестації. Трупний матеріал для дослідження отримували внаслідок пізніх абортів за медичними показниками із пологових будинків міста Вінниця. Фіксацію препаратів проводили у 10 % розчині нейтрального формаліну, забарвлення проводили гематоксиліном, еозином та толуїдиновим синім за модифікацією Ніссля. Для морфометричного дослідження застосовували комп'ютерну гістометрію (Toup View). Статистичні цифрові дані були опрацьовані на персональному комп'ютері за допомогою Microsoft Excel 2016 та програмного забезпечення "Statistica 6.1". Нами було встановлено, що у плодів людини в терміні 14-15 тижнів внутрішньоутробного розвитку були виявлені ядра трійчастого, відвідного та присінково-завиткового нервів. Ядро лицевого нерву на стадії 14-15 тижнів гестації представлено поодинокими полігональними нервовими клітинами

з еозинофільною цитоплазмою. Найбільшу площу мало ядро відвідного нерву, найменшу - завиткове ядро присінково-завиткового нерву. Найбільша площа нейронів була у ядрах присінково-завиткового нерву, найменша - у ядрі відвідного та лицевого нервів. На 14-15 тижнів внутрішньоутробного розвитку плодів людини площу ядра клітини можна було визначити лише у ядрах присінково-завиткового нерву, тоді як ядра клітин у трійчастого, лицевого та відвідного нервів були представлені нервовими клітинами кулястої форми з ядром, в якому відмічалося базофільне ядерце та гомогенна еозинофільна цитоплазма. Таким чином, у плодів людини 14-15 тижнів внутрішньоутробного розвитку були виявлені відмінності у розмірах та площах ядер черепних нервів і нейронів, які формують ядра в ділянці моста.
Ключові слова: *плоди людини, гестаційний вік, ембріональний розвиток, міст, ядра моста, нейрони ядер моста.*

Author's contribution

Lopatkina O. P. - research, methodology and writing of the original draft, data visualization.
Tykholaz V. O. - review writing and editing, formal analysis and validation, resources.
Shkolnikov V. S. - supervision, project administration.
Zalevskyi L. L. - software, conceptualization.

DOI: 10.31393/morphology-journal-2024-30(2)-05 Reports of Morphology, Vol. 30, №2, Pages 37-43

ISSN 1818-1295 eISSN 2616-6194

REPORTS OF MORPHOLOGY

Official Journal of the Scientific Society of Anatomists, Histologists, Embryologists and Topographic Anatomists of Ukraine

journal homepage: https://morphology-journal.com

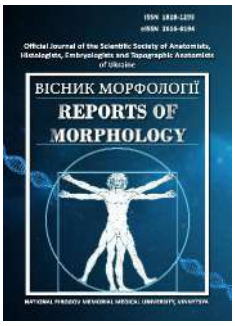

Fetal ultrasound anatomy and morphometric parameters of the tibia

Komar T. V., Khmara T. V., Protsak T. V., Zamorskii I. I., Kovalchuk P. Ye. Halaturnyk I. B.

Bukovinian State Medical University, Chernivtsi, Ukraine

ARTICLE INFO

Received: 22 January 2024

Accepted: 13 March 2024 2024

UDC: 611.98-047.37-026.572.2

CORRESPONDING AUTHOR

e-mail: komar.tetiana.ls14@bsmu.edu.ua

Komar T. V.

CONFLICT OF INTEREST

The authors have no conflicts of interest to declare.

FUNDING

Not applicable.

DATA SHARING

Data are available upon reasonable request to corresponding author.

Ultrasound screening is one of the most informative methods of visualizing fetal development during pregnancy. During standard ultrasound examinations, the length of the femur of the fetus is measured. However, if any skeletal dysplasia or intrauterine growth retardation is suspected, additional measurement of other long tubular bones should be performed. The aim of the work was to investigate the morphometric parameters of the lengths of the right and left tibia bones and to establish correlations between them and the lengths of the corresponding fibula, lower limb and crown rump length of the fetus during the fetal period of human ontogenesis. Intravital ultrasound examination of the leg bones of 38 human fetuses was performed at the medical center "YUZKO MEDICAL CENTER" in accordance with the cooperation agreement. Built-in capabilities of MS Excel were used for statistical calculations. The established data on the fetal morphometry of tibial lengths indicate relatively uniform growth of the right and left tibias during the fetal period of human ontogenesis: the length of the right tibia increases from 24.77±2.25 mm to 65.32±2.20 mm, and the length of the left tibia increases from 25.19±1.63 mm to 65.78±1.81 mm. The analysis of correlations between the length of the right and left tibia bones, the length of the fibula bones, the length of the lower limbs and the crown rump length in human fetuses aged from 4 to 10 months of intrauterine development allowed to reveal reliable strong and medium strength reliable and unreliable, mostly direct, connections in all age groups. The obtained morphometric parameters of tibia bones in fetuses of different gestational periods are important additional dimensions of fetobiometry, which can be used if a detailed assessment of the state of fetal development is necessary and in case of suspicion of congenital anomalies.

Keywords: *ultrasound diagnostics, tibia, morphometry, fetus, human.*

Introduction

Philippe Jeanty, MD, well-known in obstetrics and gynecology, made a significant contribution to the study of fetal ultrasound anatomy, biometry, diagnosis of congenital anomalies and for the first time traced the dynamics of fetal growth, described the growth of long tubular bones, as well as abdominal circumference and subsequently estimated the weight of the fetus. The scientist devoted his dissertation work to fetometry - the assessment of fetal growth by measuring the parameters of long tubular bones. At this very early stage in the development of ultrasound imaging, when ultrasound still only vaguely distinguished bones, Philippe Jeanty undertook a large-scale project to measure all the major long tubular bones (humerus, femur, ulna, radius, tibia and fibula) in a large number of fetuses and developed charts morphometric parameters of the long tubular bones of the fetus to determine the gestational age, which still do not lose their relevance [26].

Today, ultrasound screening remains one of the most informative methods of visualizing the normal development of the fetus during certain periods of pregnancy. This method allows not only to assess the general condition of the fetus, but also to determine the morphometric parameters of organs and structures, which is important for timely diagnosis of any birth defects or anomalies [1, 20].

Measurement of the length of the long tubular bones of the fetus is used to analyze the fetal anatomy and estimate the gestational age. In addition, this parameter is key for the early detection of chromosomal abnormalities and osteochondrodysplasias [7, 12, 27]. In conventional ultrasound examinations, the length of the femur of the fetus is usually measured, but in case of suspicion of any skeletal dysplasia or intrauterine growth retardation, it is necessary to additionally measure other long tubular bones for a more detailed assessment of the condition of the fetus.

Triple screening ultrasound examination of pregnant women makes it possible to detect anomalies and

deviations in the development of the fetus. Researchers are interested in the intermediate period of the ontogenesis of the fetus, which corresponds to the period of development from 16 to 28 weeks of the intrauterine period. It is at this time that all organs and systems of the fetus are actively forming, coinciding with the second standard ultrasound screening. Despite certain difficulties of ultrasound diagnostics, its effectiveness in detecting fatal skeletal anomalies ranges from 94 % to 96 %. Abnormalities of the lower extremity in general, such as campomelia, sirenomelia, and phocomelia, are rarely found in the literature. Instead, congenital malformations of the tibia or fibula, such as hemimelia, hypoplasia, congenital false joint, or congenital curvature, are more commonly noted. Most often, congenital malformations and anomalies of the shin bones are unilateral (31 %) [3, 8, 13, 23].

Modern international standards of fetal growth rate are presented in the INTERGROWTH-21 program, which was developed for comprehensive monitoring of normal fetal development around the world. Curves of the growth rate of the fetus help to understand the normogenesis of the fetus and the occurrence of pathological changes in its development. It is ultrasound diagnostics that allows you to visualize all planes of the fetus, which are necessary for accurate biometric measurements. The fetal growth profile includes 12 biometric parameters: biparietal diameter, occipital-frontal diameter, head circumference, transverse and sagittal diameters of the abdomen, abdominal circumference, lengths of the femur, tibia, fibula, humerus, radius, and ulna [13, 21]. Measurement of the length of the long tubular bones is also used to determine the age and time of death of the fetus in case of its intrauterine death [14].

At present, it is the combination of imaging parameters obtained with the help of ultrasound diagnostics, computer and magnetic resonance imaging that allows not only to detect congenital malformations, but also to predict mortality before the birth of a child [4, 11, 19]. Possible applications of these measurements include: intrauterine diagnosis of fetal growth retardation [6], congenital malformations of limbs, determination of gestational age, archaeological dating of fetuses, forensic research [9, 20], introduction of ultrasound modeling in medical education [12]. Our study of the morphometric parameters of the lower leg bones during the fetal period of human ontogenesis is a continuation of our own research.

The aim of the work was to investigate the morphometric parameters of the lengths of the right and left tibia bones and to establish correlations between them and the lengths of the corresponding fibula, lower limb and crown rump length of the fetus during the fetal period of human ontogenesis.

Materials and methods

Intravital ultrasound examination of the shin bones of 38 human fetuses was performed using a 3.5 MHz convex sensor on a Voluson E8 ultrasound scanner (manufactured by General Electric, 2013) in the medical center "YUZKO MEDICAL CENTER" in accordance with the cooperation agreement. Measurements were performed according to standardized protocols by an experienced sonologist. The length of the tibia was determined by measuring the distance between the extreme points of the proximal and distal epiphyses. Lateral and medial cuneiform bones, which are used as reference points for measurement in adults, have not yet been determined in fetuses of this age. The tibia was measured in a plane so that the latter was as close as possible to the angle of passage of the ultrasound beam so that the full length of the bone was visualized and was not obscured by the shadow of the adjacent bone parts. If any abnormality was detected in the fetus during the ultrasound diagnosis, the fetus was not included in the sample. The study was conducted in accordance with the main bioethical provisions of the Council of Europe Convention on Human Rights and Biomedicine (from 04.04.1997), the Helsinki Declaration of the World Medical Association on the ethical principles of conducting scientific medical research with human participation (1964-2013), order of the Ministry of Health of Ukraine № 690 dated 23.09.2009, the Commission on Biomedical Ethics of the Bukovinian State Medical University (Protocol № 3 dated 16.11.2023) did not detect any violations of moral and legal norms during the conduct of research work.

The built-in features of MS Excel were used to perform statistical calculations, including the calculation of the arithmetic mean and standard deviation. Comparison between study groups was performed using the non-parametric Mann-Whitney test, which was performed in the Excel environment. The level of significance of individual indicators relative to the corresponding ones in different age periods of human fetal development is determined. In addition, the Pearson correlation coefficient was determined between the morphometric indicators of the length of the tibia and the lengths of the fibula, lower limb and crown rump length in human fetuses of 4-10 months.

Results

As a result of the research, morphometric characteristics of the length of the right and left tibia bones in human fetuses of 4-10 months were established (Table 1).

Measurements of the length of the tibia of fetuses of the indicated age showed that the length of the right tibia increased by 2.64 times, from 24.77±2.25 mm to 65.32±2.20 mm, and the length of the left tibia increased by 2.61 times, from 25.19±1.63 mm to 65.78±1.81 mm (Fig. 1-8, see Table 1).

During the analysis of the obtained data, two active periods of tibial bone growth were revealed: from the end of the 5th to the end of the 6th month of intrauterine development and during the 7th month of the fetal period of development. At the same time, a slowdown in the growth of the right and left tibia bones is observed in the 4th and 10th months of intrauterine development (Fig. 9).

In the period of human fetal development, the length of

Table 1. The length of tibia bones in human fetuses aged 4-10 months (M±σ).

Gestation period	Number of fetuses (n)	Length of tibia (mm)	
		right	left
4 months	6	24.77±2.25	25.19±1.63
5 months	6	30.78±2.27*	31.04±2.16*
6 months	6	39.96±2.07*	40.82±1.91*
7 months	6	47.27±1.49*	48.56±1.32*
8 months	5	54.05±1.41*	54.93±1.01*
9 months	5	60.48±1.72*	61.13±1.46*
10 months	4	65.32±2.20*	65.78±1.81*

Notes: * - the level of significance between individual indicators relative to the previous month of gestation ($p<0.05$).

Fig. 1. Sonogram of the tibia and fibula bones of a human fetus at 16 weeks and 4 days of gestation. TIB - length of the tibia; FIB - length of the fibula.

Fig. 2. Sonogram of the tibia of a human fetus at 18 weeks 6 days of gestation. TIB - length of the tibia.

the right lower limb increases from 44.87±3.33 mm to 192.1±5.7 mm, and the length of the left lower limb increases from 44.45±3.19 mm to 194.1±5.9 mm (Table 2).

During the analysis of correlations between the length of the right and left tibia bones in human fetuses aged from 4 to 10 months of intrauterine development, reliable strong direct correlations were found in all age groups (r= from 0.71 to 0.89). Between the length of the right tibia and the right fibula in 4-month-old fetuses, a reliable strong direct

Fig. 3. Sonogram of the tibia of a human fetus at 20 weeks and 2 days of gestation. TIB - length of the tibia.

Fig. 4. Sonogram of the tibia of a human fetus at 21 weeks and 6 days of gestation. TIB - length of the tibia.

Fig. 5. Sonogram of the tibia of a human fetus at 22 weeks and 4 days of gestation. TIB - length of the tibia.

Fig. 6. Sonogram of the tibia of a human fetus at 29 weeks 6 days of gestation. TIB - length of the tibia.

Fig. 7. Sonogram of the tibia of a human fetus at 31 weeks and 3 days of gestation. TIB - length of the tibia.

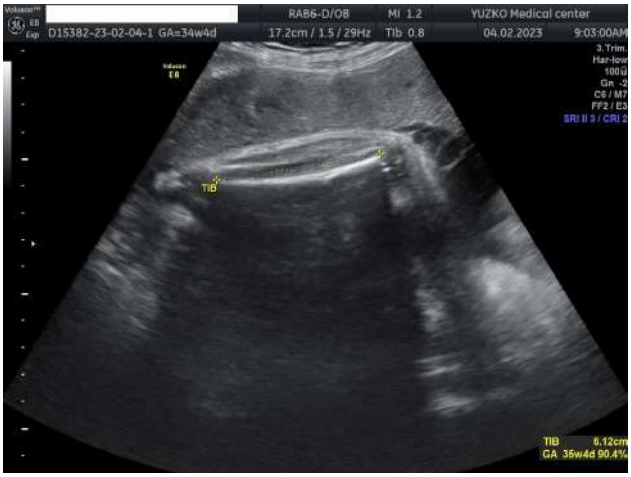

Fig. 8. Sonogram of the tibia of a human fetus at 34 weeks and 4 days of gestation. TIB - length of the tibia.

correlation was established (r=0.97), in 7-month-old fetuses there was an unreliable inverse correlation of medium strength (r=-0.38), in all other age groups - reliable and unreliable direct correlations of average strength (r= from 0.32 to 0.62). When analyzing correlations between the length of the right tibia and the length of the right lower limb, unreliable weak direct correlations were found in fetuses of 5, 8 and 10 months (r= from 0.10 to 0.21), unreliable and reliable direct correlations of medium strength in fetuses 4 and 9 months (r=0.36 and 0.50), in 6-month-old fetuses - reliable medium strength inverse correlations (r=-0.57). In fetuses of 7 months, correlations between the length of the right tibia and the length of the right lower limb are absent.

During the assessment of correlations between the length of the right tibia and crown rump length, the following was found: unreliable weak direct correlations in fetuses of almost all age groups (r= from 0.10 to 0.29), with the exception of fetuses of 8 and 9 months of age, in which unreliable average direct correlations (r=0.31 and 0.32).

According to the results of the study of the correlation dependence between the length of the left tibia and the length of the left lower limb, reliable and unreliable direct correlations of average strength were found in fetuses of 8-10 months (r= from 0.39 to 0.59), reliable inverse correlations of average strength in fetuses of 6 months of age (r=-0.57). In fetuses of 5 months, unreliable weak direct correlations (r=0.28) were established, and in fetuses of 4 and 7 months,

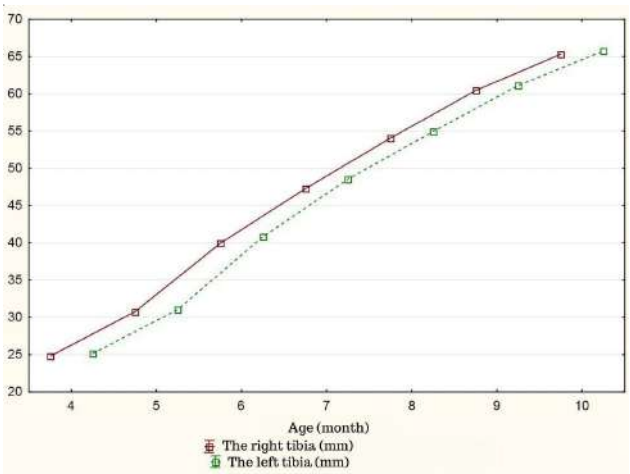

Fig. 9. Dynamics of changes in the length of tibia bones in fetuses aged 4-10 months.

Table 2. The length of the lower limbs in human fetuses aged 4-10 months (M±σ).

Gestation period	Number of fetuses (n)	Length of the lower limb (mm)	
		right	left
4 months	20	44.87±3.33	44.45±3.19
5 months	21	73.55±6.56*	74.06±6.51*
6 months	19	100.2±2.9*	99.40±2.65*
7 months	15	126.9±2.7*	124.4±3.5*
8 months	10	141.1±1.3*	141.8±1.4*
9 months	8	161.1±2.7*	161.5±3.9
10 months	9	192.1±5.7*	194.1±5.9*

Notes: * - the level of significance between individual indicators relative to the previous month of gestation (p<0.05).

correlations between the length of the left tibia and the length of the left lower limb were not observed.

Evaluating the correlations between the length of the left tibia and the length of the left fibula, the following was established: strong reliable direct correlations in fetuses of 4 months of age (r=0.97), reliable and unreliable direct correlations of medium strength in fetuses of 5, 6, 8 and 9 months (r= from 0.44 to 0.66), unreliable weak direct correlations in fetuses of 10 months (r=0.25).

In fetuses of 7 months, correlations between the length of the left tibia and the length of the left fibula were not observed. During the analysis of correlations between the length of the left tibia and crown rump length, we found the following: in fetuses aged from 7 to 10 months of intrauterine development, reliable and unreliable direct correlations of medium strength are observed (r= from 0.40 to 0.54), in 4- and 5-month-old fetuses - unreliable weak direct correlations (r=0.13 and 0.19), and in 6-month-old fetuses, reliably strong inverse correlations (r=-0.98) were established.

Discussion

Thus, the conducted morphometric study made it possible to evaluate the correlations between the lengths of the right and left tibia bones, right and left fibula bones and lower limbs in human fetuses of 4-10 months, as well as fetuses crown rump length. Two periods of intensive growth of the length of the right and left tibia bones were established, namely: from the end of the 5th month to the end of the 6th month of intrauterine development and during the 7th month of the fetal period of human ontogenesis. The periods of slow growth of the tibia are the 4th and 10th months of gestation.

Undoubtedly, an integral part of prenatal examination is ultrasound diagnostics, which is highly informative and safe, and every year not only the technical capabilities of ultrasound machines, but also the system for assessing the development of the fetus are improved. R. Yousefpour Shahrivar et al. [28] emphasize the need for further research in this field, which will contribute to more effective detection of fetal abnormalities based on ultrasound.

Our study confirms the opinion of some authors [2, 11], who claim that ultrasound measurement of the bones of the lower leg is simpler than that of the forearm. This is because the tibia and fibula are similar in size and location, making them easier to visualize with ultrasound. Despite the difficulty of accurate diagnosis, the frequency of detection of fatal anomalies of the skeleton using ultrasound is 94-96%. Even if an anomaly of the musculoskeletal system is diagnosed, not all prenatal diagnostics are complete, in some cases additional examination is required after childbirth [13, 22]. Although ultrasonography plays almost the most important role in detecting skeletal abnormalities [17, 25], some authors believe that genetic tests at the molecular level should be used to confirm chromosomal mutations and improve the accuracy of prenatal diagnosis [16].

In the sources of literature [10, 12] we find data that most often congenital malformations and anomalies of tibia bones are unilateral, however, we did not detect differences in the growth of the right and left tibia bones, changes in their structure and developmental anomalies in the examined fetuses.

The periods of intensive growth of the lengths of the right and left tibia bones that we established are partially consistent with existing data [1, 14]. However, we did not have information about the peculiarities of the course of pregnancy, the presence of concomitant diseases of the mother, or the peculiarities of her diet.

Graphs of changes in the length of long tubular bones are widely used in clinical practice to track the growth of children. They were developed on the basis of detailed studies of normal bone development of different age groups. In 2006, the World Health Organization published the child development standards of the World Health Organization, which were widely used in practice [15]. However, some researchers even today question their use, because they do not take into account the characteristics of different populations and emphasize the need to have local standards of fetal biometrics [24, 30].

Plots of CT measurements against published sonographic values for age also showed strong and significant correlations, suggesting that the data can be used interchangeably [29].

Fetal growth retardation often complicates the course of the antenatal and postnatal periods, but currently there is no definitive treatment other than delivery. It is believed that the development of unified international protocols for the early recognition, follow-up and optimal management of fetuses with growth retardation will be able to improve the perinatal outcomes of such pregnancies [10]. Growth assessment protocols can potentially help prevent stillbirth, which is often associated with fetal growth retardation [5]. Existing studies during intrauterine development indicate the absence of significant gender differences in the length and structure of the tibia. However, gender differences in the ratio of femur to tibia were determined in adults ($p<0.05$) [18].

Conclusions

1. There were no significant differences in the length of the right and left tibia bones during the fetal period of human ontogenesis, and therefore the right and left tibia bones grow evenly.

2. It was established that an intensive increase in the length of the right and left tibia bones is observed from the end of the 5th to the end of the 6th month and during the 7th month of intrauterine development. The periods of slow increase in their length are the 4th and 10th months of intrauterine development.

3. Between the length of the right and left tibia bones, the length of the fibula bones, the lower limbs and the crown rump length in human fetuses of different gestational periods, multiple reliable and unreliable, mostly direct, medium-strength relationships were established.

References

[1] Aggarwal, N., & Sharma, G. L. (2020). Fetal ultrasound parameters: Reference values for a local perspective. The *Indian Journal of Radiology & Imaging,* 30(2), 149-155. doi: 10.4103/ijri.IJRI_287_19

[2] Baschat, A. A. (2018). Planning management and delivery of the growth- restricted fetus. *Best Pract Res Clin Obstet Gynaecol,* 49, 53-65. doi: 10.1016/j.bpobgyn.2018.02.009

[3] Basso, M., Camurri, V., Frediani, P., & Boero, S. (2018). A rare case of tibial hemimelia, surgical technique and clinical results. *Acta Orthop Traumatol Turc,* 52(4), 315-519. doi: 10.1016/j.aott.2017.11.004

[4] Broere-Brown, Z. A., Schalekamp-Timmermans, S., Jaddoe, V. W. V., & Steegers, E. A. P. (2019). Deceleration of fetal growth rate as alternative predictor for childhood outcomes: a birth cohort study. *BMC Pregnancy Childbirth*, 19(1), 216. doi: 10.1186/s12884-019-2358-8

[5] Butler, E., Hugh, O., & Gardosi, J. (2022). Evaluating the Growth Assessment Protocol for stillbirth prevention: progress and challenges. *Journal of Perinatal Medicine*, 50(6), 737-747. doi: 10.1515/jpm-2022-0209

[6] Cupello, A. J., Ambrosio, J. D., & de Vasconcellos, H. A. (1995). Growth of the tibia and fibula bones in human fetuses. *Bulletin de l'Association Des Anatomistes*, 79(246), 17-20. PMID: 8541605

[7] Deguchi, M., Tsuji, S., Katsura, D., Kasahara, K., Kimura, F., & Murakami, T. (2021). Current Overview of Osteogenesis Imperfecta. *Medicina* (Kaunas), 57(5), 464. doi: 10.3390/medicina57050464

[8] Dobbe, A. M., & Gibbons, P. J. (2017). Common paediatric conditions of the lower limb. *J Paediatr Child Health,* 53(11), 1077-1085. doi: 10.1111/jpc.13756

[9] Fewtrell, M. S., Loh, K. L., Chomtho, S., Kennedy, K., Hawdon, J., & Khakoo, A. (2008). Quantitative ultrasound (QUS): a useful tool for monitoring bone health in preterm infants? *Acta Paediatr,* 97(12), 1625-1630. doi: 10.1111/j.1651-2227.2008.00992.x

[10] Giouleka, S., Tsakiridis, I., Mamopoulos, A., Kalogiannidis, I., Athanasiadis, A., & Dagklis, T. (2023). Fetal Growth Restriction: A Comprehensive Review of Major Guidelines. *Obstetrical & Gynecological Survey,* 78(11), 690-708. doi: 10.1097/OGX.0000000000001203

[11] Hani, S., Chalouhi, G., Lakissian, Z., & Sharara-Chami, R. (2019). Introduction of Ultrasound Simulation in Medical Education: Exploratory Study. *JMIR Med Educ,* 5(2), e13568. doi: 10.2196/13568

[12] Hugh, O., Cowan, J., Butler, E., & Gardosi, J. (2023). Fetal size vs growth: comparative analysis of three models of growth velocity based on third trimester estimated fetal weights for identifying stillbirth risk. *Am J Obstet Gynecol,* 2023, S0002-9378(23)02188-9. Online ahead of print. doi: 10.1016/j.ajog.2023.12.029

[13] Khmyzov, S., Yakushkin, Y., & Katsalap, Y. (2021). Нестабільність колінного суглоба за умов уроджених вад розвитку нижніх кінцівок (огляд літератури) [Knee joint instability in conditions of congenital malformations of the lower extremities (literature review)]. *Ортопедія, травматологія та протезування=Orthopaedics Traumatology and Prosthetics,* 1, 80-85. doi: 10.15674/0030-59872021180-85

[14] Kim, M. J., Hutcheon, J. A., Lee, A. F., & Liauw, J. (2024). Autopsy-Based Growth Charts May under-Detect Fetal Growth Restriction at Autopsy. *Fetal and Pediatric Pathology,* 1-10. doi: 10.1080/15513815.2023.2299491

[15] Kiserud, T., Piaggio, G., Carroli, G., Widmer, M., Carvalho, J., Neerup Jensen, L., ... & Platt, L. D. (2017). The World Health Organization fetal growth charts: a multinational longitudinal study of ultrasound biometric measurements and estimated fetal weight. *PLoS medicine,* 14(1), e1002220. doi: 10.1371/journal.pmed.1002220

[16] Lee, S. H., Kim, T. H., Lee, H. H., Park, J., Chung, S. H., & Jeon, D. S. (2013). Length measurement of fetal long bone and fetal anomaly detection. *Webmed Central Obstetrics and Gynaecology*, 4(5), WMC004236. doi: 10.9754/journal.wmc.2013.004236

[17] Levitskyi, A. F., & Benzar, I. M. (2019). *Основи діагностики, лікування та реабілітації вад розвитку опорно-рухового апарату в дітей [Basics of Diagnosis, Treatment and Rehabilitation of Developmental Defects of the Musculoskeletal System in Children].* Тернопіль: Укрмедкнига=Ternopil: Ukrmedknyg.

[18] Matsubara, Y., Higaki, T., Tani, C., Kamioka, S., Harada, K., Aoyama, H. … & Awai, K. (2020). Demonstration of Human Fetal Bone Morphology with MR Imaging: A Preliminary Study. *Magnetic Resonance in Medical Sciences,* 19(4), 310-317. doi: 10.2463/mrms.mp.2019-0105

[19] Mascherpa, M., Pegoire, C., Meroni, A., Minopoli, M., Thilaganathan, B., Frick, A., & Bhide, A. (2023). Prenatal prediction of adverse outcome using different charts and definitions of fetal growth restriction. *Ultrasound Obstet Gynecol.* Online ahead of print. doi: 10.1002/uog.27568

[20] Merz, E., Pashaj, S., & Wellek S. (2023). Normal Fetal Growth Profile at 10-41 Weeks of Gestation - An Update Based on 10225 Normal Singleton Pregnancies and Measurement of the Fetal Parameters Using 3D Ultrasound. *Ultraschall Med*, 44(2), 179-187. doi: 10.1055/a-1968-0018

[21] Ohuma, E. O., Villar, J., Feng, Y., Xiao, L., Salomon, L., Barros, F. C., & Papageorghiou, A. T. (2021). Fetal growth velocity standards from the Fetal Growth Longitudinal Study of the INTERGROWTH-21 st Project. *Am J Obstet Gynecol,* 224(2), 208. doi: 10.1016/j.ajog.2020.07.054

[22] Pang, H. Q., & Gao, Q. Q. (2021). Prenatal ultrasonographic findings in Klippel-Trenaunay syndrome: A case report. *World J Clin Cases,* 9(35), 10994-10998. doi: 10.12998/wjcc.v9.i35.10994

[23] Papageorghiou, A. T., Kemp, B., Stones, W., Ohuma, E. O., Kennedy, S. H., Purwar, M., … & Villar, J. (2016). Ultrasound-based gestational-age estimation in late pregnancy. *Ultrasound Obstet Gynecol*, 48(6), 719-726. doi: 10.1002/uog.15894

[24] Parikh, L. I., Nolan III, J., Tefera, E., Driggers, R. (2014). Fetal biometry: does patient ethnicity matter? *The Journal of Maternal-Fetal & Neonatal Medicine*, 27(5), 500-504. doi: 10.3109/14767058.2013.820696

[25] Prokopchuk, N. M., Nikolenko, M. I., Korinets, Ya. M., & Ivaniv, Yu. A. (2023). Оцінка результатів пренатальної діагностики вроджених вад розвитку плоду у жінок в різні терміни гестації [Evaluation of the results of prenatal diagnostics of congenital defects of fetal development in women in different terms of gestation]. *Перспективи та інновації науки. Педагогіка. Психологія. Медицина=Prospects and Innovations of Science. Psychology. Pedagogy. Medicine,* 10(28), 796-808. doi: 10.52058/2786-4952-2023-10(28)-796-808

[26] Romero, R. (2021). Giants in Obstetrics and Gynecology Series: Philippe Jeanty, MD, PhD, a pioneer in the study of fetal anatomy, biometry, growth, and congenital anomalies. *Am J Obstet*

Gynecol, 225(1), 3-9. doi: 10.1016%2Fj.ajog.2021.03.043
[27] Tsai, A., Laor, T., Estroff, J. A., & Kasser, J. R. (2018). Constant inhibition in congenital lower extremity shortening: does it begin in utero? *Pediatric Radiology*, 48(10), 1451-1462. doi: 10.1007/s00247-018-4153-5
[28] Yousefpour Shahrivar, R., Karami, F., & Karami, E. (2023). Enhancing Fetal Anomaly Detection in Ultrasonography Images: A Review of Machine Learning-Based Approaches. *Biomimetics* (Basel), 8(7), 519. doi: 10.3390/biomimetics8070519
[29] Victoria, T., Shakir, N. U., Andronikou, S., Edgar, J. C., Germaine, P., Epelman, M., … & Jaramillo, D. (2016). Normal Fetal Long Bone Length from Computed Tomography: Potential Value in the Prenatal Evaluation of Skeletal Dysplasias. *Fetal Diagnosis and Therapy,* 40(4), 291-297. doi: 10.1159/000444184
[30] Žaliūnas, B., Jakaite, V., Kurmanavičius, J., Bartkevičiene D., Norvilaite, K., & Passerini, K. (2022) Reference values of fetal ultrasound biometry: results of a prospective cohort study in Lithuania. *Arch Gynecol Obstet,* 306(5), 1503-1517. doi: 10.1007/s00404-022-06437-z

ФЕТАЛЬНА УЛЬТРАЗВУКОВА АНАТОМІЯ І МОРФОМЕТРИЧНІ ПАРАМЕТРИ ВЕЛИКОГОМІЛКОВОЇ КІСТКИ

Комар Т. В., Хмара Т. В., Процак Т. В., Заморський І. І., Ковальчук П. Є., Халатурник І. Б.

Ультразвуковий скринінг є одним із найінформативніших методів візуалізації розвитку плода під час вагітності. Під час стандартних ультразвукових досліджень вимірюють довжину стегнової кістки плода. Проте, у випадку, якщо існує підозра на будь-яку скелетну дисплазію або затримку внутрішньоутробного розвитку, необхідно провести додаткове вимірювання інших довгих трубчастих кісток. Метою роботи було дослідити морфометричні параметри довжин правої і лівої великогомілкових кісток та встановити кореляційні зв'язки між ними та довжинами відповідної малогомілкової кістки, нижньої кінцівки та тім'яно-куприковою довжиною плода впродовж плодового періоду онтогенезу людини. Прижиттєве ультразвукове дослідження кісток гомілки 38 плодів людини проведено у медичному центрі "YUZKO MEDICAL CENTER" згідно з договором про співпрацю. Для проведення статистичних розрахунків використовувалися вбудовані можливості MS Excel. Встановлені дані щодо фетальної морфометрії довжин великогомілкових кісток вказують на відносно рівномірний ріст правої і лівої великогомілкових кісток упродовж плодового періоду онтогенезу людини: довжина правої великогомілкової кістки збільшується з 24,77±2,25 мм до 65,32±2,20 мм, а довжина лівої великогомілкової кістки збільшується з 25,19±1,63 мм до 65,78±1,81 мм. Аналіз кореляційних зв'язків між довжиною правої та лівої великогомілкових кісток, довжинами малогомілкових кісток, довжиною нижніх кінцівок і тім'яно-куприковою довжиною у плодів людини віком від 4 до 10 місяців внутрішньоутробного розвитку дозволив виявити достовірні сильні та середньої сили достовірні й недостовірні, переважно прямі, зв'язки у всіх вікових групах. Отримані морфометричні параметри великогомілкових кісток у плодів різного терміну гестації є важливими додатковими розмірами фетобіометрії, котрі можуть бути використані за необхідності детальної оцінки стану розвитку плода та при підозрі на уроджені аномалії.

Ключові слова: *ультразвукова діагностика, великогомілкова кістка, морфометрія, плід, людина.*

Author's contribution

Komar T. V. - research concept and design, receiving data, analysis an interpretation of data, design of the article.
Khmara T. V. - analysis and interpretation of data, critical review, final approval.
Protsak T. V. - analysis and interpretation of data, critical review, design of the article.
Zamorskii I. I. - analysis and interpretation of data, critical review, final approval.
Kovalchuk P. Ye. - analysis and interpretation of data, critical review, final approval.
Halaturnyk I.B. - receiving data, analysis an interpretation of data, final approval.

DOI: 10.31393/morphology-journal-2024-30(2)-06 **Reports of Morphology, Vol. 30, №2, Pages 44-52**

ISSN 1818-1295 eISSN 2616-6194

REPORTS OF MORPHOLOGY

Official Journal of the Scientific Society of Anatomists, Histologists, Embryologists and Topographic Anatomists of Ukraine

journal homepage: https://morphology-journal.com

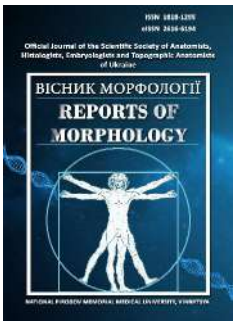

Stromal-cellular remodeling of breast tissue after silicone implant damage

Dadayan V. A.[1], Adamovych O. O.[2], Simonov V. F.[1], Kozhan V. I.[3], Poliiants A. V.[4], Hrytsenko A. P.[1], Chelpanova I. V.[2]

[1]"Grace Clinic", Kyiv, Ukraine
[2]Danylo Halytsky Lviv National Medical University, Lviv, Ukraine
[3]Korosten Central Hospital, Korosten, Ukraine
[4]Kyiv Regional Clinical Hospital, Kyiv, Ukraine

ARTICLE INFO
Received: 17 January 2024
Accepted: 19 March 2024

UDC: 618.19-091.8-06:616-089.843

CORRESPONDING AUTHOR
e-mail: ilona.med75@gmail.com
Chelpanova I. V.

CONFLICT OF INTEREST
The authors have no conflicts of interest to declare.

FUNDING
Not applicable.

DATA SHARING
Data are available upon reasonable request to corresponding author.

One of the current vectors of modern reconstructive and cosmetic surgery is augmentation mammoplasty - an operation to enlarge the mammary glands. The breast implant is well tolerated by the body, as the immunogenicity of its material is extremely low. At the same time, the silicone gel of the implant is a foreign object and the surrounding breast tissues give a stereotypical response in the form of growth of the connective tissue stroma with the formation of a capsule around the implant and the appearance of focal cellular infiltrates. Modern breast implants, unlike implants of previous decades, are more sophisticated in their structure, and the level of protection against damage is much higher. A complication associated with the long-term use (up to 20 years) of implants, where low-quality silicone or industrial silicone was used as a filler, is the penetration of low-molecular-weight particles of the implant through its shell to the surrounding tissues with the subsequent formation of silicone granules. In the vast majority, such changes develop after mechanical traumatization of the implant. The purpose of the study is to establish the morphological criteria of the reaction of breast tissue after silicone implant damage. The material for research was histological micropreparations of breast tissue from the archive of the "Grace Clinic" (Kyiv), with the mutual consent of patients who applied for repeated mammoplasty. The duration of the implants in the breast gland was from 6 to 20 years. The age range of the women was from 36 to 53 years. On preparations stained with hematoxylin and eosin, tissue biopsies of the glands of 9 patients with a diagnosis of deformation of silicone implants and violation of the integrity of their wall were presented. The micropreparations were visualized using a UlabXSP-137TLED light microscope at various magnifications and photographed with an XCAM 1080P camera. The study of histological preparations of soft tissues of the breast glands, from which silicone implants were removed, established changes in stromal-cellular elements, namely: decorated fibrous structures accumulated in the form of dense capsules with elements of local contractures; from the side of cellular elements, the most demonstrative were cellular infiltrates, which included macrophages, lymphocytes, and plasma cells, which indicated a high probability of a chronic inflammatory process. A large number of giant multinucleated cells of foreign bodies were present in practically all examined sections, which indicated the impossibility of macrophages to complete phagocytosis with lysis of the phagocytosed material, which by its chemical composition is the silicone of the implant. All the described phenomena can be interpreted as a natural reaction of the tissues to the implant, the contents of which got into the soft tissues of the breast. Thus, the presence of numerous giant multinucleated cells of foreign bodies, dense capsules with elements of local contractures, and a significant predominance of macrophages, lymphocytes, and plasma cells in cellular infiltrates over other cellular elements can be considered a morphological criterion for the reaction of breast tissue to silicone implant damage.

Keywords: *mammary/breast gland, breast implant, breast silicone implant damage, aesthetic surgery, microscopy, histopathological diagnosis, implant-associated fibrotic changes.*

Introduction

One of the relevant vectors of modern reconstructive and cosmetic surgery is augmentation mammoplasty - an operation to enlarge the mammary glands, which is most often chosen by patients [1, 20]. As a rule, the breast implant is well tolerated by the body, since the immunogenicity of its material is extremely low. At the same time, the silicone gel of the implant is a foreign object [22, 23, 32, 40]. Therefore, when it is installed, the surrounding tissues of the breast gland make a stereotypical response in the form of growth of the connective tissue stroma with the formation of a capsule around the implant and the appearance of focal cellular infiltrates [2, 10, 19, 26]. A complication of such phenomena can sometimes be the formation of Baker grade IV capsular contracture, which gives the gland incredible hardness and a bad aesthetic appearance [5, 37, 45]. In the scientific literature, there are descriptions of complications associated with the use of industrial silicone as an implant filler, which often occurred at the beginning of the development of breast implantation [10, 28, 30, 38]. In such cases, the penetration of low-molecular-weight particles of the implant through its shell to the surrounding tissues with the subsequent formation of silicone granulomas was observed [14, 16]. The authors of these studies note that most often such changes develop after mechanical damage to the implant, mainly as a result of trauma.

The scientific literature also contains data on other morphological variants of the reaction of breast tissue to the implant [11, 31, 34]. The most common among them is synovial metaplasia (transdifferentiation) [7, 27], in which epithelioid cells similar to synovial cells appear on the inner surface of the fibrous capsule bordering the implant, and in general, this structure resembles a joint [28]. In cases of mechanical damage to the implant, the formation of silicone granulomas, which are represented by multiple cystic spaces filled with silicone spherules, is not excluded. On the periphery of such spaces, fibrosis and a macrophage reaction with the formation of giant multinucleated cells of foreign bodies is observed. Such changes occur, as a rule, with extracapsular rupture of a silicone implant with a violation of the integrity of the fibrous capsule [16].

Modern breast implants, unlike implants of previous generations, are more sophisticated in their structure, and their level of protection against damage is much higher [28]. However, if injuries occur, clinical symptoms are minimal, with a relatively favorable prognosis for the occurrence of significant pathomorphological changes.

The purpose of our study was to establish the morphological criteria of the reaction of breast tissue after silicone implant damage.

Materials and methods

The work was approved at a meeting of the Bioethics Commission of Danylo Halytsky Lviv National Medical University; Protocol № 7 dated 26.06.2023 on compliance with the basic bioethical provisions of the Council of Europe Convention on Human Rights and Biomedicine (dated 04.04.1997), the Helsinki Declaration of the World Medical Association on Ethical Principles of Scientific Medical Research with Human Participation (1964-2008), and also the Order of the Ministry of Health of Ukraine № 690 dated 23.09.2009.

The material for the research was histological micropreparations of breast tissue from the archive of the "Grace Clinic" (Kyiv) with the mutual consent of patients who applied for repeated mammoplasty. Treatment included removal of damaged implants, capsulotomy due to the development of capsular fibrosis, and repeat mammoplasty.

According to the anamnesis, all patients were healthy, and none of them had signs of an autoimmune disease or other connective tissue pathology. The duration of the implants in the gland was from 6 to 20 years, and the age range of the women was 36-53 years.

A morphological study of the removed tissues was carried out. On preparations stained with hematoxylin and eosin, tissue biopsies of breast glands of 9 patients with a diagnosis of deformation of silicone implants and violation of the integrity of their wall, presence of capsular contracture are presented. On the basis of the Department of Histology, Cytology and Embryology of the Danylo Halytsky Lviv National Medical University, micropreparations were visualized using a UlabXSP-137TLED light microscope at various magnifications and photographed using an XCAM 1080P camera.

The identified morphological features of changes in the fibrous capsule were assigned to one of four types (I-IV) according to the classification of Wilflingseder et al. (1983) [8, 44], which is consistent with Baker's classification, which is used in clinical practice [1, 11, 12, 29].

Morphological criteria of breast tissue response to the implant and changes in the fibrous capsule, according to the classification of Wilflingseder et al. (1983) included a thin, loose capsule (type I), "constrictive fibrosis", absence of foreign body giant cells (type II), "constrictive fibrosis", presence of foreign body giant cells (type III), presence of inflammatory cells, foreign body granulomas, neovascularization, neuromas (IV type) [44].

Results

When studying the micropreparations, we discovered a number of changes that occurred as a result of the reaction of the gland tissues to the presence of the implant. Although the architecture and morphology of the formed fibrous capsules around the implant had a similar histological structure, they were characterized by certain differences. In all investigated cases, the capsules had a three-layer, similar histological structure. The inner layer, which was located closer to the implant, was represented by a single- or multi-layered epithelium with the presence

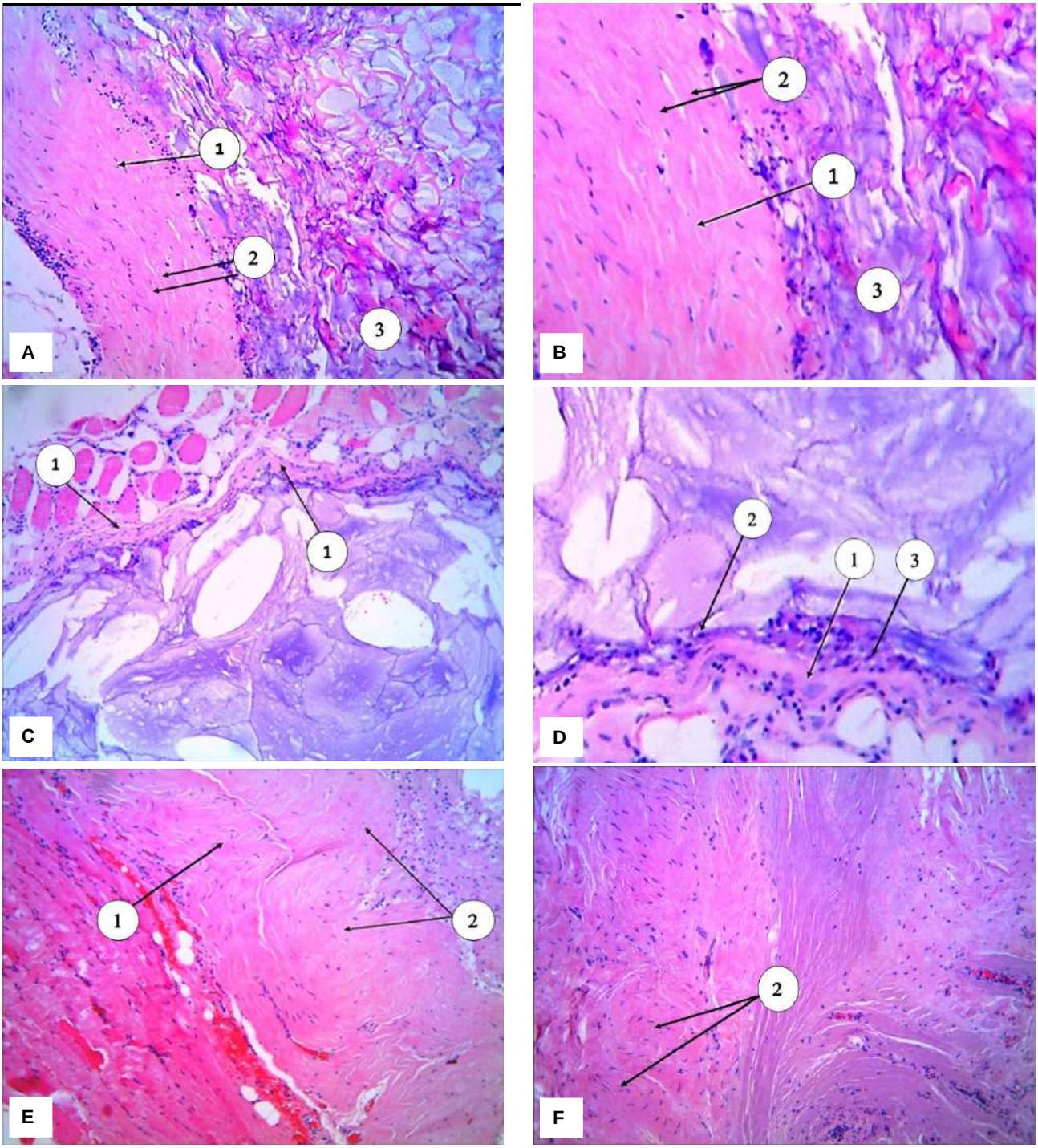

Fig. 1. Architectonics and morphology of the fibrous capsule of the breast tissue in the presence of the implant: A and B: 1 - thick fibrous capsule with a predominance of the fibrous component, 2 - parallel orientation of collagen fibers around the gel areas, 3 - gel areas. Hematoxylin-eosin. x100 (A), x400 (B); C and D: 1 - a thin connective tissue capsule around the areas of the gel, which corresponds to the 1st type according to Wilflingseder, 2 - an inflammatory cell infiltrate with a predominance of lymphocytes and plasma cells (3). Hematoxylin-eosin. x100 (C), x400 (D); E and F: 1 - wavy orientation of collagen fibers, 2 - thick bundles of collagen fibers arranged concentrically (capsular contracture). Hematoxylin-eosin. x100 (E and F).

of fibroblasts and macrophages, in isolated cases it looked like a pseudo-epithelial layer with synovial metaplasia. The middle layer was formed by loose connective tissue with widened lumens of thin-walled vessels and high cell density. The outer layer was formed by dense collagen tissue and the surface layer of blood vessels. The thickness

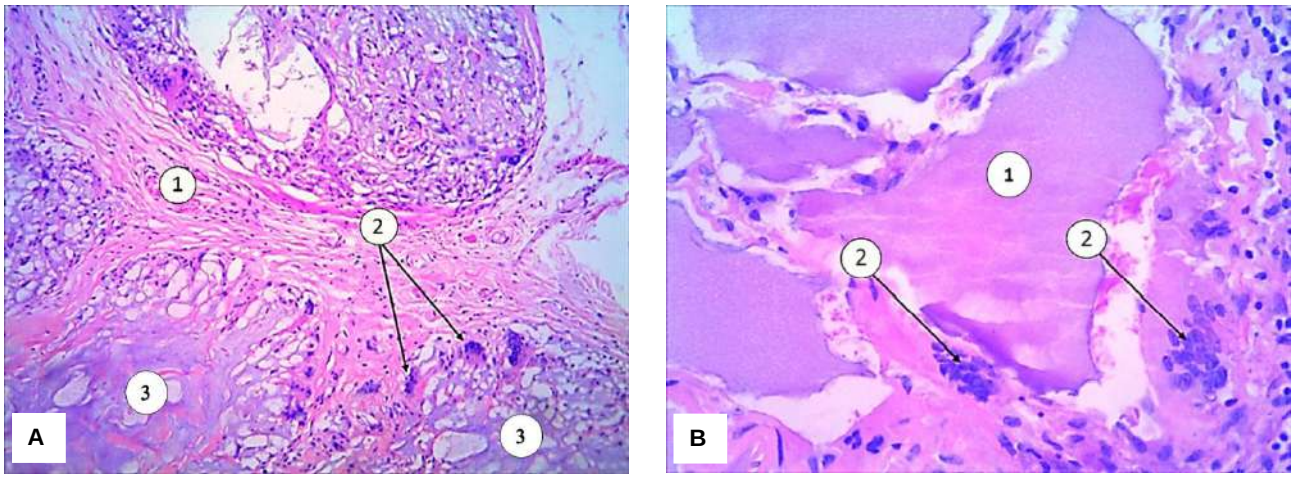

Fig. 2. Cellular response to contact with silicone gel. A: 1 - pronounced fibrous capsule around areas of gel, 2 - giant multinucleated cells of foreign bodies type, 3 - areas of gel. Hematoxylin-eosin. x100; B: 1 - areas of gel, 2 - giant multinucleated cells of foreign bodies type. Hematoxylin-eosin. x400.

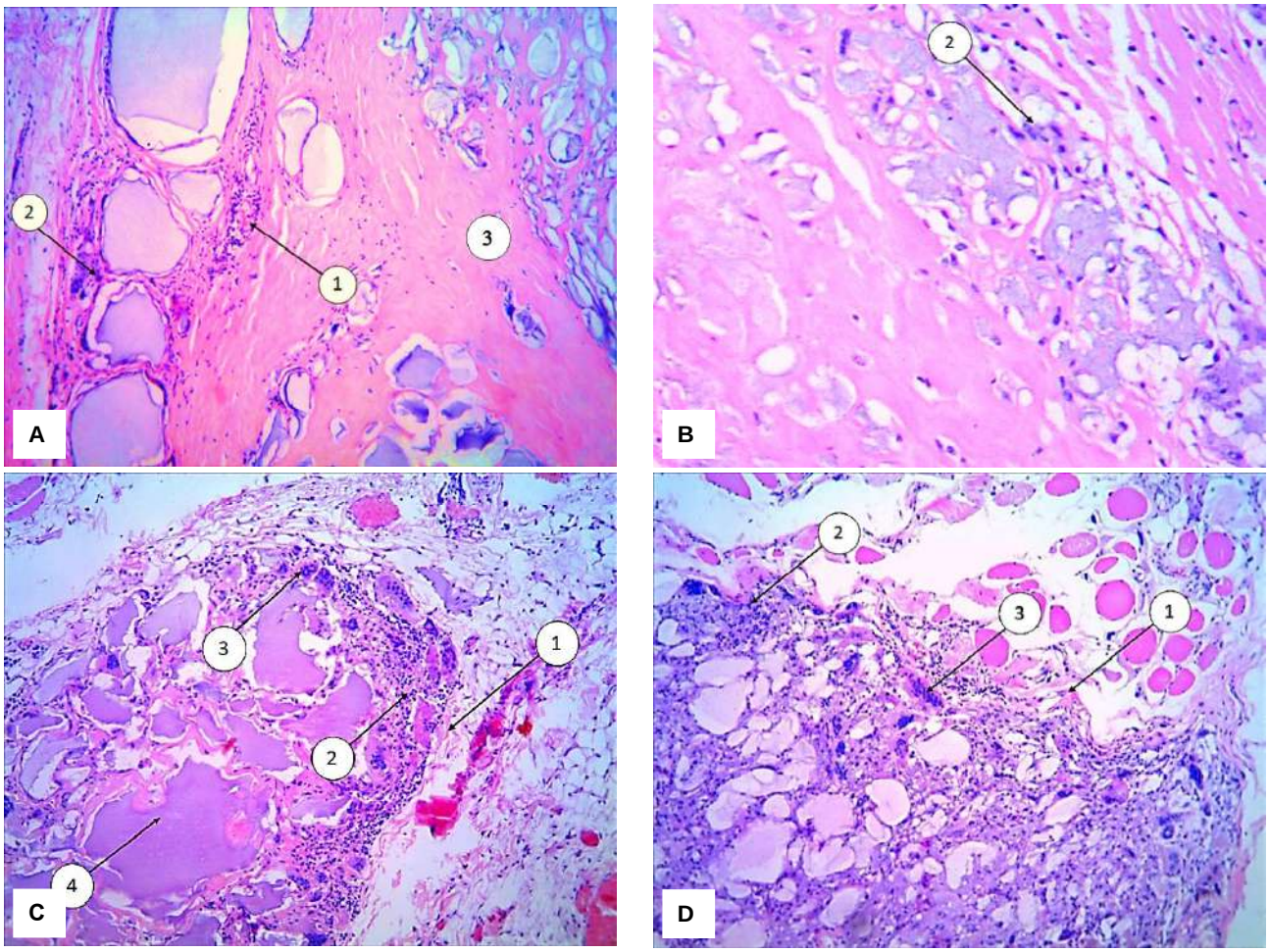

Fig. 3. Inflammatory cell infiltrate in the tissues of the breast upon contact with silicone gel of varying severity. A and B: 1 - slight inflammatory cell infiltrate with a predominance of lymphocytes and plasma cells, located perivascularly, 2 - infiltrate around the gel areas, 3 - thickened fibrous tissue with hyalinosis around the gel areas; C and D: 1 - pronounced inflammatory cell infiltrate with a predominance of lymphocytes and plasma cells, 2 - giant multinucleated foreign body-like cells, 3 - thin fibrous capsule around the gel areas, 4 - gel areas. Hematoxylin-eosin. x100 (A, C, D), x400 (B).

of the capsule varied from 2 to 8 mm, on average it was equal to 4-5 mm. Capsule thickness was measured at the thickest point of the capsule.

During the microscopic examination of preparations

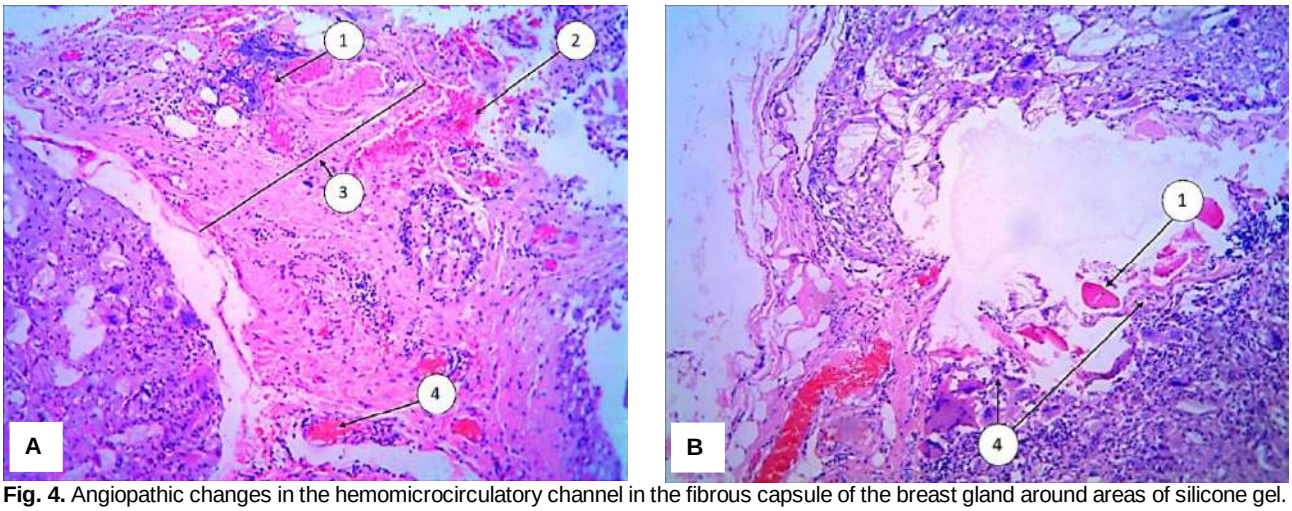

Fig. 4. Angiopathic changes in the hemomicrocirculatory channel in the fibrous capsule of the breast gland around areas of silicone gel. A, B: 1 - foci of angiomatosis, 2 - hemorrhages in the fibrous capsule, 3 - fibrous capsule, 4 - numerous thin-walled newly formed capillaries surrounded by inflammatory infiltrate. Hematoxylin-eosin. x100.

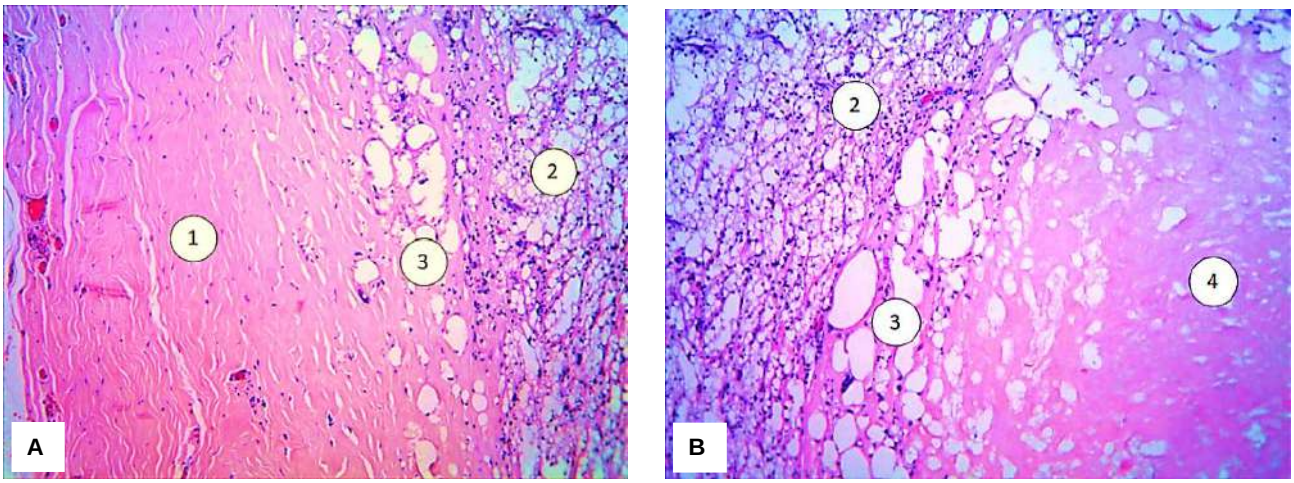

Fig. 5. The reaction of fatty connective tissue of the breast gland to the presence of silicone gel. A and B: 1 - thick fibrous wall after plastic surgery with a silicone implant, 2 - numerous groups of "light" foamy macrophages, 3 - areas of fat necrosis, 4 - area with gel masses next to fat necrosis of adipocytes. Hematoxylin-eosin. x100.

stained with hematoxylin-eosin, we analyzed in detail the morphological features of changes in the fibrous capsule in the presence of capsular contractures. Attention was paid to the structure of collagen fibers, the density of their location, the number and size of cell nuclei, the presence of lymphocytes and macrophages, macro- and microparticles of silicone, the presence of giant cells of foreign bodies and granulomas of foreign bodies, the severity of the inflammatory reaction and its differentiation (acute or chronic), localization of inflammation (focal, diffuse, perivascular, near the implant), the presence of a synovial cell layer, signs of necrosis, calcification, bleeding.

Differences in the histomorphological picture between the samples were established, including variations in cellularity, organization and density of fibers, vascularization and general structure. The location of collagen fibers in some cases was mainly oriented parallel to the capsule. Between the fibers, numerous spindle-shaped cells, which morphologically had the characteristics of myofibroblasts, could be seen. In general, cellularity decreased from the inner to the outer layer, with the outermost layer distant from the implant having few cells and mostly collagen fibers. However, in some cases, we diagnosed areas near or at the border of the implant capsule with increased or concentrated cellularity, although the capsules generally had low cellularity.

Specimens with a thickened fibrous capsule (II-IV types) predominated (Fig. 1 A, B), only in one case there was a thin non-compacted capsule, which corresponded to type I according to Wilflingseder (Fig. 1 C, D). In the composition of thickened fibrous capsules, in most cases, the correct orientation of collagen fibers was disturbed, bundles of collagen fibers were found, located concentrically and separated by individual fibroblasts and fibrocytes, which was a sign of the formation of capsular contracture (Fig. 1 E, F). Especially such changes in the orientation of collagen fibers were diagnosed in cases of damage to the implant wall and the release of the gel. The histological pattern in a

number of samples also drew attention, when the capsules consisted of one collagen layer of altered density with hyalinosis.

In all studied samples, the material of silicone granules was found surrounded by resident cells of connective tissue and migrant cells, which reacted locally in the form of clusters of macrophages with the formation of so-called giant multinucleated cells of foreign bodies (Fig. 2).

Morphological criteria of breast tissue reaction to the implant included the presence, in addition to giant multinucleated foreign body-type cells, as well as an inflammatory cell infiltrate of varying severity with a predominance of lymphocytes, plasma cells, and "light" foamy macrophages (Fig. 3). Increased accumulation of macrophages with intracellular silicon in the form of microparticles was revealed. In addition, polygonal cavities of different sizes were observed, as well as accumulation of more rounded cavities due to dissolved silicone. The number of silicone particles significantly decreased along the periphery of the implant.

In most cases, the area of the capsule adjacent to the implant had no vascularization, although it was evident throughout the capsule in a small number of specimens. Angiopathic changes in the hemomicrocirculatory channel were recorded in almost all cases. Individual vessels were dilated, and their walls were thickened, with the presence of oxyphilic amorphous masses in the lumens. Hemorrhages localized in the inner and middle layers of the capsule, as well as numerous thin-walled capillary neoplasms surrounded by inflammatory cells, were found in two samples (Fig. 4).

Certain groups of adipocytes of adipose connective tissue also underwent changes. Such cells decreased in size, lost their traditional shape, and sometimes underwent necrobiotic changes. Areas of fat necrosis were diagnosed (Fig. 5).

Discussion

To date, more than a million breast augmentation procedures using breast silicone implants have been performed in the world. A potential risk with a stable implant is still the possibility of rupture of its capsule with infiltration of silicone into the surrounding tissues and the occurrence of a number of side effects that cause discomfort or pose a threat to health. These include such local complications as pain, swelling, redness, infections, capsular contracture, implant rupture, and gel "bleeding" [9, 16, 17].

The increasing number of patients with breast implants has in turn increased the likelihood of less common complications, which include seromas or late infection, breast lymphadenopathy, granulomas in the implant capsule, which in some cases can extend beyond the fibrous capsule, desmoid tumors and large cell anaplastic lymphoma [13, 39].

The main atypical complications associated with breast implants relate to late seroma [13, 41] and the diagnosis of large cell anaplastic lymphoma [25, 38]. In addition, patients experience systemic symptoms such as chronic fatigue, arthralgias, myalgias, fever, and even cognitive dysfunction. These symptoms have been given various names such as adjuvant-induced autoimmune/ autoinflammatory syndrome due to silicone incompatibility syndrome and breast implant disease. Due to chronic immune activation, patients may develop allergies, autoimmune diseases, immune deficiencies, and, finally, lymphomas [19, 43].

Capsular contracture, based on our study and according to the data of many authors [3, 35], was the main risk for revision operations after aesthetic breast augmentation with breast implants. For example, Henriksen T. F. and co-authors [21] in 2005 found about 22% of capsular contracture as a complication after aesthetic breast plastic surgery. According to other authors, it has been established that fibrosis and capsular contracture in breast implants is a very dynamic process that does not depend on the age of the patient and the length of time the implants have been in place [26, 33]. K. Benediktsson and L. Perbeck [6] showed in their work that capsular contracture occurred during the first years in more than half of the patients. In our study, most patients developed capsular contracture in the first 3-5 years after implantation. But in some cases, the contracture did not manifest itself for many years. We could not establish cause-and-effect relationships. There is also a debate in the literature regarding the timing of capsular contracture, and according to the authors, the reasons for this have not been clarified [36].

There are various theories regarding the causes and pathomechanism of capsular contracture of breast implants, most of which consider the development of an inflammatory reaction with the induction of increased fibrosis and compaction of the capsule as the central mechanism [31]. Foreign body reaction or periprosthetic bacterial contamination are also discussed as potential triggers of the inflammatory response [4].

There are works in which it is shown that macrophages loaded with silicone play the main (central) role, stimulating fibroblasts to collagenogenesis and thus contribute to the development of capsular contracture [18, 24]. Macrophages in culture can be stimulated by silicone to release interleukin-1, which is a pro-inflammatory cytokine that plays an important role in fibroblast proliferation and differentiation [18, 42].

The results of research in recent years by Hernandez J. L. et al. [22] show conflicting opinions regarding the reaction to a foreign body: the question arises whether it is a non-specific reaction of the body or a specific activation of the immune system, whether it is the surface of the implant or particles of the surface that cause the corresponding reaction, or whether the filling of the implant, which is in contact with the body tissue due to leakage of its contents.

Thus, Dziubek M. and co-authors [15] demonstrated the results of research on silicone shells of breast

implants. Silicone gel implants showed "bleeding" of silicone particles into the periprosthetic capsule, an average of 1 million silicone particles per 1 capsule. On the other hand, no release of silicone particles was observed with saline breast implants. These data indicate that the release of particles occurs from the inner silicone gel and not from the smooth outer silicone shell.

However, Dijkman H. B. and co-authors [14], who studied saline breast implants, indicated that there are cases of silicone migration from the shell of saline breast implants, but they are very rare. The authors describe a unique case of a 66-year-old female patient with silicone migration from intact saline breast implants. The patient showed a number of symptoms indicating breast implant disease. X-ray data indicated the presence of silicone in the axillary lymph nodes, despite the integrity of the implants, confirming silicone migration. Histopathological examination revealed a reaction to a foreign body and the presence of silicone in the axillary lymph nodes. Given the salt content, the source is likely the polydimethylsiloxane breast implant shell. The rarity of documented silicone migration from intact saline breast implants, particularly in patients with breast implant disease, highlights the need for additional research into the health implications of silicone particle leakage.

It should also be taken into account that silicone implants are constantly being improved since their appearance, and a comparison between implants of different generations is impossible. There are no long-term studies on the latest generation of high-cohesive gel implants. Most of the research concerns old implants. In addition, each implant manufacturing company uses its own composition and constantly improves it.

Thus, patterns of local morphologic responses on breast implants may be of great importance as a possible starting point for the controversially discussed silicone-induced systemic immune response.

Only systematic registration of morphological reactions in the "prosthetic passport" along with additional dispensary monitoring of patients will be able to provide a realistic assessment of potential health risks for women with silicone breast implants in the future.

Conclusions

1. In the soft tissues of the mammary glands, from which silicone implants were removed according to clinical indications, a number of changes affecting, first of all, stromal-cellular elements were detected.

2. Regarding the stromal component, the accumulation of structured fibrous structures in the form of dense capsules with elements of local contractures was noted. In terms of cellular elements, the most demonstrative were cellular infiltrates, which included macrophages, lymphocytes, and plasma cells, which indicates a high probability of a chronic inflammatory process.

3. The most significant manifest sign revealed on histological preparations is a large number of giant multinucleated cells of foreign bodies, which obviously indicates the inability of macrophages to complete phagocytosis with lysis of the phagocytosed material, which by its chemical composition is the silicone of the implant.

4. The detected changes can be interpreted as a natural reaction of the tissues to a foreign object, in particular - an implant, the material of which has penetrated the soft tissues of the breast for one reason or another.

5. The risk of implant-related changes increases with prolonged implantation duration.

References

[1] Adams, Jr., W. P., & Mallucci, P. (2012). Breast augmentation. *Plastic and Reconstructive Surgery,* 130(4), 597e-611e. doi: 10.1097/PRS.0b013e318262f607

[2] Akilbekova, D., & Bratlie, K. M. (2015). Quantitative Characterization of Collagen in the Fibrotic Capsule Surrounding Implanted Polymeric Microparticles through Second Harmonic Generation Imaging. *PLoS One,* 10(6), e0130386. doi: 10.1371/journal.pone.0130386

[3] Bachour, Y., Bargon, C. A., de Blok, C. J. M., Ket, J. C. F., Ritt, M. J. P. F., & Niessen, F. B. (2018). Risk factors for developing capsular contracture in women after breast implant surgery: A systematic review of the literature. *J. Plast. Reconstr. Aesthet. Surg.,* 71(9), e29-e48. doi: 10.1016/j.bjps.2018.05.022

[4] Bachour, Y., Poort, L., Verweij, S. P., van Selms, G., Winters, H. A. H., Ritt, M. J. P. F., ... Budding, A. E. (2019). PCR Characterization of Microbiota on Contracted and Non-Contracted Breast Capsules. *Aesthetic Plast Surg*, 43(4), 918-926. doi: 10.1007/s00266-019-01383-9

[5] Bachour, Y., Verweij, S. P., Gibbs, S., Ket, J. C. F., Ritt, M. J. P. F., Niessen, F. B., & Mullender, M. G. (2018). The aetiopathogenesis of capsular contracture: A systematic review of the literature. *J Plast Reconstr Aesthet Surg,* 71(3), 307-317. doi: 10.1016/j.bjps.2017.12.002

[6] Benediktsson, K., & Perbeck, L. (2006). Capsular contracture around saline-filled and textured subcutaneously-placed implants in irradiated and non-irradiated breast cancer patients: five years of monitoring of a prospective trial. *J Plast Reconstr Aesthet Surg,* 59(1), 27-34. doi: 10.1016/j.bjps.2005.08.005

[7] Berger, R., Ribas Filho, J. M., Malafaia, O., Nassif, P. A. N., Silva, E. N., Silva, A. B. D. D., ... & Noronha, L. (2021). Histological evaluation of capsules formed by texturized silicone implants with and without polyester mesh coverage (Parietex®). A study on female rats. *Acta Cir Bras,* 36(5), e360505. doi: 10.1590/ACB360505

[8] Bergmann, P. A., Liodaki, M. E., Mauss, K. L., Lange, T., Gebhard, M., Mailander, P., & Siemers, F. (2012). Histological and immunohistochemical study of capsular contracture in an animal model-a comparison of two implants according to a modification of Wilflingseder's classification. *Handchir Mikrochir Plast Chir,* 44(4), 220-226. doi: 10.1055/s-0032-1312653

[9] Cohen, Tervaert, J. W., Mohazab, N., Redmond, D., van Eeden, C., & Osman, M. (2022). Breast implant illness: scientific evidence of its existence. *Expert Rev Clin Immunol,* 18(1), 15-29. doi: 10.1080/1744666X.2022.2010546

[10] Colaris, M. J. L., Ruhl, T., & Beier, J. P. (2022). Effects of Silicone Breast Implants on Human Cell Types In Vitro: A Closer Look on Host and Implant. *Aesthetic Plast Surg,* 46(5):2208-2217. doi: 10.1007/s00266-021-02762-x

[11] de Bakker, E., van den Broek, L. J, Ritt, M. J. P. F., Gibbs, S., & Niessen, F. B. (2018). The Histological Composition of Capsular Contracture Focussed on the Inner Layer of the Capsule: An Intra-Donor Baker-I Versus Baker-IV Comparison. *Aesthetic Plast Surg,* 42(6), 1485-1491. doi: 10.1007/s00266-018-1211-1

[12] de Faria Castro, F. E., & Castro, C. (2022). Magnetic resonance classification proposal for fibrous capsules in breast silicone implants. *Clin Imaging,* 91, 26-31. doi: 10.1016/j.clinimag.2022.08.010

[13] Di Napoli, A., Pepe, G., Giarnieri, E., Cippitelli, C., Bonifacino, A., Mattei, M., ... Giovagnoli, M. R. (2017). Cytological diagnostic features of late breast implant seromas: From reactive to anaplastic large cell lymphoma. *PLoS One,* 12(7), e0181097. doi: 10.1371/journal.pone.0181097

[14] Dijkman, H. B. P. M., Slaats, I., & Bult, P. (2021). Assessment of silicone particle migration among women undergoing removal or revision of silicone breast implants in the Netherlands. *JAMA Netw Open,* 4(9), e2125381. doi: 10.1001/jamanetworkopen.2021.25381

[15] Dziubek, M., Laurent, R., Bonapace-Potvin, M., Gaboury, L., Danino, M. A. (2023). Silicone particles in capsules around breast implants: Establishment of a new pathological methodology to assess the number of particles around breast implants. *Ann Chir Plast Esthet,* 68(1), 19-25. doi: 10.1016/j.anplas.2022.08.002

[16] Fleury, E. F. C. (2020). Silicone Induced Granuloma of Breast Implant Capsule (SIGBIC) diagnosis: Breast Magnetic Resonance (BMR) sensitivity to detect silicone bleeding. *PLoS One,* 15(6), e0235050. doi: 10.1371/journal.pone.0235050

[17] Friedrich, M., Krämer, S., Friedrich, D., Kraft, C., Maass, N., & Rogmans, C. (2021). Difficulties of Breast Reconstruction - Problems That No One Likes to Face. *Anticancer Research,* 41(11), 5365-5375. doi: 10.21873/anticanres.15349

[18] Gabasa, M., Arshakyan, M., Llorente, A., Chuliá-Peris, L., Pavelescu, I., Xaubet, A., & Alcaraz, J. (2020). Interleukin-1β Modulation of the Mechanobiology of Primary Human Pulmonary Fibroblasts: Potential Implications in Lung Repair. *Int J Mol Sci,* 21(22), 8417. doi: 10.3390/ijms21228417

[19] Gorgy, A., Barone, N., Nepon, H., Dalfen, J., Efanov, J. I., Davison, P., & Vorstenbosch, J. (2023). Implant-based brest surgery and capsular formation: when, how and why? - a narrative rewiew. *Annals of Translational Medicine*, 11(11), 385. doi: 10.21037/atm-23-131

[20] Heidekrueger, P. I., Juran, S., Patel, A., Tanna, N., & Broer, P. N. (2016). Plastic surgery statistics in the US: evidence and implications. *Aesthetic Plastic Surgery*, 40(2), 293-300. doi: 10.1007/s00266-016-0611-3

[21] Henriksen, T. F., Fryzek, J. P., Hölmich, L. R., McLaughlin, J. K., Kjøller, K., Høyer, A. P., … Friis, S. (2005). Surgical intervention and capsular contracture after breast augmentation: a prospective study of risk factors. *Ann Plast Surg*, 54(4), 343-351. doi: 10.1097/01.sap.0000151459.07978.fa

[22] Hernandez, J. L., Park, J., Yao, S., Blakney, A. K., Nguyen, H. V., Katz, B. H., … Woodrow, K. A. (2021). Effect of tissue microenvironment on fibrous capsule formation to biomaterial-coated implants. *Biomaterials,* 273, 120806. doi: 10.1016/j.biomaterials.2021.120806

[23] Hortolam, J. G., Carvalho, J. F., & Appenzeller, S. (2013). Connective tissue diseases following silicone breast implantation: where do we stand? *Clinics* (Sao Paulo), 68(3), 281. doi: 10.6061/clinics/2013(03)e01

[24] Huang, S. Q., Chen, Y., Zhu, Q., Zhang, Y. M., Lei, Z. Y., Zhou, X., & Fan, D. L. (2022). In Vivo and In Vitro Fibroblasts' Behavior and Capsular Formation in Correlation with Smooth and Textured Silicone Surfaces. *Aesthetic Plast Surg*, 46(3), 1164-1177. doi: 10.1007/s00266-022-02769-y

[25] Iwahira, Y., Nakagami, G., & Sanada, H. (2022). Risk factors for capsular contracture after breast reconstruction with tissue expanders and silicone implants in nonirradiated patients: A retrospective observational cohort study. *Medicine* (Baltimore), 101(48), e31837. doi: 10.1097/MD.0000000000031837

[26] Jimenez, R. B., Packowski, K., Horick, N., Rosado, N., Chinta, S., Koh, D. J., … Liao, E. C. (2023). The Timing of Acute and Late Complications Following Mastectomy and Implant-based Reconstruction. *Ann Surg,* 278(1), e203-e208. doi: 10.1097/SLA.0000000000005574

[27] Jiménez-Heffernan, J. A., Bárcena, C., & Muñoz-Hernández, P. (2018). Cytological features of breast peri-implant papillary synovial metaplasia. *Diagn Cytopathol*, 46(9), 769-771. doi: 10.1002/dc.23947

[28] Kaoutzanis, C., Winocour, J., Unger, J., Gabriel, A., & Maxwell. G. P. (2019). The Evolution of Breast Implants. *Semin Plast Surg,* 33(4), 217-223. doi: 10.1055/s-0039-1696985

[29] Kim, J. H., Nam, S. E., Sung J. Y., Song K. Y., Bang B. S., Lee E. K. (2021). The Value of Capsule Thickness on Breast Ultrasound as an Indicator of the Severity of Capsular Contracture and Its Correlation with the Baker Classification. *Aesthetic Plast Surg,* 46(2), 621-629. doi: 10.1007/s00266-021-02544-5

[30] Kolesnik, J., Hörner-Rieber, J. O. P., Kechedzhyev, V. V., Levyk, O. M., Kuzmemko, V. O., Kabakov, A. O. (2019). Імплантат-асоційована анапластична крупноклітинна лімфома (огляд літератури) [Implant-associated anaplastic large cell lymphoma (literature review)]. *Клінічна онкологія=Clinical Oncology*, 9, 4(36), 1-5. doi: 10.32471/clinicaloncology.2663-466X.36-4.26626

[31] Larsen, A., Rasmussen, L. E., Rasmussen, L. F., Weltz, T. K., Hemmingsen, M. N., Poulsen, S. S., … & Herly M. (2021). Histological Analyses of Capsular Contracture and Associated Risk Factors: A Systematic Review. *Aesthetic Plast Surg,* 45(6), 2714-2728. doi: 10.1007/s00266-021-02473-3

[32] Levy, Y., Rotman-Pikielny, P., Ehrenfeld, M., & Shoenfeld, Y. (2009). Silicone breast implantation-induced scleroderma: description of four patients and a critical review of the literature. *Lupus,* 18(13), 1226-1232. doi: 10.1177/0961203309347795

[33] Lista, F., Austin, R. E., Saheb-Al-Zamani, M., & Ahmad, J. (2020). Does Implant Surface Texture Affect the Risk of Capsular Contracture in Subglandular Breast Augmentation and Breast Augmentation-Mastopexy? *Aesthet Surg J*, 40(5), 499-512. doi: 10.1093/asj/sjz241

[34] Meshkin, D. H., Firriolo, J. M., Karp, N. S., & Salibian, A. A. (2023). Management of complications following implant-based breast reconstruction: a narrative review. *Ann Transl Med,* 11(12), 416. doi: 10.21037/atm-23-1384

[35] Mohan, A. S., Sullivan, J., Tenenbaum, M. M., Broderick, K. B., & Myckatyn, T. M. (2024). Toward a Consensus Aproach for Assessing Capsular Contracture Severity and Progression: A Systematic Review. *Plast Reconstr Surg,* 153(1), 7-22. doi: 10.1097/PRS.0000000000010573

[36] Paolini, G., Firmani, G., Briganti, F., Macino, M., Nigrelli, S.,

Sorotos, M., ... & Santanelli di Pompeo, F. (2023). Assessment of Risk Factors for Rupture in Breast Reconstruction Patients with Macrotextured Breast Implants. *Aesthetic Plast Surg,* 47(2), 517-530. doi: 10.1007/s00266-022-03118-9

[37] Pereira Leite, L., Correia Sá, I., & Marques, M. (2013). Etiopatogenia e Tratamento da Contractura Capsular Mam?ria [Etiopathogenesis and treatment of breast capsular contracture]. *Acta Med Port,* 26(6), 737-745. doi: 10.20344/amp.5083

[38] Peterson, M. N., Giblon, R. E., Achenbach, S. J., Davis, J. M. 3rd, TerKonda, S. P., & Crowson, C. S. (2023). The Incidence and Outcomes of Breast Implants Among 1696 Women over more than 50 Years. *Aesthetic Plast Surg*, 47(6), 2268-2276. doi: 10.1007/s00266-023-03535-4

[39] Rubio, S. N., Lannegrand, Menéndez, B., Duque Muñoz, M., Montes Fernández M, & Ciudad Fernández, M. J. (2020). Uncommon complications of breast prostheses. *Radiologia,* 62(4), 266-279. doi: 10.1016/j.rx.2020.01.008

[40] Safran, T., Nepon, H., Chu, C. K., Winocour, S., Murphy, A. M., Davison, P. G. … & Vorstenbosch, J. (2021). Current Concepts in Capsular Contracture: Pathophysiology, Prevention, and Management. *Semin Plast Surg,* 35(3), 189-197. doi: 10.1055/s-0041-1731793

[41] Spear, S. L., Rottman, S. J., Glicksman, C., Brown, M., & Al-Attar, A. (2012). Late seromas after breast implants: theory and practice. *Plast Reconstr Surg,* 130(2), 423-435. doi: 10.1097/PRS.0b013e3182589ea9

[42] Susini, P., Nisi, G., Pierazzi, D. M., Giardino, F. R., Pozzi, M., Grimaldi, L., & Cuomo, R. (2023). Advances on Capsular Contracture-Prevention and Management Strategies: A Narrative Review of the Literature. *Plast Reconstr Surg Glob Open,* 11(6), e5034. doi: 10.1097/GOX.0000000000005034

[43] Watad, A., Rosenberg, V., Tiosano, S., Cohen Tervaert, J. W., Yavne, Y., Shoenfeld, Y., … & Amital, H. (2018). Silicone breast implants and the risk of autoimmune/rheumatic disorders: a real-world analysis. *Int J Epidemiol*, 47(6), 1846-1854. doi: 10.1093/ije/dyy217

[44] Wilflingseder, P., Hoinkes, G., & Mikuz, G. (1983). Tissue reactions from silicone implant in augmentation mammaplasties. *Minerva Chir*, 38(12), 877-880. PMID: 6350933

[45] Zhang, X. R., Chien, P. N., Trinh, X. T., Nam, S. Y., & Heo, C. Y. (2022). Comparison of Formation of Capsule Among Different Breast Silicone Implants. *In Vivo,* 36(6), 2756-2766. doi: 10.21873/invivo.13012

СТРОМАЛЬНО-КЛІТИННА ПЕРЕБУДОВА ТКАНИН ГРУДНОЇ ЗАЛОЗИ ПІСЛЯ УШКОДЖЕНЬ СИЛІКОНОВОГО ІМПЛАНТА

Дадаян В. А., Адамович О. О., Сімонов В. Ф., Кожан В. І., Поліянц А. В., Гриценко А. П., Челпанова І. В.

Одним з актуальних векторів сучасної реконструктивної та косметичної хірургії є аугментаційна мамопластика - операція зі збільшення грудних залоз. Грудний імплант толерується організмом добре, оскільки імуногенність його матеріалу є надзвичайно низькою. Водночас силіконовий гель імпланта є чужорідним об'єктом і оточуючі його тканини грудної залози дають стереотипну відповідь у вигляді розростання сполучнотканинної строми з формуванням капсули навколо імпланта та появи вогнищевих клітинних інфільтратів. Сучасні грудні імпланти, на відміну від імплантів попередніх десятиліть, за своєю структурою є більш досконалими, а рівень захисту від ушкоджень є набагато вищий. Ускладненням, пов'язаним з довготривалим використанням (до 20 років) імплантів, де в якості наповнювача використовували силікон низької якості або промисловий силікон, є проникнення низькомолекулярних частинок імпланта через його оболонку до оточуючих тканин з подальшим утворенням силіконових гранульом. У переважній більшості такі зміни розвиваються після механічної травматизації імпланта. Мета дослідження - встановити морфологічні критерії реакції тканин грудної залози після ушкоджень силіконового імпланта. Матеріалом для досліджень слугували гістологічні мікропрепарати тканин грудних залоз з архіву клініки "Grace Clinic" (м. Київ), за двостороннім погодженням з пацієнтками, що звернулися з метою повторної мамопластики. Тривалість перебування імплантів у грудній залозі становила від 6 до 20 років. Віковий діапазон жінок був у межах від 36 до 53 років. На препаратах, забарвлених гематоксиліном та еозином, були представлені біоптати тканин залоз 9-ох пацієнток з діагнозом деформації силіконових імплантів та порушенням цілісності їхньої стінки. Мікропрепарати візуалізували за допомогою світлового мікроскопа UlabXSP-137TLED при різних збільшеннях та фотографували камерою XCAM 1080P. Вивчення гістологічних препаратів м'яких тканин грудних залоз, з котрих були видалені силіконові імпланти, встановило зміни у стромально-клітинних елементах, а саме: оформлені волокнисті структури накопичувались у вигляді щільних капсул з елементами локальних контрактур; зі сторони клітинних елементів найбільш демонстративними були клітинні інфільтрати, у складі яких перебували макрофаги, лімфоцити та плазмоцити, що свідчило про високу ймовірність перебігу хронічного запального процесу. Практично в усіх досліджуваних зрізах були присутні велика кількість гігантських багатоядерних клітин сторонніх тіл, що свідчило про неможливість завершення макрофагами фагоцитозу з лізисом фагоцитованого матеріалу, котрий за своїм хімічним складом є силіконом імпланта. Усі описані явища можна трактувати як природну реакцію тканин на імплант, вміст котрого потрапив до м'яких тканин грудної залози. Таким чином, морфологічним критерієм реакції тканин грудної залози на пошкодження силіконового імпланта можна вважати наявність численних гігантських багатоядерних клітин сторонніх тіл, щільних капсул з елементами локальних контрактур та суттєвої переваги макрофагів, лімфоцитів та плазмоцитів у клітинних інфільтратах над іншими клітинними елементами.

Ключові слова: *молочна/грудна залоза, грудний імплант, пошкодження грудного силіконового імпланта, естетична хірургія, мікроскопія, гістопатологічна діагностика, імплант-асоційовані фіброзні зміни.*

Author's contribution

Dadayan V. A. - conceptualization, research (results of study), methodology and writing of the original draft.
Adamovych O. O. - methodology and writing of the original draft, review & editing.
Simonov V. F. - conceptualization, research (results of study), review & editing, formal analysis and validation.
Kozhan V. I. - research (results of study), project administration.
Poliiants A. V. - conceptualization, methodology and writing of the original draft, resources, software.
Hrytsenko A. P. - conceptualization, research (results of study), resources, software.
Chelpanova I. V. - methodology and writing of the original draft, review & editing, data visualization.

DOI: 10.31393/morphology-journal-2024-30(2)-07 Reports of Morphology, Vol. 30, №2, Pages 53-60

ISSN 1818-1295 eISSN 2616-6194

REPORTS OF MORPHOLOGY

Official Journal of the Scientific Society of Anatomists, Histologists, Embryologists and Topographic Anatomists of Ukraine

journal homepage: https://morphology-journal.com

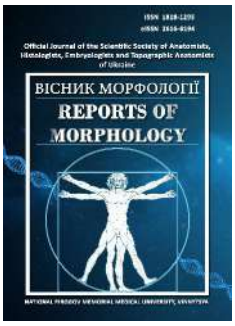

Morphological features of enamel in fluorosis of different degrees of severity

Marchenko A. V., Nikolishyna E. V., Ilenko N. M., Nikolishyn I. A., Kostyrenko O. P., Cherniak V. V.
Poltava State Medical University, Poltava, Ukraine

ARTICLE INFO
Received: 30 January 2024
Accepted: 29 March 2024

UDC: 616.314.13-053

CORRESPONDING AUTHOR
e-mail: allamarchen@ukr.net
Marchenko A. V.

CONFLICT OF INTEREST
The authors have no conflicts of interest to declare.

FUNDING
Not applicable.

DATA SHARING
Data are available upon reasonable request to corresponding author.

The occurrence of dental fluorosis is facilitated by a violation of enamel mineralization caused by fluorides, which enter the human body in excess during its development and formation and have a toxic effect on enamel blasts. However, the molecular mechanisms involved in the pathogenesis of fluorosis are not fully understood. Enamel formation is a complex process involving cell proliferation and differentiation through epithelial-mesenchymal sequential secretion of matrix proteins, tissue-specific transport of ions including calcium and fluoride, and precipitation and alignment of enamel crystals through interactions between organic and inorganic molecules. Understanding the morphological features of enamel changes during fluoride intoxication of the human body in the endemic region allows us to clearly understand the need for a comprehensive solution to this medical and social problem. The aim was to study the morphological features of enamel in fluorosis in residents of the endemic region of Ukraine, in particular the Poltava region. The work examines different groups of teeth (both intact and affected by fluorosis) removed for orthodontic or clinical indications in men and women aged 17 to 40 years. Morphological signs were studied first on native, and later on histochemically stained sections. It was established that the violation of the structure of the enamel layer of the teeth in mild and severe fluorosis is characterized by both partial and complete violation of the movement of the enamel prisms with signs of destruction. Fragmentation and homogeneity throughout the entire thickness were found in some areas of the enamel. When evaluating histochemically stained sections of teeth affected by fluorosis, it was established that dystrophic changes in the enamel structure and accumulation of acidic glycosaminoglycans in the lesions are more characteristic of mild and moderate forms. Under the conditions of a severe form of fluorosis, complete destruction of the prisms, fragmentation of the lamella, homogenization of areas on the entire enamel layer, which is due to the uneven distribution of acidic mucopolysaccharides, have been established. Morphologically and histochemically dystrophic changes in the areas of the affected enamel are confirmed by uneven distribution and accumulation of acidic glycosaminoglycans. An assessment of the effect of fluoride intoxication on the state of tooth enamel was carried out, which will allow to expand the possibilities of preventive measures for related specialists, as well as to create and develop additional treatment methods that will contribute to the improvement of physical and aesthetic indicators of teeth. dental health.
Keywords: *enamel structure, fluorosis, glycosaminoglycans, mineralization.*

Introduction

A feature of the abiotic conditions of a number of regions of the globe is the increased content of fluoride ion in drinking water, which cannot but affect the health of the population [1, 4, 19, 21]. The drinking water of the region of Ukraine, in particular of the Poltava region, along the line Karlivka - Poltava - Myrhorod, in addition to the increased level of fluoride (up to 15 mg/l at the norm of 0.5-1.5 mg/l), has a reduced calcium content [2, 7, 11, 30]. A number of industries (enamel, aluminum, thermal power plants) increase the fluorine content in the environment, as does the application of phosphorus fertilizers to the soil [12, 24, 36]. Exposure to various sources of fluoride, such as indoor coal burning or consumption of large amounts of tea in non-fluoridated areas, is a risk factor for dental fluorosis

[29]. As a result, fluorosis of teeth and bones and general hyperfluorosis of the body develops [21, 23, 27, 28]. However, the toxic effect of hyperfluorosis requires further study, in particular, the relationship between tooth morphogenesis and the development of fluorosis [20].

The primary effect of fluoride ion is related to its interaction with calcium, magnesium, iron, copper ions, alkaline groups of biopolymers. In the secondary case, there is activation of adenylate cyclase and calcium messenger systems, inhibition of protein synthesis and a number of enzymes. Tertiary action is determined by a change in the hormonal balance [5, 10]. With the accumulation of excess fluoride in the hard tissues of bones and teeth, in addition to the normal fluorination of hydroxyapatite with the formation of strong crystals of isomorphic monofluoroapatite (possible centers of crystallization), hyperfluorination occurs with the appearance of calcium phosphate and calcium fluoride crystals that are close to amorphous, also poorly soluble in water, but such coming from the enamel prism system due to the lack of isomorphism to hydroxyapatite or monofluoroapatite [25, 35]. The primary mineralization of enamel takes place in the early period of its formation. Secondary mineralization is due to the influx of minerals from the blood through the dentinal tubules, its zones - Schreger lines, lamellae and prismless enamel. Tertiary mineralization begins after teeth erupt due to the entry of substances from the oral fluid, its structure is the organization of hydroxyapatite crystals in the striae of Retzius. According to the opinion of Gasyuk A. P., the development of dental fluorosis occurs at the stages of primary and secondary mineralization [8]. At the stage of tertiary mineralization, the enamel of those teeth whose morphogenesis led to susceptibility to the action of fluoride is affected [15, 17, 18].

The purpose of this work is to study the morphological features of enamel in fluorosis in residents of Ukraine, in particular, the Poltava region.

Materials and methods

The work is a fragment of the initiative research work of the Poltava State Medical University: "Development of pathogenetic prevention of pathological changes in the oral cavity of people with internal diseases" (state registration number 0121U108263), completion date 2021-2025. The design of the study excluded the possibility of identifying individuals. Ethical standards, patient rights and confidentiality were not violated. The research was conducted in accordance with ethical and moral-legal requirements and does not contradict the basic bioethical norms of the Declaration of Helsinki, the Council of Europe Convention on Human Rights and Biomedicine (1977), the relevant provisions of the WHO and the laws of Ukraine (Minutes of the meeting of the Commission on Biomedical Ethics of the Poltava State Medical University № 201 dated 27.01.2022).

The object of our morphological study were incisors, canines, premolars and molars of the upper and lower jaws, which were removed according to orthodontic (or clinical) indications in male and female persons aged 17 to 40 years. In the set, seven teeth are intact, 20 teeth were affected by fluorosis: six of them - a mild form, six - a moderate form, and eight teeth - a severe form.

The classification recommended by WHO is used, according to which 5 forms of dental fluorosis are distinguished: doubtful, very mild, mild, moderate and severe fluorosis.

A visual assessment of the extracted teeth was carried out, their preparation for the production of grindings, the formation of thick and thin grindings (30-50 microns and 100-200 microns). Morphological features were first studied on native, and later on histochemically stained sections. The staining technique was as follows: the slides were immersed in a 10% solution of NH4Cl and placed in a thermostat at a temperature of 37 °C for 6-12 hours, after which they were immersed for 15-30 minutes in an alcohol solution of Sudan III. Subsequently, they were rinsed in distilled water and immersed in a solution of iodic acid for 5-10 minutes, washed again with two to three portions of distilled water and stained with Schiff's reagent for 10-30 minutes. Then it was washed again with water for 10 minutes and stained with alcian blue solution for 10-30 seconds. After washing, the sections were dehydrated, illuminated and fixed in polystyrene. A MBS-9 binocular magnifier (magnification x16, x32) and a Rathanow M-79053 light microscope (with image magnification from 80 to 252 times) were used to examine the slices.

PAS, Alcian blue, and Sudan III histochemical stains were used to determine the presence and changes in the distribution of lipoproteins, glycosaminoglycans, and proteoglycans.

Results

The obtained results indicate that the morphological pathohistological picture is characteristic of mild, moderate and severe forms of fluorosis. Study of slides of intact teeth and those affected by mild fluorosis yielded the following results.

On the surfaces of intact teeth, bundles of enamel prisms form longitudinal and transverse Hunter-Schreger bands (Fig. 1). Fissures, grooves, and pits contain histochemically stained PAS-positive fibrous structures surrounded by alcian-positive material. The enamel-dentine boundary is defined by a blue-green colored line. Enamel plates are contoured with a less saturated, but rather bright blue color. Enamel prisms from the enamel-dentine border to the surface of the enamel are followed by intense blue rod color, less saturated inter-rod gaps - light blue color. Under conditions of high magnification, it was established that bundles of enamel prisms, which were intensively colored in blue, alternated with inter-rod zones, where the intensity of coloring was much lower.

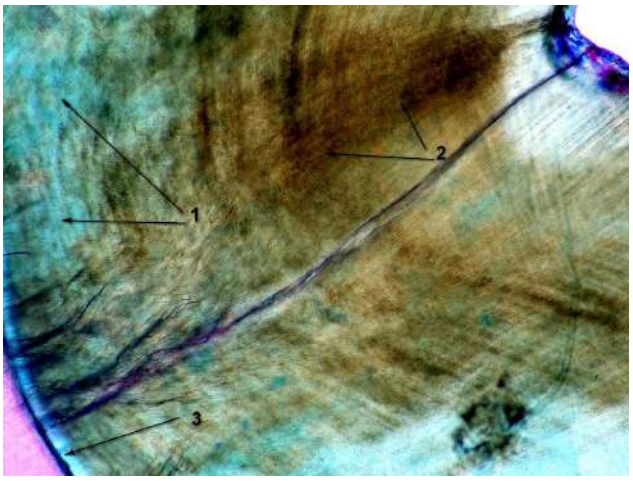

Fig. 1. Enamel of an intact tooth. 1 - enamel rod; 2 - longitudinal and transverse Hunter-Schreger bands; 3 - enamel-dentin border. Staining: Sudan III + PAS + Alcian blue. Light microscope MBS-9, x16.

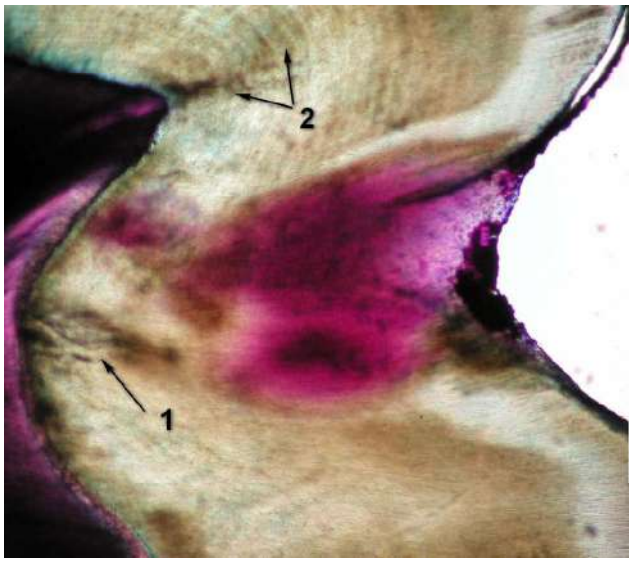

Fig. 2. Fluorosis, mild form. 1 - violation of enamel prism architecture and 2 - violation of the course of the striae of Retzius. Staining: Sudan III + PAS + Alcian blue. Light microscope Rathanow M-79053, x80.

In contrast to the slides of intact teeth, changes in the enamel of the slides of teeth affected by mild fluorosis are observed. On native and histochemically stained sections, there is a thickening of the cuticular layer, the pattern of lamellae becomes more pronounced, an uneven color and increased transparency of enamel appear, which can be explained by atypical architecture of enamel prisms and a shift in the directionality of the Retzius striae (Fig. 2).

PAS + Alcian blue positive fibrous structures are morphologically determined. When visually evaluating the macropreparation (extracted teeth, from which grindings were made), these are areas of noticeable white dots or spots. When analyzing the slides under high magnification of the microscope, the enamel prism changes its color, so we can assume that the process of mineralization of the enamel is increasing. This happens due to the redistribution of acidic glycosaminoglycans (Fig. 3).

Visually present brown mottling of the enamel, that is, moderate fluorosis of the teeth, has a slightly different morphological picture.

Clinically, dental fluorosis of a moderate degree is characterized by destructive changes in the enamel and the presence of brown spots. Morphologically moderate form of fluorosis is characterized by the following. Dotted pigmentation of the enamel surface can be traced on the section, which spreads from the outer border, sometimes to the entire thickness, almost to the enamel-dentine border (Fig. 4). The morphological picture demonstrates the presence of foci of destruction of bundles of enamel prisms, their partial homogenization or complete destruction. The orientation of the course of the enamel prisms is partially or completely lost. This phenomenon is characterized by the blue coloration of areas of accumulation of acidic glycosaminoglycans.

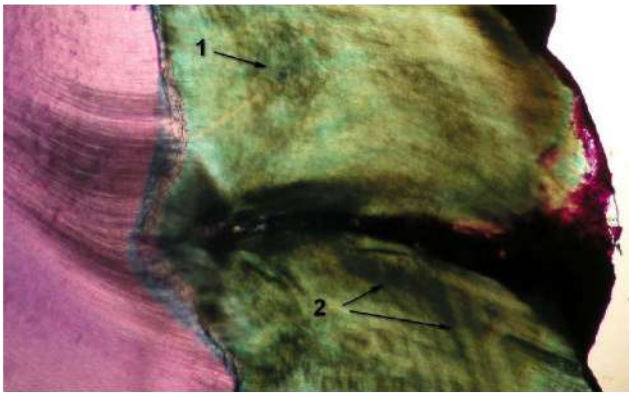

Fig. 3. Fluorosis, mild form. Violation of mineralization by striae of Retzius. 1 - enamel rod; 2 - destruction of striae of Retzius. Staining: Sudan III + PAS + Alcian blue. Light microscope Rathanow M-79053, x252.

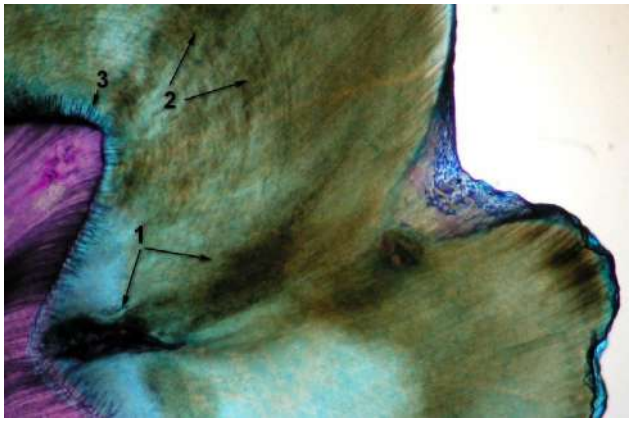

Fig. 4. Fluorosis, moderate form. The presence of foci of destruction of bundles of enamel prisms. 1 - enamel prism destruction; 2 - longitudinal and transverse Hunter-Schreger bands; 3 - enamel-dentine boundary. Staining: Sudan III + PAS + Alcian blue. Light microscope MBS-9, x32.

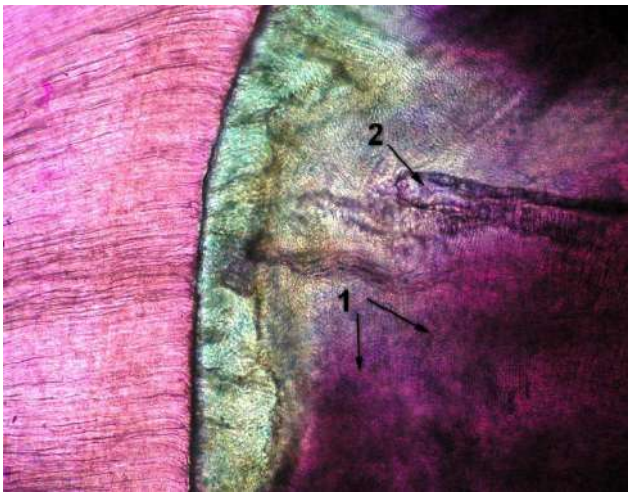

Fig. 5. Fluorosis, severe form. Homogeneous areas of cavernous structures. 1 - enamel prism destruction; 2 - cavernous structures. Staining: Sudan III + PAS + Alcian blue. Light microscope Rathanow M-79053, x252.

At high magnification of the microscope, the morphological picture was as follows. Areas of brown spotting were clearly defined. Visually intact areas are morphologically changed, because according to their location, the enamel prisms have gait disturbances. The outer enamel layer is structurally broken, the enamel layer from the enamel-dentine border contains only isolated bundles of enamel prisms. Both the outer and inner layers of enamel were painted blue from light to saturated color, which indicated the content of acidic mucopolysaccharides.

Severe fluorosis (total pigmentation, with areas of enamel destruction) was morphologically characterized by an uneven distribution of acidic mucopolysaccharides. Some areas of the enamel have sharply expressed violations of the structure.

After examination of slides of teeth with severe fluorosis under a polarizing microscope, morphological changes in the structure of the enamel were established: in the surface layer of the enamel, areas of total pigmentation and destruction had a heterogeneous structure. In the deep enamel layers of the native slides with areas of enamel destruction towards the enamel-dentine border, there was an intensification of the pattern: both Hunter-Schreger bands and striae of Retzius. Areas of enamel destruction are areas of structureless zones of an amorphous substance. The direction of movement of the enamel prisms was completely destroyed, uniform homogeneous areas with the formation of cavernous structures were traced throughout the thickness of the enamel (Fig. 5). These areas were located next to the fragmented lamellae, the enamel prisms there were partially or completely destroyed.

Thus, the morphological study of both native tooth slides and histochemically stained ones established changes in the enamel structure depending on the period of the toxic effect of fluoride on the body.

Discussion

Enamel is a unique tissue in vertebrates, its epithelial ameloblast cells secrete a number of matrix proteins that are broken down by enzymes during enamel mineralization. Any genetic or environmental disturbance will result in certain recognizable defects. Thus, depending on the specificity of the changes, a teratogenic event can be established retrospectively. Advances in this field allow the use of enamel defects as tools for the diagnosis of molecular disorders. The multifunctionality of enamel peptides is currently identified from their chemical role in mineralization to cellular signaling, which is the source of specific innovations in regenerative medicine [16]. Some studies discuss the current state of enamel tissue engineering and a new perspective on the future possibilities of regeneration of this unique tissue [22]. The analysis of numerous literary sources contains both experimental and clinical studies of the toxic effect of fluoride on the human body or animals. Animal models contribute to clinical applications by addressing disease pathogenesis. Rodent models are used to study dental fluorosis, as rat incisors erupt continuously and all stages of enamel development are present [32]. In general, fluoride promotes damage to other tissues, particularly chondrocytes, by regulating autophagy and apoptosis. This indicates that with long-term fluorine contamination and blocking of chondrocyte development, exposure to fluorine is a risk factor for cartilage development [34]. A certain percentage of researchers of the biochemical composition of enamel and the role of the protein matrix at the stages of mineralization confirm the conditionality of destructive changes and track these relationships in their experimental works [15, 28].

Analysis of caries indicators of permanent teeth in children, taking into account endemic features, demonstrates the connection of this disease with fluorosis. That is why, depending on the nature of the region, scientists offer various preventive measures [1, 2].

M. A. Buzalaf et al. [6] believe that despite the causal relationship between fluoride exposure and dental fluorosis, other factors likely account for its severity. There are observations that certain ethnic groups are more susceptible to this disease. Therefore, studies were carried out on the genetic susceptibility of different species of rodents to dental fluorosis, which aimed to evaluate the overall profile of apatite crystals in the enamel matrix of mice susceptible (strain A/J) or resistant (strain 129P3/J) to dental fluorosis by means of analysis with using atomic force microscopy.

The formation of tooth enamel is a change of successive stages, starting with presecretory, then secretory, through a short transition to the maturation stage, which is followed by apoptosis of ameloblasts and eruption of teeth in the oral cavity [9].

D. V. Kalashnikov et al. [13] determined the peculiarities of the process of enamel biomineralization in different

anatomical areas of the tooth. E. C. Küchler et al. [14] established that the polymorphism of the nonomogenin enamel matrix genes is associated with dental fluorosis. When conducting a quantitative study of the pore volume fraction of human fluorotic enamel filled with resin infiltrate, it was established that organic substances, tightly bound water and air remained in the enamel pores after impregnation with resin [31]. Under the condition of different clinical conditions of the hard tissues of the tooth, the morphological structure of the enamel has certain features. This feature may be associated with a decrease in enamel density, which is associated with a decrease in the number of prisms in non-carious tooth pathology and an increase in the spaces between them [33].

Summarizing the results of our morphological study, it should be noted that there is a negative effect of excess fluoride for the body in general and for tooth enamel in particular. The study of both native and histochemically stained sections shows the morphological changes that develop in enamel during fluoride intoxication of different duration and intensity.

The basis of our results were the studies of Aoba T. [3], in which it is stated that fluoride is involved in many aspects of the formation of calcium phosphate in vivo and has a huge impact on both the process and the nature and properties of the formed mineral. In the process of enamel mineralization during amelogenesis, it is assumed that free fluoride ions in the liquid phase accelerate the hydrolysis of the acidic precursor and increase the driving force for the growth of the apatite mineral. However, an excess of fluoride leads to abnormal formation of enamel, slowing down the maturation of tissues.

The work of Robinson C. and co-authors [26] contains a description of the effect of fluoride on biological processes, which is reflected in the formation of tooth tissues, especially tooth enamel. Attention is primarily focused on the mechanisms that, if disturbed, can lead to dental fluorosis. The turbidity characteristic of fluoridated enamel is the result of incomplete formation of apatite crystals. Matrix proteins associated with the mineral phase, which are usually decomposed and removed to allow for final crystal growth, are retained to some extent in the fluorinated fabric. Concentrations of fluoride and magnesium increase here, and carbonates decrease. The morphology of the crystal surface at the nanolevel changes, as does the functional morphology of ameloblasts at the maturation stage. The inclusion of fluoride in enamel apatite leads to the formation of more stable crystals. Such changes in crystal chemistry and morphology, including stronger ionic and hydrogen bonding, also lead to stronger binding of matrix proteins and proteolytic enzymes. This leads to a decrease in degradation and an increase in the content of protein components in mature tissue. This is most likely the cause of porous fluoro enamel, as matrix protein removal is necessary for normal crystal growth. To resolve the question of the role of cellular changes and the exact causes of protein retention, more detailed studies of changes in cell function, effects on specific types of proteins, and nanochemistry of apatite crystal surfaces are needed.

According to Gil-Bona A. and Bidlack F. B. [9] enamel-specific proteins and proteases are crucial for the correct formation of enamel. Recent proteomic analyzes have identified many other proteins whose roles in enamel formation remain to be elucidated. Although the exact protein composition of healthy tooth enamel is still unknown, it is clear that the amount and composition of organic material is different in damaged enamel. Why these differences affect both the pre-eruption mineralization process and the properties of erupted teeth will become clear when proteomics protocols are adjusted for inter-species variability, tooth size, sample size and ephemeral organic content of forming teeth. A summary of current knowledge and published data on the proteomics of healthy and diseased tooth enamel, including advances in forensic applications and animal disease modeling, highlights how recent proteomics discoveries contribute to our underestimation of the complexity and temporal changes in extracellular matrix composition during tooth enamel formation.

On the slides of visually unchanged teeth, the structure of the enamel has increased clarity of the course of the enamel prisms and Retzius striae. An uneven distribution of acidic glycosaminoglycans and neutral mucopolysaccharides is determined. Homogenization of alcian-positive masses and PAS-positive fibrous structures is determined in the affected areas. Histochemical examination shows a change in the color of homogeneous amorphous areas, which is traced from the outer surface to the enamel-dentine border of the tooth section.

The morphological changes found on the slides are obviously caused by the toxic effect of excess fluoride in one or another period of mineralization of the teeth. Excessive intake of fluorine to the body during the period of primary and secondary mineralization is especially harmful for tooth enamel. In the affected areas, fluoride continues to act even after teething, as a result - areas of total pigmentation and destruction (erosive-destructive form of fluorosis), because in the weakened area, fluoride continues to act even after teething. In the case of fluoride intoxication, only during tertiary mineralization (coming from saliva), the surface layers of the enamel are affected by fluorosis (doubtful, very weak, weak).

The results of morphological studies are a justification for further scientific developments and the introduction of new treatment methods in dentistry, in particular those involving the adhesive technique of tooth surface restoration.

Conclusions

1. In the area of endemic fluorosis, in the absence of preventive measures for the population during the period of primary, secondary or tertiary mineralization of tooth enamel, fluoride intoxication can lead to irreversible structural consequences.

2. Changes can be manifested starting from atypical architecture of enamel prisms and a violation of the directionality of Retzius striae to the appearance of areas of enamel destruction - structureless zones of amorphous substance, caverns, in which the direction of movement of enamel prisms over the entire thickness of enamel is completely destroyed.

3. Factors that have a direct impact on the morphogenesis of fluorosis during all stages of mineralization can increase or, conversely, decrease the severity of this endemic disease.

4. In the areas affected by fluorosis, the predominance of dystrophic and necrotic changes causes varying degrees of disruption of the architecture of the entire enamel layer. The spread of degenerative processes in the enamel has a tendency to spread both to the surface of the lesion and to the depth.

5. For the prevention of dental fluorosis, it is extremely important to understand the toxic effect of fluoride on ameloblasts during a certain period of enamel mineralization and to eliminate or maximally weaken the pathogenic effect of the factor.

References

[1] Al-Omoush, S. A., Al-Tarawneh, S., Abu-Awwad, M., Sartawi, S., Elmanaseer, W., & Alsoleihat, F. (2021). Comparison of oral health indicators between two places of endemic dental fluorosis in Jordan. *The Saudi Dental Journal,* 33(7), 707-712. doi: 10.1016/j.sdentj.2020.04.004

[2] Amosova, L. I., Kaskova, L. F, Pavlenkova, O. S., Khmil, O. V., Novikova, S. Ch., & Ulasevych, L. P. (2024). Analysis of indicators of caries of permanent teeth in children according to the endemic features of the Poltava region. *Polski Merkuriusz Lekarski: Organ Polskiego Towarzystwa Lekarskiego*, 52(1), 112-116. doi: 10.36740/Merkur202306107

[3] Aoba, T. (1997). The effect of fluoride on apatite structure and growth. *Critical Reviews in Oral Biology & Medicine,* 8(2), 136-153. doi: 10.1177/10454411970080020301

[4] Arheiam, A., Aloshiby, A., Gaber, A., & Fakron, S. (2022). Dental fluorosis and its associated factors amongst libyan schoolchildren. *International Dental Journal*, 72(6), 853-858. doi: 10.1016/j.identj.2022.04.010

[5] Aulestia, F. J., Groeling, J., Bomfim, G. H. S., Costiniti, V., Manikandan, V., Chaloemtoem, A., … & Lacruz, R. S. (2020). Fluoride exposure alters Ca2+ signaling and mitochondrial function in enamel cells. *Science Signaling,* 13(619), eaay0086. doi: 10.1126/scisignal.aay0086

[6] Buzalaf, M. A., Barbosa, C. S., Leite, A. D. L., Chang, S. R., Liu, J., Czajka-Jakubowska, A., & Clarkson, B. (2014). Enamel crystals of mice susceptible or resistant to dental fluorosis: an AFM study. *Journal of Applied Oral Science: Revista FOB,* 22(3), 159-164. doi: 10.1590/1678-775720130515

[7] Cury, J. A., Ricomini-Filho, A. P., Berti, F. L. P., & Tabchoury, C. P. (2019). Systemic effects (risks) of water fluoridation. *Brazilian Dental Journal,* 30(5), 421-428. doi: 10.1590/0103-6440201903124

[8] Gasyuk, P. A., Gasyuk, A. P., Danylchenko, S. I., & Gasyuk, N. V. (2016). *Морфо- і гістогенез основних стоматологічних хвороб [Morpho- and histogenesis of the main dental diseases].* Видавництво: ФОП Пархін В. В.= Publisher: FOP Parkhin V. V.

[9] Gil-Bona, A., & Bidlack, F. B. (2020). Tooth enamel and its dynamic protein matrix. *International Journal of Molecular Sciences,* 21(12), 4458. doi: 10.3390/ijms21124458

[10] Gong, Q. M., Ling, J. Q., & Wei, X. (2023). Research progress in the pathogenesis mechanism of dental fluorosis. *Zhonghua kou Qiang yi xue za zhi=Zhonghua Kouqiang Yixue Zazhi=Chinese Journal of Stomatology,* 58(3), 217-223. Advance online publication. doi: 10.3760/cma.j.cn112144-20221013-00526

[11] Grynova, M., Safranov, T., Chugai, A., Grynyov, R., Soloshych, I., & Velychko, R. (2022). Fluorides as an indicator of physiological completeness of mineral composition of drinking waters of separate regions of Ukraine. *Journal of Ecological Engineering,* 23(2), 41-49. doi: 10.12912/27197050/145131

[12] Gu, L. S., Wei, X., & Ling, J. Q. (2020). Etiology, diagnosis, prevention and treatment of dental fluorosis. *Zhonghua kou Qiang yi xue za zhi=Zhonghua Kouqiang Yixue Zazhi=Chinese Journal of Stomatology*, 55(5), 296-301. doi: 10.3760/cma.j.cn112144-20200317-00156

[13] Kalashnikov, D. V., Hasiuk, P. A., Vorobets, A. B., Rosolovska, S. O., Kindiy, D. D., Hrad, A. O., & Zubchenko, S. G. (2020). Features of the course of enamel biomineralization processes in various anatomical areas of the tooth. *Wiadomosci lekarskie,* 73(5), 864-867. doi: 10.36740/WLek202005105

[14] Küchler, E. C., Dea Bruzamolin, C., Ayumi Omori, M., Costa, M. C., Antunes, L. S., Pecharki, G. D., … & Brancher, J. A. (2018). Polymorphisms in nonamelogenin enamel matrix genes are associated with dental fluorosis. *Caries Research,* 52(1-2), 1-6. doi: 10.1159/000479826

[15] Li, Y. B., Li, F., Guo, S., Gao, L., Guo, R. M., Lu, L. W., & Zhang, Y. X. (2021). Microscopic observation of the enamel microstructures of SD rats with different degrees of fluorosis. *Zhonghua kou Qiang yi xue za zhi=Zhonghua Kouqiang Yixue Zazhi=Chinese Journal of Stomatology,* 56(12), 1261-1266. doi: 10.3760/cma.j.cn112144-20210916-00414

[16] Lignon, G., de la Dure-Molla, M., Dessombz, A., Berdal, A., & Babajko, S. (2015). Enamel: a unique self-assembling in mineral world. *Medicine Sciences: M/S,* 31(5), 515-521. doi: 10.1051/medsci/20153105013

[17] Limandri, S., Galván Josa, V., Valentinuzzi, M. C., Chena, M. E., & Castellano, G. (2016). 3D scanning electron microscopy applied to surface characterization of fluorosed dental enamel. *Micron,* 84, 54-60. doi: 10.1016/j.micron.2016.02.001

[18] Marin, L. M., Cury, J. A., Tenuta, L. M., Castellanos, J. E., & Martignon, S. (2016). Higher fluorosis severity makes enamel less resistant to demineralization. *Caries Research*, 50(4), 407-413. doi: 10.1159/000447270

[19] Martignon, S., Bartlett, D., Manton, D. J., Martinez-Mier, E. A., Splieth, C., & Avila, V. (2021). Epidemiology of erosive tooth wear, dental fluorosis and molar incisor hypomineralization in the American continent. *Caries Research*, 55(1), 1-11. doi: 10.1159/000512483

[20] Martinez-Mier, E. A., Shone, D. B., Buckley, C. M., Ando, M., Lippert, F., & Soto-Rojas, A. E. (2016). Relationship between enamel fluorosis severity and fluoride content. *Journal of Dentistry,* 46, 42-46. doi: 10.1016/j.jdent.2016.01.007

[21] Moimaz, S. A., Saliba, O., Marques, L. B., Garbin, C. A., & Saliba, N. A. (2015). Dental fluorosis and its influence on children's life. *Brazilian Oral Research,* 29, S1806-83242015000100214. doi: 10.1590/1807-3107BOR-2015.vol29.0014

[22] Pandya, M., & Diekwisch, T. G. H. (2019). Enamel biomimetics-fiction or future of dentistry. *International Journal of Oral Science,* 11(1), 8. doi: 10.1038/s41368-018-0038-6

[23] Patil, M. M., Lakhkar, B. B., & Patil, S. S. (2018). Curse of fluorosis. *Indian Journal of Pediatrics,* 85(5), 375-383. doi: 10.1007/s12098-017-2574-z

[24] Pérez-Pérez, N., Torres-Mendoza, N., Borges-Yáñz, A., & Irigoyen-Camacho, M. E. (2014). Dental fluorosis: concentration of fluoride in drinking water and consumption of bottled beverages in school children. *The Journal of Clinical Pediatric Dentistry,* 38(4), 338-344. doi: 10.17796/jcpd.38.4.e77h557k0005077n

[25] Priyadharsini, N., Malathi, N., Tamizhchelvan, H., & Dineshkumar, T. (2015). Dental fluorosis: a histological study using light and confocal microscopy. *Indian Journal of Dental Research: Official Publication of Indian Society for Dental Research*, 26(3), 248-251. doi: 10.4103/0970-9290.162896

[26] Robinson, C., Connell, S., Kirkham, J., Brookes, S. J., Shore, R. C., & Smith, A. M. (2004). The effect of fluoride on the developing tooth. *Caries research,* 38(3), 268-276. doi: 10.1159/000077766

[27] Sabandal, M. M., & Schäfer, E. (2016). Amelogenesis imperfecta: review of diagnostic findings and treatment concepts. *Odontology,* 104(3), 245-256. doi: 10.1007/s10266-016-0266-1

[28] Saldarriaga, A., Rojas-Gualdrón, D. F., Restrepo, M., Bussaneli, D. G., Fragelli, C., de Cássia Loiola Cordeiro, R., … & Jeremias, F. (2021). Clinical changes in the severity of dental fluorosis: a longitudinal evaluation. *BMC Oral Health,* 21(1), 366. doi: 10.1186/s12903-021-01729-3

[29] Sharashenidze, M., Tkeshelashvili, V., & Nanobashvili, K. (2020). Dental fluorosis prevalence, severity and associated risk factors in pre-school aged children residing in fluoride deficient regions of Georgia. *Georgian Medical News,* 306, 57-61.

[30] Sheshukova, O. V., Trufanova, V. P., Bauman, S. S., Kazakova, K. S., Polishchuk, T. V., Mosiienko, A. S., & Lyakhova, N. A. (2023). Affection on caries and its complications of temporary teeth of children in a region with excess fluorine content in drinking water. *Polski merkuriusz lekarski: organ Polskiego Towarzystwa Lekarskiego*, 51(6), 620-623. doi: 10.36740/Merkur202306107

[31] de Sousa, F. B., Lelis, I. M. P., Figueiredo, R. C. B. Q., Pires, A. C., & Gerlach, R. F. (2017). Quantitative study of the proportion of the pore volume of human fluorotic enamel filled by resin infiltrant. *Archives of Oral Biology,* 82, 134-140. doi: 10.1016/j.archoralbio.2017.06.017

[32] Suzuki, M., & Bartlett, J. D. (2019). Rodent dental fluorosis model: extraction of enamel organ from rat incisors. *Methods in Molecular Biology* (Clifton, N.J.), 1922, 335-340. doi: 10.1007/978-1-4939-9012-2_30

[33] Tkachenko, I. M., Brailko, N. N., Kovalenko, V. V., Nazarenko, Z. J., & Sheshukova, O. V. (2018). Morphological study of enamel and dentin teeth with carious process and non-carious lesions. *Wiadomosci Lekarskie,* 71(5), 1002-1005. PMID: 30176630

[34] Wang, Y., Li, A., Mehmood, K., Hussain, R., Abbas, R. Z., Javed, M. T., …& Zhang, H. (2021). Long-term exposure to the fluoride blocks the development of chondrocytes in the ducks: The molecular mechanism of fluoride regulating autophagy and apoptosis. *Ecotoxicology and Environmental Safety,* 217, 112225. doi: 10.1016/j.ecoenv.2021.112225

[35] Wei, Y., Zeng, B., Zhang, H., Chen, C., Wu, Y., Wang, N., … & Shen, L. (2018). Comparative proteomic analysis of fluoride treated rat bone provides new insights into the molecular mechanisms of fluoride toxicity. *Toxicology Letters,* 291, 39-50. doi: 10.1016/j.toxlet.2018.04.00

[36] Wiener, R. C., Shen, C., Findley, P., Tan, X., & Sambamoorthi, U. (2018). Dental fluorosis over time: a comparison of National health and nutrition examination survey data from 2001-2002 and 2011-2012. *Journal of Dental Hygiene: JDH,* 92(1), 23-29. PMID: 29500282

МОРФОЛОГІЧНІ ОСОБЛИВОСТІ ЕМАЛІ ПРИ ФЛЮОРОЗІ РІЗНОГО СТУПЕНЯ ВАЖКОСТІ

Марченко А. В., Ніколішина Е. В., Іленко Н. М., Ніколішин І. А., Костиренко О. П., Черняк В. В.

Виникненню флюорозу зубів сприяють порушення мінералізації емалі, які викликані фторидами, що надходять до організму людини в надлишковій кількості в період її розвитку та формування, токсично впливають на енамелобласти. Однак молекулярні механізми, задіяні в патогенезі флюорозу, до кінця не вивчені. Формування емалі - це складний процес, що включає проліферацію та диференціацію клітин через епітеліально-мезенхімальну послідовну секрецію матричних білків, тканинно-специфічний транспорт іонів, включаючи кальцій і фторид, а також преципітацію та вирівнювання кристалів емалі через взаємодію між органічними та неорганічними молекулами. Розуміння морфологічних особливостей змін емалі при фтористій інтоксикації організму людини в ендемічному регіоні допомагає усвідомити необхідність комплексного вирішення даної медичної та соціальної проблеми. Метою роботи стало вивчити морфологічні особливості емалі при флюорозі у жителів ендемічного регіону України, зокрема Полтавського регіону. Досліджували різні групи зубів (як інтактні, так і уражені флюорозом), котрі видалили за ортодонтичними або клінічними показаннями в осіб чоловічої та жіночої статі віком від 17 до 40 років. Морфологічні особливості вивчали первинно на нативних, у подальшому - на гістохімічно забарвлених шліфах. Встановлено, що порушення будови шару емалі зубів при ураженні флюорозом від слабкого до тяжкого ступеня характеризується як частковим, так і повним порушенням ходи емалевих призм, з ознаками деструкції. Виявлено фрагментацію і гомогенезацію на всю товщу в окремих ділянках емалі. При оцінці гістохімічно забарвлених шліфів зубів, уражених флюорозом, встановлено, що дистрофічні зміни структури емалі та накопичення кислих глікозаміногліканів у вогнищах ураження більшою мірою характерно для слабкої та помірної форми. За умов тяжкої форми флюорозу встановлено повне руйнування призм, фрагментація ламел, гомогенізація ділянок на весь шар емалі, що обумовлено нерівномірним розподілом кислих мукополісахаридів. Морфологічно та гістохімічно в ділянках ураженої емалі дистрофічні зміни знаходять своє підтвердження в нерівномірному розподілі та накопиченні кислих глікозаміногліканів. Оцінка впливу фтористої інтоксикації на стан емалі зубів дозволить розширити можливості профілактичних заходів суміжним спеціалістам, а також створити та розробити додаткові лікувальні методи, котрі сприятимуть покращенню фізичних та естетичних норм стоматологічного здоров'я.

Ключові слова: *структура емалі, флюороз, глікозаміноглікани, мінералізація.*

Author's contribution

Marchenko A. V. - conceptualization, methodology, writing of the original draft.
Nikolishyna E. V. - conceptualization, research, review writing and editing.
Ilenko N. M. - software, formal analysis and validation.
Nikolishyn I. A. - research, review writing and editing, project administration, software, resources.
Kostyrenko O. P. - formal analysis and validation, project administration, software, resources.
Cherniak V. V. - project administration, review writing and editing.

DOI: 10.31393/morphology-journal-2024-30(2)-08 Reports of Morphology, Vol. 30, №2, Pages 61-68

ISSN 1818-1295 eISSN 2616-6194

REPORTS OF MORPHOLOGY

Official Journal of the Scientific Society of Anatomists, Histologists, Embryologists and Topographic Anatomists of Ukraine

journal homepage: https://morphology-journal.com

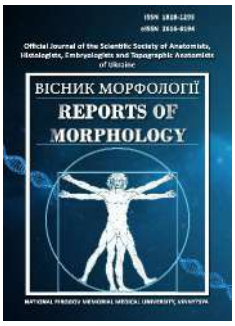

Pathomorphological features of confirmed bronchogenic cyst with atypical localization

Khoroshun E. M.[1], Nehoduiko V. V.[1], Vorovskyi O. O.[2], Makarov V. V.[3], Bunin Yu. V.[1], Smolyannik K. M.[3]

[1]Military Medical Clinical Center of the Northern Region of the Command of the Medical Forces of the Armed Forces of Ukraine, Kharkiv, Ukraine
[2]National Pirogov Memorial Medical University, Vinnytsya
[3]Kharkiv National Medical University, Kharkiv, Ukraine

ARTICLE INFO
Received: 07 February 2024
Accepted: 03 April 2024

UDC: 616.233:575.113.1:618.11-006.2-089:616-073.75:611.018

CORRESPONDING AUTHOR
e-mail: vorovskiysurgery@ukr.net
Vorovskyi O. O.

CONFLICT OF INTEREST
The authors have no conflicts of interest to declare.

FUNDING
Not applicable.

DATA SHARING
Data are available upon reasonable request to corresponding author.

Among all formations of the mediastinum in the adult population, cysts make up about 20 %, of which more than 60 % are bronchogenic cysts, where up to 50% have an asymptomatic course, and therefore in most cases are detected accidentally. Regardless of the course and origin, cysts are subject to complete surgical removal. In connection with the clinical and radiological polymorphism of bronchogenic cysts, histological confirmation of the origin of the cysts does not lose its relevance. The purpose of the work is to study and highlight the pathomorphological characteristics of a cyst localized in the pericardium. Using video-assisted thoracic surgery (VATS) and thoracotomy approaches, 16 people aged 28 to 62 with cystic lesions of the mediastinum were operated on. The patients underwent radiographic examination, computed tomography with intravenous contrast injection and, in 2 cases, magnetic resonance imaging. Ultrasound examination was performed on 6 patients in whom cystic lesions were a diagnostic finding. The location of the cyst, maximum diameter, density, and calcification were evaluated. Clinically and radiologically, asymptomatic pericardial (coelomic) cysts were detected in 2 persons in the prevascular department. In the visceral part of the mediastinum, 3 patients had a pericardial cyst, 10 patients were diagnosed with 10 bronchial cysts with parenchymal and perihilar localization, among which one patient was diagnosed with an asymptomatic bronchial cyst with an atypical localization in the pericardium. In the paravertebral part of the mediastinum, 1 paraesophageal cyst was established, which was intimately connected with the lower third of the thoracic part of the esophagus. All types of cysts were histologically confirmed. Statistical processing of the obtained results was carried out using the Excel program. After a clinical examination of a patient with a pericardial cyst of the visceral mediastinum, right VATS surgery and removal of the cyst was performed. Histological examination of fragments of the cyst wall showed the presence of multi-rowed ciliated cylindrical epithelium, pronounced infiltration by lymphoid elements with hemorrhages and foci of fibrotization in separate areas. The histological structure of the removed pericardial cyst confirmed its bronchogenic origin. So, we discovered a rare form of abnormality of embryonic growth of the ventral part of the foregut with localization of a bronchogenic cyst in the anterior-inferior mediastinum on the right, which significantly expanded the understanding of the disease.

Keywords: *bronchogenic cyst, radiography, video-assisted thoracic surgery, histology.*

Introduction

The mediastinum is a rather complex anatomical space, where accurate diagnosis of the localization of any lesion remains quite problematic today, which cannot but affect the results of treatment. Previous anatomical classifications of the mediastinum and their definitions do not always coincide with the conclusions of modern instrumental diagnostic methods. Therefore, on the basis of cross-sectional imaging of the mediastinum, the International Thymic Malignancy Interest Group (ITMIG) developed and adopted a new clinical classification that divides the mediastinum into three sections: prevascular (anterior), visceral (middle) and paravertebral (posterior)

sections [1, 27].

The frequency of detection of cysts in the adult population is about 20 % of the total number of detected neoplasms of the mediastinum. Often they arise as a result of disorders of embryonic development. And depending on the morphological component, the following types of cysts are distinguished:

1) bronchial cysts - capsular one-chamber formations, which are filled with liquid content and are most often located in the visceral (middle) and paravertebral parts of the mediastinum;

2) cysts of the digestive tract - capsular one- and two-chamber, oval, can connect with the esophagus [3], forming a fistula; usually located in the paravertebral section of the mediastinum;

3) pericardial cysts - thin-walled oval or pear-shaped formations connected by a stalk to the pericardial cavity. They are located mainly in the right phrenic-cardiac angle (as a coelomic cyst). It is believed that a third of mediastinal cysts are pericardial cysts. They are usually asymptomatic and appear accidentally, most often in people aged 40-50 [2].

Cysts are divided into congenital cysts, including bronchogenic cysts, esophageal cysts, gastrointestinal cysts, coelomic cysts (pericardial and mesothelial), thymic cysts, and acquired cysts, which are less common and are represented mainly by thoracic duct cysts and lymphangiomas. Bronchogenic cysts are congenital cystic malformations of the respiratory tract that arise as a result of abnormal budding of the bronchial tree during embryogenesis and account for 50-60 % of the total number of mediastinal cysts. It should be noted that bronchogenic cysts are quite rare, their frequency is 1 case per 42,000-68,000 [9, 19]. They can be diagnosed at any age, but are more often reported in young people and adolescents than in adults [17, 23].

In most patients, the presence of cysts is asymptomatic, sometimes symptoms associated with compression of mediastinal structures appear. Cysts are single-chambered and, rarely, multi-chambered. Typically, the cyst wall is a thin fibrous capsule with few smooth muscle cells, which is lined by secretory respiratory epithelium (columnar or cuboidal ciliated epithelium) and may contain cartilage, glandular tissue, and smooth muscle fibers. This epithelium can be metaplastic [23]. Bronchogenic cysts are characterized by a parenchymal (intrapulmonary) or perihilar location. However, rare localizations were observed, including the neck [23], pericardium [8], esophagus [5].

Less than 6 % of all neoplasms of the mediastinum are pericardial cysts [6], which can be detected accidentally during radiography, sometimes they can disappear spontaneously [18]. A pericardial cyst develops as a result of violations of the embryogenesis of the pericardial leaves and the impossibility of fusion of the mesenchymal lacuna, which forms the pericardial sac. This leads to metamorphosis in the cyst wall, consisting of a thin layer of fibrous tissue lined by a single layer of mesothelial cells. Most pericardial cysts are found in the right anterior costo-diaphragmatic angle (70 %), but it can be located in any part of the mediastinum near the heart. The incidence is reported to be 1:100,000 patients, although this is probably an underestimate, as more than 50 % remain clinically "silent" and are usually discovered incidentally. Pericardial cysts are usually less than 5.0 cm in diameter. Differential diagnosis should be carried out with any bronchogenic neoplasm, pericardial lipoma, thymoma, mediastinal teratoma, Morganhi hernia, cyst-duplication of the gastrointestinal tract, cystic sequestration of the lungs, mesothelium-lined cyst, post-traumatic cyst and hydatid cyst, and other cystic formations of the mediastinum [6, 22, 26].

Taking into account the fact that mediastinal formations in most cases have an asymptomatic course, they are most often detected accidentally, during a chest X-ray, which must be performed in two projections.

A mediastinal cyst can be diagnosed accidentally during echocardiography of intracardiac hemodynamic disorders. Computed tomography is a method with which it is often possible to predetermine the nature of the lesion. Single cases of malignancy of bronchogenic cysts are described in the scientific literature. J. Whooley et al. [29] first reported a squamous cell carcinoma arising in the paratracheal region from a bronchogenic cyst. Computed tomography provides the fastest results regarding the presence of signs of malignancy. Cysts have low density, thin (imperceptible) walls, little or no septa, and no contrast enhancement. Cystic lesions (proteinaceous, infected, or hemorrhagic) may be misinterpreted as solid due to tissue areas or blood clots. Dual-energy computed tomography with intravenous contrast can help distinguish cystic from solid lesions using digital iodine subtraction techniques (intravenous contrast). This allows differentiation of tissue enhancement from hemorrhagic/proteinaceous fluid, as well as differentiation of calcium due to different intensity of contrast accumulation [24].

For the diagnosis of hypermetabolic lesions of cysts, a number of scientists promote the use of a fairly modern study, such as fluorodeoxyglucose-positron emission tomography/computed tomography (FDG-PET/CT) with individualized radioactive indicators, which can be used in each specific case for the diagnosis of metastatic lesions. neuroendocrine lesions and other suspected malignant neoplasms [24].

Magnetic resonance imaging can be used as a means of solving problems, especially when it is difficult to distinguish cystic from solid lesions on a computer tomography and characterize complex cystic lesions, more clearly determine the presence of infiltrative disease [24].

Most authors consider operative removal of cysts of any type as the "gold standard" instead of a therapeutic approach, according to their observations of patients with

cystic lesions who underwent radical surgery, had excellent results [26].

As for the approach to the choice of the method and accesses of surgical intervention, at the current stage we are observing a transition from highly traumatic thoracotomy (anterolateral or lateral) to minimally invasive surgery (MIS). The possibilities of MIS application are directly related to the progress of development of medical technology and corresponding surgical instruments. MIS became possible with the introduction of video-assisted thoracic surgery (VATS) [4] or robotic assisted thoracic surgery (RATS), and the development of endoscopic instruments expanded the indications for the use of MIS and became the "gold" standard. In particular, RATS not only improved the quality of life of patients, but also the ergonomic indicators of the professional activity of doctors [9, 12].

The purpose of the work is to study and highlight the pathomorphological characteristics of a cyst localized in the pericardium.

Materials and methods

During the period January 2010 - December 2023, 16 (100 %) people aged 28 to 62 with cystic lesions of the mediastinum were diagnosed and treated in the conditions of the Military Medical Clinical Center of the Northern Region of the Command of the Medical Forces of the Armed Forces of Ukraine. The average age of the patients was 42.5±0.5 years. There were 12 (75.0 %) men, 4 (25.0 %) women. There was no significant difference in the average age between men and women ($p>0.5$).

All patients were informed about the nature of the study and signed an informed consent for the diagnostic examination and the type of surgical intervention using personal data. The patient could refuse to participate in the study or stop participating at any time. The research was conducted confidentially, only the patients were informed about their results. In scientific publications, only generalized data without personalized information were presented. Only the operator had access to the information. No harm was caused to the patients from the conducted research. The study was approved by the ethics committee of the Military Medical Clinical Center of the Northern Region of the Command of the Medical Forces (Protocol No. 1 dated January 26, 2024).

In 10 (62.5 %) patients, the clinical course was asymptomatic, and the mediastinal cyst was detected during the examination of the chest X-ray. Other 6 patients (37.5 %) had specific symptoms. The location and type of mediastinal cysts were determined with the help of appropriate instrumental diagnostic methods. The diameter of the cysts was 4.0±1.0 cm on average. The average size of bronchogenic cysts was 4.5±0.5 cm, and 3.7±0.5 cm in pericardial cysts.

Thus, in the prevascular department, clinical and radiological signs indicated the presence of asymptomatic pericardial (coelomic) cysts in 2 persons (12.5 %), the sizes of which in diameter were 3.5 cm and 4.5 cm. Cysts of the thymus gland were not detected during the study.

In the visceral part of the mediastinum, 3 patients (18.75 %) had a pericardial cyst, of which 2 (12.5 %) asymptomatic cysts were located in the left cardiodiaphragmatic angle, and 1 (6.25 %) - above the left ventricle with signs of clinical compression. Also, in the visceral part of the mediastinum, 10 patients (62.5 %) had 10 (62.5 %) bronchial cysts with a diameter of 4.0 to 6.5 cm, of which in 4 patients (25.0 %) they were localized intrapulmonary (parenchymal), 5 (31.25 %) - perihilar, and in 1 patient (6.25 %) was diagnosed with an asymptomatic bronchial cyst with atypical localization in the pericardium.

In the paravertebral part of the mediastinum, 1 (6.25 %) paraesophageal cyst with a diameter of 4.4 cm was found, which was intimately connected to the lower third of the thoracic part of the esophagus.

In all patients (100 %), according to the examination protocol, in order to clarify the type of vascularization of the formation, radiography of the chest organs was combined with computer tomography with intravenous injection of contrast. Ultrasound examination was performed in 6 (37.5 %) patients, where cystic lesions were a diagnostic finding. FDG-PET/CT was not used in these studies.

Magnetic resonance imaging was used in 2 (12.5 %) patients with a bronchial cyst with perihilar localization and 1 (6.25 %) with a paraesophageal cyst in order to rule out an infiltrative process. With the help of the above studies, it was established that there was no significant difference in size between the types of cysts.

In 10 (62.5 %) cases, the contents of the cyst were mucoid, in 5 (31.25 %) - serous, and in 1 (6.25 %) - blood clots. Membranes were present in 2 (12.50 %) cysts, and cartilage (bronchogenic cysts) in 1 (6.25 %).

"Open" surgical approaches included lateral thoracotomy in 5 (31.25%) cases. VATS was performed in 11 (68.75 %) cases.

In one case, an *atypical location of a bronchial cyst was established (Report of an atypical case)*. The sick serviceman Ye., 38 years old, was hospitalized in the surgical department of the surgical clinic of the Military Medical Clinical Center of the Northern Region of the Command of the Medical Forces due to a pericardial cyst for further examination and operative treatment. Clinically and laboratory examined. Survey radiography of the chest organs was performed with the help of the radiographic diagnostic KRD-50 complex "INDIASCOP-01" (Ukraine). Multispiral computed tomography (MSCT) of the chest organs was performed on the "Revolution EVO" machine with a tomograph step of 0.5 mm. Surgery performed: VATS on the right, revision, cyst removal of the visceral mediastinum, sanitation and drainage of the right pleural cavity according to Bülau under general anesthesia with one-lung intubation (left) and artificial lung ventilation.

Video thoracoscopy was performed on the OLYMPUS VISERA 4K UHD OTV-S400, 2021 video endoscopic stand. Pericardial cyst tissue fragments were taken for histological examination, for which the excised samples were fixed in 40 % neutral formalin and embedded in paraffin according to generally accepted methods [11]. After paraffin fixation, sections with a thickness of 5-6 μm were made, which were stained with hematoxylin and eosin. Complex pathomorphological studies were performed on a Primo Star microscope (Carl Zeiss) with a magnification of x280. An AxioCam (ERc 5s) high-resolution 8-bit digitizing digital camera with a pixel size of 2.2 μm and Carl Zeiss AxioCam (ERc5s) Configuration Tool software were used for image documentation. In the postoperative period, before and after the removal of pleural drainage, control X-rays of the chest organs were performed. The lungs were expanded, fluid and air in the pleural cavity on the right were not determined.

Statistical processing of the obtained results was carried out using the Excel program (Microsoft Office, USA).

Results

All 16 patients underwent surgical removal of the cyst. In 14 (87.5 %) cases, complete removal of the cyst was performed, and in 2 (12.5 %) cases - partial removal (due to intimate fusion with the aorta).

All types of cysts were histologically confirmed. Bronchogenic cysts were characterized by a cystic wall with a mucous membrane, which was lined with respiratory epithelium, where metaplasmic dysplasia was observed in 4 (25.0 %) cases, the presence of bronchial glands was established, and in 1 (6.25 %) case - 2 areas of cartilage. The paraesophageal cyst was characterized by the presence of a mucous membrane lined with ciliated columnar epithelium characteristic of the gastrointestinal tract, with areas of nonkeratinizing squamous epithelium and the presence of a smooth muscle layer with moderate degenerative changes.

Patient E., 38 years old, underwent a multispiral computed tomography of the chest organs (Fig. 1). During the examination, a neoplasm of a rounded shape, size 33.00 x 30.00 mm, of inhomogeneous structure with a liquid component and clear contours, without signs of invasion into adjacent anatomical structures, was found in the area of the anterior mediastinum on the right.

During the operation, a revision of the thoracic cavity was carried out and in the projection of the anterior-inferior mediastinum on the right, the presence of interpleural adhesions and a rounded neoplasm measuring 33.00 x 30.00 mm, which was dense and limited in mobility, was established. With the help of the Covidien LigaSure Maryland device, the neoplasm was gradually isolated from the surrounding tissues and removed from the pleural cavity. Figure 2 shows the thoracoscopic visualization of the cyst and the stage of separation of the cyst after cutting it off from the pericardium.

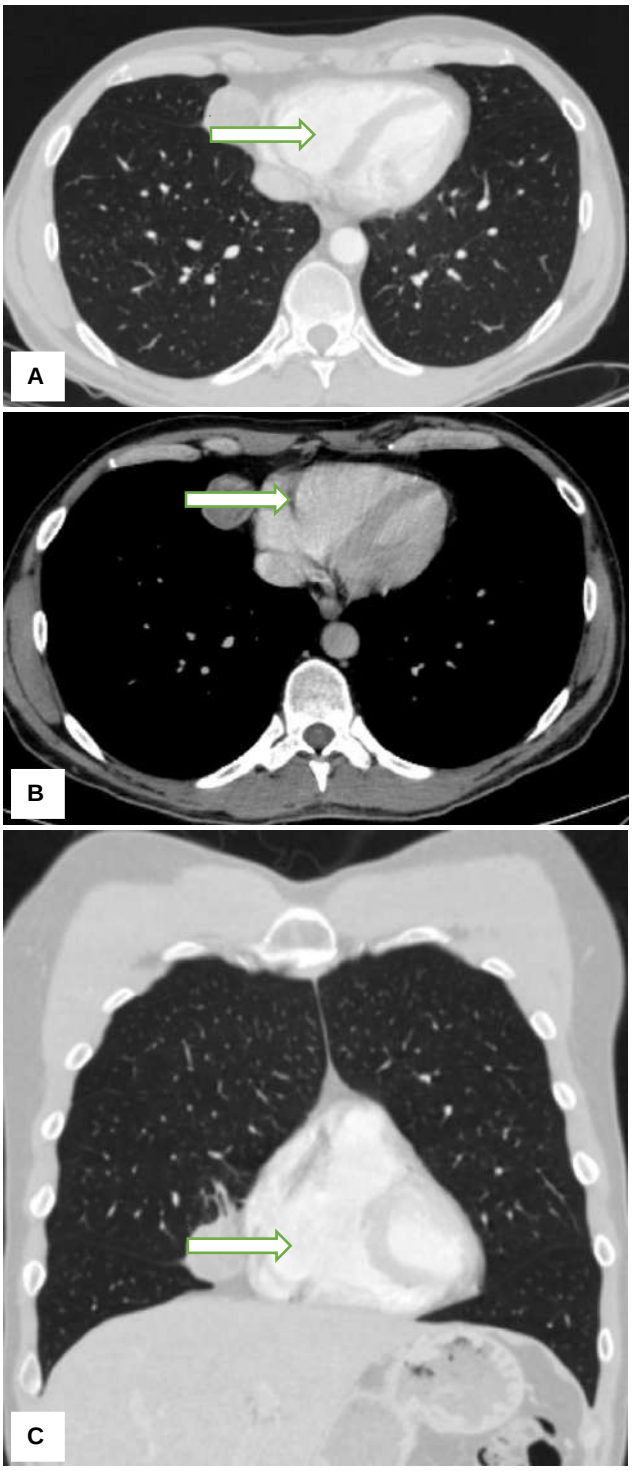

Fig. 1. Primary computer tomography of patient E., 38 years old. Right anterior mediastinum. A rounded neoplasm with clear contours without signs of invasion into adjacent anatomical structures (white arrows). A, B - axial projection; C - coronal projection.

The external macroscopic view of the pericardial cyst after removal from the pleural cavity is presented in Figure 3.

When the cyst was opened, up to 8 ml of cloudy liquid

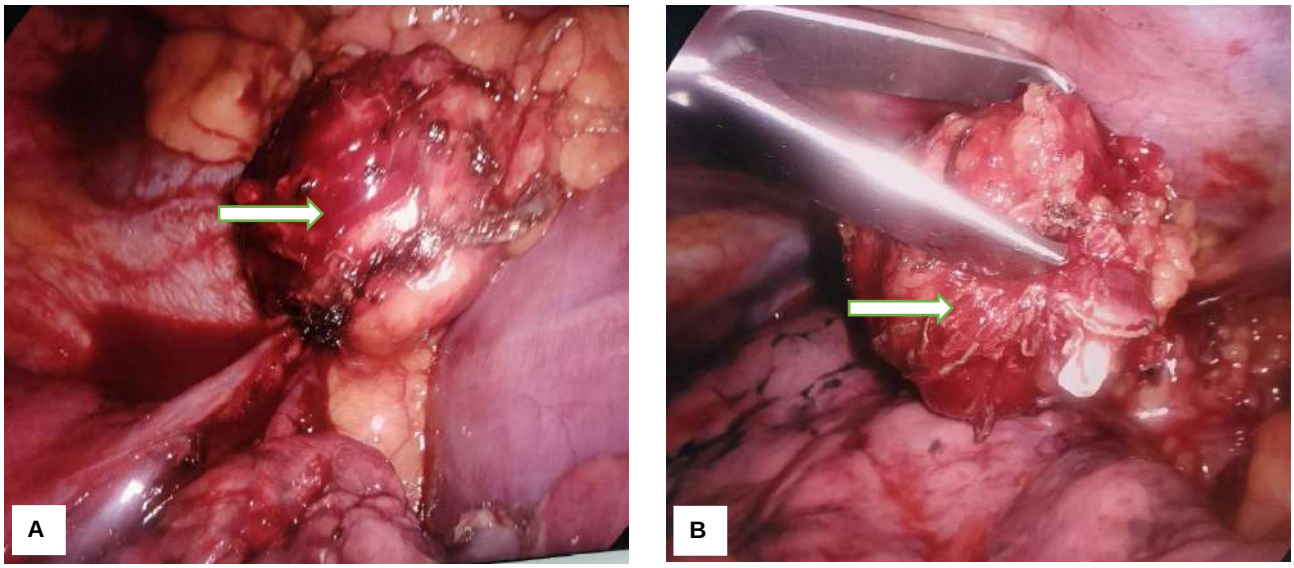

Fig. 2. A - thoracoscopic visualization of a pericardial cyst (white arrow); B - cyst removal (white arrow) after cutting from the pericardium.

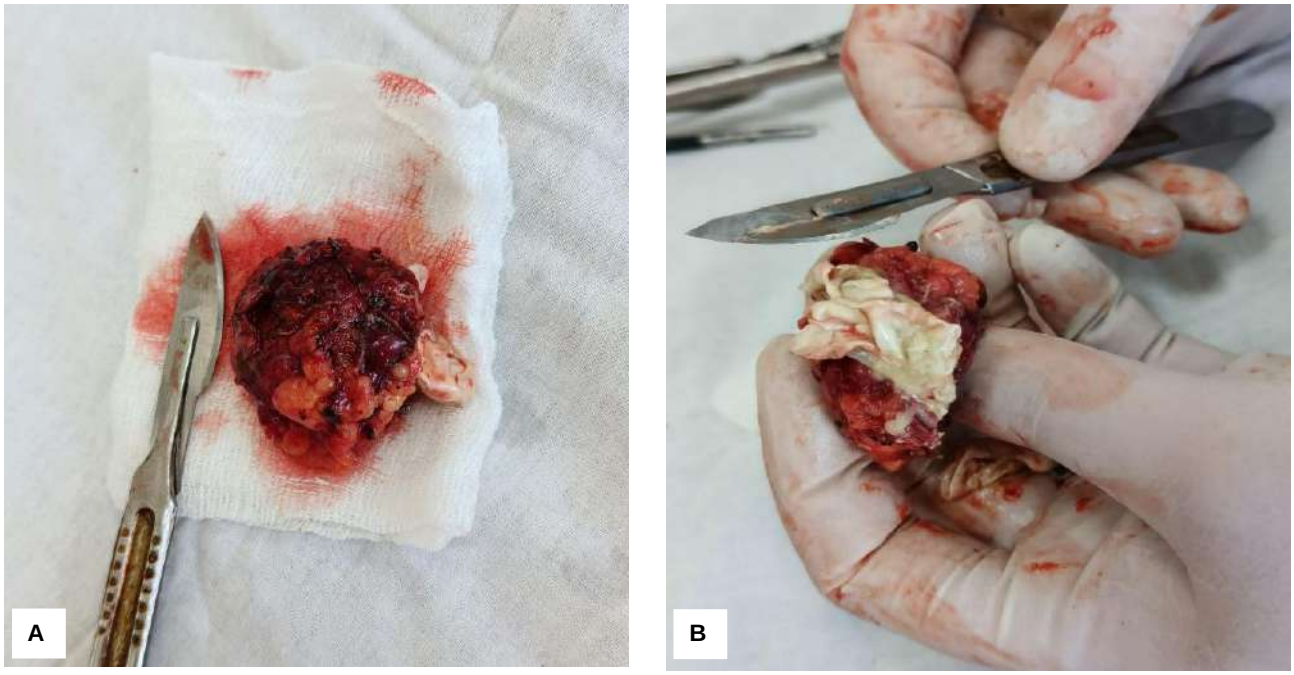

Fig. 3. Macropreparation. A - removed cyst. Macropreparation. B - cyst on autopsy.

was removed, the inner layer of the cyst was white. The cyst was soft to the touch.

The microscopic structure of the removed cyst is shown in Figures 4 and 5. The wall of the cyst was lined with multi-row ciliated cylindrical epithelium, marked infiltration by lymphoid elements with multiple hemorrhages was observed. In some areas, dilated venous vessels with foci of fibrotization were visualized. The histological structure of the removed pericardial cyst confirmed by us its bronchogenic origin.

The microscopic picture of the cyst is characterized by one or several tissues that are characteristic of the trachea or bronchi. Characteristically, they are lined, usually, with ciliated, multi-layered columnar epithelium, which was determined during histological examination. In the absence of ciliated epithelium, squamous cell metaplasia may occur, which should always be emphasized and the drugs should be examined histologically. The patient's absence in the anamnesis of lung disease and accompanying parenchymal and bronchial inflammation, together with the histological examination, confirmed the presence of a bronchogenic cyst with a localization that is not characteristic of bronchogenic cysts.

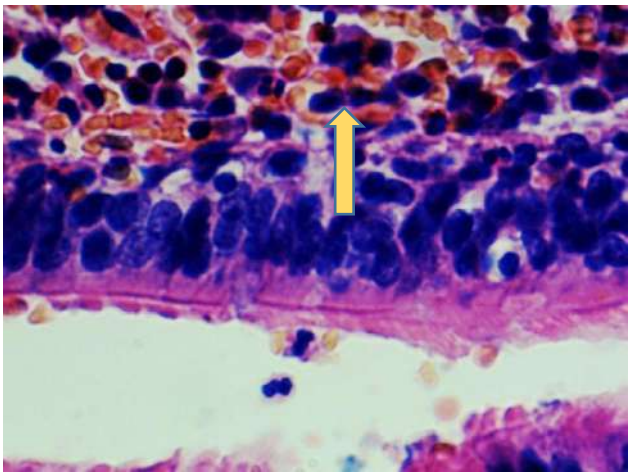

Fig. 4. Section of the pericardial bronchogenic cyst wall. Multi-row ciliated cylindrical epithelium (black arrow). Lymphoid elements with multiple hemorrhages in the wall (yellow arrow). Hematoxylin-eosin. x280.

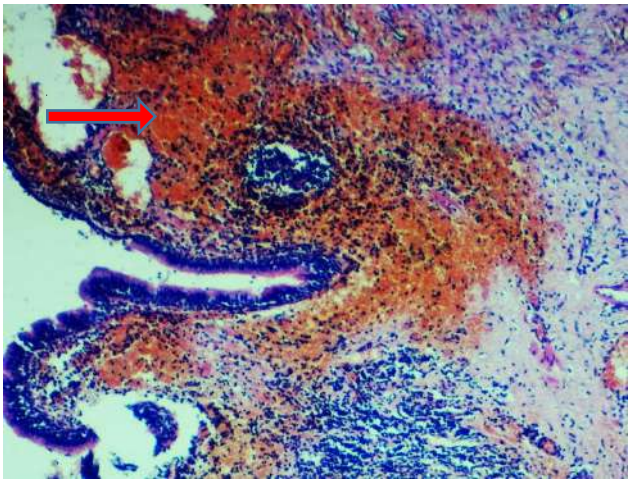

Fig. 5. Section of the pericardial bronchogenic cyst wall. Areas of fibrotization (red arrow). Hematoxylin-eosin. x56.

Discussion

Mediastinal cysts can be of pericardial, intestinal or bronchogenic origin [30].

Since the article deals with bronchogenic cysts, we note that this is a congenital formation that arises from the respiratory epithelium [20]. Bronchogenic cysts were first described in 1859 [9].

Bronchogenic cysts are rare congenital anomalies of the foregut, usually localized in the mediastinum and lungs [14]. It is during the formation of the tracheobronchial tree from the embryonic ventral foregut, which forms the respiratory system, that aberrant budding and branching leads to the formation of bronchogenic cysts [19, 25]. The location of the bronchogenic cyst depends on the embryological stage of development at which the anomaly occurs. If malformations of the respiratory tract occur in the early stages of pregnancy, then bronchogenic cysts are usually localized in the mediastinum, if in later stages, then in the lungs [15]. Bronchogenic cysts can usually form in the 6th week of pregnancy from abnormal growth of a tracheal diverticulum. They are characterized by the presence of respiratory (ciliated) epithelium. Histologically, they also contain cartilage, fibrous tissue, smooth muscle and mucous glands. These cysts are located near the trachea or main stem bronchi. Sometimes you can find a connection of the cyst with the tracheobronchial tree.

There are three types of bronchogenic cysts: mediastinal, intrapulmonary, and ectopic, and the mediastinal type predominates [10, 13].

From the point of view of the localization of bronchogenic cysts, according to many studies, they can be found in any organ, but most of them are found in the chest, or in the parenchyma of the lungs, or in the mediastinum, in addition, they occur in the cervical, diaphragmatic paravertebral, scapular, pericardial, retroperitoneal, omentum, perianal regions and thymus [15, 19, 20, 28]. In a recent study, Liu X. et al. [16], which is devoted to the study of ectopic double primary bronchogenic cysts, describes the case of Xinlong, and provides important evidence for the further determination of the pathogenesis of bronchial cysts.

It should be noted that from the point of view of differential diagnosis, bronchogenic cysts are a problem, because they are characterized by clinical and radiological polymorphism, they can be confused with echinococcosis. Histological differential diagnosis includes: cystic teratoma, bronchopulmonary sequestration, esophageal cyst, chronic abscess [15].

Bronchogenic cysts are subject to complete surgical excision, and the final diagnosis is established with the help of histopathological examination of the surgical specimen [7]. Histologically, one can find elements of normal bronchial structures with respiratory-type epithelium (ciliated pseudo-multilayered columnar epithelial goblet-shaped cells, often filled with mucin) in the composition of cysts. The wall of the cyst usually consists of fibrous connective tissue, which has serous-mucous bronchial glands (but not always), hyaline cartilage, smooth muscles, elastic fibers [9].

Previously, only symptomatic cysts were subject to surgical removal, later indications were extended to asymptomatic cysts due to the 25 % frequency of their complications, such as infection, development of clinical symptoms, and increase in cyst size [9, 12, 21].

In our case, a 38-year-old man was hospitalized with a suspected pericardial cyst for further examination and operative treatment. With the help of multispiral computed tomography of the chest organs, a dense neoplasm of a rounded shape, 3.3 x 3.0 cm in size, of an inhomogeneous structure with a liquid component and clear contours, without signs of invasion into adjacent anatomical structures, was revealed in the area of the anterior-inferior mediastinum on the right. Note that 70 % of pericardial cysts are located precisely in the right cardiodiaphragmatic angle [12].

That is, the age, sex of the patient, localization, size of the cyst (<5.0 cm) tended to assess the identified cyst as

pericardial. However, the histological examination of the tumor removed during the operation revealed a cystic lesion, the wall of which is lined with multi-row cylindrical ciliated epithelium with foci of infiltration by lymphoid elements with multiple hemorrhages, foci of fibrotization, but without signs of cytological atypia, which made it possible to make the final diagnosis - bronchogenic cyst and avoid misdiagnosis.

Conclusions

1. The successful experience of detecting a bronchogenic cyst in an atypical location, which is confirmed histologically, allows you to avoid a false diagnosis.

2. The obtained results make it possible to significantly improve the understanding of the pathomorphological picture of bronchogenic cysts.

References

[1] Ahuja, J., Strange, C. D., Agrawal, R., Erasmus, L. T., & Truong, M. T. (2023). Approach to Imaging of Mediastinal Masses. *Diagnostics,* 13(20), 3171. doi: 10.3390/diagnostics13203171

[2] Barrios, P., & Patino, D. A. (2022). Surgical indications for mediastinal cysts - a narrative review. *Mediastim,* 6, 31. doi: 10.21037/med-22-27

[3] Benfaddoul, O., Hajjine, A., Bellasri, S., Slioui, B., Roukhsi, R., Hammoune, N. … & Atmane, E. (2022). Paraesophageal Cyst: A Case Report. *Journal of Clinical Case Studies Reviews & Reports J Clin Stud Rev Rep*, 4(3), 1-2. doi: 10.47363/JCCSR/2022(4)210

[4] Bertolaccini, L., & Rocco, G. (2019). History and development of minimally invasive surgery: VATS surgery. *Shanghai Chest,* 3, 16. doi: 10.21037/shc.2019.03.01

[5] Ceniceros-Cabrales, A. P., & Sánchez-Fernández, P. (2018). Esophageal bronchogenic cyst: an uncommon cause of dysphagia in adults. Case report and literature review. *Cirugia y Cirujanos*, 86(2), 187-190. doi: 10.24875/CIRUE.M18000027

[6] Collins, K., L., Zakharious, F., Mandal, A. K. J., & Missouris, C. G. (2018). Pericardial Cyst: Never Too Late to Diagnose. *Journal of Clinical Medicine,* 7(11), E399. doi: 10.3390/jcm7110399

[7] Erbenová, A., Placrová, B., Špůrková, Z., & Horák, P. (2021). Bronchogenic cyst of gastric cardia - case report and literature review. *Rozhl Chir,* 100(10), 507-511. doi: 10.33699/PIS.2021.100.10.507-511

[8] Escalante, J. M., Molina, G., Rincón, F. M., Acosta Buitrago, L. M., & Perez Rivera, C. J. (2021). Giant intrapericardial bronchogenic cyst associated with congestive heart failure and atrial fibrillation: a case report. *Journal of Cardiothoracic Surgery,* 16, 1-5. doi: 10.1186/s13019-021-01412-2

[9] Gross, D. J., Briski, L. M., Wherley, E. M., & Nguyen, D. M. (2023). Bronchogenic cysts: a narrative review. *Mediastinum,* 7, 26. doi: 10.21037/med-22-46

[10] Gu, X., Zhu, L., Li, Y., Yin, B., & Wang, Z. (2023). Imaging Findings and Misdiagnosis of Bronchogenic Cysts: A Study of 83 Cases. *J Belg Soc Radiol,* 107(1), 81. doi: 10.5334/jbsr.3214

[11] Gutzwiller, L. G., & Crouch, C. (2023). *Methodology for Formalin Fixed Paraffin Embedded Cardiac Tissue Analysis*. Haslam Scholars Projects. 6 p. https://trace.tennessee.edu/utk_haslamschol/25

[12] Hsu, D. S., Banks, K. C., & Velotta, J. B. (2022). Surgical approaches to mediastinal cysts: clinical practice review. *Mediastinum,* (6), 32. doi: 10.21037/med-22-20

[13] Lau, C. L., & Davis, R. D. (2004). *The mediastinum. In: Sabiston's Textbook of Surgery.* (17th.) (Ch. 56). (pp. 1738-1739). Philadelphia, Pa, USA: Elsevier.

[14] Limaïem, F., Ayadi-Kaddour, A., Djilani, H., Kilani, T., & El Mezni, F. (2008). Pulmonary and mediastinal bronchogenic cysts: a clinicopathologic study of 33 cases. *Lung,* 186(1), 55-61. doi: 10.1007/s00408-007-9056-4

[15] Limaiem, F., & Mlika, M. (2023). *Bronchogenic Cyst.* In: StatPearls [Internet]. Treasure Island (FL): StatPearls Publishing; 2024 Jan. Available from: https://www.ncbi.nlm.nih.gov/books/NBK536973/

[16] Liu, X., Sun, T., Hong, T., & Zhang, H. (2023). Ectopic double primary bronchogenic cysts: a case description Xinlong. *Quant Imaging Med Surg,* 13(9), 6310-6316. doi: 10.21037/qims-23-247

[17] Mlika, M., Abdennadher, M., Ayadi, R., Braham, E., Ismail, O., Marghli, A., & Mezni, F. (2022). Mediastinal cysts: a 52-case retrospective study. *La Tunisie Medicale*, 100(1), 44-48. PMID: 35822331

[18] Moffa, A. P., Stoppino, L. P, Loizzi, D, & Milillo, P. (2018). Spontaneous disappearance of a pericardial cyst: case report and literature review. *Korean J Thorac Cardiovasc Surg*, 51, 72-75. doi: 10.5090/kjtcs.2018.51.1.72

[19] Mir, Z. M., Wang, A., Winthrop, A., & Kolar M. (2018). Scapular Bronchogenic Cyst in a Girl Presenting as Recurrent Cellulitis: A Case Report and Review of the Literature. *Case Rep Pediatr,* 2018, 7463724. doi: 10.1155/2018/7463724

[20] Núñez-Rocha, R. E., Perez, V., Urango, M. L., Mejia, M., Palau, M., & Herrera-Almario, G. (2023). Extrapulmonary bronchogenic cyst: A case report. *Int J Surg Case Rep,* 110, 108706. doi: 10.1016/j.ijscr.2023.108706

[21] Osman, N. I., Bratt, D. G., Downey, A. P., Esperto, F., Inman, R. D., & Chapple, C. R. (2021). A systematic review of surgical interventions for the treatment of bladder pain syndrome/interstitial cystitis. *European Urology Focus*, 7(4), 877-885. doi: 10.1016/j.euf.2020.02.014

[22] Ramireddy, K., Golamari, R. R., Minupuri, A., Zheng, S., & Menetrey, J. (2020). Bronchogenic Cyst Presenting as Acute Pericarditis. *Cureus,* 12(6), e8874. doi: 10.7759/cureus.8874

[23] Santos, I., Barros, J., Lopes, T., Mesquita, M., Barroso, L., & Amado, I. (2019). Bronchogenic cyst of the neck in an elder patient: a case.report. *International Journal of Surgery Case Reports*, 64, 128-132. doi: 10.1016/j.ijscr.2019.10.013

[24] Shah, A., & Rojas, C. A. (2023). Imaging modalities (MRI, CT, PET/CT), indications, differential diagnosis and imaging characteristics of cystic mediastinal masses: a review. *Mediastinum,* 7(25), 3. doi: 10.21037/med- 22-31

[25] Schittny, J. (2017). Development of the lung. *Cell and Tissue Research,* 367(3), 427-444. doi: 10.1007/s00441-016-2545-0

[26] Szolkowska, M., Szczepulska-Wojcik, E., Maksymiuk, B., Burakowska, B., Winiarski, S., Gatarek, J., … & Langfort, R. (2019). Primary mediastinal neoplasms: a report of 1,005 cases from a single institution. *Journal of Thoracic Disease,* 11(6), 2498. doi: 10.21037/jtd.2019.05.42

[27] Tomiyama, N. (2019). Approach to the prevascular mass. *Mediastinum,* 3, 17. doi: 10.21037/med.2019.04.05

[28] Ugurlucan, M., Sayin, O. A., Felten, M., Oztas, D. M., Cakir, M. S., Barburoglu, M., … & Dayioglu, E. (2014). Intrapericardial Bronchogenic Cyst: An Unusual Clinical Entity. *Case Rep Med,*

651683. doi: 10.1155/2014/651683
[29] Whooley, J., White, A., & Soo, A. (2022). Bronchogenic cyst: a rare case of malignant transformation. *BMJ Case Rep,* 15(4), e248916. doi: 10.1136/bcr-2022-248916
[30] Wychulis, A. R., Payne, W. S., Clagett, O. T., & Woolner, L. B. (1971). Surgical treatment of mediastinal tumors: a 40 year experience. *Journal of Thoracic and Cardiovascular Surgery,* 62(3), 379-392. doi: 10.1016/S0022-5223(19)42048-5

ПАТОМОРФОЛОГІЧНІ ОСОБЛИВОСТІ ПІДТВЕРДЖЕНОЇ БРОНХОГЕННОЇ КІСТИ З АТИПОВОЮ ЛОКАЛІЗАЦІЄЮ

Хорошун Е. М., Негодуйко В. В., Воровський О. О., Макаров В. В., Бунін Ю. В., Смолянник К. М.

Серед усіх утворень середостіння у дорослого населення кісти становлять близько 20 %, з яких понад 60 % припадає на бронхогенні кісти, де до 50 % мають безсимптомний перебіг, а тому в більшості випадків виявляються випадково. Незалежно від перебігу та походження, кісти підлягають повному хірургічному видаленню. У зв'язку з клінічним і радіологічним поліморфізмом бронхогенних кіст, гістологічне підтвердження походження кіст не втрачає актуальності. Мета роботи - вивчити та висвітлити патоморфологічну характеристику кісти з локалізацією в перикарді. Із застосуванням відеоасистентної торакальної хірургії (video-assisted thoracic surgery - VATS) і торакотомічних доступів були прооперовані 16 осіб у віці від 28 до 62 років з кістозними ураженнями середостіння. Пацієнти пройшли рентгенографічне обстеження, комп'ютерну томографію з внутрішньовенним введенням контрасту та у 2 випадках - магнітно-резонансну томографію. Ультразвукове дослідження виконали 6 пацієнтам, у котрих кістозні ураження були діагностичною знахідкою. Оцінювали розташування кісти, максимальний діаметр, щільність, кальцифікацію. У передваскулярному відділі клінічно та рентгенологічно виявили безсимптомні перикардіальні (целомічні) кісти у 2-х осіб. У вісцеральному відділі середостіння 3 пацієнти мали перикардіальну кісту, у 10 пацієнтів діагностували 10 бронхіальних кіст з паренхіматозною та перигілярною локалізацією, серед яких в одного пацієнта діагностували безсимптомну бронхіальну кісту з атиповою локалізацією в перикарді. У паравертебральному відділі середостіння встановлена 1 параезофагеальна кіста, котра була інтимно злучена з нижньою третиною грудного відділу стравоходу. Всі види кіст були гістологічно підтверджені. Статистичну обробку отриманих результатів проводили за допомогою програми Excel. Після клінічного обстеження пацієнта з кістою перикарда вісцерального відділу середостіння виконана операція VATS справа та видалення кісти. Гістологічне дослідження фрагментів стінки кісти показало наявність багаторядного війчастого циліндричного епітелія, виражену інфільтрацію лімфоїдними елементами з геморагіями та осередками фіброзизації на окремих ділянках. Гістологічна будова видаленої кісти перикарда підтвердила її бронхогенне походження. Отже, нами виявлена рідкісна форма аномалії ембріонального росту вентральної частини передньої кишки з локалізацією бронхогенної кісти в передньо-нижньому середостінні справа, що значно розширило розуміння хвороби.

Ключові слова: *бронхогенна кіста, рентгенографія, відеоасистентна торакальна хірургія, гістологія.*

Author's contribution

Khoroshun E. M. - project administration.
Nehoduiko V. V. - conceptualization, research, data visualization.
Vorovskyi O. O. - methodology and writing of the original draft, review writing and editing.
Makarov V. V. - supervision, formal analysis and validation.
Bunin Yu. V. - data visualization, resources.
Smolyannik K. M. - resources, software.

DOI: 10.31393/morphology-journal-2024-30(2)-09 Reports of Morphology, Vol. 30, №2, Pages 69-75

ISSN 1818-1295 eISSN 2616-6194

REPORTS OF MORPHOLOGY

Official Journal of the Scientific Society of Anatomists, Histologists, Embryologists and Topographic Anatomists of Ukraine

journal homepage: https://morphology-journal.com

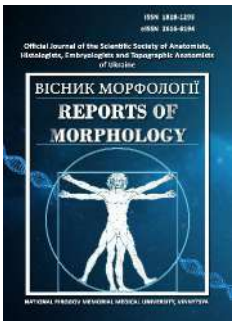

Morphological state of lungs of rats under the influence of Vipera berus berus venom

Lasavutz V. S.[1], Yaremenko L. M.[1], Butska L. V.[2], Lavrynenko V. Y.[2], Zhehulovych Z. Y.[1]

[1]Bogomolets National Medical University, Kyiv, Ukraine
[2]Educational and Scientific Center "Institute of Biology and Medicine", Taras Shevchenko National University of Kyiv, Kyiv, Ukraine

ARTICLE INFO
Received: 14 February 2024
Accepted: 08 April 2024

UDC: 61:612.2:615.9.616.2:616-008

CORRESPONDING AUTHOR
e-mail: vladyslav.lasavuts@gmail.com
Lasavutz V. S.

CONFLICT OF INTEREST
The authors have no conflicts of interest to declare.

FUNDING
Not applicable.

DATA SHARING
Data are available upon reasonable request to corresponding author.

About 5.4 million snake bite cases are registered worldwide every year. About half of them cause 81,000-138,000 deaths or disabled 400,000 people. Despite this, this problem is neglected in many countries in Asia, Africa and Latin America. It is believed that death from snakebites is associated with poverty since the lack of proper access to medical facilities in such sections of the population causes the development of fatal complications. The purpose of the study is to study the morphological state of rats' lungs under exposure to Vipera berus berus venom. Experimental studies were carried out on white, non-linear male rats. Animals were conditionally divided into control and experimental groups, ten individuals each. Experimental rats were injected intraperitoneally with a semi-lethal dose (LD^{50}) (1.576 mg/g^{-1}) of Vipera berus berus venom in a physiological solution. Animals of the control group were injected intraperitoneally with only a physiological solution. Rats were removed from the experiment 24 hours after exposure to the poison and anaesthetized by cervical dislocation. Lung tissue samples were taken for microscopic examination. Fixation of the material and preparation of paraffin blocks were carried out according to generally accepted methods. Staining of histological preparations of the lungs was carried out with hematoxylin and eosin, according to Masson, and the PAS+"Hale" reaction was carried out according to the Mowry method. Histological preparations were studied using an SEO SCAN light microscope. The toxic effect of Vipera berus berus venom caused significant changes in the vascular, stromal and parenchymal components, which was confirmed by histological, histochemical and morphometric data. In the lungs of experimental animals, the vascular bed is primarily restructured, forming coagulopathies and thrombosis. The development of DIC syndrome and haemorrhages accompanies an increase in the permeability of the vessel wall. Inflammatory phenomena are found in the bronchi and respiratory departments' walls. There is a remodelling of the respiratory department components, with the formation of significant areas of dis- and atelectasis and zones of emphysema, which is confirmed morphometrically.

Keywords: *vipers, lungs, poison, inflammation, rats.*

Introduction

About 5.4 million cases of snakebites are registered around the world every year. About half of them cause 81,000-138,000 deaths or disabled 400,000 people. Despite this, this problem is neglected in many countries in Asia, Africa and Latin America. It is believed that death from the bites of snakes and other animals with poisonous glands, in particular scorpions, is associated with poverty since the lack of proper access to medical facilities in such sections of the population causes the development of fatal complications [7, 12, 14, 15]. However, changes in climatic conditions and human settlement of territories endemic to these species of animals lead to the fact that the risk groups expand significantly and include not only low-income residents of these regions [8, 13, 19, 38]. The consequences of snake bites in children and pregnant women are especially severe. In the first case, the immaturity of the immune system and low body weight compared to adults becomes the cause of the development of severe complications [1, 9, 21]. In the second case, as a result of disorders of the coagulation system and, accordingly, haemorrhages or thrombosis, it is possible to terminate pregnancies at different times [17, 23, 28].

The venom produced by snakes consists of a significant variety of components, among which the largest share are proteins and peptides with different molecular weights [18, 22, 25]. Most of the components have a synergistic effect, which causes the rapid effect of toxins on the victim's body [6, 20, 31]. Snide venom leads to significant structural changes in the cardiovascular, respiratory, excretory, endocrine, immune, and nervous systems [4, 5, 33].

Today, scientists worldwide actively study the components of snake toxins [24, 30, 30]. First of all, this is explained by the wide range of effects of the poison on the victim's body, as well as the possibilities of using it for medical purposes and making antidotes. The toxins of snakes from different families vary considerably [27, 29, 34]. However, it was established that many structural elements are identical for all snakes [36]. In Europe, the most common vipers are Vipera berus berus and Vipera berus nikolskii, which determines our exceptional attention to the study of the toxins of these types of snakes and the specifics of their effect on the body of victims [2, 26, 37].

To date, no data describe the full range of histological changes in the lungs during bites of poisonous snakes. Few available studies do not reveal the main pathogenetic links in developing one or another complication from the respiratory system under these conditions. In particular, there is a complete lack of data in the literature regarding the effect of Vipera berus berus viper toxins on the structure and functions of the respiratory system, which explains the importance of our study.

The purpose of the study is to study the morphological state of rats' lungs under exposure to Vipera berus berus venom.

Materials and methods

Experimental studies were carried out on white, non-linear male rats. For preliminary acclimatisation, the animals were kept for seven days in the animal husbandry of the Taras Shevchenko National University of Kyiv and later in laboratory conditions in compliance with temperature and light regimes [10]. Rats received standard chow and water ad libitum. The National Institutes of Health Guidelines performed all experiments for the Care and Use of Laboratory Animals and the European Council Directive of November 24, 1986, on the Care and Use of Laboratory Animals (86/609/EEC). The research was approved and confirmed by the bioethics commission of the NSC "Institute of Biology and Medicine" of Taras Shevchenko Kyiv National University (protocol No. 2 dated 08.19.2021).

Vipera berus berus venom was obtained from V. N. Karazin Kharkiv National University. Freeze-dried native venom was stored at -20 °C and dissolved in saline immediately before the experiment.

The animals were conditionally divided into a control and an experimental group of 10 individuals. Experimental rats were injected intraperitoneally with a semi-lethal dose (LD50) (1.576 mg/g-1) of Vipera berus berus venom in a physiological solution. Animals of the control group were injected intraperitoneally with only a physiological solution. Rats were removed from the experiment 24 hours after exposure to the poison and anaesthetized by cervical dislocation.

Lung samples of animals of all groups were taken for microscopic examination. The pieces were fixed in a 10 % formalin solution for one day. Next, the pieces were dehydrated in alcohols of increasing concentration and embedded in paraffin blocks. Histological preparations of lungs were stained with hematoxylin and eosin, according to Masson (to detect collagen fibres), and the PAS+"Hale" reaction was performed according to the Mowry method (detection of glycoproteins and glycosaminoglycans in the intercellular substance of connective tissue) [16]. Histological preparations were studied using an SEO SCAN light microscope and photo-documented using a Vision CCD Camera with a system of image output from histological preparations.

Morphometric studies were carried out using the visual analysis system of histological preparations. Images from histological preparations were displayed on a computer monitor using a MICROmed SEO SCAN microscope and a Vision CCD Camera. Morphometric studies were conducted using SEO programs ImageLabBio, ImageJ and STATISTICA 10.0. The research was carried out in the specified terms of the experiment in preparations stained with hematoxylin and eosin.

Morphometrically, the relative share of blood vessels, bronchi, lymphoid tissue and the respiratory department was determined, in which the relative share of lung tissue with unchanged histostructure, atelectasis, disatelectase, and emphysematously changed lung tissue was measured.

The obtained digital material was processed using variational statistics using the Student's t-test. Arithmetic mean values (M), arithmetic mean errors (m), variation coefficients, and mean square deviations were calculated. Changes were considered reliable at $p \leq 0.05$.

Results

Histological examination of the lungs of experimental animals after the bite of the viper Vipera berus berus showed that significant destructive and inflammatory changes of all constituent components occur in the organ. Hemotoxins provoked hemodynamic disorders with the remodelling of vessel walls, in particular, increased permeability, which leads to swelling of the wall, disorganisation of the amorphous component and fibres, and perivascular, interstitial and peribronchial connective tissue. An increase in the number of glycoproteins in their composition is confirmed by pronounced PAS-positive properties and redistribution and an increase in the number of sulfated glycosaminoglycans with Hale-positive properties (Fig. 1).

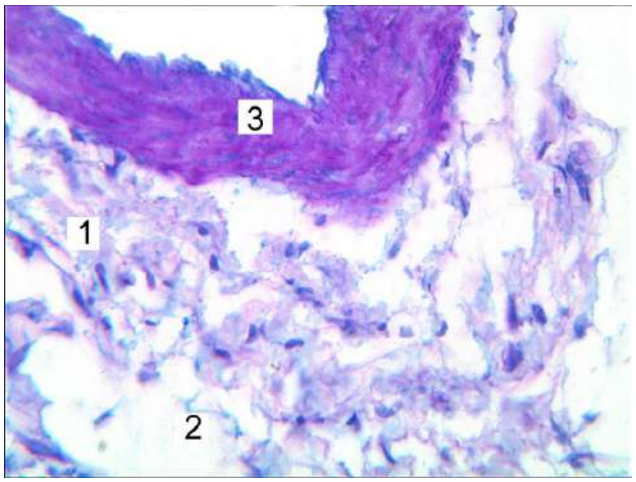

Fig. 1. Histochemical changes in a white rat's lung under exposure to the viper Vipera berus berus. Collagen fibres of perivascular connective tissue with weakly expressed PAS-positive properties (1) and intensively expressed "Hale" positive properties of glycosaminoglycans (2), arterial media (3). Staining according to the Mowry method. x400.

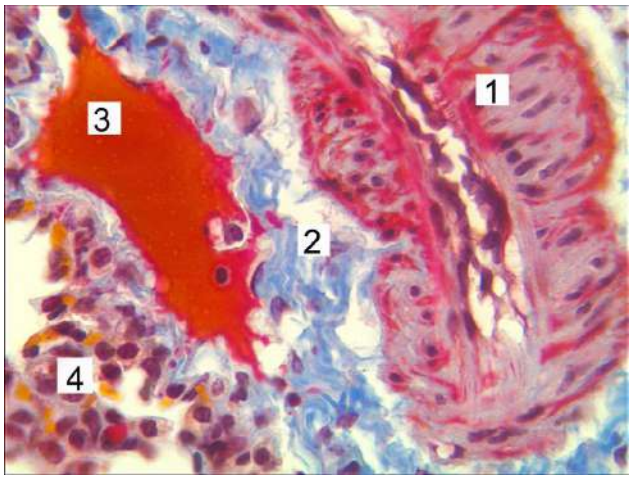

Fig. 2. Microscopic changes in a white rat's lung under viper Vipera berus berus exposure. Swollen artery media (1), disorganisation of adventitia fibres (2), and perivascular accumulation of fibrin (3). Staining by the MSB (OKH) method. x400.

Table 1. The ratio of structural components of animal lungs after exposure to steppe viper venom (M±m).

Indicator	Intact group	Vipera berus berus
Vessels, %	4.821±0.213	6.33±0.252*
Bronchi, %	5.472±0.264	12.24±0.46*
Lymphoid tissue, %	6.751±0.232	15.05±0.55*
Respiratory department, %	82.96±3.84	66.38±2.89*

Note: * - values significantly differ from the indicators of the control group of animals (p<0.001).

The toxic effect of Vipera berus berus venom provokes choalugopathy, manifested histologically by stasis, erythrocyte sludge, and blood clots. Blood circulation disorders are accompanied by the accumulation of fibrin intra- and extravascularly, which confirms the development of DIC syndrome (Fig. 2).

Morphometrically, a significant increase in the average value of the vascular area was established by 1.31 times (p<0.001) relative to the value of the intact group. The average values of the bronchi and lymphoid tissue area also increased progressively by 2.24 and 2.23 times (p<0.001) relative to the average values of the intact group. Accordingly, the average indicator of the respiratory department decreases significantly and is 0.80 relative to the intact value (Table 1).

In the lungs' respiratory department, the alveoli's wall is mainly thickened due to oedema and infiltration by histo- and leukocyte series cells. Extensive dys- and atelectasis areas and emphysematously changed lung tissue zones are revealed (Fig. 3).

It was morphometrically investigated that under the conditions of exposure to Vipera berus berus viper toxins in the lungs of experimental animals, the relative proportions of dys- and atelectasis, emphysematously changed lung tissue increased reliably by 6.03, 7.15, and 2.00 times (p<0.001) relative to the parameters of the intact group. Accordingly, the average value of lung tissue with unchanged histostructure, which is 0.31 relative to the value of the intact group, progressively decreases (Table 2).

Alteration of vessel walls is also manifested by diapedesis of formative elements into alveolar lumens. Activation of inflammatory processes in the respiratory tract of the lungs is characterised by the presence of inflammatory local conglomerates of macrophages, lymphocytes, and neutrophils, mainly in the loci of atelectasis (Fig. 4).

In the areas of haemorrhages, the presence of macrophages with brightly "Hale"-positive lumps of hemosiderin, which results from pathological accumulation and breakdown of haemoglobin in erythrocytes, was

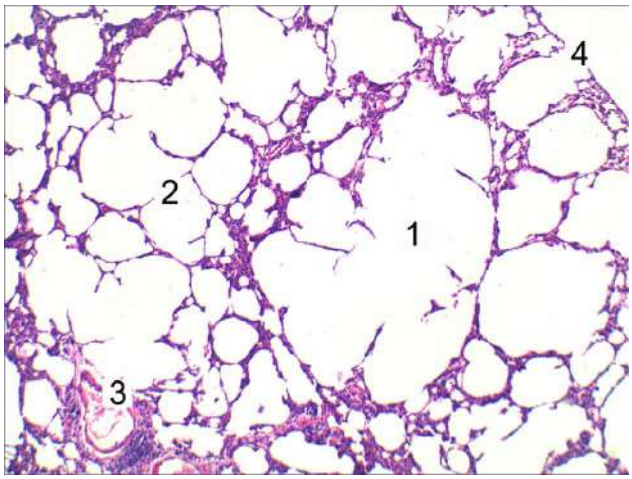

Fig. 3. Microscopic changes in a white rat's lung under viper Vipera berus berus exposure. Emphysematously changed alveoli (1), thin interalveolar septa (2), destructively changed vessel (3), and thin pleura (4). Staining with hematoxylin and eosin. x 100.

Table 2. The ratio of the structural components of the respiratory department of the lungs of animals under exposure to the poison Vipera berus berus (M±m).

Groups	Indicators			
	The relative proportion of lung tissue with unchanged histostructure, %	Relative share of atelectasis, %	The relative proportion of dysatelectases, %	The relative share of emphysematous changed lung tissue, %
Intact group	82.82±3.91	3.552±0.151	5.280±0.241	8.352±0.393
Vipera berus berus	26.06±1.25*	25.38 ±1.23*	31.85±1.49*	16.71±0.81*

Note: * - values significantly differ from the indicators of the control group of animals (p<0.001).

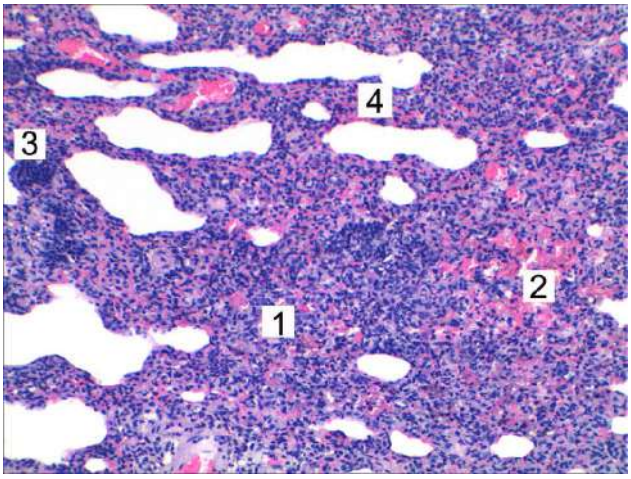

Fig. 4. Histological changes in a white rat's lung under exposure to the viper Vipera berus berus. Zones of atelectasis (1), diapedesis diffuse haemorrhages (2), local leukocyte infiltrates (3), thickened, infiltrated alveolar walls (4). Staining with hematoxylin and eosin. x100.

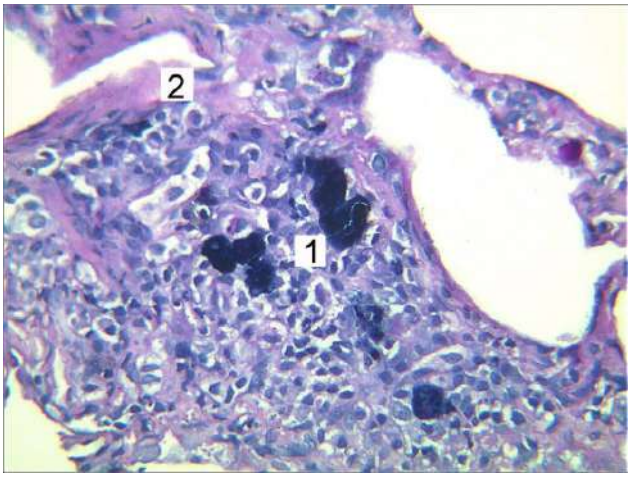

Fig. 5. Histochemical changes in a white rat's lung under exposure to the viper Vipera berus berus. Macrophages with an accumulation of brightly "Hale"-positive hemosiderin grains in the areas of atelectasis (1), moderately PAS-positive reticular fibres of the stroma (2). Staining according to the Mowry method. x400.

detected histochemically (Fig. 5).

Bronchi are characterised by wall damage with alteration of all membranes. In most fields of view, in the parenchyma of the lungs and mainly in the wall of the bronchi, voluminous inflammatory infiltrates in which lymphocytes and macrophages are detected (Fig. 6).

Bronchial obstruction due to bronchospasm is observed in part of the bronchi, not only of small bronchi but also of

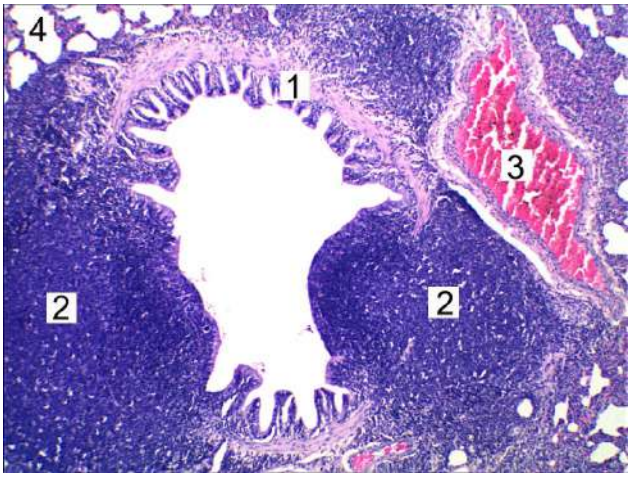

Fig. 6. Microscopic changes in a white rat's lung under viper Vipera berus berus exposure. Alteration of the wall of the bronchus (1), voluminous inflammatory infiltrates in the wall of the bronchus (2), full-blooded vein (3), and respiratory department (4). Staining with hematoxylin and eosin. x100.

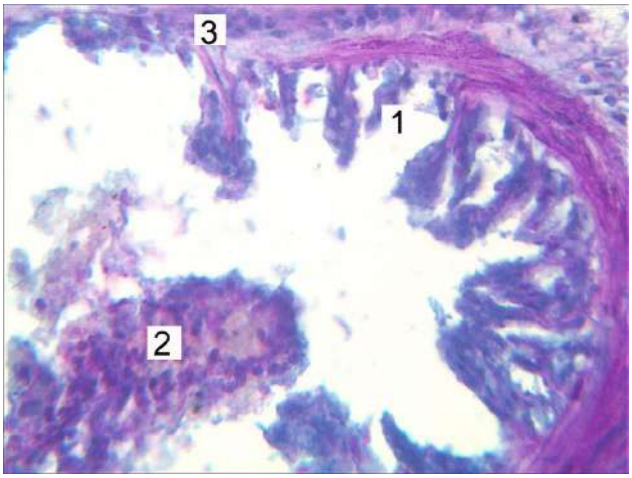

Fig. 7. Histochemical changes in a white rat's lung under exposure to the viper Vipera berus berus. Destruction of the epithelial plate of the wall (1), serous-mucous content in the lumen with moderately expressed PAS-positive properties (2), and alteration of the media (3). Staining according to the Mowry method. x200.

medium diameter. The ciliated epithelium of the mucous membrane is swollen, fragmented in many areas and desquamated in the lumen. Serous-mucous content with cellular detritus, which has bright PAS-positive properties, is determined in the lumen of the bronchi (Fig. 7).

Destructive damage to the respiratory epithelium is detected in most fields of observation; however, restoration of the epithelial plate due to interstitial cells is determined in some areas.

Discussion

Thus, histological studies of the lungs of experimental animals after being bitten by the viper Vipera berus berus showed the development of significant destructive and inflammatory changes in all constituent components. The toxic effect of Vipera berus berus venom provoked coagulopathy. Blood circulation disorders were accompanied by the accumulation of fibrin intra- and extravascularly, which confirmed the development of the syndrome of disseminated intravascular blood coagulation. In the areas of haemorrhages, the presence of macrophages with brightly "Hale"-positive lumps of hemosiderin was histochemically revealed, which is the result of pathological accumulation and breakdown of haemoglobin in erythrocytes. Morphometrically, a reliable increase in the average value of the vascular area by 1.31 times ($p<0.001$) relative to the value of the intact group was established. The average values of the bronchi and lymphoid tissue area also increased progressively by 2.24 and 2.23 times ($p<0.001$) relative to the average values of the intact group. It was morphometrically investigated that under the conditions of exposure to Vipera berus berus viper toxins in the lungs of experimental animals, the relative proportions of dys- and atelectasis, emphysematously changed lung tissue increased reliably by 6.03, 7.15, and 2.00 times ($p<0.001$) relative to the parameters of the intact group.

The results of separate in-depth studies demonstrate the characteristics of broncho-pulmonary complications after bites of various types of snakes.

A. L. Ferrara and co-authors [11], in an experimental study, established that the secretory PLA2 poison of Naja mossambica mossambica leads to the development of an inflammatory process in the lungs associated with the activation of macrophages. It is known that PLA2 can hydrolyse the fatty acids of phospholipids of cell membranes. Among all species, their secretory PLA2 (sPLA2) represents the most prominent family, a low molecular weight Ca^{2+}-dependent enzyme. During the activation of the inflammatory cascade, sPLA2 is released into biological fluids and stimulates the activity of cells of the immune system, in particular, macrophages. In this case, under the influence of the enzyme, the authors observed increased production of cytokines by alveolar macrophages. They also demonstrated that sPLA2 of groups IIA and X stimulates the production of vascular endothelial growth factors A and C (VEGF-A and VEGF-C) by lung macrophages through a receptor-mediated mechanism. In addition, this enzyme from snake venom enhanced the activity of neutrophils. It induced the activity of its own cytosolic PLA2, leading to the production of arachidonic acid metabolites. It stimulated the synthesis of cytokines - TNF-α, IL-6 and IL-10, leading to a robust inflammatory process in lung tissue.

A rare complication in patients after a hump-nosed viper bite (Hypnale hypnale or Hump-nosed viper) was found by Srirangan A. et al. [34]. Pulmonary bleeding under conditions of moderate changes in the coagulogram was recorded in the early stages after venom inoculation. In addition, signs of severe blood stagnation and swelling of the lung tissue were observed. The authors suggest that the cause of the mentioned symptoms is the presence in the venom of a significant number of SVMPs, which are key participants in the development of coagulopathies.

Many authors in recent studies have described marked histological changes in the respiratory system due to the bite of Crotalus durissus terrificus. Examination of lung tissue samples 2, 6, and 12 hours after subcutaneous administration of crotoxin to mice revealed such changes as a decrease in the area of the alveolar sacs and an increase in the thickness of the alveolar walls. Stagnant phenomena, haemorrhages, infiltration of lung tissue by polymorphonuclear leukocytes, presence of foamy macrophages, and increased permeability of lung vessels were recorded. The growth of myeloperoxidase activity was determined in the homogenates. It has also been established that crotoxin from the venom of this viper species has a neurotoxic effect. It is a β-neurotoxin that induces the blockade of impulses in neuromuscular synapses, suppressing the release of acetylcholine from presynaptic membranes and postsynaptic desensitisation of nicotinic receptors, causing flaccid paralysis of the respiratory muscles. In addition, crotoxin PLA2 leads to the degradation of cell membrane phospholipids, the initiation of the arachidonic acid cascade and the production of prostaglandin E2 (PGE2), which is associated with myo- and neurotoxicity and the activation of the immune response [30].

According to the literature, the venom of the viper Crotalus durissus cascavella causes changes in the histological architecture of the bronchial tree, bronchioles and alveoli due to the development of emphysema and atelectasis. The specified structural organisation violations are accompanied by moderate swelling of the lung tissue, which is associated with the direct toxic effect of the poison. Also, a characteristic feature of the toxin is the induction of acute damage to the respiratory system, which is morphologically manifested by inflammatory infiltration of the lungs by lymphocytes and plasma cells [3].

Conclusions

The toxic effect of Vipera berus berus venom caused significant changes in the vascular, stromal and

parenchymal components, which was confirmed by histological, histochemical and morphometric data. In the lungs of experimental animals, the priority is the remodelling of the vascular bed, with the formation of coagulopathies and thrombosis. The development of DIC syndrome and haemorrhages accompanies an increase in the permeability of the vessel wall. Inflammatory phenomena are found in the bronchi and respiratory departments' walls. There is a remodelling of the respiratory department components, with the formation of significant areas of dis- and atelectasis and zones of emphysema, which is confirmed morphometrically.

References

[1] Alekseeva, A. S., Tretiakova, D. S., Chernikov, V. P., Utkin, Yu. N., Molotovsky, J. G., Vodovozova, E. L., … Boldyrev, I. A. (2017). Heterodimeric V. nikolskii phospholipases A2 induce aggregation of the lipid bilayer. *Toxicon,* 133, 169-179. doi: 10.1016/j.toxicon.2017.05.015

[2] Al-Sadoon, M. K., Diab, M. S., Bauomy, A. A., & Abdel Moneim, A. E. (2014). Cerastes cerastes gasperetti venom induced hematological alterations and oxidative stress in male mice. *J Pure Appl Microbiol,* 8(Suppl 2), 693-702.

[3] Azevedo, E., Figueiredo, R. G., Pinto, R. V., Ramos, T. C. F., Sampaio, G. P., Bulhosa Santos, R. P., … Trindade, S. C. (2020). Evaluation of systemic inflammatory response and lung injury induced by Crotalus durissus cascavella venom. *PLoS One,* 15(2), e0224584. doi: 10.1371/journal.pone.0224584

[4] Balija, T., Leonardi, A., Brgles, M., Sviben, D., Kurtovic, T., Halassy, B., … Krizaj, I. (2020). Biological activities and proteomic profile of the venom of Vipera ursinii ssp., a very rare Karst Viper from Croatia. *Toxins* (Basel), 12(3), 187. doi: 10.3390/toxins12030187

[5] Bhagwat, K., & Amar, L. (2013). Blood hemoglobin, lactate dehydrogenase and total creatine kinase combinely as markers of hemolysis and rhabdomyolysis associated with snake bite. *Int J Toxicol Pharmacol Res,* 5(1), 5-8.

[6] Bhattacharya, S., Krishnamurthy, A., Gopalakrishnan, M., Kalra, S., Kantroo, V., Aggarwal, S., … Surana, V. (2020). Endocrine and metabolic manifestations of snakebite envenoming. *Am J Trop Med Hyg,* 103(4), 1388-1396. doi: 10.4269/ajtmh.20-0161

[7] Bolon, I., Durso, A. M., Mesa, S. B., Ray, N., Alcoba, G., Chappuis, F., … Ruiz de Castaneda, R. (2020). Identifying the snake: first scoping review on practices of communities and healthcare providers confronted with snakebite across the world. *PLoS One,* 15(3), e0229989. doi: 10.1371/journal.pone.0229989

[8] Canas, C. A., Castro-Herrera, F., & Castano-Valencia, S. (2021). Clinical syndromes associated with Viperidae family snake envenomation in southwestern Colombia. *Trans R Soc Trop Med Hyg,* 115(1), 51-56. doi: 10.1093/trstmh/traa081

[9] Castro, A. C., Escalante, T., Rucavado, A., & Gutierrez, J. M. (2021). Basement membrane degradation and inflammation play a role in the pulmonary hemorrhage induced by a P-III snake venom metalloproteinase. *Toxicon*, 197, 12-23. doi: 10.1016/j.toxicon.2021.04.012

[10] Dobrelia, N. V., Boitsova, L. V. & Danova, I. V. (2015). Правова база для проведення етичної експертизи доклінічних досліджень лікарських засобів з використанням лабораторних тварин [Legal basis for ethical examination of preclinical studies of drugs using laboratory animals]. *Фармакологія та лікарська токсикологія=Pharmacology and Drug Toxicology,* (2), 95-100.

[11] Ferrara, A. L., Galdiero, M. R., Fiorelli, A., Cristinziano, L., Granata, F., Marone, G., … Loffredo, S. (2021). Macrophage-polarizing stimuli differentially modulate the inflammatory profile induced by the secreted phospholipase A2 group IA in human lung macrophages. *Cytokine*, 138, 155378. doi: 10.1016/j.cyto.2020.155378

[12] Gunas, V., Maievskyi, O., Raksha, N., Vovk, T., Savchuk, O., Shchypanskyi, S., & Gunas, I. (2023). Protein and peptide profiles of rats' organs in scorpion envenomation. *Toxicology Reports, 1*0, 615-620. doi: 10.1016/j.toxrep.2023.05.008

[13] Gunas, V., Maievskyi, O., Raksha, N., Vovk, T., Savchuk, O., Shchypanskyi, S., & Gunas, I. (2023). The Activity of Metalloproteases and Serine Proteases in Various Organs after Leiurus macroctenus Envenomation. *Journal of Toxicology,* 2023. Article ID 5262729. doi: 10.1155/2023/5262729

[14] Gutiérrez, J. M., Calvete, J. J., Habib, A. G., Harrison, R. A., Williams, D. J., & Warrell, D. A. (2017). Snakebite envenoming. *Nat Rev Dis Primers,* 3, 17063. doi: 10.1038/nrdp.2017.63

[15] Herzig, V., Cristofori-Armstrong, B., Israel, M. R., Nixon, S. A., Vetter, I., & King, G. F. (2020). Animal toxins - nature's evolutionary-refined toolkit for basic research and drug discovery. *Biochem Pharmacol,* 181, 114096. doi: 10.1016/j.bcp.2020.114096

[16] Horalskyi, L. P., Khomych, V. T., & Kononskyi, O. I. (2011). *Основи гістологічної техніки і морфофункціональні методи досліджень у нормі та при патології [Fundamentals of histological technique and morphofunctional research methods in normal and pathology].* Житомир, Полісся=Zhytomyr: Polissya.

[17] Islam, K., Seth, S., Roy, A., & Datta, A. K. (2020). Predictors of renal complications in children with hematotoxic snakebite. *Indian Pediatrics,* 57(5), 427-430.

[18] Leonardi, A., Sajevic, T., Pungerčar, J., & Križaj, I. (2019). Comprehensive study of the proteome and transcriptome of the venom of the most venomous european viper: Discovery of a new subclass of ancestral snake venom metalloproteinase precursor-derived proteins. *J Proteome Res*, 18(5), 2287-2309. doi: 10.1021/acs.jproteome.9b00120

[19] Malina, T., Krecsák, L., Westerström, A., Szemán-Nagy, G., Gyémánt, G., M-Hamvas, M., … Vasas, G. (2017). Individual variability of venom from the European adder (Vipera berus berus) from one locality in Eastern Hungary. *Toxicon,* 135, 59-70. doi: 10.1016/j.toxicon.2017.06.004

[20] Naik, B. N., Bhalla, A., Sharma, N., Mokta, J., Singh, S., Gupta, P., … Dutta, P. (2018). Pituitary dysfunction in survivors of Russell's viper snake bite envenomation: A prospective study. *Neurol India,* 66(5), 1351-1358. doi: 10.4103/0028-3886.241378

[21] Nova, Z., Skovierova, H., & Calkovska, A. (2019). Alveolar-capillary membrane-related pulmonary cells as a target in endotoxin-induced acute lung injury. *Int J Mol Sci,* 20(4), 831. doi: 10.3390/ijms20040831

[22] Olaoba, O. T., Karina Dos Santos, P., Selisstre-de-Araujo, H. S., & Ferreira de Souza, D. H. (2020). Snake venom metalloproteinases (SVMPs): a structure-function update. *Toxicon X*, 7, 100052. doi: 10.1016/j.toxcx.2020.100052

[23] Pach, S., Le Geyt, J., Gutiérrez, J. M., Williams, D., Maduwage, K. P., Habib, A. G., … Halbert, J. (2020). Paediatric snakebite envenoming: the world's most neglected 'Neglected Tropical Disease'? *Arch Dis Child,* 105(12), 1135-1139. doi: 10.1136/

archdischild-2020-319417
[24] Palamarchuk, M., Bobr, A., Mudrak, A., Gunas, I., Maievskyi, O., Samborska, I., … Ostapchenko, L. (2023). Proteolytic Homeostasis in the Tissue of the Spleen and the Heart of Rats Injected with the Venom of Vipera berus berus and Vipera berus nikolskii. *Curr Apl Sci Technol*, 6(23), 1-13. doi: 10.55003/cast.2023.06.23.015
[25] Paloschi, M. V., Pontes, A. S., Soares, A. M., & Zuliani, J. P. (2018). An update on potential molecular mechanisms underlying the actions of snake venom L-amino acid oxidases (LAAOs). *Curr Med Chem,* 25(21), 2520-2530. doi: 10.2174/0929867324666171109114125
[26] Paolino, G., Di Nicola, M. R., Pontara, A., Didona, D., Moliterni, E., Mercuri, S. R., … & Pampena, R. (2020). Vipera snakebite in Europe: a systematic review of a neglected disease. *J Eur Acad Dermatol Venerol,* 34(10), 2247-2260. doi: 10.1111/jdv.16722
[27] Puzari, U., & Mukherjee, A. K. (2020). Recent developments in diagnostic tools and bioanalytical methods for analysis of snake venom: A critical review. *Anal Chim Acta,* 1137, 208-224. doi: 10.1016/j.aca.2020.07.054
[28] Ramirez-Cruz, M. P., Smolinske, S. C., Warrick, B. J., Rayburn, W. F., & Seifert, S. A. (2020). Envenomations during pregnancy reported to the national poison data system, 2009-2018. *Toxicon,* 186, 78-82. doi: 10.1016/j.toxicon.2020.07.029
[29] Roldán-Padrón, O., Castro-Guillén, J. L., García-Arredondo, J. A., Cruz-Pérez, M. S., Díaz-Peña, L. F., Saldaña, C., … García-Gasca, T. (2019). Snake venom hemotoxic enzymes: biochemical comparison between Crotalus species from Central Mexico. *Molecules,* 24(8), 1489. doi: 10.3390/molecules24081489
[30] Samborska, I. A., Maievskyi, O. Y., Ahafonov, K. V., & Kovalchuk, O. I. (2020). Ultrastructural changes in the lungs of 1-2 months-old rats in the conditions of hyperhomocysteinemia. *Світ медицини та біології=World of Medicine and Biology,* 1(71), 214-217. doi: 10.26724/2079-8334-2020-1-71-214-217
[31] Sarkar, S., Sinha, R., Chaudhury, A. R., Maduwage, K., Abeyagunawardena, A., Bose, N., … McCulloch, M. (2021). Snake bite associated with acute kidney injury. *Pediatr Nephrol,* 2021, 1-12. doi: 10.1007/s00467-020-04911-x
[32] Sartim, M. A., Souza, C. O. S., Diniz, C. R. A. F., da Fonseca, V. M. B., Souza, L. O., Peti, A. P. F., … Sampaio, S. V. (2020). Crotoxin-induced mice lung impairment: role ofnicotinic acetylcholine receptors and COX-derived prostanoids. *Biomolecules,* 10(5), 794. doi: 10.3390/biom10050794
[33] Simoes, L. O., Alves, Q. L., Camargo, S. B., Araujo, F. A., Hora, V. R. S., Jesus, R. L. C., … Silva, D. F. (2021). Cardiac effect induced by Crotalus durissus cascavella venom: morphofunctional evidence and mechanism of action. *Toxicol Lett,* 337, 121-133. doi: 10.1016/j.toxlet.2020.11.019
[34] Srirangan, A., Pushpakumara, J., & Wanigasuriya, K. (2020). A life-threatening complication due to pulmonary haemorrhage following hump-nosed viper bite. *BMC Pulm Med,* 20(1), 35. doi: 10.1186/s12890-020-1070-9
[35] Ullah, A. (2020). Structure-function studies and mechanism of action of snake venom L-amino acid oxidases. *Front Pharmacol,* 11, 110. doi: 10.3389/fphar.2020.00110
[36] Waiddyanatha, S., Silva, A., Siribaddana, S., & Isbister, G. K. (2019). Long-term effects of snake envenoming. *Toxins* (Basel), 1(4), 193. doi: 10.3390/toxins11040193
[37] Zinenko, O., Tovstukha, I., & Korniyenko, Y. (2020). PLA2 Inhibitor Varespladib as an Alternative to the Antivenom Treatment for Bites from Nikolsky's Viper Vipera berus nikolskii. *Toxins* (Basel), 12(6), 356. doi: 10.3390/toxins12060356

МОРФОЛОГІЧНИЙ СТАН ЛЕГЕНЬ ЩУРІВ ЗА УМОВ ВПЛИВУ ОТРУТИ ГАДЮК VIPERA BERUS BERUS

Ласавуц В. С, Яременко Л. М., Буцька Л. В., Лавриненко В. Є., Жегулович З.Є.

В усьому світі щороку реєструють близько 5,4 млн випадків укусів змій. Приблизно половина з них стає причиною 81 000-138 000 смертей або призводить до інвалідності 400 000 людей. Не дивлячись на це, дана проблема є занедбаною в багатьох країнах Азії, Африки та Латинської Америки. Вважають, що смерть від укусів змій асоційована з бідністю, оскільки відсутність належного доступу до медичних закладів у таких прошарків населення зумовлює розвиток летальних ускладнень. Метою дослідження є вивчення морфологічного стану легень щурів за умов впливу отрути гадюк Vipera berus berus. Експериментальні дослідження проводили на білих нелінійних щурах самцях. Тварин умовно розподіляли на дві групи - контрольну і дослідну по 10 особин в кожній. Дослідним щурам внутрішньоочеревинно вводили напівлетальну дозу (LD^{50}) (1,576 мг/г$^{-1}$) отрути Vipera berus berus на фізіологічному розчині. Тваринам контрольної групи внутрішньоочеревинно вводили лише фізіологічний розчин. Виводили щурів з експерименту через 24 години після впливу отрути під анестезією, знеживлюючи шляхом цервікальної дислокації. Для мікроскопічного дослідження вилучали зразки тканини легень. Фіксацію матеріалу та приготування парафінових блоків проводили за загальноприйнятими методиками. Забарвлення гістологічних препаратів легень здійснювали гематоксиліном та еозином, за Массоном, проводили ШИК+"Хейл" реакцію за методом Моурі. Гістологічні препарати вивчали за допомогою світлового мікроскопа SEO SCAN. Токсичний вплив отрути гадюки Vipera berus berus спричинив значні зміни судинного, стромального та перенхіматозного компонентів, що підтверджується гістологічними, гістохімічними та морфометричними даними. В легенях дослідних тварин першочергово відбувається перебудова судинного русла, з формуванням коагулопатій, тромбозів. Підвищення проникності стінки судин супроводжується розвитком ДВЗ-синдрому та крововиливами. В стінці бронхів та респіраторному відділі виявляються запальні явища. Відбувається ремоделювання компонентів респіраторного відділу з формуванням значних площ дис- та ателектазів, зон емфіземи, що підтверджується морфометрично.

Ключові слова: *гадюки, легені, отрута, запалення, щури.*

Author's contribution

Lasavutz V. S. - research, writing of the original draft.
Yaremenko L. M. - conceptualization, research, review writing and editing.
Butska L. V. - project administration.
Lavrynenko V. Y. - software, resources.
Zhehulovych Z. Y. - validation.

DOI: 10.31393/morphology-journal-2024-30(2)-10 **Reports of Morphology, Vol. 30, №2, Pages 76-83**

ISSN 1818-1295 eISSN 2616-6194

REPORTS OF MORPHOLOGY

Official Journal of the Scientific Society of Anatomists, Histologists, Embryologists and Topographic Anatomists of Ukraine

journal homepage: https://morphology-journal.com

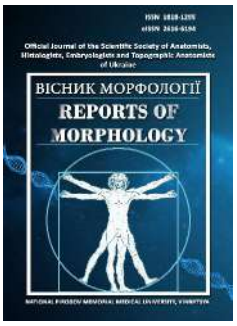

Modeling of individual teleroentgenometric indicators using the "Cephalometrics for orthognathic surgery" method in Ukrainian young women with a wide face type and orthognathic bite

Nesterenko Ye. A.[1], Dzevulska I. V.[2], Gunko I. P.[1], Karpenko I. A.[1], Datsenko G. V.[1], Prokopenko S. V.[1], Datsenko Yu. O.[1]

[1]National Pirogov Memorial Medical University, Vinnytsya, Ukraine
[2]Bogomolets National Medical University, Kyiv, Ukraine

ARTICLE INFO
Received: 07 February 2024
Accepted: 11 April 2024

UDC: 616.714.1-071.3(477)

CORRESPONDING AUTHOR
e-mail: tikhonova_123@ukr.net
Nesterenko Ye. A.

CONFLICT OF INTEREST
The authors have no conflicts of interest to declare.

FUNDING
Not applicable.

DATA SHARING
Data are available upon reasonable request to corresponding author.

The study of individual normative cephalometric parameters in individuals of different sexes and ages is important for the "Cephalometrics for orthognathic surgery method", as it allows to accurately diagnose abnormalities and develop personalized treatment plans. This contributes to achieving better aesthetic results, reducing the risk of complications and increasing the effectiveness of surgical interventions. Taking into account age, sex, and face type helps predict long-term changes and adapt the treatment plan to obtain optimal results. In addition, it improves assessment accuracy and standardizes evidence-based approaches, making it easier to compare results between clinics. Thus, individual regulatory parameters are key to successful orthognathic surgery. The purpose of the study is to build and analyze regression models of teleroentgenometric indicators using the "Cephalometrics for orthognathic surgery" method in Ukrainian young women with a wide face type. 25 Ukrainian young women with an orthognathic bite and a wide face type underwent a cephalometric study using the "Cephalometrics for orthognathic surgery" (COGS-method) method. For the correct modeling of cephalometric parameters, their division into three groups was applied (Dmitriev M. O., 2016, 2017): the first group - basic metric characteristics of the skull; the second group - teleroentgenometric indicators by which it is possible to change the parameters of the upper and lower jaws with the help of orthognathic surgery; the third group - indicators that characterize the position of each tooth relative to each other, cranial structures and the profile of the soft tissues of the face. Construction of regression models was carried out in the license package "Statistica 6.0". Only reliable models with a coefficient of determination R^2 of at least 0.60 were subject to further analysis. It was found that in young women with a wide face, using the COGS method, 6 models of teleroentgenometric indicators were built out of 33 possible, which were included in the second and third groups depending on the indicators of the first group (R^2= from 0.601 to 0.705, p<0.01-0.001); out of 19 possible, 16 indicator models were built, which were included in the third group depending on the indicators of the first and second groups (R^2= from 0.614 to 0.983, p<0.01-0.001). The analysis of the models showed that most often the regression equations of the indicators included in the second and third groups, depending on the indicators of the first group, include the distance P-PTV and N-CC according to Ricketts, N-Se according to Schwarz, N-S and S-Ar according to Roth-Jarabak, Ar-Pt and Pt-N according to the COGS method (7.69 % each), as well as the value of the H angles according to Schwarz and N-S-Ba according to Bjork; and to the indicator models that were included in the third group depending on the indicators of the first and second groups - the value of the distances ANS-Me, N-B, N-A, N-Pog, B-Pog, N-CC according to Ricketts, PNS-N, Ar-Go and ANS-PNS, as well as the magnitude of the angles N-A-Pog, N-S-Ba according to Bjork, MP-HP, as well as Por-NBa according to Ricketts.

Keywords: *regression analysis, teleroentgenography, cephalometry according to the method "Cephalometrics for orthognathic surgery", young women, facial types, orthognathic bite.*

Introduction

Pathology of the dental and jaw system has become widespread. Thus, fractures of the maxillofacial area requiring further orthodontic treatment are not uncommon. In a study by Daneste H. and Bayat P. [7], it was found that 65% of patients with fractures of the maxillofacial area were men, 35 % were women, and the average age was 38.5 years. Lefort I fracture was found in 25 % of patients, Lefort II in 31 %, and Lefort III in 11 %. The causes of fracture of the upper jaw in 46% were car accidents, in 26 % violence, and in 27 % accidents at work and during sports. On the example of one hospital in Togo, it was found that the occurrence rate of Lefort fractures was 15.2 cases. As in the previous study, the main group consisted of individuals of working age of 34.43±11.98 years. Lefort II fracture occurred in 51.06 % of cases. Treatment was surgical in 99.34 % [12].

The prevalence of backbite in the world is about 1.0 % to 1.5 % according to various estimates. The prevalence of Brodie's bite is from 0.5 to 2.3 %. The prevalence of scissor bite is from 0.5 to 5.9 % [18]. Data from the examination of children in one of the regions of Saudi Arabia showed that more than half of the examinees had Class I malocclusion (anterior crossbite, posterior crossbite, open bite, etc.). More than 20% of the participants needed orthodontic treatment [2].

The significant prevalence of various types of orthodontic pathology can be explained by the fact that bad oral habits (thumb sucking, use of a pacifier) greatly contribute to the emergence of pathological types of bite, such as posterior crossbite [13].

Such a number and spread of orthodontic pathology led to the search for tools and techniques to facilitate planning and predicting the results of orthodontic intervention.

Lateral cephalometry, which was proposed in 1931 by Broadbent, is used to characterize facial morphology, predict the growth of the facial skeleton, plan orthodontic treatment, and evaluate treatment outcomes. Cephalometric analyses, which have increased in number in recent decades, provide angular and linear measurements useful for diagnostic purposes and orthodontic treatment planning [11, 28]. At the same time, there are still ongoing discussions about whether it is necessary to conduct a routine cephalometric examination in every case of a patient seeking orthodontic care [16, 30].

Evaluation of economic efficiency is an equally important component in orthodontic practice [19]. M. Bengtsson and co-authors [5] planned the treatment of persons with severe class III malocclusion with 2- and 3-dimensional techniques, comparing costs with benefits. A study involving 57 people showed that the 2-dimensional technique had a large cost advantage and required a significantly lower radiation dose compared to the 3-dimensional technique. In addition, an active discussion is taking place regarding the comparison of the clinical effectiveness of 2-dimensional and 3-dimensional techniques of cephalometric research [28].

In 2015, Burstone C. J. passed away, who, in co-authorship with various researchers, in particular Legan H., in 1979 developed a new method of cephalometric analysis of lateral teleroentgenograms, known as Cephalometrics for orthognathic surgery or the Burstone Legan analysis, which became widely used throughout the world [25]. At the same time, like many other methods of analysis, its main drawback is its inapplicability to different ethnic groups. In addition, the accuracy decreases due to the failure to take into account other factors - sex, age, type of face, etc. Thus, the effective application of this method of analysis is possible only by carrying out research on the local population, taking into account these and other important factors.

The purpose of the study is to build and analyze regression models of teleroentgenometric indicators using the "Cephalometrics for orthognathic surgery" method in Ukrainian young women with a wide face type.

Materials and methods

25 young women (YW) with a wide facial type according to Garson [27] (aged 16 to 20 years), who belonged in three generations to residents of Ukraine of the Caucasian race and had a physiological bite as close as possible to the orthognathic one, underwent a cephalometric study using the "Cephalometrics" method for orthognathic surgery" (COGS method) [6]. The OnyxCeph^{3}™ software, version 3DPro, from Image Instruments GmbH, Germany (software license #URSQ-1799) was used for the study. Primary teleradiograms, which were obtained using a

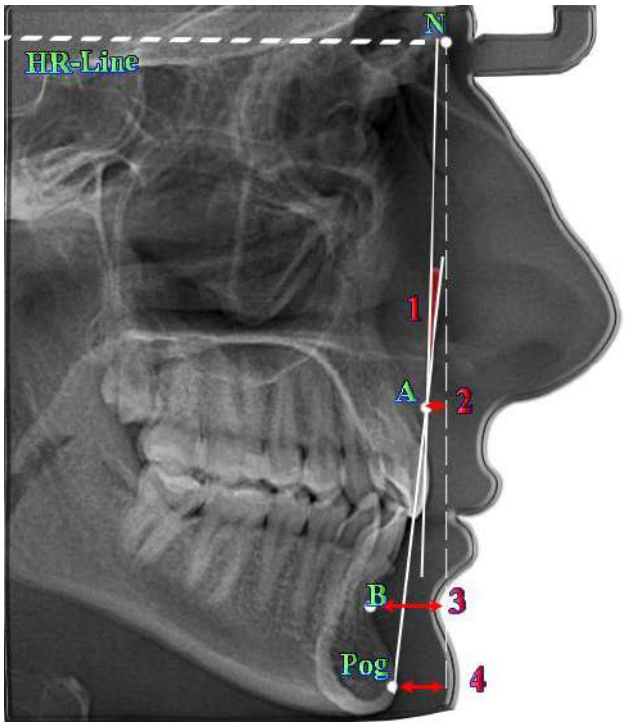

Fig. 1. The second group of teleroentgenometric indicators according to COGS-method: 1 - angle N-A-Pog (°); 2 - distance N-A (mm); 3 - distance N-B (mm); 4 - distance N-Pog (mm).

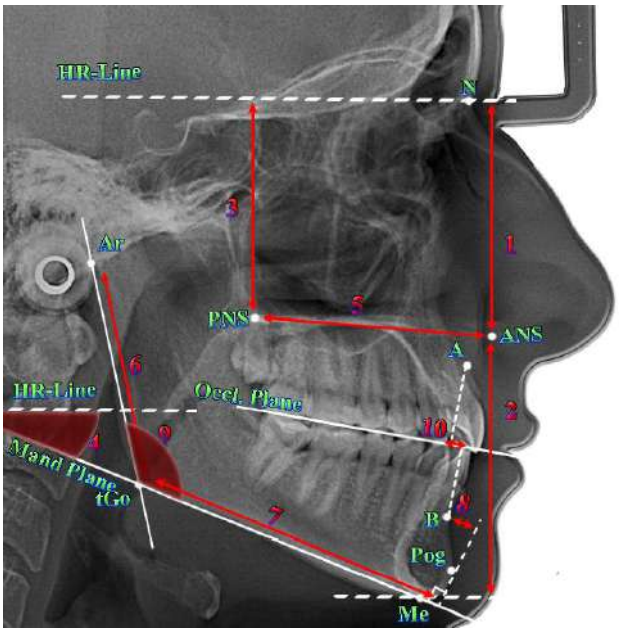

Fig. 2. The second group of teleroentgenometric indicators according to COGS-method: 1 - distance N-ANS (mm); 2 - distance ANS-Me (mm); 3 - distance PNS-N (mm); 4 - angle MP-HP (°); 5 - distance ANS-PNS (mm); 6 - distance Ar-Go (mm); 7 - distance Go-Pog (mm); 8 - distance B-Pog (mm); 9 - angle Ar-Go-Gn (°); 10 - distance A-B (mm).

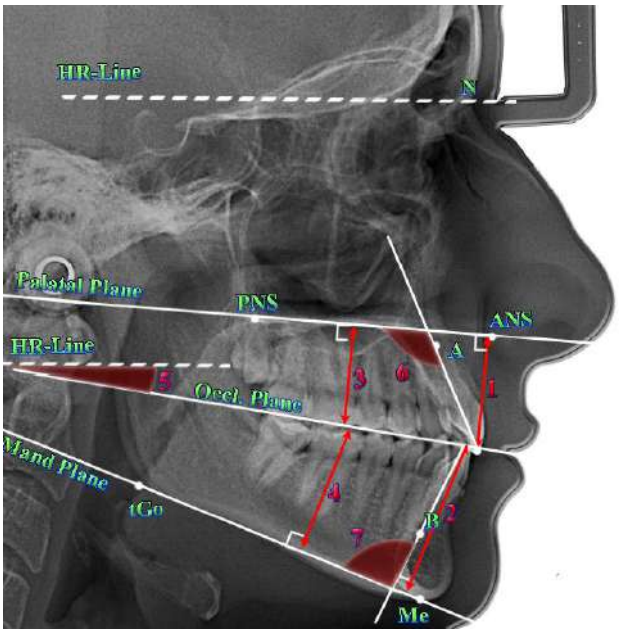

Fig. 3. The third group of teleroentgenometric indicators according to COGS-method: 1 - distance 1u-NF (mm); 2 - distance 1l-MP (mm); 3 - distance 6u-NF (mm); 4 - distance 6l-MP (mm); 5 - angle OP-HP (°); 6 - angle Max1-NF (°); 7 - angle Mand1-MP (°).

Veraviewepocs 3D Morita dental cone beam tomograph, taken from the database of the Research Center and the Department of Pediatric Dentistry of the National Pirogov Memorial Medical University, Vinnytsya (all YW applied to the private dental clinic "Vinintermed" for diagnostic examination and gave voluntary consent for the further use of the obtained results in our study).

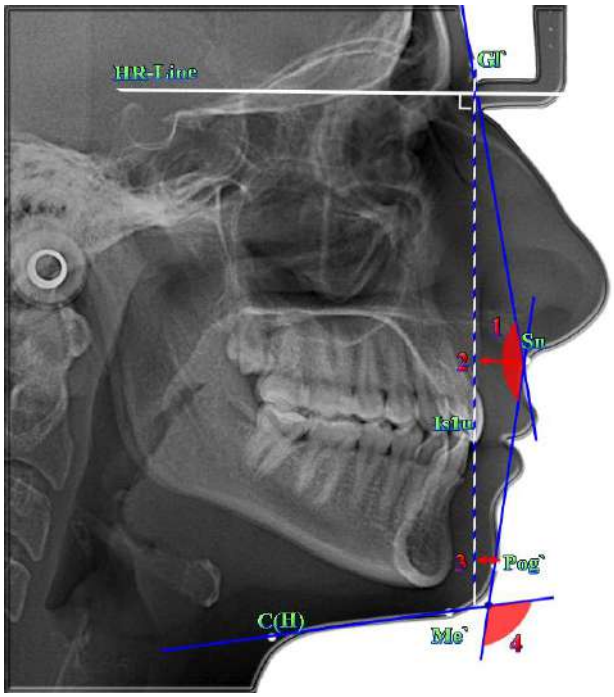

Fig. 4. The third group of teleroentgenometric indicators according to COGS-method, which characterize the shape of the facial profile: 1 - angle Gl'-Sn-Pog' (°); 2 - distance Gl'-Sn (mm); 3 - distance Gl'-Pog' (mm); 4 - angle Sn-Gn'-C (°).

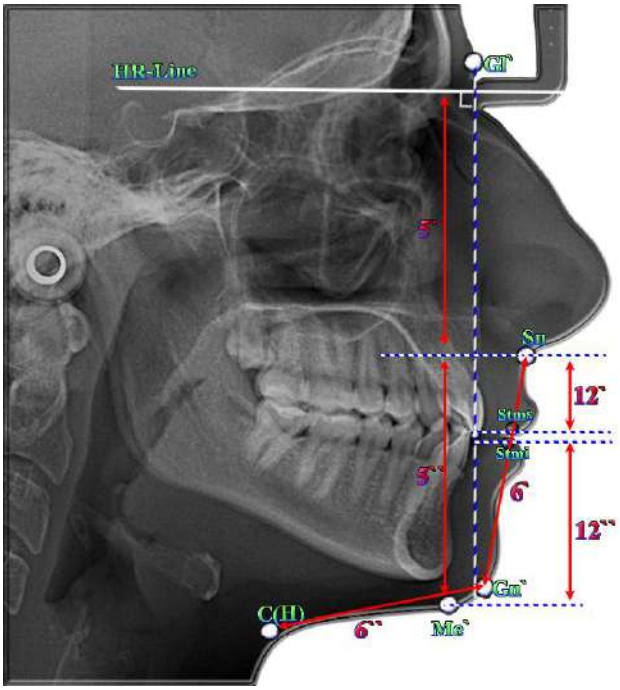

Fig. 5. The third group calculated teleroentgenometric indicators according to COGS-method, which characterize the *shape of the facial profile*: 5 - ratio Gl'-Sn(5')/Sn-Me'(5") (%); 6 - ratio Sn-Gn'(6')/C-Gn'(6") (%); and *the position and shape of the lips*: 12 - ratio Sn-Stms(12')/Stmi-Me'(12") (%).

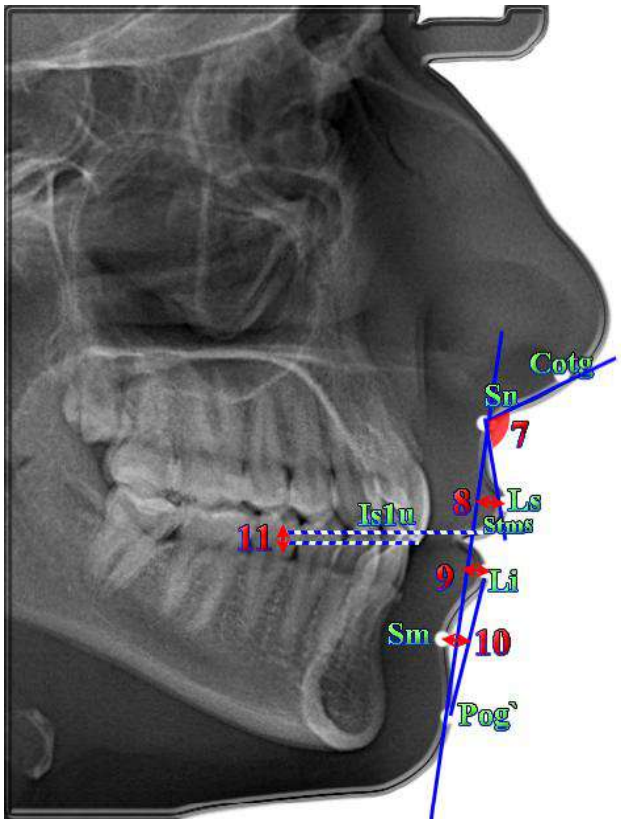

Fig. 6. The third group of teleroentgenometric indicators according to COGS-method, which characterize the position and shape of the lips: 7 - angle Cotg-Sn-Ls (°); 8 - distance Ls-(Sn-Pog') (mm); 9 - distance Li-(Sn-Pog') (mm); 10 - distance Sm-(Li-Pog') (mm); 11 - distance Stms-I (mm).

Committee on Bioethics of National Pirogov Memorial Medical University, Vinnytsya (protocol № 8 From 30.09.2021) found that the studies do not contradict the basic bioethical standards of the Declaration of Helsinki, the Council of Europe Convention on Human Rights and Biomedicine (1977), the relevant WHO regulations and laws of Ukraine.

For the correct modeling of teleroentgenometric indicators, we used their division into three groups proposed by Dmitriev M. O. [9, 10]:

the first group - basic cranial indicators, which usually do not change during surgical and orthodontic treatment. Because in the COGS methodology, only distances Ar-Pt (mm) and Pt-N (mm) belong to them, we also used the following most common cephalometric indicators of other authors: Schwarz N-Se distance (mm), Roth-Jarabak N-S distance (mm), Ricketts N-CC distance (mm), Steiner S-E distance (mm); S-Ar distance according to Roth-Jarabak (mm), P-PTV distance according to Ricketts (mm), S-Ar' distance according to Roth-Jarabak (mm), angle H according to Schwarz (°), POr-NBa angle according to Ricketts (°), angle N-S-Ba by Bjork (°), angle N-S-Ar according to Bjork (°), ratio N-S:S-Ar' according to Bjork;

the second group - teleroentgenometric indicators, which can be used to change the width, length, angles and position of the upper and lower jaws with the help of orthognathic surgery (Fig. 1, 2);

the third group - teleroentgenometric indicators that characterize the position of each individual tooth relative to each other, cranial structures (Fig. 3) and the profile of the soft tissues of the face (Fig. 4, 5, 6).

In order to build models of teleroentgenometric indicators according to the COGS method, the method of step-by-step regression analysis in the license package "Statistica 6.0" was applied. When conducting this analysis, we observed the following conditions: 1) the final version of the regression equation must have a coefficient of determination R^2 of at least 0.60 (thus, the accuracy of the description of the modeled feature is at least 60.0 %); 2) the value of the F-criterion should be at least 2.5 (thus, the contribution of the variable to the total regression equation will be sufficiently significant); 3) the number of free members included in the regression equation should be as minimal as possible.

Results

Out of 33 possible, in Ukrainian YW with an orthognathic bite and a wide face type, 6 reliable regression equations of teleroentgenometric indicators were built, which were included in the *second* and *third* groups according to the COGS method, depending on the value of the indicators of the *first* group with a coefficient of determination greater than 0.60:

distance value N-ANS=8.132 + 0.259 x N-Se - 0.401 x P-PTV + 0.240 x S-Ar (R^2=0.705, $F_{(3.20)}$=15.93, p<0.001, Std.Error of estimate=1.423);

distance value ANS-Me=134.7 + 1.372 x N-CC - 0.985 x N-S - 1.211 x H + 0.626 x Ar-Pt + 0.446 x Por-NBa (R^2=0.601, $F_{(5.18)}$=5.43, p<0.01, Std.Error of estimate=2.637);

distance value 1I-MP=51.16 + 1.238 x N-CC - 0.355 x N-S - 0.517 x H + 0.162 x N-S-Ba - 0.575 x Pt-N (R^2=0.615, $F_{(5.18)}$=5.74, p<0.01, Std.Error of estimate=1.693);

angle value OP-HP=8.049 - 1.009 x P-PTV - 1.757 x N-CC + 0.520 x N-Se - 0.607 x Ar-Pt + 0.833 x Pt-N (R^2=0.661, $F_{(5.18)}$=7.01, p<0.001, Std.Error of estimate=2.611);

angle value Mand1-MP=70.46 + 4.197 x N-Se - 0.987 x S-Ar - 3.937 x N-S - 0.908 x P-PTV + 4.150 x N-S:S-Ar' (R^2=0.639, $F_{(5.18)}$=6.39, p<0.01, Std.Error of estimate=3.563);

distance value Ls-(Sn-Pog')=-4.875 - 0.683 x S-E + 0.121 x N-S-Ba - 0.150 x P-PTV (R^2=0.623, $F_{(3.20)}$=11.03, p<0.001, Std.Error of estimate=0.936);

where, here and in the following equations, R^2 - coefficient of determination; $F_{(!)}$=! - critical $_{(!)}$ and obtained (!) Fisher's test value; p - confidence level; Std.Error of estimate - standard error of estimate.

Coefficients of determination of the regression equations of the *distance values N-A* (R^2=0.278, p<0.05), *N-B* (R^2=0.314, p<0.01), *N-Pog* (R^2=0.479, p<0.01), *PNS-N* (R^2=0.365, p<0.01), *ANS-PNS* (R^2=0.391, p<0.01), *Go-Pog* (R^2=0.385, p<0.05), *B-Pog* (R^2=0.222, p<0.05), *A-B*

(R^2=0.122, p>0.05), *1u-NF* (R^2=0.210, p>0.05), *6u-NF* (R^2=0.582, p<0.001), *Gl'-Pog'* (R^2=0.288, p<0.01), *Li-(Sn-Pog')* (R^2=0.344, p<0.05) and *Stms-I* (R^2=0.447, p<0.05); *angles values N-A-Pog* (R^2=0.391, p<0.05), *Max1-NF* (R^2=0.359, p<0.05), *Gl'-Sn-Pog'* (R^2=0.126, p>0.05), *Sn-Gn'-C* (R^2=0.328, p<0.05) and *Cotg-Sn-Ls* (R^2=0.420, p<0.05); and *the values of the ratios Gl'-Sn/Sn-Me'* (R^2=0.575, p<0.001), *Sn-Gn'/C-Gn'* (R^2=0.103, p>0.05) and *Sn-Stms/Stmi-Me'* (R^2=0.576, p<0.001) in Ukrainian young women with a wide face type had a value of less than 0.60 and therefore have no significant value for practical dentistry. The regression equations of the *distance values Ar-Go, 6l-MP, Gl'-Sn, Sm-(Li-Pog')* and the *angles values MP-HP, Ar-Go-Gn* in Ukrainian young women with a wide face type are not constructed at all.

Out of 19 possible, in Ukrainian YW with an orthognathic bite and a wide face type, 16 reliable regression equations of teleroentgenometric indicators were built, which were included in the *third* group according to the COGS method, depending on the value of the indicators of the *first* and *second* groups with a coefficient of determination greater than 0.60:

distance value 1u-NF=7.181 + 0.399 x ANS-Me - 0.285 x N-Pog - 0.899 x S-Ar' - 0.364 x A-B + 0.260 x N-A + 0.839 x S-E - 0.214 x Por-NBa (R^2=0.889, $F_{(7.16)}$=18.38, p<0.001, Std.Error of estimate=0.842);

distance value 1l-MP=-16.20 + 0.502 x ANS-Me + 0.228 x N-A + 0.226 x N-CC + 0.077 x N-S-Ba + 0.094 x MP-HP (R^2=0.910, $F_{(5.18)}$=36.50, p<0.001, Std.Error of estimate=0.817);

distance value 6u-NF=23.43 + 0.333 x ANS-Me + 0.171 x N-CC - 0.356 x PNS-N - 0.111 x N-S-Ba - 0.075 x N-B (R^2=0.821, $F_{(5.18)}$=16.47, p<0.001, Std.Error of estimate=0.867);

distance value 6l-MP=2.511 + 0.358 x ANS-Me + 0.284 x Ar-Go - 0.185 x P-PTV - 0.118 x Ar-Go-Gn + 0.122 x N-A-Pog (R^2=0.878, $F_{(5.18)}$=25.86, p<0.001, Std.Error of estimate=0.887);

angle value OP-HP=0.162 + 0.843 x N-Pog - 1.637 x A-B + 0.732 x N-A-Pog - 1.593 x N-B (R^2=0.983, $F_{(4.19)}$=271.0, p<0.001, Std.Error of estimate=0.573);

angle value Max1-NF=32.62 + 0.985 x N-B + 0.979 x Go-Pog + 0.702 x ANS-PNS - 0.674 x Ar-Go - 0.893 x PNS-N + 1.044 x N-ANS (R^2=0.691, $F_{(6.17)}$=6.33, p<0.01, Std.Error of estimate=3.527);

angle value Mand1-MP=83.80 + 0.394 x N-Se + 0.609 x N-A-Pog - 1.613 x MP-HP - 0.562 x N-Pog + 0.984 x ANS-PNS - 0.681 x Ar-Go (R^2=0.868, $F_{(6.17)}$=18.65, p<0.001, Std.Error of estimate=2.218);

angle value Gl'-Sn-Pog'=7.836 + 0.741 x N-A-Pog - 0.339 x N-B (R^2=0.614, $F_{(2.21)}$=16.69, p<0.001, Std.Error of estimate=3.870);

distance value Gl'-Sn=-15.99 + 0.832 x N-A + 0.400 x N-CC (R^2=0.654, $F_{(2.21)}$=19.86, p<0.001, Std.Error of estimate=2.137);

distance value Gl'-Pog'=23.41 + 0.914 x N-Pog - 0.167 x N-S-Ba (R^2=0.917, $F_{(2.21)}$=116.0, p<0.001, Std.Error of estimate=1.670);

value of the ratio Gl'-Sn/Sn-Me'=76.18 + 2.992 x Pt-N - 1.867 x Por-NBa - 1.201 x ANS-Me (R^2=0.694, $F_{(3.20)}$=15.15, p<0.001, Std.Error of estimate=7.071);

value of the ratio Sn-Gn'/C-Gn'=105.9 + 2.496 x ANS-Me - 7.267 x N-B - 6.771 x N-ANS + 4.127 x PNS-N + 4.977 x N-A - 2.326 x MP-HP (R^2=0.710, $F_{(6.17)}$=6.93, p<0.001, Std.Error of estimate=13.37);

angle value Cotg-Sn-Ls=112.9 + 5.669 x B-Pog + 1.076 x N-A-Pog + 1.612 x S-Ar - 0.455 x Ar-Go-Gn - 0.698 x ANS-Me (R^2=0.640, $F_{(5.18)}$=6.40, p<0.01, Std.Error of estimate=5.728);

distance value Ls-(Sn-Pog')=1.417 + 0.077 x N-A-Pog - 0.475 x S-E + 0.098 x N-S-Ba - 0.326 x B-Pog (R^2=0.806, $F_{(4.19)}$=19.75, p<0.001, Std.Error of estimate=0.689);

distance value Li-(Sn-Pog')=-11.13 + 0.144 x N-A-Pog - 0.475 x Ar-Pt + 0.115 x N-S-Ba + 0.317 x ANS-PNS - 0.591 x B-Pog (R^2=0.829, $F_{(5.18)}$=17.50, p<0.001, Std.Error of estimate=0.906);

value of the ratio Sn-Stms/Stmi-Me'=90.02 - 1.116 x Pt-N + 1.488 x B-Pog + 0.341 x MP-HP + 0.543 x Por-NBa (R^2=0.709, $F_{(4.19)}$=11.57, p<0.001, Std.Error of estimate=3.409).

Coefficients of determination of the regression equations of the *distances Sm-(Li-Pog')* (R^2=0.437, p<0.01) and *Stms-I* (R^2=0.455, p<0.05); angle *value Sn-Gn'-C* (R^2=0.389, p<0.05) in Ukrainian young women with a wide face type had a value of less than 0.60 and therefore have no significant value for practical dentistry.

Discussion

Thus, in Ukrainian YW with an orthognathic bite and a wide facial type, using the "Cephalometrics for orthognathic surgery" method, 6 reliable regression models of teleroentgenometric indicators were built out of 33 possible, which are included in the *second* and *third* groups depending on the indicators of the *first* group with a coefficient of determination greater than 0.60 (R^2= from 0.601 to 0.705, p<0.01-0.001). Most often, these regression equations include: the distance P-PTV (15.38 %) and N-CC (11.54 %) according to Ricketts, N-Se according to Schwarz (11.54 %), N-S (11.54 %) and S-Ar (7.69 %) according to Roth-Jarabak, Ar-Pt and Pt-N according to the COGS method (7.69 % each), as well as the value of the angles H according to Schwarz and N-S-Ba according to Bjork (7.69 % each).

Also, in Ukrainian YW with an orthognathic bite and a wide facial type, using the "Cephalometrics for orthognathic surgery" method, 16 reliable regression models of teleroentgenometric indicators were built out of 19 possible, which are included in the *third* group depending on the indicators of the *first* and *second* groups with a coefficient of determination greater than 0.60 (R^2 = from 0.614 to 0.983, p<0.01-0.001). Most often, these regression equations include: ANS-Me distances (9.86 %), N-B (7.04 %), N-A, N-

Pog and B-Pog (5.63 % each), N-CC according to Ricketts, PNS-N, Ar -Go and ANS-PNS (4.23 % each), as well as the value of the angles N-A-Pog (9.86 %), N-S-Ba according to Bjork (7.04 %), MP-HP (5.63 %) and Por-NBa according to Ricketts (4.23 %).

The establishment of ethnic characteristics and other variables that can influence changes in normative indicators of odontometric parameters is actively conducted in various scientific institutions [26, 29]. In the study of Amjad Al Taki et al. [1], 71 lateral cephalometric images were analyzed according to the Legan-burstone method of Circassian adults with normal occlusion. The results showed that Circassians have a more convex facial profile, a setback lower jaw and an increased nasolabial angle compared to Caucasians.

The researchers measured 25 anthropometric variables according to the Holdaway-Burstone method in 25 Iranian men and 25 women with good occlusion and balanced faces. Statistical analysis showed significant differences between men and women in several parameters, such as chin-neck angle, nasolabial angle, Merrifield Z-angle, facial convexity angle, thickness of soft tissues of the chin and upper lip, respectively, not all Holdaway norms can be applied to the Iranian population [3]. Another study of Iranians using different cephalometric methods identified significant characteristics of attractive profiles, which were compared with norms for Caucasians. It was found that such indicators as the angle of the soft tissues of the face, the protrusion of the nose, the curve of the upper lip, the nasolabial angle and others have statistical significance in the formation of attractive profiles. Age and sex did not affect the attractiveness of profiles [14].

A study of 100 Egyptian adults aged 18-25 years showed that, according to Holdaway-Burstone analysis, their faces are more convex, their lips are more prominent, and their nasolabial angles are sharper compared to white population standards. Men had more convex faces and protruding lips than women [4].

Teleroentgenograms of 100 Kurds were analyzed using Holdaway and Legan-Burstone cephalometry methods. According to the Holdaway analysis, Kurds have a significantly smaller angle of soft facial tissues, nose protrusion, and thickness of the upper lip compared to Caucasians. At the same time, the values of such parameters as the angle of the face, the convexity of the skeleton, the thickness of the upper lip, and others, turned out to be significantly greater in Kurds [17].

50 individuals aged 18 to 30 years from the southern states of India were subjected to lateral cephalometric analysis according to Burston and Legan. The South Indian population had increased mandibular protrusion, lower lip, upper lip, and deep mentolabial sulcus in both males and females compared to the norm. An increase in the angle between the lower part of the face and the neck was observed in men from southern India [24].

Maharashtrian men have a straighter profile, lower vertical height and reduced mandibular deviation compared to Caucasian men, while Maharashtrian women have a convex profile, reduced vertical height and reduced mandibular deviation according to COGS analysis [20].

Significant progress in the study of teleroentgenometric parameters was achieved by Ukrainian scientists when working with local populations. Thus, the peculiarities of the craniotype and facial types of men from different regions of Ukraine were established [15], the peculiarities of teleradiographic parameters according to the method of Schwarz A. M. were investigated, in particular, the parameters of the root length of the incisors and canines of the upper and lower jaws, models were created for building the correct shape of the teeth arches in young men with a wide face depending on the characteristics of odontometric and cephalometric indicators. In general, in most works, special importance was attached to the study of the relationships between the investigated odontometric parameters and the types of the faces of the examinees [21, 22, 23].

93 lateral cephalometric images of Ukrainian adolescents with a normal bite were studied and discrepancies were found in the position of the central incisors of the upper and lower jaws depending on the ANB angle compared to the results of S.S. Steiner. Reliable incisor position models for Ukrainian teenagers were built using Steiner's method, and the coefficient of determination for boys was from 0.542 to 0.796, and for girls - from 0.503 to 0.622. The study confirmed the relationship of the ANB angle with the characteristics of the position of the upper and lower incisors and revealed ethnic differences [8].

Conclusion

1. With a coefficient of determination higher than 0.60 in YW with an orthognathic bite and a wide face using the COGS method, 6 regression models of teleroentgenometric indicators were built out of 33 possible, which were included in the second and third groups depending on the indicators of the first group (R^2= from 0.601 to 0.705) and out of 19 possible - 16 indicator models that were included in the third group depending on the indicators of the first and second groups (R^2= from 0.614 to 0.983).

2. In YW with an orthognathic bite and a wide face, the values of the distances P-PTV (15.38 %) and N-SS (11.54 %) are most often among the indicators of the *first* group, which were included in the models of indicators of the *second* and *third* groups according to the COGS method Ricketts, N-Se by Schwarz (11.54 %) and N-S by Roth-Jarabak (11.54 %); and among the indicators of the *first* and *second* groups that were included in the models of indicators of the *third* group - the value of the distances ANS-Me (9.86 %), N-B (7.04 %), N-A, N-Pog and B-Pog (5.63 % each), as well as the value of the angles N-A-Pog (9.86 %), N-S-Ba by Bjork (7.04 %) and MP-HP (5.63 %).

References

[1] Al Taki, A., Yaqoub, S., & Hassan, M. (2018). Legan-burstone soft tissue profile values in a Circassian adult sample. *Journal of orthodontic science,* 7(1), 18. doi: 10.4103/jos.JOS_27_18

[2] Alwadei, S. H., Hattan, A. A., Faqihi, K., Alhawiatan, A., Alwadei, F., & Alwadei, A. (2023). Prevalence of malocclusion and orthodontic treatment needs among Saudi primary school male children aged 6-12 years: A cross-sectional study. *Journal of International Oral Health,* 15(1), 106-112. doi: 10.4103/jioh.jioh_159_22

[3] Amini, F., Razavian, Z. S., & Rakhshan, V. (2016). Soft tissue cephalometric norms of Iranian class I adults with good occlusions and balanced faces. *International orthodontics,* 14(1), 108-122. doi: 10.1016/j.ortho.2015.12.003

[4] Bagwan, A. A., Al-Shennawy, M. I., & Alskhawy, M. M. (2015). Evaluation of soft tissue parameters for adults with accepted occlusion using Legan and Burstone analysis. *Tanta Dental Journal,* 12(1), 1-6. doi: 10.1016/j.tdj.2014.06.004

[5] Bengtsson, M., Wall, G., Becktor, J. P., & Rasmusson, L. (2019). A comparison of cost-effectiveness of computer-assisted 2- and 3-dimensional planning techniques in orthognathic surgery. *British Journal of Oral and Maxillofacial Surgery,* 57(4), 352-358. doi: 10.1016/j.bjoms.2019.03.012

[6] Burstone, C. J., James, R. B., Legan, H., Murphy, G. A., & Norton, L. A. (1979). Cephalometrics for orthognathic surgery. *J. Oral. Surg,* 36, 269-277. PMID: 273073

[7] Daneste, H., & Bayat, P. (2022). The prevalence of maxillary fractures in trauma patients referred to Shahid Rajaei hospital in Shiraz from 2011 to 2021. *Journal of Craniomaxillofacial Research,* 9(2), 81-85. doi: 10.18502/jcr.v9i2.11738

[8] Dmitriev, M., Gunas, V., Polishchuk, S., Olkhova, I., & Kumar, A. (2020). Modeling of Central Incisors Position Indicators in boys and girls according to CC. Steiner method for Forensic Dental Identification. *Journal of Indian Academy of Forensic Medicine,* 42(3), 155-160. doi: 10.5958/0974-0848.2020.00043.3

[9] Dmitriev, M. O. (2016). Кореляції основних краніальних показників з характеристиками верхньої та нижньої щелеп у мешканців України юнацького віку [Correlations of main cranial index with characteristics of upper and lower jaws among residents in Ukraine of adolescent age]. *Світ медицини та біології=World of Medicine and Biology*, 4(58), 24-29.

[10] Dmitriev, M. O. (2017). Зв'язки кутових міжщелепних показників з характеристиками положення зубів та профілем м'яких тканин лиця у мешканців України юнацького віку [Links of angular inter-jaws indices with the characteristics of the closure plane, the position of the teeth and the soft-tissue profile of the face in the youth of Ukraine]. *Світ медицини та біології=World of Medicine and Biology,* 2(60), 51-59.

[11] Durão, A. P. R., Morosolli, A., Pittayapat, P., Bolstad, N., Ferreira, A. P., & Jacobs, R. (2015). Cephalometric landmark variability among orthodontists and dentomaxillofacial radiologists: a comparative study. *Imaging science in dentistry,* 45(4), 213-220. doi: 10.5624/isd.2015.45.4.213

[12] Fabien, D. M., Haréfétéguéna, B., Mathieu, M., Motandi, I., Bertrand, E. T., & Tarcissus, K. (2022). Epidemiology and management of Lefort fractures at the Sylvanus Olympio University Hospital of Lom? (Togo). Advances in Oral and Maxillofacial Surgery, 8, 100376. doi: 10.1016/j.adoms.2022.100376

[13] Galán-González, A. F., Domínguez-Reyes, A., & Cabrera-Domínguez, M. E. (2023). Influence of bad oral habits upon the development of posterior crossbite in a preschool population. *BMC Oral Health,* 23(1), 923. doi: 10.1186/s12903-023-03572-0

[14] Ghorbanyjavadpour, F., & Rakhshan, V. (2019). Factors associated with the beauty of soft-tissue profile. *American Journal of Orthodontics and Dentofacial Orthopedics*, 155(6), 832-843. doi: 10.1016/j.ajodo.2018.07.020

[15] Gunas, I. V., Shinkaruk-Dykovytska, M. M., Kotsyura, O. O., Orlovskiy, V. O., Dmytrenko, S. V., Shayuk, A. V., & Glushak, A. A. (2017). Differences of craniotype distribution and types of face among apparently healthy men from different regions of Ukraine. *Folia morphologica*, 76(3), 473-477. doi: 10.5603/FM.a2017.0017 PMID: 28198529

[16] Helal, N. M., Basri, O. A., & Baeshen, H. A. (2019). Significance of cephalometric radiograph in orthodontic treatment plan decision. *J Contemp Dent Pract,* 20(7), 789-7793. PMID: 31597797

[17] Imani, M. M., Hosseini, S. A., Arab, S., & Delavarian, M. (2018). Characterization of soft tissue cephalometric norms of Kurdish population of Iran. *J Res Med Dent Sci,* 6(1), 335-342. doi: 10.5455/jrmds.20186155

[18] Ize-Iyamu, I. N., & Otaren, J. N. (2023). The prevalence of Brodie bite in untreated orthodontic patients in Nigeria. *Journal of orthodontic science,* 12(1), 2. doi: 10.4103/jos.jos_34_22

[19] Jermyn, O., Bister, D., & Jin, H. (2022). Cost-effectiveness of orthodontics: a systematic review. *European Journal of Orthodontics,* 44(5), 566-577. doi: 10.1093/ejo/cjac019

[20] Joshi, S., Punamiya, S., Naik, C., Mhatre, B., Garad, A., & Chabalani, D. (2022). A study to evaluate cephalometric hard tissue profile of maharashtrian population for orthognathic surgery. *Indian Journal of Dental Sciences,* 14(2), 68-73. doi: 10.4103/IJDS.IJDS_60_21

[21] Marchenko, A. V., Shinkaruk-Dykovytska, M. M., Pozur, T. P., Gunas, V. I., & Orlovskiy, V. O. (2020). Models of individual linear dimensions necessary for the construction of the correct form of dental arches in young men with a wide face, depending on the features of odontometric and cephalometric indicators. *Wiadomosci lekarskie* (Warsaw, Poland: 1960), 73(6), 1103-1107. PMID: 32723934

[22] Marchenko, A. V., Gunas, I. V., Petrushanko, T. O., Serebrennikova, O. A., & Trofimenko, Yu. Yu. (2017). Computer-tomographic characteristics of root length incisors and canines of the upper and lower jaws in boys and girls with different craniotypes and physiological bite. *Wiadomosci Lekarskie* (Warsaw, Poland: 1960), 70(3 pt 1), 499-502. PMID: 28711896

[23] Marchenko, A. V., Prokopenko, O. S., Dzevulska, I. V., Zakalata, T. R., & Gunas, I. V. (2021). Mathematical modeling of teleroentgenographic parameters according to the method of Schwarz AM depending on the basic cephalometric parameters in Ukrainian young men and young women with different face types. *Wiadomosci Lekarskie* (Warsaw, Poland: 1960), 74(6), 1488-1492. PMID: 34159943

[24] Murali, P. S., Saidath, K., Achalli, S., Mohammed, A., Soans, C. R., & Nayak, U. S. (2020). Soft Tissue Cephalometric Norms for Orthognathic Surgery in South Indian Population. *Indian Journal of Forensic Medicine & Toxicology,* 14(4), 257-265. doi: 10.37506/ijfmt.v14i4.11482

[25] Nanda, R., & Roberts, W. E. (2015). Charles J. Burstone, 1928-2015. *American Journal of Orthodontics and Dentofacial*

Orthopedics, 148(1), 190-191. doi: 10.1016/j.ajodo.2015.04.010

[26] Nojima, M. D. C. G., Oliveira, T. C. P., Copello, F. M., Silva, I. M. C. C., & Nojima, L. I. (2020). Cephalometric profile norms for southeastern african-brazilian adults according to the legan-burstone analysis: a pilot study. *Revista Científica do CRO-RJ* (Rio de Janeiro Dental Journal), 5(1), 29-34. doi: 10.29327/24816.5.1-6

[27] Proffit, U. R., Fildz, G. U., & Saver, D. M. (2006). *Современная ортодонтия* (перевод с английского Д. С. Персина) [*Modern orthodontics* (translation from English by D. S. Persina)]. M.: МЕДпресс-информ=M.: MEDpress-inform.

[28] Silva, M. B. G. D., & Sant'Anna, E. F. (2013). The evolution of cephalometric diagnosis in orthodontics. *Dental press journal of orthodontics,* 18, 63-71. doi: 10.1016/j.bjoms.2019.03.012

[29] Singh, R., Awasthy, A., Krishna, B. P., Mazhar, H., Soni, S. K., & Thomas, A. E. (2021). Do We Vary from Caucasians! Cephalometric Analysis for Orthognathic Surgery in Chhattisgarhi Population. *Journal of Maxillofacial and Oral Surgery*, 21, 1237-1243. doi: 10.1007/s12663-021-01559-4

[30] Stupar, I., Yetkiner, E., Wiedemeier, D., Attin, T., & Attin, R. (2018). Influence of lateral cephalometric radiographs on orthodontic treatment planning of class II patients. *The open dentistry journal,* 12, 296-302. doi: 10.2174/1874210601812010296

МОДЕЛЮВАННЯ ІНДИВІДУАЛЬНИХ ТЕЛЕРЕНТГЕНОМЕТРИЧНИХ ПОКАЗНИКІВ ЗА МЕТОДОМ "CEPHALOMETRICS FOR ORTHOGNATHIC SURGERY" В УКРАЇНСЬКИХ ДІВЧАТ ІЗ ШИРОКИМ ТИПОМ ОБЛИЧЧЯ ТА ОРТОГНАТИЧНИМ ПРИКУСОМ

Нестеренко Є. А., Дзевульська І. В., Гунько І. П., Карпенко І. А., Даценко Г. В., Прокопенко С. В., Даценко Ю. О.

Дослідження індивідуальних нормативних цефалометричних параметрів у осіб різної статі і віку є важливим для методу "Cephalometrics for orthognathic surgery", оскільки дозволяє точно діагностувати аномалії та розробляти персоналізовані плани лікування. Це сприяє досягненню кращих естетичних результатів, знижуючи ризик ускладнень і підвищуючи ефективність хірургічних втручань. Врахування вікових, статевих особливостей, типу обличчя допомагає прогнозувати довгострокові зміни та адаптувати план лікування для отримання оптимальних результатів. Крім того, це підвищує точність оцінки і стандартизує науково обґрунтовані підходи, що полегшує порівняння результатів між клініками. Таким чином, індивідуальні нормативні параметри є ключовими для успішної ортогнатичної хірургії. Мета дослідження - побудова та аналіз регресійних моделей телерентгенометричних показників за методикою "Cephalometrics for orthognathic surgery" в українських дівчат із широким типом обличчя. 25 українським дівчатам із ортогнатичним прикусом і широким типом обличчя проведено цефалометричне дослідження за методикою "Cephalometrics for orthognathic surgery" (COGS-метод). Для коректного моделювання цефалометричних параметрів застосовано їх розподіл на три групи (Дмітрієв М. О., 2016, 2017): перша група - базові метричні характеристики черепа; друга група - телерентгенометричні показники за якими за допомогою ортогнатичної хірургії можливо змінювати параметри верхньої та нижньої щелеп; третя група - показники які характеризують положення кожного зуба відносно один одного, черепних структур та профілю м'яких тканин обличя. Побудова регресійних моделей проведена в ліцензійному пакеті "Statistica 6.0". Подальшому аналізу підлягали лише достовірні моделі з коефіцієнтом детермінації R^2 не менше 0,60. Встановлено, що у дівчат із широким обличчям за COGS-методом із 33 можливих побудовано 6 моделей телерентгенометричних показників які увійшли до другої та третьої груп в залежності від показників першої групи (R^2= від 0,601 до 0,705, p<0,01-0,001), а також із 19 можливих побудовано 16 моделей показників, які увійшли до третьої групи в залежності від показників першої та другої груп (R^2= від 0,614 до 0,983, p<0,01-0,001). Аналіз моделей показав, що найчастіше до регресійних рівнянь показників які увійшли до другої та третьої груп в залежності від показників першої групи входять величина відстаней P-PTV і N-CC за Ricketts, N-Se за Schwarz, N-S і S-Ar за Roth-Jarabak, Ar-Pt і Pt-N за COGS-методом (по 7.69 %), а також величина кутів H за Schwarz і N-S-Ba за Bjork; а до моделей показників які увійшли до третьої групи в залежності від показників першої та другої груп - величина відстаней ANS-Me, N-B, N-A, N-Pog, B-Pog, N-CC за Ricketts, PNS-N, Ar-Go і ANS-PNS, а також величина кутів N-A-Pog, N-S-Ba за Bjork, MP-HP, а також Por-NBa за Ricketts.

Ключові слова: *регресійний аналіз, телерентгенографія, цефалометрія за методикою "Cephalometrics for orthognathic surgery", дівчата, типи обличчя, ортогнатичний прикус.*

Author's contribution

Nesterenko Ye. A. - research, methodology and original project writing, data visualization, formal analysis, software.
Dzevulska I. V. - conceptualization.
Gunko I. P. - project administration.
Karpenko I. A. - validation.
Datsenko G. V. - review writing and editing.
Prokopenko S. V. - review writing and editing.
Datsenko Yu. O. - validation.

Signed for print 03.06.2024
Format 60x84/8. Printing offset. Order № 3826. Circulation 100.
Vinnytsia. Printing house “TVORY”, Nemyrivske shose St., 62a,
Vinnytsya, 21034
Phone: 0 (800) 33-00-90, (096) 97-30-934, (093) 89-13-852,
(098) 46-98-043
e-mail: tvory2009@gmail.com
http://www.tvoru.com.ua